Universität Bremen*

Centre for Human Genetics

FUNCTIONAL EVALUATION OF HMGB1 AS IMMUNE THERAPEUTIC EFFECTOR MOLECULE FOR CELL-BASED VACCINATION STRATEGIES

Dissertation to obtain the degree
Doctor Rerum Naturalium (Dr. rer. nat.)

Submitted to the Doctoral Committee
of the faculty of Biology and Chemistry (FB 02)

by Saskia Willenbrock

March 2013

First examiner: Prof. Dr. Jörn Bullerdiek
Centre for Human Genetics
University of Bremen

Second examiner: Prof. Dr. Andreas Dotzauer
Department of Virology
University of Bremen

Thesis defence: 24 April 2013

Parts of this work have been supported by the German Research Foundation (DFG) funded interdisciplinary Collaborative Research Centre Transregio 37 (CRC / TR37) with the title ‘Micro- and Nanosystems in Medicine - Reconstruction of Biological Functions’ (Sub-project A2 ‘Laser-based transfection of hematopoietic stem cells’).

Declaration / Erklärung

Herewith I, Saskia Willenbrock, born on 28.12.1980, declare that for writing this dissertation 'Functional evaluation of HMGB1 as therapeutic immune effector molecule for cell-based vaccination strategies' the following three statements apply:

1. I completed the dissertation submitted without any unauthorized aid.
2. I only used those sources and aids as referenced.
3. I acknowledged and referenced any uses of the works of other authors properly.

Hiermit erkläre ich, Saskia Willenbrock, geboren am 28.12.1980, dass für das Verfassen der vorliegenden Dissertation ‘Functional evaluation of HMGB1 as immune therapeutic effector molecule for cell-based vaccination strategies’ folgende drei Aussagen zutreffen:

1. Ich habe die Arbeit ohne unerlaubte fremde Hilfe angefertigt.
2. Ich habe keine anderen als die von mir angegebenen Quellen und Hilfsmittel benutzt.
3. Ich habe die den benutzten Werken wörtlich oder inhaltlich entnommenen Stellen als solche kenntlich gemacht.

Bremen, 06.03.2013

_____

Saskia Willenbrock

„Man kann meist viel mehr tun, als man sich gemeinhin zutraut."

Aenne Burda

Contents

1. Introduction

1.1. Comparative aspects on canine and human neoplasias

Cancer is a major public health problem worldwide. In 2008, 12.7 million new cases of cancer were diagnosed and 7.6 million people died from the disease. This number represents 13 % of all deaths around the world. Of there, lung, stomach, liver, colon, breast and prostate cancer cause the most cancer deaths each year [1]. A prediction of the World Health Organization (WHO) states that deaths from cancer worldwide are continuously increasing with an estimated number of 13.1 million deaths in 2030. More than 30 % of cancer deaths (39 % for men and 19 % for women) are considered to be caused by exposure to influential risk factors (e.g. smoking, bad dietary, lack of physical activity, excessive alcohol consumption) and can be avoided by changing the lifestyle [1, 2].

Extensive research in human cancer medicine is carried out to decipher the processes involved in the development and metastasis of tumours. To establish and improve anticancer therapies, numerous animal models for different human cancer types are available as comparative living systems recapitulating the natural history of cancers and their response to therapeutic agents [3, 4]. Genetically engineered (transgenic and knockout) or immunocompromised murine xenografts with implanted tumour cell lines or tissues are most widely-used as *in vivo* models providing insight in the biology and genetics of human cancers. Mouse models have been extremely useful, but significant limitations are the specific differences between the species and the lack of spontaneous tumour development [3, 5].

Moreover, some physiopathologic characteristics caused by naturally occurring tumours cannot be resembled that closely by induced xenografts tumours. Thus, animal models in which cancers are spontaneously occurring, have gained considerable interest in human cancer research.

The dog is one of the companion animals being considered as an important model system. Canine neoplasias are developing spontaneously in the context of an intact immune system within a syngeneic host and tumour microenvironment enabling new prospects for cancer immunotherapy [5-7]. With their human counterparts, the spontaneous tumours in dogs have been described to share many epidemiologic, histopathologic and biologic features (e.g. tumour progression, metastatic pattern) that are difficult to reproduce in other animal model systems [5, 8, 9]. In dogs,

recurrences as well as similar response rates to conventional chemotherapy protocols are also observed as present in humans [5, 9, 10].

Similar to humans, in dogs cancer is one of the leading natural cause of death. Regardless of age, one of four dogs is reported to die of cancer, while for older individuals with an age of 10 years the death rate with one of two is much higher [11]. Dogs develop tumours at similar sites as humans, but twice as frequently [8]. Therefore, the cancer development in dogs can be observed at an accelerated pace and the response to novel cancer therapeutic options can be tested faster to success with transferable results for humans [8]. Dogs share also many environmental risk factors as exposure to carcinogenic substances (including passive tobacco smoking) and effects induced by living conditions such as bad nutrition with their human owners [12]. Furthermore, the dog receives very good medical health care which in turn leads to a detailed surveillance of cancer development, progression and success of tumour therapy [13, 14]. The superior health care provides also the benefit to obtain adequate tumour samples, non-neoplastic tissue biopsies as well as blood or bone marrow during medical check-up or surgery [10].

Several distinct canine cancers such as osteosarcoma, mammary carcinoma, oral melanoma, oral squamous cell carcinoma, nasal tumours, lung carcinoma, soft tissue sarcomas, and malignant non-Hodgkin's lymphoma (NHL) are known to have the same naturally occurring tumour mechanisms as their human counterparts making them relevant for comparative therapeutic studies [8, 10]. A recent review by Marconato *et al.* in 2012 underlines the similarities between canine and human NHL including the clinical, clinical-pathological and histological correspondence as well as the genomic instability [15-17]. With the analysis of chromosomal copy number aberrations in dogs by comparative genomic hybridisation (CGH), the detection of genomic imbalances was possible in canine NHL. Compared to human CGH analyses, recurrent chromosome aberrations in canine NHL were also present, but lower than in human NHL showing less copy number aberrations [15, 17, 18]. Notable differences were also found e.g. in the distribution of subtypes of T-cell and B-cell lymphomas in the human and canine population. In detail, in dogs T-zone and nodal marginal zone lymphomas are common and rare in humans. In contrast, Burkitt-like and follicular lymphomas are infrequent in dogs and occurring more often in people [15, 19].

The incidence rates for certain tumour types like e.g. canine osteosarcoma and non-Hodgkin's lymphoma are reported to be significantly higher than those observed for humans increasing the potential of serving as appropriate model for the human malignancy [10].

The release of the entire canine genome sequence in 2005 revealed a strong genetic similarity to the human genome [20]. It turned out that many genes are present in a preserved order with up to 95 % synteny between dog and man concerning different chromosome segments [21]. This information offers the opportunity to investigate the development and biologic behaviour of tumours and to identify cancer-associated target genes comparatively in human and dog patients, which provides reciprocal benefit for both species [13, 22]. The characterisation of the molecular structure and function of the target genes and the respective proteins is a prerequisite to elucidate their involvement in pathogenic processes. With the identification of molecular targets, the establishment of gene-therapeutic strategies or diagnostic approaches is strongly facilitated. The development of advanced technologies and highly validated research methodologies enabled the identification of new genes which are also related to cancer [23].

Two targets which are generally known to contribute to carcinogenesis and other pathogenic processes in humans are high-mobility group box 1 (HMGB1) and the receptor for advanced glycation end products (RAGE) as one of its receptors. The genetic structure of the canine homologues of these genes was characterised by Murua Escobar *et al*. in 2003 for *HMGB1* [24] and in 2006 for *RAGE* [25] creating a basis for comparative oncology research in dogs.

Based on these data, during this thesis further basic research on the canine HMGB1 and RAGE was carried out. Furthermore, this thesis covers research that has been conducted in other areas than structure, function and expression of canine cancer-related genes, which can also contribute valuable findings to the establishment of preclinical therapies against cancer.

1.2. HMGB1 - nuclear and extracellular functions

The high-mobility group box protein 1 (also designated as HMG-1 or amphoterin) is a ubiquitously expressed non-histone nuclear protein with double function belonging to the HMG-protein-superfamily [26, 27]. HMGB1 is highly conserved amongst almost all eukaryotic cells. The human protein is composed of 215 amino acids (aa) and has a size of ~30 kDa. The comparison of various species showed that the human

HMGB1 protein sequence is 100 % identical to canine HMGB1 [24] and 99 % identical to mouse, rat, bovine, and porcine HMGB1 [28-31]. Due to the 100 % identity between human and dog HMGB1 is an interesting protein in terms of comparative oncology. The protein structure of HMGB1 is composed of two homologous DNA binding domains (boxes A and B) and a highly negatively charged, acidic C-terminal domain of about 30 asparagine and glutamine residues [32, 33]. The A and B boxes are consisting each of three α-helices which are stabilized by a hydrophobic core and arranged in an L-shape [34].

Nuclear HMGB1 plays a role as DNA-binding protein to sustain nucleosome structure and acts as architectural transcription factor [35]. HMGB1 binds structure-specific to the minor groove of the DNA and is able to induce transient bends or kinks into parts of linear DNA thereby directly influencing the attachment of other transcription factors to their target sequence in a positive or negative way [36-38]. In this function, HMGB1 is reported to modulate the activity of a number of transcription factors including retinoblastoma protein (pRb) [39], members of the Rel/NFκB family [40], the tumour suppressor p53 [41] and its homologue p73 [42] and steroid hormone receptors [43-45].

HMGB1 has also the ability to bind to damaged DNA. The protein is in this role reported to be a key player enhancing nucleotide excision repair and chromatin modification after DNA damage [46, 47]. In terms of cancer, it was demonstrated that HMGB1 has also a higher affinity to the anticancer drug cisplatin forming complexes with DNA [48-50]. HMGB1 inhibits the repair of these cisplatin-DNA adducts leading to an enhanced sensitivity of cells to cisplatin [51-53]. The generation of HMGB1 knockout mice dying 24 h after birth from hypoglycemia and an improper regulation of the glucocorticoid receptor revealed that HMGB1 is indispensable for live [54].

Apart from its intranuclear role, HMGB1 can be localized in the extracellular matrix exerting function as a proinflammatory cytokine which was firstly identified in 1999 by Wang *et al.* [55]. The effects of HMGB1 in its cytokine function are mediated by its functional domains. The B box mediates proinflammatory activity recapitulating the capacity of the full-length protein [56-59] while the A box was shown to act as an antagonist [56, 60-62].

Two main ways of HMGB1 release are known at present: passive and active release. In necrotic or damaged cells dying inadvertently in a traumatic way, HMGB1 is passively released and takes part in the mediation of inflammation, immune system

activation, tissue repair, induces the migration and activation of dendritic cells (DCs) and attracts leukocytes to the inflammated areas [57, 63-65]. HMGB1 thereby functions as an indicator forwarding the dimension of tissue injury to the immune system [66]. In contrast to necrotic cells, cells undergoing apoptosis were initially described to be HMGB1 non-secreting as the protein stays tightly associated to the chromatin [63]. Some later reports revealed that apoptotic cells can also release HMGB1, and this extracellular HMGB1 is tolerated by the immune system instead of mediating proinflammatory effects [67, 68].

It was shown that the caspase-dependent reversible oxidation of the cysteine aa residue 106 (Cys106) in the presence of reactive oxygen free radicals play the central role in the modulation of HMGB1 activity [69]. Cys106 is localised within the cytokine-inducing, inflammation mediating B box [56, 62] and is essential for interaction of HMGB1 with Toll-Like Receptor (TLR) 4 [70]. The fully reduced form of HMGB1 has chemoattractant activity, while HMGB1 with cytokine activity contains a disulfide bridge between the Cys23 and Cys45 and a reduced Cys106 [71]. This cysteine oxidation mechanism for HMGB1 activity regulation is not only existent in apoptotic cells but also hypothesised to control the proinflammatory function of HMGB1 *in vivo*, where a largely oxidative extracellular environment is present during inflammatory processes [71].

Besides passive release, HMGB1 actively can be released from activated immune cells including monocytes, macrophages, dendritic cells, pituicytes, natural killer cells, endothelial cells and platelets [72-78]. Those cells release HMGB1 as a response to exogenous bacterial products (e.g. LPS or CpG-DNA) [55, 79] or endogenous host stimuli causing cellular responses like inflammation, sepsis, development of acute lung injury as well as stimulation of cytokine expression and secretion [55, 72, 75, 80]. Monocytes/macrophages were stimulated *in vitro* with LPS, TNF-α or IL-1β and found to release HMGB1 in a time-dependent manner delayed by several hours in comparison to other proinflammatory cytokines [55, 72, 80]. *In vivo* increased serum levels of HMGB1 could be detected in BALB/c mice beginning approximately 8 h after onset of endotoxemia as well as in a model of sepsis and reaching highest levels after 12-20 h in comparison to other ‘early’ proinflammatory cytokines [55, 62, 81]. As well cells not belonging to the immune system such as adenocarcinoma derived tumour cell lines and mouse intestinal epithelial cells were shown to be capable to secrete HMGB1 [82-85]. Before active secretion, HMGB1 was reported to undergo

extensive acetylation of specific lysine residues [86]. The protein accumulates in the cytoplasm as the re-entry to the nucleus is blocked by the modifications [86] and is released via non-classical pathway by exocytosis of secretory lysosomes [87].
HMGB1 plays a complex role in the development and progression of cancer. The gene is found to be overexpressed in some types of cancers like human gastrointestinal stromal tumours [88], and gastrointestinal adenocarcinomas [89], human malignant melanomas [90], breast [91, 92], and prostate cancer [93], canine osteosarcomas and fibrosarcomas [94], in human leukaemia cell lines [95], and human and canine Non-Hodgkin lymphoma [96, 97]. Accordingly, extracellular HMGB1 is supposed to play a key role in the promotion of tumour growth, because it is accredited to cause angiogenic effects by increasing the expression of angiogenesis-related cytokines and growth factors [98, 99].

1.3. Receptors of HMGB1

Once released, the extracellular effect is mediated by interaction with at least five different membrane receptors as the receptor for advanced glycation end products (RAGE) [100], the Toll-like receptors (TLR)-2, -4 and -9 [58, 59, 101, 102], triggering receptor expressed on myeloid cells-1 (TREM-1) [103], and the glycosyl phosphatidylinositol-anchored CD24 membrane protein [71, 104, 105]. RAGE was the first identified receptor for HMGB1, but it was hypothesised that interaction of HMGB1 solely with RAGE could not lead to all the effects provoked by HMGB1. Later on, signalling via alternative receptors like the above-mentioned TLRs was discovered.
HMGB1 interacts with TLR-2 and TLR-4 via an epitope in its B box. This enables cells of the innate immune system to respond to various exogenous and endogenous stimuli [57-59] leading to cell activation (e.g. macrophages) and NFκB-dependent expression of proinflammatory cytokines [59, 101, 106].
TLR-9 is essential for recognition of unmethylated microbial CpG-DNA inducing macrophages, monocytes and DCs to secret proinflammatory cytokines leading to the elimination of microbial pathogens by activation of plasmacytoid DCs and B-cells [79, 107-110]. Synthetic short single stranded unmethylated oligonucleotides with a CpG motif (CpG-ODN) are also interacting in the same way as microbial CpG-DNA with TLR-9, thus being attractive for therapeutic vaccine strategies aiming at the stimulation of immune responses in the focus of e.g. infectious diseases or cancer [79, 111-113]. HMGB1 itself was also identified as a CpG-ODN binding protein [79,

102]. Triggered by CpG-ODN, HMGB1 is able to enhance TLR9-dependent cytokine responses inside the cell, whereas extracellular HMGB1 helps to accelerate the formation of CpG-DNA/TLR-9 complexes [79]. Another study published in the same year indicated that the TLR-9 dependent activation by DNA containing immune complexes is mediated by HMGB1 and RAGE. These findings demonstrate a previously unknown close relationship between those three proteins [102, 114].

Physiological and pathophysiological outcomes of HMGB1 in interaction with the cell surface have been mostly associated to RAGE signalling [115]. As described previously, RAGE was the first receptor being identified to interact with HMGB1 [100]. Therefore, the focus in this thesis is set on RAGE in reference to receptors interacting with HMGB1.

1.4. RAGE

RAGE is a member of the immunoglobulin superfamily of cell surface molecules which was initially identified to act as a receptor for advanced glycation end products (AGEs) [116, 117]. Later, it was shown that RAGE interacts, besides the AGEs, with multiple ligands including HMGB1, members of the calcium-binding S100 protein family, amyloid-β and macrophage-1 antigen [100, 118-120]. Depending on the ligands, RAGE has been described to be involved in a variety of human immune system dysfunctions and inflammatory disorders [119, 121-123], Alzheimer's disease [118, 124, 125, reviewed also in 126], in diabetes and its associated disorders such as atherosclerosis [122, 127-130], impaired wound healing [131], and various cancers [reviewed in 132].

RAGE is expressed in numerous cells like endothelial cells, vascular smooth muscle cells, neurons, macrophages / monocytes [133]. High expression levels of RAGE were detected in lung tissue [134], atherosclerotic plaques [128, 135] and in the brain of rats during embryonic development while becoming lower in adult tissues [100]. As well large amounts of RAGE are observed in pathologic states like those described above.

The gene encoding the human RAGE consists of 11 exons / introns. The protein is composed of three extracellular immunoglobulin-like domains (V, C1 and C2), a single transmembrane domain (TM), and a short highly charged C-terminal cytosolic domain essential for cell signalling [116, 122]. The V-domain was identified as the ligand-binding domain. The interaction of HMGB1 with RAGE is mediated by a region consisting partly of the B box and the acidic C-terminal domain of the molecule [60].

Characterisation of the canine RAGE revealed a total identity of 77.6 % to the human counterpart [25].

Besides the full-length RAGE several naturally occurring splice variants were detected in humans characterised by C-terminal or N-terminal truncations lacking the TM and cytosolic tail or the ED domain respectively [136-143, reviewed also in 144]. The C-terminal truncated forms are released into the extracellular compartment interacting there as a soluble binding partners for RAGE ligands, but the exact biological role of this soluble variants remains still to be elucidated. Those soluble RAGE variants can exist in different isoforms which include RAGEv1, formed through alternative splicing, and esRAGE, generated by shedding of the extracellular domain from transmembrane RAGE [145, 146, reviewed also in 147].

In general, the diverse variants of RAGE are discussed to act as mechanisms for receptor regulation by competitive inhibition [reviewed in 148, 149]. An imbalance between the full-length RAGE and its soluble variants was reported to be involved inter alia in several clinical settings which were previously accredited to the full-length receptor including immune-mediated diseases (e.g. rheumatoid arthritis) [121, 150], Alzheimer's disease [125, 126, 151], diabetes mellitus type 1 and 2 [152-158], atherosclerosis [127, 159-161], neurodegenerative diseases as for example multiple sclerosis or amyotrophic lateral sclerosis (ALS) [162-164], and cancer [reviewed in 132, 165]. The analysis of RAGE splicing variants expressed in canines will be discussed later within this thesis.

1.5. HMGB1 signalling via RAGE

HMGB1 in its role as a ligand of RAGE is supposed to be involved in growth and actin mobilisation in normal cells [166]. Regarding tumour biology the RAGE-HMGB1 ligand-receptor complex regulates proliferation, migration and metastasis of tumour cells by activation of signal transduction pathways like p21ras, mitogen activated protein (MAP) kinases, p38, JNK (c-Jun NH_2-terminal kinase), cdc42/rac and p44/p42, which in turn leads to activation of the transcription factor nuclear factor kappa B (NFκB) [61, 167-171].

In vivo and *in vitro* experiments by Taguchi *et al*. published in the year 2000 demonstrated that the blockade of the RAGE/HMGB1 complex significantly suppressed local tumour growh and metastasis by application of a soluble RAGE variant (sRAGE) and anti-RAGE or anti-HMGB1 antibodies [170]. These findings provided a wide range of potential therapeutic options targeting at the blockade of

RAGE/HMGB1 complex in terms of cancer as well as inflammatory processes. Since then, the application of sRAGE *in vitro* and *in vivo* in several animal models targeting at the treatment of different human diseases was effectively realised [121, 131, 172-175]. Nevertheless, the sRAGE blocking strategy needs to be considered carefully, because it has been shown that sRAGE seems to have more effects than simply blocking the function of full-length RAGE as cell surface receptor [176, 177]. Besides blocking of the RAGE/HMGB1 complex with sRAGE, alternative strategies for therapeutic HMGB1 inhibition have been evaluated so far. An inhibitory synthetic RAGE-binding C-terminal HMGB1 motif was shown to prevent the metastasis of melanoma cells *in vivo* by blocking the RAGE/HMGB1 complex [60]. Further, several experimental methods for therapeutic HMGB1 inhibition are focussing on the neutralisation of HMGB1 using anti-HMGB1 antibodies or on the administration of the inhibitory HMGB1 A box to block the ligand-receptor interaction [62, reviewed in 178]. Neutralising anti-HMGB1 antibodies were shown to inhibit the release of inflammatory cytokines, but a prevention of HMGB1 secretion cannot be accomplished with this strategy [55, 62, 176, 179].

A deregulated expression of both, HMGB1 and RAGE, was found in various types of human neoplasias including breast, colon, prostate, pancreatic, lung and oesophageal cancers and glioma being strongly associated with the aggressive potential and metastasis of the tumour cells [reviewed in 165, 180]. In dogs, only few analyses targeting at the expression of HMGB1 and RAGE have been performed so far [24, 25, 94].

As previously mentioned, lymphoma is a commonly occurring spontaneous neoplasia in dogs similar to human non-Hodgkin's lymphoma. Data concerning expression of HMGB1 and RAGE in lymphomas are rare [96, 97, 181] lacking the simultaneous analysis of both genes. During this thesis, the expression patterns of HMGB1 and RAGE were analysed in a set of canine lymphomas and control samples. Due to the previously described high similarity of the human and canine RAGE and HMGB1 proteins especially in their interacting domains, those targets could serve for future development and evaluation of tumour therapeutic approaches providing benefit for humans as well as dogs.

In contrast to the proinflammatory and tumour progressing functions of HMGB1, there is much evidence that HMGB1 induces also beneficial effects. HMGB1 can mediate the activation of immune responses to confine infections, and to promote tissue

remodelling and repair [182-184]. In addition, HMGB1 is discussed to have precondition ability. A low level of HMGB1 was shown, by binding to TLR-4, to act as a stressful stimulus reducing injury significantly in various disease states [185, 186]. It seems that the HMGB1 mediated effects are varying from beneficial to pathological in a concentration-dependent manner [182, 184]. From the inflammatory, immune system activating potential of HMGB1 benefits can be drawn to develop new therapeutic strategies aiming at cancer immunotherapy. In combination with RAGE, HMGB1 was shown to be essential for DC activation, maturation and chemotactic migration [187-189]. DCs are the most professional antigen presenting cells (APC) playing a major role in the initiation and regulation of immune responses [190]. Blocking the HMGB1-RAGE complex was reported to inhibit the maturation of DCs [187, 191, 192]. The DC migration towards peripheral lymph nodes was also shown to be mediated by RAGE *in vivo* [189]. In turn, activated DCs themselves also are able to secrete HMGB1 in response to inflammatory stimuli resulting in an 'autocrine-loop' playing a significant role in the proliferation, survival, and functional polarisation of naïve T-cells [65, 192]. Recently it has been also shown that stimulation with recombinant HMGB1 has a proliferative effect on canine peripheral blood mononuclear cells (PBMC) [193].

1.6. Cancer immunotherapy

Cell-based vaccination therapy with tumour antigen-loaded DCs has become of special interest as promising immunotherapeutic approach for treatment of cancer. Cancer immunotherapy is based on the assumption, that cancer cells have the ability to evade the host immune system, in part by expressing immunosuppressive cytokines, which prevent the activation of tumour reactive T-cells [194]. An immunization strategy is to stimulate the immune system for the detection of cancer cells and to induce an immune response by DC application. DCs can be easily generated *ex vivo* by differentiation from hematopoietic stem cells, PBMCs, or monocytes under cytokine-stimulating conditions [195].

DC vaccines were used successfully for the first time in patients with non-Hodgkin's lymphoma who had failed conventional chemotherapy [196]. In this clinical trial, autologous DCs were pulsed *ex vivo* with immunoglobulin idiotype obtained from the patient's tumour and re-injected to stimulate host anti-tumour immunity by priming DC mediated T-cell responses [196].

Up to now, the current approaches are still challenging because those DC vaccines in some cases show less immunogenic potential, e.g. by the DC maturation state influencing the migration activity [197, 198]. To improve the therapeutic utility of DC vaccines in terms of antigen presentation, co-stimulation and cytokine production, several strategies are followed. Those strategies are using DNA, mRNA, viruses to genetically modify DCs for endogenous expression and processing of tumour-associated antigens or immune response factors or to express cytokines, chemokines, and other co-stimulatory molecules [199, 200].

One approach, aiming at the development of an effective DC vaccine strategy for enhancement host anti-tumour responses is addressed by an interdisciplinary collaborate research centre Transregio 37 (CRC / TR37). Parts of this thesis were conducted to support the development of this immunotherapeutic approach.

Within the CRC / TR37, the establishment of a genetically engineered recombinant HMGB1-secreting DC vaccine with enhanced immunostimulatory potential in the dog as model organism is aspired. In detail, one goal of this project is to achieve a highly efficient method for transfection of canine haematopoietic stem cells (HSC) with HMGB1 expression plasmids using the novel femtosecond (fs)-laser technology. In addition, the expansion and differentiation of the modified stem cells to cHMGB1 expressing DC are examined. The application of the engineered DCs as a vaccine in dogs and the characterisation of the migration behaviour of those DCs *in vivo* are also aimed in this project.

To follow therapeutic approaches as described in the CRC / TR37 targeting at *in vivo* application of genetically 'engineered' stem or primary cells, high transfection efficiencies are necessary. To introduce nucleic acids or other molecules deliberately into eukaryotic cells, transfection is an essential biological key technique used in areas of basic research and consequently for implementation of gene-therapeutic approaches. Standard non-viral transfection, e.g. via chemical-based liposome-mediated or cationic methods and the physical method of electroporation, have been shown to be sufficient for fast proliferating cells, but inadequate for transfection of stem cells or primary cells as to unsatisfactory efficiencies or cell toxic side effects [201-204]. Stem cells like e.g. HSCs are regarded to be notoriously difficult to transfect [205]. Transduction with viral vectors as an alternative to the non-viral transfection also revealed limitations and pitfalls in terms of biosafety, inflammatory potential and efficiency [204, 206]. Against the background of the

described limitations, the difficult isolation and availability of limited stem cell populations, novel strategies besides the conventional transfection methods are needed.

The opto-perforation of the cell membrane using fs-laser pulses is a new, very versatile method for cell-type independent transfection selectively targeting single cells [207, 208]. In contrast to the commonly used electroporation perforating the whole cell membrane, fs-laser pulses are focused on a small region of the membrane. The shortness of the laser pulse causes almost no heating due to the fact that the applied pulse duration is shorter than the duration of thermal conveyance (picoseconds to nanoseconds). Thus, thermal shock and mechanical damage can be neglected in this context [207, 209, 210]. The application of fs-laser pulses leads to a precise and gentle opening of a transient pore in membrane with less than one micrometer in diameter affecting only a small volume of some femtoliters allowing the diffusion of extracellular nucleic acids or other molecules into the cell [209].

Another novel approach for achieving enhanced transfection efficiencies is the application of nanoparticles for introduction of nucleic acids and other biomolecules into cells. Especially gold nanoparticles (AuNP) are currently focussed in research due to their outstanding characteristics in terms of biocompatibility, chemical stability, surface functionalisation properties, electrodensity and affinity to biomolecules such as DNA when those AuNPs have an electrical charge [211, 212]. AuNP can be generated by various methods, predominantly relying on chemical reactions or gas pyrolysis [213]. Those methods are bearing the risk of impurities emerging during generation or formation of agglomerates [213]. A new technique generating stabilizer-free AuNP by pulsed laser ablation in liquids (PLAL) has been shown to be a powerful tool to obtain highly pure colloidal particles without any chemical surface modifications making those particles interesting for biomedical applications [214, 215]. Those positively charged PLAL-AuNPs were recently shown to easily adsorb unmodified, negatively charged DNA oligonucleotides providing an interesting tool for improvement of DNA transfection of difficult cells [216].

After successful transfection, a next step to be performed within the CRC / TR37 is the expansion and differentiation of the genetically modified stem cells to recombinant HMGB1 expressing DCs. For the characterisation of the trafficking patterns of such administrated DC vaccines, suitable non-invasive, non-toxic *in vivo* imaging methods are needed to monitor the fate and migration of transplanted cells.

One strategy for non-invasive *in vivo* imaging of applied DCs is the tracking via DC-specific fluorophore-coupled antibodies. In humans, DC specific antibodies directed against CD40, CD80, and CD83 are commonly used for characterisation of the DC maturation state [217]. Those antibodies might also be used for quantification, separation and specific immunological or direct *in vivo* visualisation. Up to now, the availability of antibodies binding specifically to canine DCs is severely limited, making the detection of DCs in canine tissues challenging [217].

Another powerful option for cellular in vivo tracking appears to be the magnetic resonance imaging (MRI) technique as promising clinically transferable tool, with high spatial resolution, a long effective imaging window, and fine signal intensity [218-220]. In order to detect transplanted cells by MRI, the cells must be labelled with an effective contrast agent. Due to their low toxicity and high biocompatibility, different types of superparamagnetic iron oxide (SPIO) nanoparticles with strong T2*-specific signal extinctions are widely used for labelling of different cell types [220-225]. SPIOs can be incorporated easily by endocytosis without requirement of transfection agents which could affect the viability of cells [226]. It was shown that DCs can be labelled as well effectively with SPIO and successfully detected via MRI [226-231]. Thus, MRI in combination with SPIOs might be a suitable, clinically feasible modality to monitor the migration behaviour of implanted cells *in vivo*.

1.7. Areas of research within this thesis

The thesis presented herein is divided into the following four main fields.

- In the first part of the thesis, basic research on the canine HMGB1 and RAGE concerning the analysis of expression patterns, structural and functional characterisation was carried out. In detail, the naturally occurring splice variants of the RAGE were characterised and the expression RAGE and HMGB1 in canine lymphoma was analysed. In addition *in silico* sequence homology analyses of the canine cytokines IL-1α, IL-1β, and TNF-α to several other mammalian species were performed.
- The second topic deals with the establishment of two novel transfection methods using fs-laser based opto-perforation on the one hand and the application of positively charged AuNPs in combination with DNA on the other hand.
- The focus in the third part lies on the functional analysis of modified cells. Herein the induction of HMGB1 secretion from a mammary epithelial cell line

by cytokine stimulation and the response of canine B-cell lymphoma cells to CpG-oligonucleotide DSP30 and IL-2 stimulation are presented.

- The last topic of this thesis introduces methodologies for the non-invasive *in vivo* imaging of cells including the generation of antibody fragments targeting canine DCs and cell tracking of SPIO nanoparticle labelled cells via MRI.

2. Materials and Methods

2.1. Cell culture

2.1.1. MTH53A

The MTH53A canine mammary cell line, derived from epithelial healthy canine mammary tissue, was provided by the Centre for Human Genetics, University of Bremen, Bremen, Germany. The cells were cultivated in medium 199 (Gibco, Karlsruhe, Germany) supplemented with 10 % heat-inactivated fetal calf serum (FCS) (PAA Laboratories GmbH, Coelbe, Germany), 200 U/ml (U; unit) penicillin and 200 ng/ml streptomycin (Biochrom AG, Berlin, Germany).

2.1.2. CD34+ human umbilical cord blood stem cells (hUCBCs)

CD34+ selected and expanded hUCBCs were provided by the department of Neurology, Hannover Medical School, Hannover, Germany. The cord blood was obtained from healthy pregnant women with non-complicated pregnancies at spontaneous term-deliveries (38-40 weeks of gestation) or by Caesarean section after informed written consent, respectively, as approved by the Institutional Review Board, project #3037 on June 17th, 2006.

2.2. *In vitro* SPIO cell labelling

Cell labelling was performed with the commercially available superparamagnetic iron oxide (SPIO) suspension ENDOREM® (Guerbet S.A., Roissy, France). This infusion suspension contains particles with an approximate size of 80 to 150 nm and has a total iron content of 11.2 mg/ml.

A total of $5X10^6$ MTH53A cells or CD34+ hUCBCs was seeded in a 25 cm^2 cell culture flask with 5 ml of the respective cultivation medium. For labelling, 41.15 µl SPIO suspension (=130 pg iron oxide nanoparticles/cell) was added to the seeded cells followed by an overnight incubation at 37°C in 5 % CO_2. After SPIO incubation, the viability of the labelled cells and unlabelled cells as controls was assessed by trypan blue staining.

2.3. Prussian blue staining

After SPIO labelling, cells were fixed with 4 % paraformaldehyde, washed with 1X Phosphate Buffered Saline (PBS; Biochrom AG, Berlin, Germany) and incubated with a 1:1 solution of 5 % potassium ferrocyanide and 5 % hydrochloric acid for 30 min. The ferric iron (iron(III) oxide; Fe_2O_3) of the intracellular SPIO particles reacts with potassium ferrocyanide to form ferric ferrocyanide (= Prussian blue), a water-insoluble, blue precipitate. A final washing step with 1x PBS was performed before visualization of the internalized particles was carried out under light microscopy.

2.4. Agar gel phantom construction for *in vitro* MRI scans

For *ex vivo* MRI detection of SPIO-labelled cells, 250 ml of a hand-warm bubble-free 1 % agar (Carl Roth GmbH & Co. KG, Karlsruhe, Germany) solution (in dH_2O) were prepared and put into an empty pipette tip box (Greiner Bio-One, Frickenhausen, Germany). For generation of sample wells, an unskirted 96-well PCR plate (Eppendorf AG, Hamburg, Germany) was placed onto the surface of the liquid agar solution. After polymerisation of the agar, the 96 well-plate was removed and the sample wells were ready for cell loading.

The SPIO-labelled cells were trypsinised after incubation with SPIOs and the cell number was determined. Defined numbers of cells were aliquoted into 1.5 ml cups (Eppendorf AG, Hamburg, Germany) as indicated in the results. The aliquoted cells were centrifuged for 10 min at 1,000 rpm (room temperature), the supernatant was discarded and the pellet was resuspended in 30 µl of hand-warm 4 % gelatine (AppliChem, Darmstadt, Germany)/dH_2O solution. The cell-gelatine mixture was pipetted into the wells of the agar gel phantom and air bubbles were removed. The phantom was cooled at 4°C until the gelatine was solidified. As controls, additionally to unlabelled cells, 1.0 µl or 1.5 µl SPIO solution (1.0 T MRI and 7.0 T MRI, respectively) and 30 µl culture medium were prepared by mixing 30 µl of the 4 % gelatine solution and loading the samples into the wells of the agar gel phantom. Finally, to embed the loaded samples evenly in the agar phantom, the top was covered with 1 % agar gel solution. After polymerisation, the construct was stored at 4°C until MRI analysis.

2.5. *In vivo* experiment with SPIO labelled CD34+ hUCBCs

In vivo imaging of SPIO-labelled hUCBCs was performed in a transgenic mutant SOD1-ALS mouse. The G93A-ALS mouse model (B6SJL-Tg(SOD1-G93A)1Gur/J) is bred and maintained at the animal facility of Hannover Medical School.

The SPIO-labelling of the cells was carried out as described in the '*In vitro* SPIO cell labelling' section. The injection of the SPIO-labelled hUCBCs in the SOD1-ALS mouse was performed by Prof. Dr. Susanne Petri of the Department of Neurology, Hannover Medical School, and is described in the corresponding publication (Willenbrock *et al.*, 2012b; Journal: IN VIVO).

2.6. *In vitro* and *in vivo* MRI scan parameters

2.6.1. *In vitro* MRI

The scans of the prepared agar gel phantom, loaded with SPIO-labelled cells and respective controls, were performed in a clinical whole-body MR imaging system at 1.0 T (Magnetom Expert, Siemens Healthcare, Erlangen, Germany) and a Bruker Pharmascan 70/16 7.0 T MR-tomograph for small laboratory animals (Bruker BioSpin MRI GmbH, Ettlingen, Germany).

For 1.0 T analysis, a T2*-weighted gradient echo fl2d 20 sequence with a repetition time (TR) of 800 ms and an echo time (TE) of 26.0 ms, slice thickness of 2.0 mm, flip angle (FA) of 20°, field of view (FoV) of 201X230, 168X256 and two repetitions was used and the data analysis was carried out by dicomPACS version 5.2 (Oehm and Rehbein, Rostock, Germany).

To scan the agar gel phantom in the 7.0 T MRI, an 8 cm volume resonator designed for MRI analysis of rats was used. The agar gel phantom was trimmed with a scalpel to fit into the 8 cm volume resonator. The parameters for the 7.0 T scan were as follows: T2*-weighted flash 2D sequence, TR/TE = 200/20, slice thickness 2.0 mm, FA = 90°, one repetition.

Data were analysed using ImageJ, version 1.41 (NIH, Bethesda, MD, USA) extended by the Bruker Opener plugin version 2008/04/22 (Fraunhofer Institute for Biomedical Engineering, St. Ingbert, Germany).

2.6.2. *In vivo* MRI

In vivo MRI was performed by Dr. Martin Meyer, Institute of Laboratory Animal Science and Research Cluster of Excellence 'REBIRTH' (AG36), Hannover Medical School, on a 7.0 T Bruker Pharmascan 70/16 (Bruker Biospin) equipped with a 6 cm volume resonator using Paravision 5.0. A T2* multi-gradient echo (MGE) with the following parameters was used: TR = 1500 ms, TE = 9 ms, FA = 30°, slice thickness = 1 mm. The G93A-ALS mouse was scanned at day 0 (injection day) and day 4 to detect the injected SPIO-labelled cells and to analyse if cell migration could be visualized.

2.7. PCR and DNA cloning

PCR amplification of DNA fragments was done using gene specific primers and GoTaq flexi DNA polymerase (Promega, Mannheim, Germany) according the manufacturers' instructions in a Thermoblock Mastercycler Gradient (Eppendorf AG, Hamburg, Germany) or a Trio Thermoblock 48 (Biometra GmbH, Göttingen, Germany). The PCR conditions varied depending on the annealing temperatures of the used primers and the fragment length of the amplified PCR product.

The amplified PCR products were separated on a 1.5 % agarose gel, eluted using QIAquick Gel Extraction Kit (QIAGEN, Hilden, Germany) and ligated into the corresponding expression vector.

The ligated expression vectors were transformed into thermocompetent *Escherichia coli* (*E. coli*) DH5α bacteria cells (Invitrogen AG, Carlsbad, CA, USA) as described by Inoue *et al*. (1990). For long-term storage, glycerol stocks were prepared by the addition of 1 ml bacteria culture into sterile aliquots of 1 ml 60 % glycerol and frozen at -80°C.

Plasmid isolation was done using QIAprep Spin Miniprep Kit (Qiagen, Hilden, Germany) following the manufacturers' protocol. Verification of the constructed plasmids was done by double restriction digest with suitable restriction enzymes and sequencing (Eurofins MWG GmbH, Ebersberg, Germany).

Sequence data analysis was done using DNASTAR Lasergene software (DNASTAR Inc., Madison, WI, USA). Large scales of plasmids were isolated using the PureYield™ Plasmid Maxiprep System (Promega, Madison, WI, USA).

2.8. Mammalian expression vector constructs

2.8.1. pIRES-hrGFP II expression vectors

Different variants of recombinant pIRES-hrGFP II (Stratagene, La Jolla, CA, USA) vector constructs were generated, carrying the *hrGFP* gene (pIREShrGFP) and the gene of interest. The bicistronic expression cassette of the different constructed vectors permits the simultaneous but separate expression of the inserted genes of interest and of *hrGFP* showing successful transfection of the cells with the respective vector by green fluorescence.

2.8.1.1. pIRES-hrGFP II-*rHMGB1*+FLAG

This expression vector variant contains the canine *HMGB1* coding sequence (CDS) (GenBank ID: AY135519.1) without the terminal stop codon resulting in an HMGB1 fusion protein with a recombinant short 3x FLAG peptide sequence at its C-terminal part to differentiate via immunohistochemistry between endogenous and expressed recombinant HMGB1 protein (rHMGB1+FLAG).

DNA fragments were amplified by PCR (forward primer: EcoRI-B1-CFA-FWD, 5'-GGAATTCCACCATGGGCAAAGGAGA-3'; reverse primer: NotI-B1-CFA-REV, 5'-GCGCGGCCGCTTATTCATCATCATC-3').

Cloning of the PCR amplicons into the pIRES-hrGFP II expression vector was performed as described in the 'PCR and DNA cloning' section. Verification of the constructed plasmids was done by NotI/EcoRI double restriction digest and sequencing.

2.8.1.2. pIRES-hrGFP II-*rHMGB1*

This vector contains the complete *HMGB1* CDS (GenBank ID: AY135519.1) with its terminal TAA stop codon and was constructed to make sure that the 3x FLAG-tail has no effect on the function of the recombinant HMGB1 (rHMGB1) protein.

DNA fragments were amplified by PCR (forward primer: EcoRI-B1-CFA-FWD, 5'- GGAATTCCACCATGGGCAAAGGAGA-3'; reverse primer: NotI-B1-CFA-Rev/-TAA, 5'-AAGAATGATGATGATGAAGCGGCCGCGC-3').

Cloning of the PCR amplicons into the pIRES-hrGFP II expression vector was performed as described in the 'PCR and DNA cloning' section. Verification of the constructed plasmids was done by NotI/EcoRI double restriction digest and sequencing.

2.8.1.3. pIRES-hrGFP II-*eIL-12*

DNA encoding for eIL-12 (Vetsuisse-Faculty, University of Zürich) was amplified by PCR (forward primer: NotI_IL-12_f, 5'-CGGCGGCCGCATATGTGCCCGCCGCGC-3'; reverse primer: NotI_IL-12_r, 5'-CGGCGGCCGCAACTGCAGGATACGG-3'). The DNA contains the p35 and p40 IL-12 subunit cDNAs (p35: Acc. No. Y11129; p40: Acc. No. Y11130) separated by an IRES element, both IL-12 subunits are translated separately and then processed by the cell to a joint complex.
Cloning of the PCR amplicons into the pIRES-hrGFP II expression vector was performed as described in the 'PCR and DNA cloning' section. Verification of the constructed plasmid was done by NotI restriction digest and sequencing.

2.8.2. HMGB1-GFP fusion protein expressing vector

The pEGFP-C1-HMGB1 expression vector, containing the complete coding sequence of the canine HMGB1 gene, was constructed and provided by Dr. Andreas Richter, Centre for Human Genetics of the University of Bremen, Germany. Expression of this vector leads to the formation of a HMGB1-GFP fusion protein. The protein coding sequence of the canine HMGB1 was amplified by PCR (forward primer: EcoRI-B1-CFA-FWD, 5'-CGGAATTCCACCATGGGCAAAGGAGA-3'; reverse primer: KpnI-B1-CFA-REV, 5'-GATGATGATGAATAAGGTACCGC-3). Cloning of the PCR amplicons into the pIRES-hrGFP II expression vector was performed as described in the 'PCR and DNA cloning' section. Verification of the constructed plasmid was done by EcoRI/KnpI double restriction digest and sequencing.

2.9. Transient transfection

2.9.1. FuGENE® HD transfection

The transient transfection assays were performed in 6-well plates with approximately 3×10^5 or 4×10^5 cells per well and 2 ml medium. An amount of 2 µg of the corresponding vector constructs was transfected into MTH53A cells according to the manufacturer's instructions using 3 or 5 µl in 100 µl H_2O FuGENE® HD (FHD) transfection reagent (Roche, Mannheim, Germany). For details concerning the used cell number and volume of FHD reagent *c.f.* the publications of Durán & Willenbrock *et al.* (2011) and Willenbrock *et al.* (2012).

2.9.2. Gold nanoparticle (AuNP) and magnet-assisted transfection (MATra)

In comparison to the conventional FHD transfection method, five additional different transfection protocols were evaluated:

- Commercially available AuNPs (Plano-AuNP; 20 nm; Plano GmbH, Wetzlar, Germany) combined with FHD
- Stabilizer-free PLAL-AuNP (size 1 (d50 = 28.5 nm and d90 = 43.4 nm hydrodynamic sizes; 14 ± 3 nm Feret diameter) combined with FHD
- Stabilizer-free laser-generated PLAL-AuNP size 2 (d50 = 52.4 nm and d90 = 78.6 nm hydrodynamic sizes; 41 ± 8 nm Feret diameter) combined with FHD
- MATra using MA Lipofection Enhancer (PromoKine, Heidelberg, Germany)
- MATra using MATra-A Reagent (PromoKine, Heidelberg, Germany)

These transfection methods were performed in the co-publication of Durán & Willenbrock *et al*. (2011) and carried out by Carolina Durán. The PLAL-AuNP were generated and provided by Dr. Annette Barchanski (Laser Zentrum Hannover e.V., Hannover, Germany) and Prof. Dr. Stephan Barcikowski (Chair of Technical Chemistry I, University of Duisburg-Essen and Center for Nanointegration Duisburg-Essen (CeNIDE)). Details concerning the different transfection methods and the generation of PLAL-AuNPs can be found in the relevant publication.

2.10. Transfection efficiency analyses

2.10.1. Fluorescence microscopy

The transfected MTH53A cells were incubated for 48 h in culture medium. After incubation, the cells were washed with 1x PBS, fixed with phosphate-buffered formaldehyde (4 %, pH 7.4, 10-15 min) at room temperature and washed again with 1x PBS. Nucleic DNA was stained using Vectashield Mounting Medium with DAPI (4'-6-diamidino-2-phenylindole, Vector Laboratories, Burlingame, CA, USA) and the uptake of plasmid DNA was verified by fluorescence microscopy using an Axioskop microscope or Axio Imager.Z1 fluorescence microscope (both Carl Zeiss MicroImaging GmbH, Jena, Germany).

2.10.2. Flow cytometry for transfection efficiency analysis

In order to determine the transfection efficiency, GFP expression of pIRES-hrGFP II-*rHMGB1*+FLAG and pIRES-hrGFP II-*eIL-12* transfected MTH53A cells was analysed measuring green fluorescence by flow cytometry in comparison to untransfected native MTH53A cells.

The flow cytometry analyses were carried out by Carolina Durán. Details can be found in the relevant publication of Durán & Willenbrock *et al.* (2011).

2.11. Induction of HMGB1 release by cytokine stimulation

Approximately 400,000 MTH53A cells were plated in 6-wells and transfected as described previously with the pIRES-hrGFPII-*rHMGB1*+FLAG vector construct to differentiate between the recombinant HMGB1 (rHMGB1+FLAG) and endogenous HMGB1 (eHMGB1). To induce the release of HMGB1 the cells were stimulated 24 h after transfection with 50 ng/ml canine TNF-α (R&D Systems, Minneapolis, USA) or 100 U/ml canine IFN-γ (R&D Systems, Minneapolis, USA) for different time periods (6, 24, 48 h) at 37°C and 5 % CO_2. After incubation the conditioned medium and the MTH53A cells were harvested for HMGB1 Western blotting and HMGB1 ELISA.

2.12. Live cell imaging using laser scanning microscopy

Live cell imaging of pEGFP-C1-HMGB1 transfected MTH53A cells was performed for visualization of HMGB1 release after stimulation with TNF-α.

400,000 MTH53A cells were seeded in glass-bottom-dishes (MatTek Corporation, Ashland, USA). Cultivation and transfection were performed as described previously. 24 h after transfection the cells were stimulated with 50 ng/ml canine TNF-α (R&D Systems, Minneapolis, USA) for induction of HMGB1 release. Live cell imaging was performed at the Laser Zentrum Hannover e.V. (LZH) for 50 h on an uniquely modified multiphoton laser scanning system (Zeiss Axiovert S100) consisting of a femtosecond-laser system (Chameleon Ultra II, Coherent Inc., tuneable wavelength 690 nm-1040 nm; femtosecond = fs, 10^{-15} sec.) and a custom built scanning and detection module. Used parameters: 37°C, 5 % CO_2, 900 nm wavelength, 2.71 V amplifier voltage, 8 mW (80 Mega-Hertz) pulse energy. Images were recorded in 30 µm 3D-stacks with 1.5 µm layer distance and 256 x 256 pixel resolution all 30 minutes.

2.13. Protein analyses

2.13.1. SDS PAGE and HMGB1 Western blot

48 h after transfection and stimulation of MTH53A cells the cell-conditioned medium was harvested and the adherent cells were lysed using cell lysis buffer (50 mM Tris, pH 7.8, 150 mM NaCl, 1 % Nonidet P-40). Cellular debris was removed by centrifugation for 10 min at 1000 rpm and the supernatants were collected.

The presence of recombinant and endogenous HMGB1 in the harvested cell-conditioned medium or in lysed MTH53A cells was assayed before and after cytokine treatment by Western blotting analysis and quantified using the HMGB1 ELISA Kit II (Shino-Test Corporation, Kanagawa, Japan).

For Western blot analysis equal volumes of the harvested samples were heated for 5 min at 95°C in reducing sample buffer, fractioned by sodiumdodecylsulfate-polyacrylamide gel electrophoresis (SDS-PAGE) (4 % stacking gel, 12 % running gel) and transferred to a polyvinylidene difluorid (PVDF) membrane with 0.2 µm pore size (PALL Corporation, New York, USA) in order to examine the protein biosynthesis of recombinant HMGB1. Membranes were probed using a 1:5,000 dilution of primary HMGB1 antibody [HAP46.5] (Abcam plc, Cambridge, UK) and 1:10,000 dilution of goat anti mouse IgG (H&L):HRP (AbD Serotec, Martinsried/Planegg, Germany) secondary antibody (HRP; horseradish peroxidase). To exclusively detect recombinant rHMGB1+FLAG protein, a monoclonal ANTI-FLAG® M2-Peroxidase (HRP) antibody (Sigma-Aldrich Corp., St. Louis, MO, USA) was used in a dilution of 1:10,000. Visualisation was done by chemiluminescence using 3.3'-diaminobenzidine (DAB) substrate (Sigma-Aldrich Corp., St. Louis, MO, USA).

2.13.2. HMGB1 enzyme-linked immunosorbent assay (ELISA)

To determine the HMGB1 level in the cell-conditioned medium and MTH53A cell lysates after cytokine stimulation the Shino-Test HMGB1 ELISA Kit II was used according to the manufacturer's instructions.

The samples were concentrated before ELISA measurement from 200-450 µl lysate and 500 µl medium to 20 µl end volume via 10 kilo Dalton (kDa) Roti-Spin Midi-10 columns (Carl Roth GmbH, Karlsruhe, Germany). The absorbance of the performed ELISA was read at 455 nm in a Synergy HT multi-detection microplate reader (BioTek Instruments GmbH, Bad Friedrichshall, Germany) using KC4 software

(Kineticalc for Windows, version 3.4, BioTek Instruments GmbH). The levels of HMGB1 were calculated with reference to standard curves of purified recombinant HMGB1 at various dilutions (1.25, 2.5, 5.0, 10.0, 20.0, 40.0, 80.0 ng/ml) and in consideration of the concentrations factors.

2.13.3. Immunofluorescence

The immunofluorescence analyses were carried out in collaboration with Carolina Durán.

To confirm biological functionality of the recombinant proteins expressed in pIRES-hrGFPII-*eIL-12* and pIRES-hrGFP II-*rHMGB1*+FLAG transfected MTH53A cells, immunofluorescence directed against eIL-12 and canine HMGB1 was performed. For transfection, the previously described FHD method was chosen. The microscopy for analysis of the immunofluorescence was carried out using a Leica DMI 6000 fluorescence microscope (Leica Microsystems GmbH, Wetzlar Germany).

2.13.3.1. Equine IL-12

MTH53A cells were fixed 24 h after transfection in 4 % paraformaldehyde/PBS for 20 min at room temperature, permeabilised with Triton X-100 (Sigma-Aldrich Corp., St. Louis, MO, USA) and blocked. Immunofluorescence was carried out using the primary goat IgG anti-p35 polyclonal antibody (IL-12 p35, Santa Cruz Biotechnology, Inc.; Santa Cruz, CA, USA) in a dilution of 1:40 and the secondary donkey anti-goat antibody (IgG-TR, Santa Cruz Biotechnology, Inc.; Santa Cruz, CA) in a dilution of 1:180.

2.13.3.2. Canine HMGB1

The expression of canine HMGB1 was evaluated in MTH53A cells. Cells were prepared as described for the equine IL-12 expression. For transfection, different protocols were applied which are described in detail in the corresponding publication of Durán & Willenbrock *et al.* (2011).

Twenty four hours after transfection with tree different protocols (details of the protocols can be found in the corresponding publication of Durán & Willenbrock *et al*., 2011), immunofluorescence was performed using an anti-HMGB1 mouse monoclonal antibody (HMGB1 antibody [HAP46.5], Abcam, Cambridge, UK) with a dilution of 1:60 and a goat anti-mouse antibody (DyLightTM 549-TFP ester, Jackson ImmunoResearch, West Grove, PA, USA) with a dilution of 1:220.

2.14. Toxicity and viability analyses

2.14.1. Cell viability staining

Viability of 24 h TNF-α or IFN-γ pIRES-hrGFP II-*rHMGB1*+FLAG transfected MTH53A and untransfected MTH53A stimulated cells was assessed by Trypan Blue exclusion (Invitrogen, Carlsbad, USA), which detects necrotic cells.

To verify if incubation with TNF-α or IFN-γ may lead to apoptosis or necrosis and thus possibly to a release of HMGB1, double staining with Annexin V-PE / propidium iodide (PI) was performed using the 'Annexin V-PE Apoptosis Detection Kit' (PromoCell GmbH, Heidelberg, Germany). This assay distinguishes between apoptotic and necrotic cells.

A number of approximately 400,000 MTH53A cells was seeded in 1-well Falcon CultureSlides (Becton, Dickinson and Company, Heidelberg, Germany), transfected with pIRES-hrGFPII-*rHMGB1*+FLAG and treated with TNF-α or IFN-γ for 6, 24, and 48 h as described in the section 2.11. 'Induction of HMGB1 release by cytokine stimulation'. After incubation, the culture medium was replaced by 500 µl 1x Annexin V Binding Buffer. For detection of phosphatidyl serine exposure on the external leaflet of the plasma membrane during apoptosis, Annexin V-PE reagent was added showing an orange-red staining.

Necrotic cell detection was performed by adding propidium iodide (PromoCell GmbH, Heidelberg, Germany) in a concentration of 30 µM. PI is a nucleic acid intercalator passing only through disturbed cell membranes staining the nuclei of necrotic cells with a light red fluorescence.

The cells were incubated for 15 minutes at room temperature in the dark, washed wice with 1x PBS after incubation and fixed for 10 min using 4 % phosphate-buffered formaldehyde (pH 7.4). The cells were analyzed by fluorescence microscopy using an Axioskop microscope with a rhodamine filter (Carl Zeiss, Oberkochen, Germany).

2.14.2. Flow cytometry for cell toxicity analysis

Staining with PI was used to identify the percentage of dead cells after transfection. The flow cytometry cell toxicity analyses were carried out by Carolina Durán. Details can be found in the relevant publication of Durán & Willenbrock *et al.* (2011).

2.14.3. Proliferation assay

Proliferation of cells in response to each transfection protocol was evaluated using a colorimetric cell proliferation ELISA (Roche Applied Science, Mannheim, Germany) which measures the incorporation of 5-bromo-2-deoxyuridine (BrdU) into DNA by ELISA using an anti-BrdU monoclonal antibody. The absorbance was read with a Synergy HT multi-mode microplate reader (BioTek Instruments GmbH, Bad Friedrichshall, Germany) and exported with Excel 2003 software (Microsoft, Unterschleißheim, Germany).

The proliferation assay was performed by Carolina Durán. Details can be found in the relevant publication of Durán & Willenbrock *et al.* (2011).

3. Results

3.1. Structural and functional characterisation of HMGB1 and RAGE genes, proteins and associated cytokines

The following section describes basic research on RAGE and HMGB1. The RAGE/HMGB1 receptor/ligand complex is described to play a key role in mediation of immune responses, inflammation processes, angiogenesis as well as tumour formation and in the genesis of other diseases. Active release of HMGB1 by various cell types is stimulated by 'early' proinflammatory cytokines like TNF-α, IL-1 or IFN-γ. Thus, the characterisation of cytokines inducing the secretion of HMGB1 is also crucial for understanding the development of diseases. An *in silico* sequence homology analysis of several mammalian IL-1α, IL-1β, and TNF-α mRNA and protein structures was therefore carried out and is also described in this section.

I 'Cloning, characterisation, and comparative quantitative expression analyses of receptor for advanced glycation end products (RAGE) transcript forms.' **Sterenczak *et al*., Gene, 2009.**

Besides the initial characterisation of the complete canine *RAGE* cDNA and a sequence identity comparison to the human counterpart on DNA and protein level done by Murua Escobar *et al*. in 2006, the structural appearance of this transmembrane receptor needs to be analysed in detail. In humans, nearly 20 different natural occurring RAGE splice variants with C-terminal or N-terminal truncations, lacking of the cytosolic or transmembrane domains, were found and discussed to be acting as mechanisms for receptor regulation by competitive inhibition.

In this study RNA isolation was carried out on a set of 17 different canine tumours, seven healthy tissues, four canine and three human cancer cell lines and screened for RAGE splice variants. Subsequently, an *in silico* structural analysis determining the putative protein outcome was performed. Additionally, the ratio of the mainly found transcript variants was analysed by quantitative and relative real-time PCR.

Altogether, 24 canine and six human splice variants were characterized whereof 14 canine and four human RAGE isoforms were not described previously in other

species showing various combinations of insertions of introns, partial or complete deletion of exons and several small nuclear polymorphisms (SNPs).

The found RAGE transcripts could be classified in two categories at which the first category covers splicing variants encoding for protein forms with either the complete open reading frame or for soluble sRAGE lacking the transmembrane domain. Both variants are capable to bind extracellular ligands due to the existence of the N-terminally localised ligand binding immunoglobulin type V-domain.

The second group contains transcripts being processed by alternative exon / intron splicing and intron insertions leading to translation of mutated 'non-sense' protein forms. The most remarkable mutation found in the analysed human and canine cell lines and neoplastic as well as non-neoplastic samples was the recurrent occurrence of an intron 1 insertion.

For absolute real-time PCR quantification, a novel approach analysing the ratio between the canine functional full length or sRAGE variants and the non-sense intron 1 insertion variant transcripts was established. The analyses showed expression of both categories (sense and non-sense transcripts) in all canine samples. In detail, the screening of non-neoplastic tissues revealed a predominant expression of the full length or *sRAGE* transcript encoding for ligand binding RAGE variants in lung, testis and thyroid tissue. In contrast a higher expression of the intron 1 insertion variant was detected in ovary, pancreas, skin and spleen. In neoplastic tissue the majority of the samples showed a stronger expression of the intron 1 *RAGE* transcript variant.

I

Cloning, characterisation, and comparative quantitative expression analyses of receptor for advanced glycation end products (RAGE) transcript forms.

Sterenczak KA, Willenbrock S, Barann M, Klemke M, Soller JT, Eberle N, Nolte I, Bullerdiek J, Murua Escobar H.

Gene. 2009. 434(1-2):35-42

Own contribution:

- Cell culture handling
- Assistance in figure preparation

Gene 434 (2009) 35–42

Contents lists available at ScienceDirect

Gene

journal homepage: www.elsevier.com/locate/gene

Cloning, characterisation, and comparative quantitative expression analyses of receptor for advanced glycation end products (*RAGE*) transcript forms

Katharina A. Sterenczak [a,b], Saskia Willenbrock [a,b], Matthias Barann [b], Markus Klemke [b], Jan T. Soller [a,b], Nina Eberle [a], Ingo Nolte [a], Jörn Bullerdiek [a,b], Hugo Murua Escobar [a,b,*]

[a] *Small Animal Clinic and Research Cluster of Excellence "REBIRTH", University of Veterinary Medicine, Bischofsholer Damm 15, D-30173 Hannover, Germany*
[b] *Centre for Human Genetics, University of Bremen, Leobener Strasse ZHG, D-28359 Bremen, Germany*

ARTICLE INFO

Article history:
Received 25 April 2008
Received in revised form 16 July 2008
Accepted 31 October 2008
Available online 12 November 2008

Received by D.A. Tagle

Keywords:
Receptor for advanced glycation end products
RAGE
sRAGE
Tumour
Canis familiaris
Comparative genomics

ABSTRACT

RAGE is a member of the immunoglobulin superfamily of cell surface molecules playing key roles in pathophysiological processes, e.g. immune/inflammatory disorders, Alzheimer's disease, diabetic arteriosclerosis and tumourigenesis. In humans 19 naturally occurring *RAGE* splicing variants resulting in either N-terminally or C-terminally truncated proteins were identified and are lately discussed as mechanisms for receptor regulation. Accordingly, deregulation of sRAGE levels has been associated with several diseases e.g. Alzheimer's disease, Type 1 diabetes, and rheumatoid arthritis. Administration of recombinant sRAGE to animal models of cancer blocked tumour growth successfully. In spite of its obvious relationship to cancer and metastasis data focusing sRAGE deregulation and tumours is rare. In this study we screened a set of tumours, healthy tissues and various cancer cell lines for *RAGE* splicing variants and analysed their structure. Additionally, we analysed the ratio of the mainly found transcript variants using quantitative Real-Time PCR. In total we characterised 24 previously not described canine and 4 human RAGE splicing variants, analysed their structure, classified their characteristics, and derived their respective protein forms. Interestingly, the healthy and the neoplastic tissue samples showed in majority RAGE transcripts coding for the complete receptor and transcripts showing insertions of intron 1.

1. Introduction

The receptor for advanced glycation end products (RAGE) is a member of the immunoglobulin superfamily of cell surface molecules which binds nonenzymatically glycated adducts like advanced glycation end products (AGE). Acting as a multiligand receptor it has been described to interact with various ligands i.e. amphoterin also known as HMGB1 (Hori et al., 1995), amyloid beta (Yan et al., 1996), proteins of the S100/calgranulin family (Hofmann et al., 1999) and Mac-1 (Chavakis et al., 2003). The ligand-receptor-complexes regulate cell signalling pathways having influencing effect on cell growth and proliferation, i.e. p21ras, erk1/2 (p44/p42) MAP kinases, p38, SAPK/JNK Map kinases, rho GTPases, phosphoinostiol-3 kinase, NFkB, and cAMP response element binding protein (CREB) (Neeper et al., 1992; Yan et al., 1994; Lander et al., 1997; Deora et al., 1998; Hofmann et al., 1999; Huttunen et al., 1999; Kislinger et al., 1999; Huang et al., 2001; Huttunen et al., 2002b). In terms of pathophysiological processes RAGE has been described to be involved in various diseases including diabetic arteriosclerosis (Park et al., 1998; Cipollone et al., 2003), impaired wound healing (Goova et al., 2001), Alzheimer's disease (Yan et al., 1996; Lue et al., 2001, 2005), immune and inflammatory disorders (Hofmann et al., 1999; Schmidt et al., 2001; Hofmann et al., 2002; Chavakis et al., 2004) and various cancers (Taguchi et al., 2000; Huttunen et al., 2002a; Bartling et al., 2005; Bhawal et al., 2005; Ishiguro et al., 2005). In humans 19 naturally occurring *RAGE* splicing variants resulting in either N-terminally or C-terminally truncated proteins were identified and are currently discussed as mechanisms for receptor regulation (hRAGEsec (Malherbe et al., 1999), sRAGE1,

Abbreviations: aa, amino acid(s); Acc. No., Accession number; AGE, advanced glycation end product(s); bp, base pair(s); cAMP, cyclic adenosine monophosphate; CD, Cytosol domain; cDNA, DNA complementary to RNA; CDS, coding sequence(s); CFA, *Canis familiaris*; CREB, cAMP response element binding protein; DNA, deoxyribonucleic acid; DNase, deoxyribonuclease; EC, extracellular domain; ERK 1/2, extracellular signal-regulated kinase; esRAGE, endogenous secretory RAGE; gDNA, genomic DNA; GTPase, guanosine triphosphatase; HMG, high mobility group; HMGB1, high mobility group protein B1; JNK, C-Jun N-terminal kinase; kDa, kiloDalton; Mac-1, Macrophage-1 antigen; MAP, kinase mitogen activated protein kinase; M-MLV, Moloney murine leukemia virus; mRNA, messenger ribonucleic acid; NCBI, National Center for Biotechnology Information; NFκB, nuclear factor-kappa B; ORF, open reading frame; PCR, polymerase chain reaction; qRT-PCR, quantitative Real Time PCR; RAGE, receptor for advanced glycation end products; Ras, rat sarcoma virus; RNA, ribonucleic acid; RNase, ribonuclease; SAPK, stress-activated protein kinase; sRAGE, soluble RAGE variant (s); TM, transmembrane domain; UTR, untranslated region.

* Corresponding author. Small Animal Clinic and Research Cluster of Excellence "REBIRTH", University of Veterinary Medicine Hannover, Bischofsholer Damm 15, D-30173 Hanover, Germany. Fax: +49 511 856 7686.
E-mail address: hescobar@tiho-hannover.de (H.M. Escobar).

0378-1119/$ – see front matter © 2008 Elsevier B.V. All rights reserved.
doi:10.1016/j.gene.2008.10.027

sRAGE2, sRAGE3 (Schlueter et al., 2003), N-truncated and Secretory (Yonekura et al., 2003), Δ8-RAGE (Park et al., 2004), RageΔ, NtRAGEΔ and sRAGEΔ (Ding and Keller, 2005b), RAGE_v4-RAGE_v13 (Hudson et al., 2007). The function of these variants was unclear, but lately the described truncated RAGE protein variants were supposed to act as competitive inhibitors of the receptor either by ligand binding or displacing the full-length receptor in the membrane (Ding and Keller, 2005a; Geroldi et al., 2005). Deregulations of the naturally occurring protein isoforms are supposed to have significant effect on RAGE mediated diseases. Accordingly, deregulations of sRAGE levels have been associated with several diseases e.g. Alzheimer's disease (Emanuele et al., 2005), Type 1 diabetes (Challier et al., 2005; Forbes et al., 2005; Katakami et al., 2005; Miura et al., 2007), Type 2 diabetes (Nakamura et al., 2006; Tan et al., 2006; Yamagishi et al., 2006; Humpert et al., 2007), atherosclerosis (Falcone et al., 2005; Koyama et al., 2005), rheumatoid arthritis (Moser et al., 2005; Pullerits et al., 2005), essential hypertension (Geroldi et al., 2005), and renal disease (Kalousova et al., 2006). On the other hand Taguchi et al. (2000) were able to show that blocking of the binding of the RAGE ligand HMGB1 to the receptor, by using RAGE variants lacking the cytosolic or transmembrane domains, strongly inhibited the metastatic behaviour of glioma cells in terms of invasive growth, motility and migration. The data clearly showed that the application of soluble RAGE variants drastically suppressed the growth of tumour cells *in vitro* and *in vivo* (for review see Huttunen and Rauvala, 2004). In spite of its obvious relationship to cancer and metastasis data focusing soluble RAGE deregulations or structural aberrations and tumours is currently rare. Only recently Takeuchi et al. reported a correlation between esRAGE, RAGE, and HMGB1 and staging of chondrosarcomas classifying esRAGE expression as tumourmarker for malignancy (Takeuchi et al., 2007).

As reviewed lately by Khanna and Hunter (2005) the dog is significantly helping to reveal characteristics of human tumour biology especially of metastasis due to various similarities of the malignancies seen in both species. Generally, in the case of cancer, in dogs we find naturally spontaneously developing neoplasias which are more similar to human cancers than induced tumours used in rodent model systems in terms of presentation, histology and biology (Withrow and MacEwen, 1989, 2001; MacEwen, 1990). Additionally, dogs show similar characteristics of physiology and metabolism for most organ systems and drugs, which allows better comparability of modalities e.g. surgery, radiation, chemotherapy (Withrow and MacEwen, 2001), and new therapeutic approaches aimed at cancer treatment.

In this study we screened a set of 14 different canine tumours, healthy tissues and various canine and human cancer cell lines for *RAGE* splicing variants and analysed their structures. Additionally, we analysed the ratio of the mainly found transcript variants using quantitative and relative Real-Time PCR.

2. Methods and materials

2.1. Tissues and cell lines

The analysed canine healthy (lung, ovar, pancreas, skin, spleen, testis, thyroid) and tumour tissues (adenoma of pancreas, colon cancer, fibrosarcoma, histiocytoma, insulinoma, liver adenoma, malignant histiocytosis, malignant lymphoma, mamma tumour, mastocytoma, melanoma, splenic hemangiosarcoma, testis tumour, thyroid carcinoma, vaginal tumour) were provided by the Small Animal Clinic, University of Veterinary Medicine, Hanover, Germany. The canine cell lines CT1258 (prostate cancer), MTH53A (non neoplastic tissue of the mammary gland), MTH52C (malignant small-cell carcinoma of the mammary gland), and ZMTH3 (pleomorphic adenoma of the mammary gland) and the human cell lines Hela (cervical cancer), Li14 (lipoma), and MCF7 (breast cancer) which were used in this study, were provided by the Centre for Human Genetics, University of Bremen, Bremen, Germany.

2.2. RNA isolation and cDNA synthesis for transcript characterisation

The cultured cells were homogenized using QIAshredder spin columns (Qiagen, Hilden, Germany) while the used tissue samples were homogenized using the iron-beads QIAshredder homogenizer method (Qiagen, Hilden, Germany). Following, total RNA was isolated using the RNeasy Mini Kit according to the manufacturer's instructions (Qiagen, Hilden, Germany). To avoid genomic DNA contaminations, on-column DNase digestion with the RNase-Free DNase set (Qiagen, Hilden, Germany) was performed.

The respective total cDNA syntheses were performed using 5 μg total RNA of each sample, the adaptor poly dT primer AP2: AAG GAT CCG TCG ACA TC(17)T, and MMLV reverse transcriptase following the manufacturer's protocol (Invitrogen, Karlsruhe, Germany). The respective cDNA syntheses were performed several times during the experiments.

2.3. PCR reactions

All performed PCR reactions were designed to amplify products spanning from exon 1 to exon 11 of the canine or human *RAGE* mRNA, respectively. The PCR reactions using the total poly dT primed cDNAs of the canine cell lines and tissue samples were performed either with the primer pair 1 (up 5′GAA GCC TGG GAA GGA ACG ATG3′/lo 5′GAG AGC AAG GGG GAA GAA AAG3′) or pair 2 (up 5′CCT GGG TGC TGG TCC TCA GT3′/lo 5′TCA TGG CCC TGC TGC ACC GC TCT3′). The reactions using human templates were performed with the primer pair 5′CCT GGG TGC TGG TCC TCA GT3′ as upper primer and the primer 5′TCA AGG CCC TCC AGT ACT ACT TC3′ as lower primer for PCR reactions amplifying RAGE transcripts in human cell lines (Hela, Li14, MCF7).

The PCR reactions were performed with a "touch down" programme with the following conditions: initial denaturation at 95 °C for 5 min, followed by 10 cycles with 30 s denaturation at 95 °C, 1 min annealing by 70–60 °C with a decrease of 1 °C per cycle and an elongation at 72 °C for 1 min. The following 30 cycles were performed at 95 °C for 30 s, 60 °C for 1 min and 72 °C for 1 min, respectively.

2.4. Characterisation of RAGE transcript variants

The respective amplified PCR products were separated electrophoretically in 1.5% agarose gels and recovered using the QIAquick Gel Extraction Kit following the manufacturer's protocol (Qiagen, Hilden, Germany). The isolated fragments were cloned into the pGem-T-Easy vector system (Promega, Mannheim, Germany), transfected in thermocompetent DH5α *E. coli* cells, and verified by sequencing (MWG, Ebersberg, Germany). The received sequence data was analysed using Lasergene software (DNAStar, Madison, USA).The generated sequences were submitted to the NCBI database (GenBank accession nos: EU428788, EU428789, EU428790, EU428791, EU428792, EU428793, EU428794, EU428795, EU428796, EU428797, EU428798, EU428799, EU428800, EU428801, EU428802, EU428803, EU428804, EU428805, EU428806, EU428807, EU428808, EU428809, EU428810, EU428811, EU428812, EU428813, EU428814, EU428815, EU428816).The CDS and protein alignments were performed using various sequences from NCBI database (GenBank accession nos.: D28769, NM001048081; BAA89369, ABA18650).

2.5. Quantitative Real-time RT-PCR

2.5.1. RNA isolation and cDNA syntheses for qRT-PCR

Total RNAs from the homogenized cultured cells and tissue samples were isolated using the RNeasy Plus Mini Kit (Qiagen, Hilden,

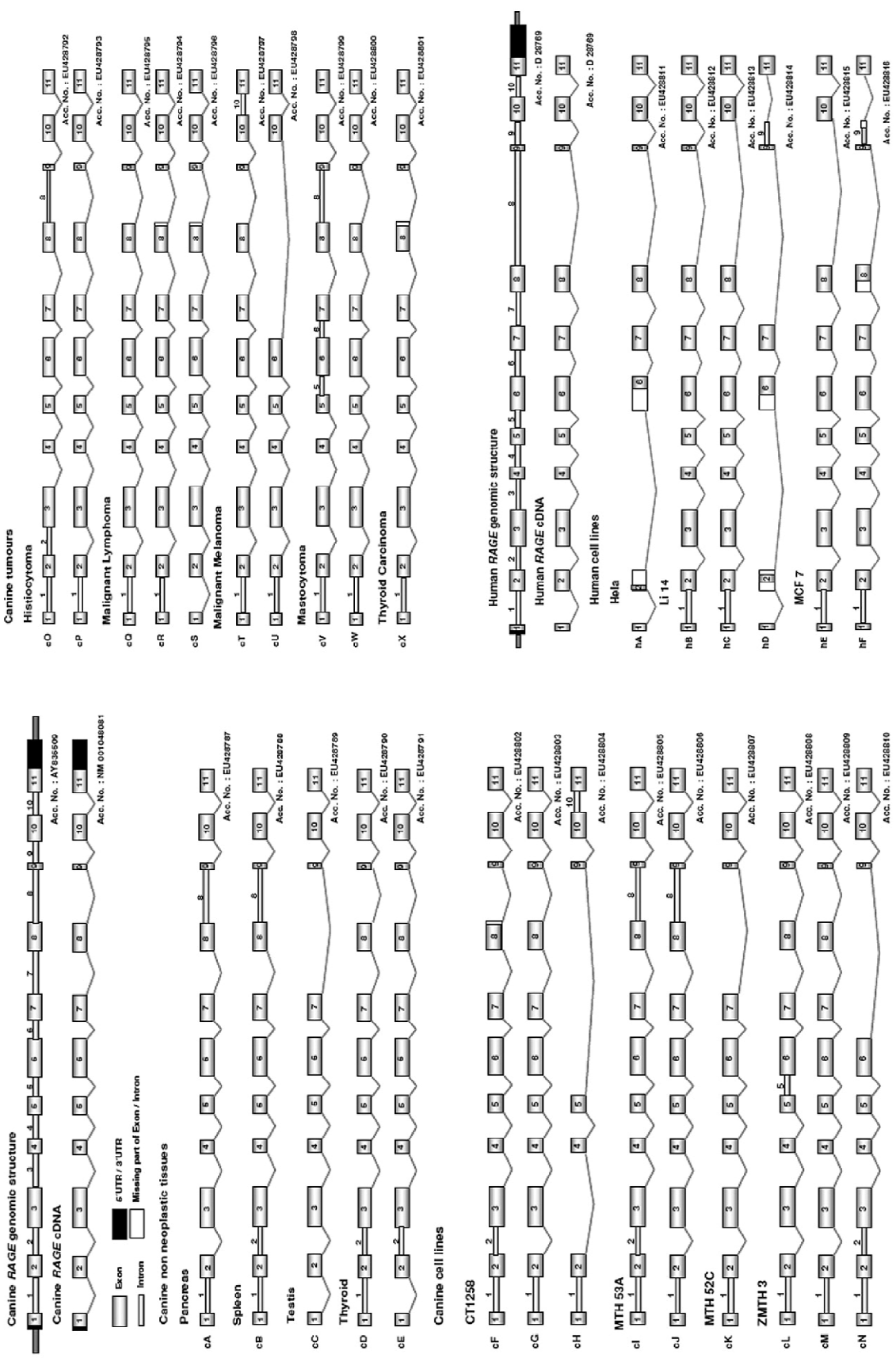

Fig. 1. *RAGE* transcript variants. Characterisation of *RAGE* transcript variants in canine non neoplastic tissues: pancreas, spleen, testis and thyroid (cA–cE), canine cell lines: CT1258, MTH 53A, MTH 52C and ZMTH3 (cF–cN), canine tumours: histiocytoma, malignant lymphoma, malignant melanoma, mastocytoma and thyroid carcinoma (cO–cX) and human cell lines: Hela, Li14 and MCF7 (hA–hF). The amplified PCR products range from the star codon in exon 1 till stop codon in exon 11. The RT PCR was performed with a poly dT primer. The transcript variants show different structural modifications like insertions of introns and deletions of both whole exons and parts of exons.

Table 1
Canine and human *RAGE* transcript variants

	Name (Fig. 1)	Structure insertion/deletion	Acc. No.	Putative protein (Fig. 2)/characteristic
Non neoplastic canine tissues				
Pancreas	cA	Insertion: intron1, intron 8	EU428787	J/non sense protein
Spleen	cB	Insertion: intron1, intron 2, intron 8	EU428788	I/non sense protein
Testis	cC	Deletion: exon 8	EU428789	A/soluble isoform, ligand binding
Thyroid	cD	Insertion: intron 1, intron 2	EU428790	C/membrane bound, no ligand binding
	cE	Insertion: intron 2	EU428791	F/membrane bound, no ligand binding
Canine cell lines				
CT1258	cF	Insertion: intron1, intron 2/deletion: 16 bp exon 8	EU428802	K/non sense protein
	cG	Insertion: intron 1	EU428803	E/membrane bound, no ligand binding
	cH	Insertion: intron 1/deletion: exon 3, exon 6, exon 7, exon 8	EU428804	No putative protein
MTH 53A	cI	Insertion: intron 1, intron 2, intron 8	EU428805	I/non sense protein
	cJ	Insertion: intron 1, intron 8	EU428806	J/non sense protein
MTH 52C	cK	Insertion: intron 1/deletion: exon 8	EU428807	M/non sense protein
ZMTH3	cL	Insertion: intron 1, intron 5	EU428808	D/membrane bound, no ligand binding
	cM	Insertion: intron 1	EU428809	E/membrane bound, no ligand binding
	cN	Insertion: intron 1, intron 2/deletion: exon 7, exon 8	EU428810	G/membrane bound, no ligand binding
Canine tumours				
Histiocytoma	cO	Insertion: intron 1, intron 2, intron 8	EU428792	I/non sense protein
	cP	Insertion: intron 1	EU428793	E/membrane bound, no ligand binding
Malignant lymphoma	cQ	Insertion: intron 1	EU428795	E/membrane bound, no ligand binding
	cR	Insertion: intron 1/deletion: 16 bp exon 8	EU428794	L/non sense protein
	cS	Deletion: 16 bp exon 8	EU428796	B/soluble isoform, ligand binding
Malignant melanoma	cT	Insertion: intron 1, intron 10	EU428797	No putative protein
	cU	Insertion: intron 1/Deletion: exon 7, exon 8, exon 9	EU428798	H/membrane bound, no ligand binding
Mastocytoma	cV	Insertion: intron1, intron 5, intron 6, intron 8	EU428799	No putative protein
	cW	Insertion: intron 1	EU428800	E/membrane bound, no ligand binding
Thyroid carcinoma	cX	Insertion: intron1/deletion: 16 bp exon 8	EU428801	L/non sense protein
Human cell lines				
Hela	hA	Deletion: 80 bp exon2, exon3, exon 4, exon 5, 120 bp exon6	EU428811	CC/membrane bound, no ligand binding
Li 14	hB	Insertion: intron 1	EU428812	AA/membrane bound, no ligand binding
	hC	Insertion: intron 1/deletion: exon 9	EU428812	BB/membrane bound, no ligand binding
	hD	Insertion: intron 9/deletion: 72 bp exon 2, exon 3, exon 4, exon 5	EU428814	No putative protein
MCF 7	hE	Insertion: intron 1/deletion: exon 9	EU428815	BB/membrane bound, no ligand binding
	hF	Insertion: intron 1, intron 9/deletion: 52 bp exon 8, 22 bp intron 9	EU428816	No putative protein

Detailed characterisation of the different respective *RAGE* transcript modifications and analyses of their derived protein isoforms.

Germany). This isolation method does not require an additional on column DNase digestion due to a direct removal of genomic DNA (gDNA) by a gDNA eliminating spin column.

The respective cDNA syntheses were performed using 250 ng total RNA of each sample, the gene specific lower primer 5′ TTCTGTCCGACCTGTGTTCAGCTT3′, and Quantiscript Reverse Transcriptase following the manufacturer's protocol (Qiagen, Hilden, Germany) with an integrated removal of genomic DNA contamination.

For absolute and relative quantification of the RAGE transcript levels RT-PCR amplifications were carried out using the Applied Biosystems 7300 Real-Time PCR System (Applied Biosystems, Darmstadt, Germany). 2 µl of each cDNA corresponding to 25 ng of total RNA was amplified in a total volume of 25 µl using universal PCR Mastermix (Applied Biosystems) with 600 nM of each primer (forward primer 1: 5′GTCTGTGGGGAGCAGTAGTAGG3′, forward primer 2: 5′TACTCCTCCACCATTGTCCCATCT3′, reverse primer: 5′ TTCTGTCCGACCTGTGTTCAGCTT3′) and 200 nM fluorogenic probe (5′ 6-FAM-AAGCCGCTGGTGCTCAACTGTA-TAMRA 3′). PCR conditions were as follows: 2 min at 50 °C and 10 min at 95 °C, followed by 45 cycles with 15 s at 95 °C and 1 min at 60 °C. All samples were measured in triplicate and for each run non-template controls and no reverse transcriptase reactions were included. Expression levels of RAGE mRNA transcripts were calculated using an amplicon-specific standard curve. For absolute quantification the transcript levels were normalised to total RNA concentration and expressed as copy number/250 ng total RNA. For relative quantification the healthy full length RAGE transcript was chosen as endogenous control. The calibrator sample was lung tissue to which all other samples were compared to determine the ratio of the relative expression level.

3. Results and discussion

3.1. Characterisation of RAGE transcript variants

In humans 19 naturally occurring *RAGE* splicing variants resulting in either N-terminally or C-terminally truncated proteins were identified and are just recently discussed as mechanisms for receptor regulation (hRAGEsec, sRAGE1, sRAGE2, sRAGE3, N-truncated and Secretory, Δ8-RAGE, RageΔ, NtRAGEΔ and sRAGEΔ, RAGE_v4 till RAGE_v13). The described truncated RAGE protein variants are discussed to act as competitive inhibitors of the receptor either by ligand binding or displacing the full-length receptor in the membrane. Deregulation of the naturally occurring protein isoforms is supposed to have significant effect on RAGE mediated diseases. Accordingly, deregulation of sRAGE levels has been associated with several diseases

Fig. 2. The canine RAGE CDS and protein structure. The different *RAGE* transcript variants characterised in canine non neoplastic tissues, cell lines, tumours and in human cell lines code for different putative protein structures: canine soluble RAGE protein isoforms with the ability to bind RAGE ligands without subsequent signalling in the cell (A, B), canine membrane bound RAGE isoforms without the competence of binding RAGE ligands (C–H), canine non sense RAGE protein isoforms (I–M) and human membrane bound RAGE protein isoforms (AA–CC).


The canine RAGE CDS and Protein structure
CDS
5'UTR
3'UTR
Acc. No. : NM 001040091
Protein
V
ED
TD
CD
Acc. No. : ABA18650
1: ED: Extracellular Domain (318 aa)
2: V: V Domain (107 aa)
3: TD: Transmembrane Domain (19 aa)
4: CD: Cytosol Domain (43 aa)
Exon
Intron
Missing part of protein or CDS
Non sense part in protein
Soluble RAGE isoform
A: Protein
Detected in: Testis tissue (cC)
B: Protein
Detected in: Malignant Lymphoma (cB)
Membrane bound RAGE isoforms
C: Protein
Detected in: Thyroid (cD)
D: Protein
Detected in: ZMTH3 (cL)
E: Protein
Detected in: CT1258 (cG)
ZMTH3 (cM)
Histiocyoma (cP)
Malignant Lymphoma (cQ)
Masocyoma (cW)
F: Protein
Detected in: Thyroid (cE)
G: Protein
Detected in: ZMTH3 (cN)
No sense RAGE protein isoforms
H: Protein
Detected in: Malignant Melanoma (cU)
I: Protein
Detected in: Spleen (cB)
MTH s3A (cI)
Histiocytoma (cO)
J: Protein
Detected in: Pancreas (cA)
MTH s3A (cJ)
K: Protein
Detected in: CT1258 (cF)
L: Protein
Detected in: Malignant Lymphoma (cR)
Thyroid Carcinoma (cX)
M: Protein
Detected in: MTH s2C (cK)
The human RAGE CDS and Protein structure
CDS
5'UTR
3'UTR
Acc. No. : D28769
Protein
1: ED: Extracellular Domain (322 aa)
2: V: V Domain (76 aa)
3: TD: Transmembrane Domain (19 aa)
4: CD: Cytosol Domain (41 aa)
Missing part of protein or CDS
Non sense part in protein
Exon
Intron
Membrane bound RAGE Isoforms
AA Protein
Detected in: U114 (hB)
BB Protein
Detected in: U114 (hC)
MCF 7 (hD)
CC Protein
Detected in: Hela (hA)

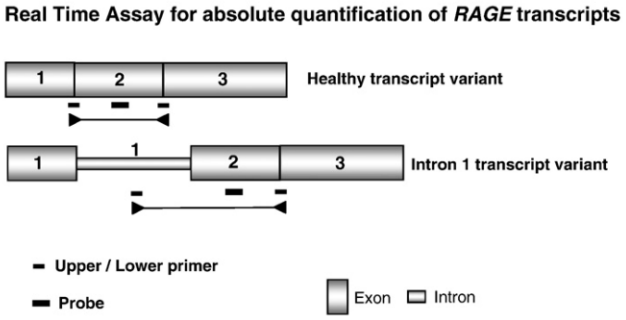

Fig. 3. Designed Real Time assay for absolute quantification of RAGE transcripts allowing differentiation of "healthy" and "intron 1" *RAGE* splicing variants. For the absolute quantification of healthy *RAGE* transcript the designed upper primer binds at the border of exon 1/exon 2, the probe anneals in exon 2 and the lower primer binds at the exon 2/exon 3 border avoiding measurement of genomic contaminations. The assay for measurement of the quantity of the intron 1 transcript variant consists of the same probe and lower primer like the healthy transcript detection, and the upper primer anneals in intron 1. Due to the upper and lower primer, transcripts which bear intron 1 but no genomic contaminations will be detected.

e.g. Alzheimer's disease, Type 1 diabetes, Type 2 diabetes, atherosclerosis, rheumatoid arthritis, essential hypertension, and renal disease. On the other hand blocking of the binding of the RAGE ligand HMGB1 to the receptor by using RAGE variants lacking the cytosolic or transmembrane domains, strongly inhibited the metastatic behaviour of glioma cells in terms of invasive growth, motility and migration (Taguchi et al., 2000). A recent study based on immunohistologic analyses reports a correlation of esRAGE and staging of chondrosarcomas classifying RAGE expression as tumourmarker for malignancy (Takeuchi et al., 2007).

In the herein screened canine 17 neoplastic and seven healthy tissue samples as well as the four canine and 3 human cell lines we found in total 24 canine and 6 human transcripts coding for 16 structural different canine and 5 different human forms. Fourteen of these found canine and four human forms were previously not described for any other species (Fig. 1, Table 1). In detail the transcripts detected in healthy tissues are characterised by various combinations of insertions of intron 1, 2 and 8 and by an observed deletion of the exon 8 (Figs. 1cA–cE). In canine cell lines the following events could be detected: various combinations of insertions of the introns 1, 2, 5, 8 and 10, a 16 bp partial deletion of exon 8, and complete deletions of the exons 3, 6, 7 and 8 (Figs. 1cF–cN). The neoplastic samples showed several insertions of introns 1, 2, 5, 6, 8 and 10, the partial 16 bp deletion of exon 8, and finally deletions of exons 7, 8 and 9 (Figs. 1cO–cX). The human cell lines showed insertion of intron 1, partial large deletions of parts of the exons 2, 6, and 8, compete deletions of the exons: 3, 4, 5, 8, and 9, and finally insertion of intron 9 with an additional deletion of parts of intron 9 (Figs. 1hA–hF).

These different transcript variants can be roughly classified into two groups. One group of splicing variants coding for full length *RAGE* transcripts or soluble *RAGE* variants which code for protein forms capable to bind extracellular ligands, and the other group showing various insertions of introns and alternative splicing of exons leading to mutated protein forms (Fig. 1,Fig. 2, Table 1). The recurrent remarkable modification in the latter group is the insertion of intron 1. This modification is seen in transcripts found in healthy tissues as well as in the cell lines and neoplastic samples. Depending on further modifications of the seen transcripts respective protein isoforms would result, missing the V — domain required for ligand binding or result in nonsense proteins (Fig. 2). Previously Yonekura et al. found a similar variant showing an insertion of intron 1 in a sample of human endothelial cells and pericytes (Yonekura et al., 2003). However, this reports the existence of these transcripts for the first time in neoplastic samples and cell lines.

3.2. Quantitative Real-Time PCR analyses

Following the assumption that the transcripts showing the intron 1 insertion are lost as competitive inhibitors we decided to quantify the ratio between these variants and variants coding for proteins capable to bind RAGE ligands in neoplastic canine samples providing naturally occurring tumour material. The designed assay discriminates genomic DNA detection, due to the position of the chosen primers (Fig. 3). The comparative quantification showed a diverse pattern (Table 2) in the analysed samples. Generally, in all screened tissue samples and cell lines, an expression of both forms could be detected varying from $1.38*10^3$ (mastocytoma) to $6.53*10^8$ (lung) transcripts for the normal splicing variant and $1.3*10^3$ (mastocytoma) to $1.88*10^6$ (lung) transcripts for the "intron 1" variant. In the screened healthy tissues the variant coding for a functional complete or soluble RAGE variant is significantly higher expressed in lung, testis and thyroid tissue showing in absolute numbers $6.53*10^8$, $6.27*10^5$ and $1.02*10^7$ more "healthy" transcripts than their respective "intron 1" variants. The pattern seen in the 17 tumour tissue samples and cell lines is quite different. The majority of samples showed a higher presence of the "intron 1" variant with the exception of a mastocytoma, which shows a similar level of both variants ($1.3*10^3$ "intron 1" to $1.38*10^3$ "healthy") and a testis tumour, which as only neoplastic sample showed a higher expression "healthy" variant (Table 2). In absolute numbers the "intron 1" variant outnumbers in the "healthy" variant 15 of the neoplastic samples with a range of 15 to 17 transcripts. The screened four cell lines showed uniformly a higher level of the intron 1 variant varying from $5.38*10^4$ to $9.17*10^4$.

However, as lately discussed by Hudson et al. (2007), the wide diversity of seen RAGE transcripts and the obvious relationship of RAGE to several pathologic findings arise many new questions. The

Table 2
Absolute Real Time quantification transcript numbers of "healthy" and "intron 1" *RAGE* transcript variants in canine healthy tissues, neoplastic samples and cell lines

	Copy no./250 ng total RNA	
	Healthy transcript	Intron 1 transcript
Non neoplastic canine tissues		
Lung	$6.53*10^8$	$1.88*10^6$
Ovar	$6.9*10^3$	$7.36*10^4$
Pancreas	$2.6*10^4$	$3.08*10^5$
Skin	$1.9*10^3$	$1.1*10^4$
Spleen	$7.1*10^3$	$8.26*10^4$
Testis	$6.27*10^5$	$5.6*10^4$
Thyroid	$1.02*10^7$	$1.9*10^5$
Canine cell lines		
CT1258	$2.98*10^3$	$5.38*10^4$
MTH 53A	$4.68*10^3$	$6.77*10^4$
MTH 52C	$9.3*10^3$	$9.17*10^4$
ZMTH3	$6.83*10^3$	$8.8*10^4$
Canine tumours		
Adenoma of pancreas	$4.26*10^3$	$5.5*10^4$
Colon cancer	$5.66*10^3$	$6.19*10^4$
Fibrosarcoma	$4.7*10^3$	$7.67*10^4$
Histiocytoma	$1.46*10^4$	$1.47*10^5$
Insulinoma	$1.7*10^4$	$2.6*10^5$
Liver adenoma	$3.9*10^3$	$2.9*10^4$
Malignant histiocytosis	$9.52*10^3$	$8.34*10^4$
Malignant lymphoma	$1.18*10^4$	$1.49*10^5$
Malignant lymphoma	$7.6*10^3$	$8.62*10^4$
Malignant lymphoma	$1.2*10^4$	$2.1*10^5$
Mammatumour	$1.5*10^4$	$5.29*10^4$
Mastocytoma	$1.38*10^3$	$1.3*10^3$
Melanoma	$4.77*10^3$	$4.14*10^4$
Splenic hemangiosarcoma	$2.17*10^4$	$1.07*10^5$
Testis tumour	$7.84*10^5$	$2.11*10^5$
Thyroid carcinoma	$5.16*10^4$	$1.53*10^5$
Vaginal tumour	$1.13*10^4$	$1.5*10^5$

growing understanding of its biology combined with the accessibility of an adequate animal model – like the dog providing naturally occurring neoplastic samples – will be of great value to elucidate the pathologic events with RAGE involvement. The here newly described 24 canine and 4 human RAGE splicing variants as well as their respective derived protein forms will further help to understand the diversity of RAGE biology. The comparative quantitative Real-Time PCR analyses of both major *RAGE* transcript classes represent a first approach to analyse, if deregulation/structural aberrations of *RAGE* can be detected at RNA level and play a role in RAGE mediated pathologic events. Anyway, further studies will be needed, to confirm at protein level the qPCR data. We tested the commercially availed RAGE antibodies for detection of recombinant canine protein but got unspecific results. This may be due to the fact that the identity of the canine RAGE protein to its human is just 77.6% (Murua Escobar et al., 2006).

However, studies done with human neoplasias using the herein generated data as basis should be a promising approach to answer the remaining questions.

Acknowledgment

This work was funded by the German Research Foundation (DFG) within the SFB/TransRegio 37.

References

Bartling, B., Hofmann, H.S., Weigle, B., Silber, R.E., Simm, A., 2005. Down-regulation of the receptor for advanced glycation end-products (RAGE) supports non-small cell lung carcinoma. Carcinogenesis 26, 293–301.

Bhawal, U.K., et al., 2005. Association of expression of receptor for advanced glycation end products and invasive activity of oral squamous cell carcinoma. Oncology 69, 246–255.

Challier, M., Jacqueminet, S., Benabdesselam, O., Grimaldi, A., Beaudeux, J.L., 2005. Increased serum concentrations of soluble receptor for advanced glycation endproducts in patients with type 1 diabetes. Clin. Chem. 51, 1749–1750.

Chavakis, T., Bierhaus, A., Al-Fakhri, N., Schneider, D., Witte, S., Linn, T., et al., 2003. The pattern recognition receptor (RAGE) is a counterreceptor for leukocyte integrins: a novel pathway for inflammatory cell recruitment. J. Exp. Med. 198, 1507–1515.

Chavakis, T., Bierhaus, A., Nawroth, P.P., 2004. RAGE (receptor for advanced glycation end products): a central player in the inflammatory response. Microbes Infect. 6, 1219–1225.

Cipollone, F., et al., 2003. The receptor RAGE as a progression factor amplifying arachidonate-dependent inflammatory and proteolytic response in human atherosclerotic plaques: role of glycemic control. Circulation 108, 1070–1077.

Deora, A.A., Win, T., Vanhaesebroeck, B., Lander, H.M., 1998. A redox-triggered ras-effector interaction. Recruitment of phosphatidylinositol 3′-kinase to Ras by redox stress. J. Biol. Chem. 273, 29923–29928.

Ding, Q., Keller, J.N., 2005a. Evaluation of rage isoforms, ligands, and signaling in the brain. Biochim. Biophys. Acta 1746, 18–27.

Ding, Q., Keller, J.N., 2005b. Splice variants of the receptor for advanced glycosylation end products (RAGE) in human brain. Neurosci. Lett. 373, 67–72.

Emanuele, E., et al., 2005. Circulating levels of soluble receptor for advanced glycation end products in Alzheimer disease and vascular dementia. Arch. Neurol. 62, 1734–1736.

Falcone, C., et al., 2005. Plasma levels of soluble receptor for advanced glycation end products and coronary artery disease in nondiabetic men. Arterioscler. Thromb. Vasc. Biol. 25, 1032–1037.

Forbes, J.M., et al., 2005. Modulation of soluble receptor for advanced glycation end products by angiotensin-converting enzyme-1 inhibition in diabetic nephropathy. J. Am. Soc. Nephrol. 16, 2363–2372.

Geroldi, D., et al., 2005. Decreased plasma levels of soluble receptor for advanced glycation end-products in patients with essential hypertension. J. Hypertens. 23, 1725–1729.

Goova, M.T., et al., 2001. Blockade of receptor for advanced glycation end-products restores effective wound healing in diabetic mice. Am. J. Pathol. 159, 513–525.

Hofmann, M.A., et al., 1999. RAGE mediates a novel proinflammatory axis: a central cell surface receptor for S100/calgranulin polypeptides. Cell 97, 889–901.

Hofmann, M.A., et al., 2002. RAGE and arthritis: the G82S polymorphism amplifies the inflammatory response. Genes Immun. 3, 123–135.

Hori, O., et al., 1995. The receptor for advanced glycation end products (RAGE) is a cellular binding site for amphoterin. Mediation of neurite outgrowth and co-expression of rage and amphoterin in the developing nervous system. J. Biol. Chem. 270, 25752–25761.

Huang, J.S., Guh, J.Y., Chen, H.C., Hung, W.C., Lai, Y.H., Chuang, L.Y., 2001. Role of receptor for advanced glycation end-product (RAGE) and the JAK/STAT-signaling pathway in AGE-induced collagen production in NRK-49F cells. J. Cell Biochem. 81, 102–113.

Hudson, B.I., Carter, A.M., Harja, E., Kalea, A.Z., Arriero, M., Yang, H., et al., 2007. Identification, classification, and expression of RAGE gene splice variants. FASEB J. 22 (5), 1572–1580.

Humpert, P.M., et al., 2007. Soluble RAGE but not endogenous secretory RAGE is associated with albuminuria in patients with type 2 diabetes. Cardiovasc. Diabetol. 6, 9.

Huttunen, H.J., Rauvala, H., 2004. Amphoterin as an extracellular regulator of cell motility: from discovery to disease. J. Intern. Med. 255, 351–366.

Huttunen, H.J., Fages, C., Rauvala, H., 1999. Receptor for advanced glycation end products (RAGE)-mediated neurite outgrowth and activation of NF-kappaB require the cytoplasmic domain of the receptor but different downstream signaling pathways. J. Biol. Chem. 274, 19919–19924.

Huttunen, H.J., Fages, C., Kuja-Panula, J., Ridley, A.J., Rauvala, H., 2002a. Receptor for advanced glycation end products-binding COOH-terminal motif of amphoterin inhibits invasive migration and metastasis. Cancer Res. 62, 4805–4811.

Huttunen, H.J., Kuja-Panula, J., Rauvala, H., 2002b. Receptor for advanced glycation end products (RAGE) signaling induces CREB-dependent chromogranin expression during neuronal differentiation. J. Biol. Chem. 277, 38635–38646.

Ishiguro, H., Nakaigawa, N., Miyoshi, Y., Fujinami, K., Kubota, Y., Uemura, H., 2005. Receptor for advanced glycation end products (RAGE) and its ligand, amphoterin are overexpressed and associated with prostate cancer development. Prostate 64, 92–100.

Kalousova, M., et al., 2006. Soluble receptor for advanced glycation end products in patients with decreased renal function. Am. J. Kidney Dis. 47, 406–411.

Katakami, N., et al., 2005. Decreased endogenous secretory advanced glycation end product receptor in type 1 diabetic patients: its possible association with diabetic vascular complications. Diabetes Care 28, 2716–2721.

Khanna, C., Hunter, K., 2005. Modeling metastasis in vivo. Carcinogenesis 26, 513–523.

Kislinger, T., et al., 1999. N(epsilon)-(carboxymethyl)lysine adducts of proteins are ligands for receptor for advanced glycation end products that activate cell signaling pathways and modulate gene expression. J. Biol. Chem. 274, 31740–31749.

Koyama, H., et al., 2005. Plasma level of endogenous secretory RAGE is associated with components of the metabolic syndrome and atherosclerosis. Arterioscler. Thromb. Vasc. Biol. 25, 2587–2593.

Lander, H.M., Tauras, J.M., Ogiste, J.S., Hori, O., Moss, R.A., Schmidt, A.M., 1997. Activation of the receptor for advanced glycation end products triggers a p21(ras)-dependent mitogen-activated protein kinase pathway regulated by oxidant stress. J. Biol. Chem. 272, 17810–17814.

Lue, L.F., et al., 2001. Involvement of microglial receptor for advanced glycation endproducts (RAGE) in Alzheimer's disease: identification of a cellular activation mechanism. Exp. Neurol. 171, 29–45.

Lue, L.F., Yan, S.D., Stern, D.M., Walker, D.G., 2005. Preventing activation of receptor for advanced glycation endproducts in Alzheimer's disease. Curr. Drug Targets CNS Neurol. Disord. 4, 249–266.

MacEwen, E.G., 1990. Spontaneous tumours in dogs and cats: models for the study of cancer biology and treatment. Cancer Metastasis Rev. 9, 125–136.

Malherbe, P., et al., 1999. cDNA cloning of a novel secreted isoform of the human receptor for advanced glycation end products and characterization of cells co-expressing cell-surface scavenger receptors and Swedish mutant amyloid precursor protein. Brain Res. Mol. Brain Res. 71, 159–170.

Miura, J., et al., 2007. Endogenous secretory receptor for advanced glycation end-products levels are correlated with serum pentosidine and CML in patients with type 1 diabetes. Arterioscler. Thromb. Vasc. Biol. 27, 253–254.

Moser, B., Hudson, B.I., Schmidt, A.M., 2005. Soluble RAGE: a hot new biomarker for the hot joint? Arthritis Res. Ther. 7, 142–144.

Murua Escobar, H., et al., 2006. Cloning and characterization of the canine receptor for advanced glycation end products. Gene 369, 45–52.

Nakamura, K., et al., 2006. Elevation of soluble form of receptor for advanced glycation end products (sRAGE) in diabetic subjects with coronary artery disease. Diabetes Metab. Res. Rev.

Neeper, M., et al., 1992. Cloning and expression of a cell surface receptor for advanced glycosylation end products of proteins. J. Biol. Chem. 267, 14998–15004.

Park, L., et al., 1998. Suppression of accelerated diabetic atherosclerosis by the soluble receptor for advanced glycation endproducts. Nat. Med. 4, 1025–1031.

Park, I.H., et al., 2004. Expression of a novel secreted splice variant of the receptor for advanced glycation end products (RAGE) in human brain astrocytes and peripheral blood mononuclear cells. Mol. Immunol. 40, 1203–1211.

Pullerits, R., Bokarewa, M., Dahlberg, L., Tarkowski, A., 2005. Decreased levels of soluble receptor for advanced glycation end products in patients with rheumatoid arthritis indicating deficient inflammatory control. Arthritis Res. Ther. 7, 817–824.

Schlueter, C., Hauke, S., Flohr, A.M., Rogalla, P., Bullerdiek, J., 2003. Tissue-specific expression patterns of the RAGE receptor and its soluble forms—a result of regulated alternative splicing? Biochim. Biophys. Acta 1630, 1–6.

Schmidt, A.M., Yan, S.D., Yan, S.F., Stern, D.M., 2001. The multiligand receptor RAGE as a progression factor amplifying immune and inflammatory responses. J. Clin. Invest. 108, 949–955.

Taguchi, A., et al., 2000. Blockade of RAGE-amphoterin signalling suppresses tumour growth and metastases. Nature 405, 354–360.

Takeuchi, A., et al., 2007. Endogenous secretory receptor for advanced glycation endproducts as a novel prognostic marker in chondrosarcoma. Cancer 109, 2532–2540.

Tan, K.C.B., et al., 2006. Association between serum levels of soluble receptor for advanced glycation end products and circulating advanced glycation end products in type 2 diabetes. Diabetologia 49, 2756–2762.

Withrow, S.J., MacEwen, E.G., 1989. Clinical Veterinary Oncology. J.B. Lippincott, Co.

Withrow, S.J., MacEwen, E.G., 2001. Small Animal Clinical Oncology. W.B. Saunders Company.

Yamagishi, S., et al., 2006. Positive association between serum levels of advanced glycation end products and the soluble form of receptor for advanced glycation end products in nondiabetic subjects. Metabolism 55, 1227–1231.
Yan, S.D., et al., 1994. Enhanced cellular oxidant stress by the interaction of advanced glycation end products with their receptors/binding proteins. J. Biol. Chem. 269, 9889–9897.
Yan, S.D., et al., 1996. RAGE and amyloid-beta peptide neurotoxicity in Alzheimer's disease. Nature 382, 685–691.
Yonekura, H., et al., 2003. Novel splice variants of the receptor for advanced glycation end-products expressed in human vascular endothelial cells and pericytes, and their putative roles in diabetes-induced vascular injury. Biochem. J. 370, 1097–1109.

'High mobility Group B1 (HMGB1) and Receptor for Advanced Glycation End Products (RAGE) Expression in Canine Lymphoma.' **Sterenczak et al., Anticancer Research, 2010.**

An imbalanced expression of HMGB1 and RAGE was reported to play a key role in many human and canine neoplasias being strongly associated with aggressive potential and progression of tumour cells. With regard to haematopoietic tumours, lymphoma is a commonly occurring neoplasia in dogs which has a spontaneous development.

To identify factors potentially involved in the formation and progression of lymphomas, the expression levels of *HMGB1* and *RAGE* were measured via relative real-time PCR and canine beta-glucuronidase gene (*GUSB*) as endogenous control. The samples included in this study are 22 canine lymphomas and three non-neoplastic lymph node samples. In detail, 15 B-cell, two T-cell, three intestinal, and two unidentified multicentric lymphomas, which could not be classified by flow cytometry, were analysed.

The expression of HMGB1 was significantly increased in all lymphoma types in comparison to the control samples (intestinal lymphoma: $p = 0.030$; B-cell lymphoma: $p = 0.001$; T-cell lymphoma: $p = 0.033$) except the two lymphoma samples of unknown origin, where no significant difference in *HMGB1* expression could be detected.

In contrast to this, the *RAGE* expression did not change significantly within all lymphoma samples when compared to the non-neoplastic control lymph nodes.

II

High mobility Group B1 (HMGB1) and Receptor for Advanced Glycation End Products (RAGE) Expression in Canine Lymphoma.

Sterenczak KA, Joetzke AE, Willenbrock S, Eberle N, Lange S, Junghanss C, Nolte I, Bullerdiek J, Simon D, Murua Escobar H.

Anticancer Research. 2010. 30(12):5043-8

Own contribution:

- Partial manuscript drafting
- Assistance in figure preparation

ANTICANCER RESEARCH *30*: 5043 5048 (2010)

High-mobility Group B1 (HMGB1) and Receptor for Advanced Glycation End-products (RAGE) Expression in Canine Lymphoma

KATHARINA A. STERENCZAK[1,2], ALEXA E. JOETZKE[1], SASKIA WILLENBROCK[1,2], NINA EBERLE[1], SANDRA LANGE[3], CHRISTIAN JUNGHANSS[3], INGO NOLTE[1], JÖRN BULLERDIEK[1,2], DANIELA SIMON[1] and HUGO MURUA ESCOBAR[1]

[1]*Small Animal Clinic and the German Research Foundation SFB Transregio 37, University of Veterinary Medicine Hannover, 30559 Hannover, Germany;*
[2]*Centre for Human Genetics, University of Bremen, Leobener Str ZHG, 28359 Bremen, Germany;*
[3]*Division of Medicine, Department of Haematology/Oncology, University of Rostock, 18057, Germany*

Abstract. *Background: Canine lymphoma is a commonly occurring, spontaneously developing neoplasia similar to human non-Hodgkin's lymphoma and, thus, is used as a valuable model for human malignancy. HMGB1 and RAGE are strongly associated with tumour progression and vascularisation. Consequently, deregulated RAGE and HMGB1 may play an important role in the mechanisms involved in lymphoma progression. Materials and Methods: Expression patterns of HMGB1 and RAGE were analysed in 22 canine lymphoma and three canine non-neoplastic control samples via real time PCR and canine beta-glucuronidase gene (GUSB) as endogenous control. Results: HMGB1 was up-regulated in the neoplastic samples, while RAGE expression remained inconspicuous. Conclusion: This study demonstrated similar mechanisms in lymphoma progression in humans and dogs due to overexpression of HMGB1, which was described in human lymphomas. RAGE remained stable in terms of expression indicating that the extracellular HMGB1-induced effects are regulated by HMGB1 itself.*

Human and canine tumours share many biological similarities including tumour progression, metastatic pattern and histology. Accordingly, these spontaneously occurring canine tumours represent a valuable model for several human neoplasias and may help to elucidate the biology of those neoplasias. Focusing on haematopoietic tumours, canine lymphoma is a commonly occurring neoplasia serving as an appropriate model for human non-Hodgkin's lymphoma. The frequency of canine lymphoma cases among haematopoietic malignancies is approximately 83%, representing 7% to 24% of all canine neoplasms (1). The response of this malignancy to chemotherapy protocols varies substantially (2). Thus, the identification of factors involved in the formation and progression of lymphomas are of significant value for future development and evaluation of therapeutic approaches, providing benefits for both species.

During tumour progression, hypoxic and necrotic regions develop as a result of fast cell proliferation. To assure a sufficient supply of oxygen, solid and haematopoietic tumours activate cellular angiogenic mechanisms by secretion of pro-angiogenetic factors such as vascular endothelial growth factor (VEGF), tumour necrosis factor alpha (TNF-α) and interleukin-8 (IL-8) (3-5). In human haematopoietic malignancies, increased angiogenesis, measured by high vascular density levels, was observed in the lymph nodes of B-cell non-Hodgkin's lymphoma and B-cell chronic lymphocytic leukaemia, as well as in bone marrow specimens from patients with childhood acute lymphoid leukaemia, acute myeloid leukaemia, chronic myelocytic leukaemia, myelodysplastic syndromes and idiopathic myelofibrosis (6-12). VEGF plays an important role in this process as a master regulator of the angiogenic switch. Sustained angiogenesis leads to disease progression described by tumour growth and metastasis. In non-Hodgkin's lymphoma, for example, circulating levels of VEGF have been shown to correlate with overall survival and event-free survival (13-15).

The high-mobility group box protein 1 (HMGB1), also known as amphoterin or HMG-1, was initially described as a DNA-binding protein but seems to act as a proinflammatory cytokine and as well as a dose-dependent mediator of

Correspondence to: Hugo Murua Escobar, Small Animal Clinic and the German Research Foundation SFB Transregio 37, University of Veterinary Medicine Hannover, Bischofsholer Damm 9, 30559 Hannover, Germany. Tel: +49 5119536382, Fax: +49 5118567686, e-mail: hescobar@tiho-hannover.de

Key Words: Canine lymphoma, HMGB1, RAGE.

0250-7005/2010 $2.00+.40

angiogenic and neo-vascularising effects (16). In response to angiogenic and inflammatory signals, HMGB1 is passively released by necrotic cells or actively secreted by activated macrophages. HMGB1 signalling itself is mediated *via* the receptor for advanced glycation end-products (RAGE) and toll-like receptors (TLR) such as TLR-2 and TLR-4. Activation of these receptors results in activation of nuclear factor kappa B (NFκB), among other factors, which itself acts as a transcriptional enhancer for RAGE, pro-inflammatory cytokines and the pro-angiogenic factor VEGF (17). Due to the positive feedback loop caused by activation of NFκB, a sustained inflammation or angiogenic reaction contributes to disease progression and, in the case of tumour development, to uncontrolled growth and metastasis (17). An *in vitro* study by Sasahira *et al*. (18) showed that the HMGB1/RAGE complex induces VEGF expression through the activation of NFκB in two human oral squamous cell carcinoma cell lines. The abrogation of the HMGB1-mediated effect was observed by down-regulation of RAGE expression *via* application of antisense S-oligodeoxynucleic acid, resulting in a significantly lower VEGF secretion (18).

In this context, a study by Wolfesberger *et al*. (19) examined the expression pattern of VEGF in canine lymphomas, demonstrating a high expression of VEGF in 60% of the analysed tumours. However, studies in human neoplasias focusing on RAGE and HMGB1 expression levels showed a significant up-regulation of RAGE and HMGB1 in pancreatic cancer, prostate cancer and colon cancer (20). In summary, the interaction of HMGB1, RAGE and VEGF is strongly associated with vascularisation and plays a key role in tumour progression. Consequently, deregulation of RAGE and HMGB1 expression may play a key role in lymphoma progression. To elucidate this, the present study analysed the expression patterns of the previously characterized canine *HMGB1* and *RAGE* genes (21-23) in a set of canine lymphomas and controls.

Materials and Methods

Tissue samples. Fine-needle aspirates of enlarged lymph nodes of 22 lymphoma-bearing dogs (19 multicentric and three intestinal lymphomas) and three inconspicuous lymph nodes were examined. The control lymph node samples were derived from dogs diagnosed with diseases other than haematopoietic neoplasia and with clinically unaltered peripheral lymph nodes. All diagnoses were cytologically or histologically confirmed. Clinical staging was performed according to the World Health Organization (WHO) clinical staging system (24) and determination of the immunophenotype of the 19 multicentric lymphomas was performed by flow cytometry (25). Among the 19 multicentric lymphomas, 15 samples showed B-cell origin, two samples were of T-cell origin and two samples could not be determined. The dogs represented 13 different breeds, namely Beagle, Dogo Argentino, German Shepherd, Golden Retriever, Hovawart, Jack Russell Terrier, Jagdterrier, Mixed-breed, Munsterlander, Pitbull, Rottweiler, Teckel and West Highland. After collection, the samples were immediately frozen in liquid nitrogen and stored at −80˚C until RNA isolation. All samples were provided by the Small Animal Clinic, University of Veterinary Medicine, Hannover, Germany.

RNA isolation and cDNA synthesis for transcript characterisation. The tissue samples were homogenised using the iron-beads QIAshredder homogeniser method (Qiagen, Hilden, Germany). Following, total RNA was isolated using the RNeasy Mini Kit (Qiagen) according to the manufacturer's instructions. To avoid genomic DNA contaminations, on-column DNase digestion with the RNase-Free DNase set (Qiagen) was performed.

The respective cDNA syntheses were performed using 250 ng total RNA of each sample and the QuantiTect Reverse Transcription Kit (Qiagen) following the manufacturer's protocol.

Quantitative real-time RT-PCR. Relative real-time PCRs were performed with the Applied Biosystems 7300 real-time PCR System (Applied Biosystems, Darmstadt, Germany). The canine Glucuronidase Beta transcript was chosen as endogenous control (26). Two μl of each cDNA corresponding to 25 ng of total RNA was amplified in a total volume of 25 μl using universal PCR Mastermix (Applied Biosystems) with 600 nM of each primer and 200 nM fluorogenic probe. The following PCR conditions were applied: 2 min at 50˚C and 10 min at 95˚C, followed by 45 cycles with 15 s at 95˚C and 1 min at 60˚C. Primer and probe sequences were as follows: *HMGB1* forward primer: 5'AAGTGAGAGCCAG ACGGG3', *HMGB1* reverse primer: 5'TCCTTTGCCCATGTTTAA TTATTTTC3', *HMGB1* probe: 5' 6-FAM-CTGGGCGACTCT GTGCCTCGCT-TAMRA3', *RAGE* forward primer: 5'GTCTGT GGGGAGCAGTAGTAGG3', *RAGE* reverse primer: 5'TTCTGTC CGACCTGTGTTCAGCTT3', *RAGE* probe: 5' 6-FAM-AAGCCGCTGGTGCTCAACTGTA-TAMRA 3', *GUSB* forward primer: 5'TGGTGCTGAGGATTGGCA3', *GUSB* reverse primer: 5'CTGCCACATGGACCCCATTC3', *GUSB* probe: 5' 6-FAM-CGCCCACTACTATGCCATCGTGTG-TAMRA 3'.

All samples were measured in triplicate and non-template controls and non-reverse transcriptase control reactions were included for each run.

A precedent absolute real-time PCR reaction was carried out with all PCR assays using the same templates and dilution steps in order to ensure the comparability between the PCR reactions showing similar amplification efficiencies appropriate for relative quantification PCRs.

For the analysis based on the ΔΔCT method, the sample within the control group with the most stable CT values for target and endogen control was defined as the calibrator for the analysis of RAGE/GUSB as well as HMGB1/GUSB relative real-time PCR.

Statistical analysis. Statistical analysis of the relative real-time PCR results applying various hypothesis test was performed with the software REST 2008, version 2.0.7 (27). REST determines whether there is a significant difference between samples and controls taking into account reaction efficiencies and using randomisation techniques. Regarding clinical parameters, a Mann-Whitney-test was performed using SPSS 15.0 statistic software (SPSS Inc., Chicago, IL, USA). The HMGB1 and RAGE expression levels were evaluated for statistical significance regarding WHO substage (substage a *vs*. substage b), WHO stage (clinical stage III and IV *vs*. V), and, additionally, for the comparison of multicentric lymphomas *vs*. control dogs and intestinal lymphomas. A p-value <0.05 was considered to be statistically significant.

Table I. *Hypothesis tests of relative HMGB1/GUSB and RAGE/GUSB real-time PCR results in canine lymphoma using the REST software. A total of 25 samples with 3 control and 22 tumour samples (3 intestinal lymphomas, 15 B-cell lymphomas, 2 T-cell lymphomas and 2 of unknown origin) were analysed. A p-value <0.05 was considered statistically significant.*

Hypothesis test: Control group *vs*. tumour group	Expression pattern of HMGB1 compared to control group (*p*-value)	Expression pattern of RAGE compared to control group (*p*-value)
All tumour samples (n=22)	Up-regulation (p=0.001)	Not significantly different (p=0.155)
Intestinal lymphoma (n=3)	Up-regulation (p=0.030)	Not significantly different (p=0.096)
B-cell lymphoma (n=15)	Up-regulation (p=0.001)	Not significantly different (p=0.07)
T-cell lymphoma (n=2)	Up-regulation (p=0.033)	Not significantly different (p=0.792)
Unknown multicentric lymphoma (n=2)	Not significantly different (p=0.135)	Not significantly different (p=0.303)

Results

Expression analyses of *HMGB1* and *RAGE* in canine lymphomas were performed using relative real-time PCR on lymph node aspirates from 22 lymphoma-bearing dogs and three dogs without haematopoietic neoplasias. Both real-time reactions were analysed using the ΔΔCT method and the results are shown in Figures 1 and 2. In both graphs, the same samples were put in the same position to compare the tumour samples directly for both candidate genes. The *HMGB1* expression (Figure 1) quotient in the tumour samples varied from 1.587 (sample seven) to 8.549 (sample three) relative to the defined calibrator. The median expression levels were 1.33 for the control group (samples 1-3), 4.22 for the intestinal lymphoma group (samples 4-6), 4.26 for the B-cell lymphoma group (samples 7-21), 3.83 for the T-cell lymphoma group (samples 22-23) and 2.13 for the unknown lymphoma group (samples 24-25). In the case of *RAGE* (Figure 2), the relative quotients varied from 0.36 (sample 10) to 18.282 (sample 3). The median expression levels were 0.55 for the control group (samples 1-3), 6.69 for the intestinal lymphoma group (samples 4-6), 1.73 for the B-cell lymphoma group (samples 7-21), 0.56 for the T-cell lymphoma group (samples 22-23) and 1.61 for the unknown lymphoma group (samples 24-25).

Samples 6 (intestinal lymphoma), 15, 20 and 21 (B-cell lymphoma) showed the highest RAGE expression levels and, accordingly, in samples 6, 20 and 21 high HMGB1 expression levels were also detected. Samples 20 and 21 had the highest *HMGB1* expression within the group of B-cell lymphomas and sample 6 showed the highest expression of *HMGB1* in the intestinal lymphoma group. Sample 15 showed an average *HMGB1* expression level.

Hypothesis tests of the relative real-time PCR results were performed using the REST software. Analysis of expression of control samples *vs*. all tumour samples showed a highly significant up-regulation of *HMGB1* (p=0.001), while *RAGE* showed no significant expression value (p=0.155). The test was also performed for all subgroups within the sample collective (intestinal lymphoma, B-cell lymphoma, T-cell lymphoma and unknown multicentric lymphoma). Comparison of the control samples *vs*. intestinal lymphomas revealed a significant difference for *HMGB1* (p=0.03) but not for *RAGE* (p=0.096). B-Cell lymphomas were significantly different to the control samples for *HMGB1* (p=0.001) but not different for *RAGE* (p=0.07). Compared to the control samples, T-cell lymphomas showed significant up-regulation of *HMGB1* expression (p=0.033) but no significant difference of RAGE expression (p=0.792). The group of multicentric lymphoma samples, which were unable to be determined by flow cytometry, showed no statistically significant difference in the expression of *HMGB1* (p=0.135) nor *RAGE* (p=0.303) in comparison to the control group. The results of the statistical analysis using the REST programme are displayed in Table I.

The Mann-Whitney test regarding the difference in the expression levels between the multicentric lymphomas and the control samples revealed significant differences for *HMGB1* (p=0.003) but not for RAGE (p=0.078). The expression of *HMGB1* and *RAGE* also showed no significant differences between multicentric and intestinal lymphomas (p=0.907 for *HMGB1* and p=0.702 for *RAGE*). WHO stage and substage of the samples were not significantly associated with *HMGB1* and *RAGE* expression values (results not shown).

Discussion

Vascularisation under normal conditions is strongly regulated by a delicate balance of pro- and anti-angiogenic molecules. In the case of tumour progression, sustained secretion of pro-angiogenic factors such as HMGB1, RAGE and VEGF is triggered by tumour microenvironmental hypoxic and necrotic areas leading to neo-vascularisation. Regarding haematological malignancies, increased vascularity was observed in B-cell non-Hodgkin's lymphoma (9) and high serum levels of VEGF were associated with poor outcome (14). In this context, a study targeting canine lymphomas showed high levels of VEGF in the analysed tumour samples, indicating an involvement of pro-angiogenic factors in lymphoma progression (19, 28).

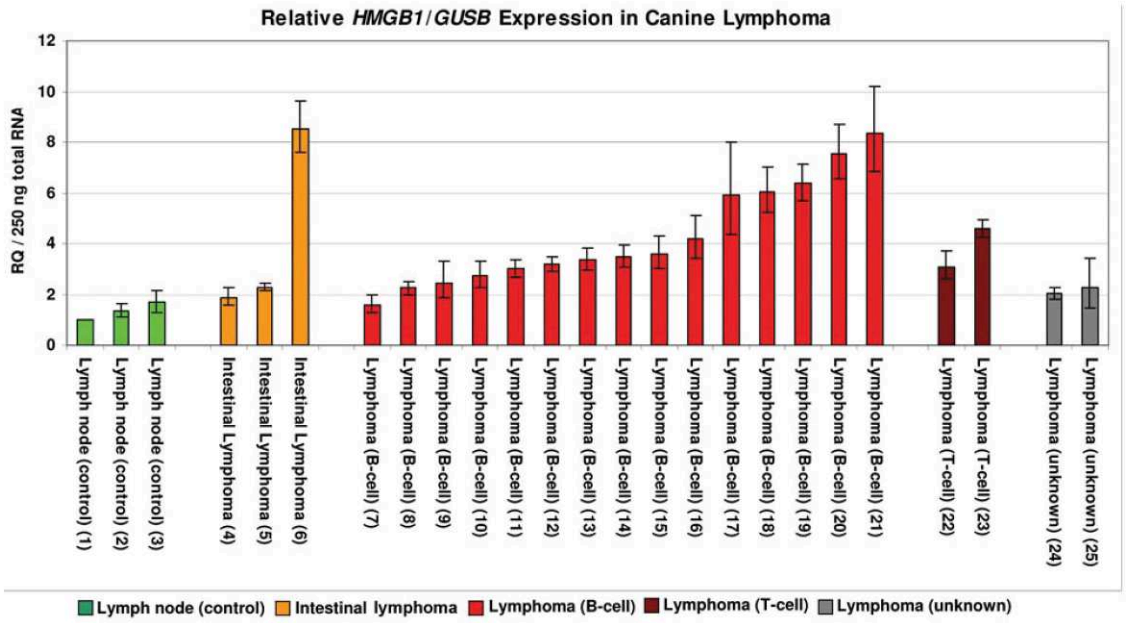

Figure 1. *Relative HMGB1/GUSB expression in canine lymphoma. A total of 25 samples were analysed. The set of samples consisted of 3 control and 22 tumour samples of the following subgroups: 3 intestinal lymphomas, 15 B-cell lymphomas, 2 T-cell lymphomas and 2 of unknown origin. Green bars: lymph node control; orange bars: intestinal lymphoma; red bars: B-cell lymphoma; brown bars: T-cell lymphoma and grey bars: lymphomas of unknown origin.*

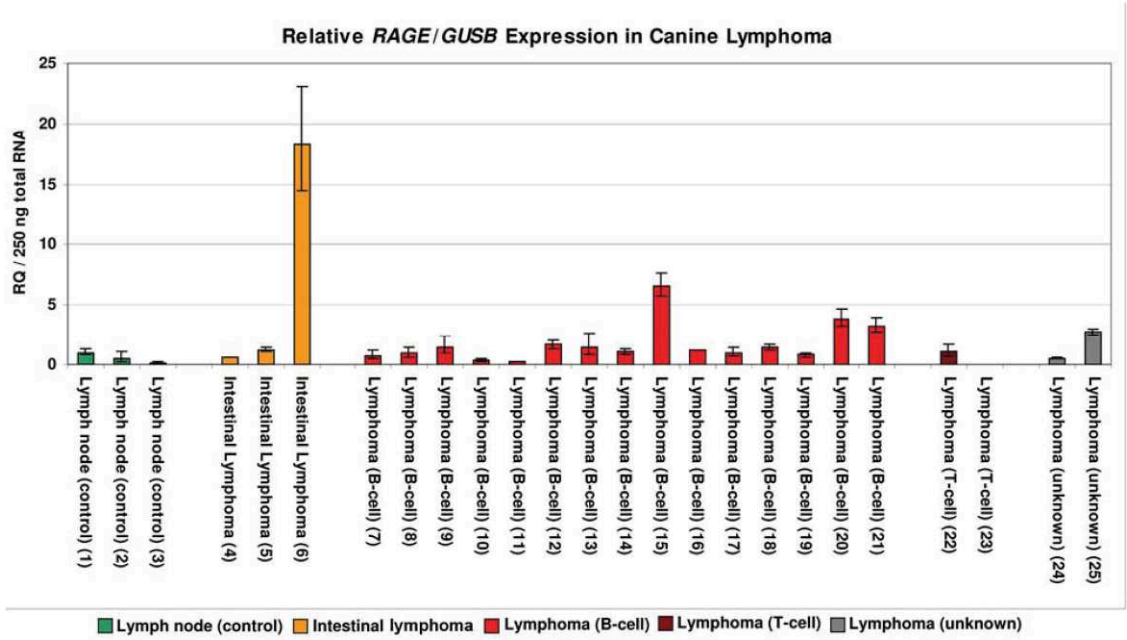

Figure 2. *Relative RAGE/GUSB expression in canine lymphoma. A total of 25 samples were analysed. The set of samples consisted of 3 control and 22 tumour samples of the following subgroups: 3 intestinal lymphomas, 15 B-cell lymphomas, 2 T-cell lymphomas and 2 of unknown origin. Green bars: lymph node control; orange bars: intestinal lymphoma; red bars: B-cell lymphoma; brown bars: T-cell lymphoma and grey bars: lymphomas of unknown origin.*

These findings raise the question whether RAGE and HMGB1 are also deregulated in lymphomas. For several other neoplasias such as pancreatic, prostate and colon cancer deregulation of the expression of HMGB1 and RAGE has been described (20).

Therefore, the present study examined the expression of *HMGB1* and *RAGE* in lymph node samples of canine lymphomas in comparison to lymph nodes from dogs without haematopoietic neoplasias. The tumour samples were cytologically and histologically confirmed and flow cytometry determined the immunophenotype of the multicentric lymphomas. The present study showed a significant up-regulation in *HMGB1* expression in the analysed lymphoma samples, while the detected *RAGE* expression did not change significantly when compared to the control samples. Furthermore, statistical analyses were performed not only with all control and all tumour samples together as groups, but also for the different subgroups of the sample collective. The sample numbers of intestinal, T-cell and unknown lymphomas were too small for an appropriate powerful statistical analysis (n=3, 2 and 2, respectively) and, consequently, more samples of both non-neoplastic and tumour types would be necessary for further analyses. However, the results of the present study indicated a trend of the expression pattern of *HMGB1* and *RAGE* in this lymphoma types.

Meyer *et al*. (29) examined the expression of HMGB1 in human non-Hodgkin lymphoma using real-time PCR and showed high levels of HMGB1 expression, while RAGE expression was not analysed. The *HMGB1* overexpression detected in the canine lymphoma samples strongly emphasises that similar HMGB1-related mechanisms exist in canine and human lymphoma progression. Furthermore, in canine lymphomas, elevated HMGB1 serum levels were detected and the prognostic value of initial and sequential serum level was suggested (30).

The *RAGE* expression data determined herein indicated that the HMGB1-induced effects in all 22 analysed lymphoma samples are regulated by the overexpression of *HMGB1* itself, while RAGE, as a receptor, remains stable in terms of expression. Using tumour tissue microarray slides, a study by Hsieh *et al*. (31), detected a borderline positive staining for RAGE antibodies in lymphoma tumours, suggesting that only certain cells or vessels on the tissue disc were stained positive, thus, indicating low levels of RAGE in the tumour slides analysed; however, that finding was not discussed further in detail by the authors. Besides the present study, there have been no significant data published concerning RAGE expression in lymphomas. In summary, the data of the present study showed significant deregulation of *HMGB1* but not *RAGE* in canine lymphoma, contradictory to the observations in many solid tumours. However, the TLR receptors 2 and 4 also participate in the complex signalling pathways induced by HMGB1 and, thus, should be considered with regard to lymphoma development and progression. Accordingly, recent studies concerning the expression of TLR receptors showed associations of expression/overexpression of these receptors in gastric carcinoma, colon cancer and breast cancer (32). Additionally, gene polymorphisms in TLR-2 and -4 gene sequences have been hypothesised as possible contributors to follicular lymphoma and mucosa-associated lymphoid tissue lymphoma (33).

The analysed samples were of 13 different dog breeds and some breeds show higher incidences in development of malignant lymphomas; for example, the German Shepherd, Beagle and Golden Retriever breeds (34). In the present study, the two highest values for HMGB1 in B-cell lymphomas were detected in a Beagle and a German Shepherd.

In conclusion, pathways leading to vascularisation and tumour progression are described by the complex interaction of all involved factors including their interactions on DNA and protein level. In the present study, it should be noted that an up-regulated HMGB1 signalling was mediated not only by RAGE, but also by TLR-2 and -4 and the extensive interactions between all factors. Thus, elucidating whether the interaction between HMGB1 and its respective receptors plays a key role in the mechanisms involved in lymphoma development and progression will be of significant value for the development of therapeutic approaches for the dog as patient and as a model system for human non-Hodgkin's lymphoma.

Acknowledgements

This work was supported in part by German Federal Ministry of Education and Research and the German Research Foundation SFB Transregio 37 (Micro- and Nanosystems in Medicine)

References

1 Withrow S and Vail DM: Withrow and MacEwen's Small Animal Clinical Oncology, fourth edition. St. Louis: Saunders Elsevier, 2007.

2 Simon D, Moreno SN, Hirschberger J, Moritz A, Kohn B, Neumann S, Jurina K, Scharvogel S, Schwedes C and Reinacher M: Efficacy of a continuous, multiagent chemotherapeutic protocol *versus* a short-term single-agent protocol in dogs with lymphoma. J Am Vet Med Assoc *232(6)*: 879-885, 2008.

3 Ono M, Torisu H, Fukushi J, Nishie A and Kuwano M: Biological implications of macrophage infiltration in human tumor angiogenesis. Cancer Chemother Pharmacol *43(Suppl)*: 69-71, 1999.

4 Moehler TM, Neben K, Ho AD and Goldschmidt H: Angiogenesis in hematologic malignancies. Ann Hematol *80(12)*: 695-705, 2001.

5 Andersson U, Erlandsson-Harris H, Yang H and Tracey KJ: HMGB1 as a DNA-binding cytokine. J Leukoc Biol *72(6)*: 1084-1091, 2002.

6 Hussong JW, Rodgers GM and Shami PJ: Evidence of increased angiogenesis in patients with acute myeloid leukemia. Blood *95(1)*: 309-313, 2000.

7 Lundberg LG, Lerner R, Sundelin P, Rogers R, Folkman J and Palmblad J: Bone marrow in polycythemia vera, chronic myelocytic leukemia, and myelofibrosis has an increased vascularity. Am J Pathol *157(1)*: 15-19, 2000.

8 Mesa RA, Hanson CA, Rajkumar SV, Schroeder G and Tefferi A: Evaluation and clinical correlations of bone marrow angiogenesis in myelofibrosis with myeloid metaplasia. Blood *96(10)*: 3374-3380, 2000.

9 Molica S, Vacca A, Ribatti D, Cuneo A, Cavazzini F, Levato D, Vitelli G, Tucci L, Roccaro AM and Dammacco F: Prognostic value of enhanced bone marrow angiogenesis in early B-cell chronic lymphocytic leukemia. Blood *100(9)*: 3344-3351, 2002.

10 Perez-Atayde AR, Sallan SE, Tedrow U, Connors S, Allred E and Folkman J: Spectrum of tumor angiogenesis in the bone marrow of children with acute lymphoblastic leukemia. Am J Pathol *150(3)*: 815-821, 1997.

11 Pruneri G, Bertolini F, Soligo D, Carboni N, Cortelezzi A, Ferrucci PF, Buffa R, Lambertenghi-Deliliers G and Pezzella F: Angiogenesis in myelodysplastic syndromes. Br J Cancer *81(8)*: 1398-1401, 1999.

12 Ribatti D, Vacca A, Nico B, Fanelli M, Roncali L and Dammacco F: Angiogenesis spectrum in the stroma of B-cell non-Hodgkin's lymphomas. An immunohistochemical and ultrastructural study. Eur J Haematol *56(1-2)*: 45-53, 1996.

13 Bertolini F, Paolucci M, Peccatori F, Cinieri S, Agazzi A, Ferrucci PF, Cocorocchio E, Goldhirsch A and Martinelli G: Angiogenic growth factors and endostatin in non-Hodgkin's lymphoma. Br J Haematol *106(2)*: 504-509, 1999.

14 Salven P, Teerenhovi L and Joensuu H: A high pretreatment serum vascular endothelial growth factor concentration is associated with poor outcome in non-Hodgkin's lymphoma. Blood *90(8)*: 3167-3172, 1997.

15 Salven P, Orpana A, Teerenhovi L and Joensuu H: Simultaneous elevation in the serum concentrations of the angiogenic growth factors VEGF and bFGF is an independent predictor of poor prognosis in non-Hodgkin lymphoma: a single-institution study of 200 patients. Blood *96(12)*: 3712-3718, 2000.

16 Schlueter C, Weber H, Meyer B, Rogalla P, Roser K, Hauke S and Bullerdiek J: Angiogenetic signaling through hypoxia: HMGB1: an angiogenetic switch molecule. Am J Pathol *166(4)*: 1259-1263, 2005.

17 van Beijnum JR, Buurman WA and Griffioen AW: Convergence and amplification of toll-like receptor (TLR) and receptor for advanced glycation end products (RAGE) signaling pathways *via* high mobility group B1 (HMGB1). Angiogenesis *11(1)*: 91-99, 2008.

18 Sasahira T, Kirita T, Bhawal UK, Ikeda M, Nagasawa A, Yamamoto K and Kuniyasu H: The expression of receptor for advanced glycation end products is associated with angiogenesis in human oral squamous cell carcinoma. Virchows Arch *450(3)*: 287-295, 2007.

19 Wolfesberger B, Guija de Arespacohaga A, Willmann M, Gerner W, Miller I, Schwendenwein I, Kleiter M, Egerbacher M, Thalhammer JG, Muellauer L, Skalicky M and Walter I: Expression of vascular endothelial growth factor and its receptors in canine lymphoma. J Comp Pathol *137(1)*: 30-40, 2007.

20 Sparvero LJ, Asafu-Adjei D, Kang R, Tang D, Amin N, Im J, Rutledge R, Lin B, Amoscato AA, Zeh HJ and Lotze MT: RAGE (Receptor for Advanced Glycation Endproducts), RAGE ligands, and their role in cancer and inflammation. J Transl Med *7*: 17, 2009.

21 Murua Escobar H, Meyer B, Richter A, Becker K, Flohr AM, Bullerdiek J and Nolte I: Molecular characterization of the canine HMGB1. Cytogen Genome Res *101*: 33-38, 2003.

22 Murua Escobar H, Soller JT, Sterenczak KA, Sperveslage JD, Schlueter C, Burchardt B, Eberle N, Fork M, Nimzyk R, Winkler S, Nolte I and Bullerdiek J: Cloning and characterization of the canine receptor for advanced glycation end products. Gene *369*: 45-52, 2006.

23 Sterenczak KA, Willenbrock S, Barann M, Klemke M, Soller JT, Eberle N, Nolte I, Bullerdiek J and Murua Escobar H: Cloning, characterisation, and comparative quantitative expression analyses of receptor for advanced glycation end products (RAGE) transcript forms. Gene *434(1-2)*: 35-42, 2009.

24 Owen LN: TNM Classification of Tumours in Domestic Animals. Geneva: World Health Organization, 1980.

25 Culmsee K, Simon D, Mischke R and Nolte I: Possibilities of flow cytometric analysis for immunophenotypic characterization of canine lymphoma. J Vet Med A Physiol Pathol Clin Med *48(4)*: 199-206, 2001.

26 Brinkhof B, Spee B, Rothuizen J and Penning LC: Development and evaluation of canine reference genes for accurate quantification of gene expression. Anal Biochem *356(1)*: 36-43, 2006.

27 Pfaffl MW, Horgan GW and Dempfle L: Relative expression software tool (REST) for group-wise comparison and statistical analysis of relative expression results in real-time PCR. Nucleic Acids Res *30(9)*: e36, 2002.

28 Zizzo N, Patruno R, Zito FA, Di Summa A, Tinelli A, Troilo S, Misino A, Ruggieri E, Goffredo V, Gadaleta CD and Ranieri G: Vascular endothelial growth factor concentrations from platelets correlate with tumor angiogenesis and grading in a spontaneous canine non-Hodgkin lymphoma model. Leuk Lymphoma *51(2)*: 291-296, 2010.

29 Meyer A, Staratschek-Jox A, Springwald A, Wenk H, Wolf J, Wickenhauser C and Bullerdiek J: Non-Hodgkin lymphoma expressing high levels of the danger-signalling protein HMGB1. Leuk Lymphoma *49(6)*: 1184-1189, 2008.

30 Meyer A, Eberle N, Bullerdiek J, Nolte I and Simon D: High-mobility group B1 proteins in canine lymphoma: prognostic value of initial and sequential serum levels in treatment outcome following combination chemotherapy. Vet Comp Oncol *8(2)*: 127-137, 2010.

31 Hsieh HL, Schafer BW, Sasaki N and Heizmann CW: Expression analysis of S100 proteins and RAGE in human tumors using tissue microarrays. Biochem Biophys Res Commun *307(2)*: 375-381, 2003.

32 Yu L and Chen S: Toll-like receptors expressed in tumor cells: targets for therapy. Cancer Immunol Immunother *57(9)*: 1271-1278, 2008.

33 Nieters A, Beckmann L, Deeg E and Becker N: Gene polymorphisms in Toll-like receptors, interleukin-10, and interleukin-10 receptor alpha and lymphoma risk. Genes Immun *7(8)*: 615-624, 2006.

34 Gough A: Breed Predispositions to Disease in Dogs and Cats. Oxford, Blackwell Publishing Ltd, 2004.

Received September 23, 2010
Revised October 22, 2010
Accepted October 26, 2010

III ‘Comparison of the human and canine cytokines IL-1(alpha/beta) and TNF-alpha to orthologous other mammalians.’ **Soller *et al.*, Journal of Heredity, 2007.**

Cytokines as e.g. IL-1α, IL-1β and TNF-α are described to play an important role in the initiation and regulation of immune responses to infectious diseases and in the development and progression of diseases like cancer in humans as well as dogs and other species. The availability of recombinant canine cytokines for development of *in vitro* and *in vivo* approaches is still limited. Therefore, an identity comparison to identify potential cross-reactivity from cytokines of other species was carried out in this work.

The mRNA and protein structures of TNF-α, IL1-α, and IL1-β of several mammalian species (human, canine, murine, rat, ovine, equine, feline, porcine, and bovine) were compared and analysed basing on the presently known sequences. In addition, the complete mRNA structures of the *IL1-α*, and *IL1-β* mRNAs were derived by *in silico* analysis of the canine genome sequence.

The general described cytokine identity in reference to the canine sequences were for the human molecules on nucleotide level 76.4 % for *IL-1β*, 79.6 % *IL1-α*, and 90.8 % for TNF-α. The respective proteins the similarity indices were 62.8 % for *IL-1β*, 68.5 % for *IL1-α*, and 91.0 % for TNF-α. Comparison of murine vs. canine sequences revealed similarities of 43.9 % for *IL1-α*, 71.7 % for *IL-1β*, and 80.4 % for TNF-α. The corresponding *in silico* determined protein similarities were 57.1 % for *IL1-α*, 53.8 % for *IL-1β*, and 78.2 % for TNF-α.

Concerning the functional domains and sequence motifs, the analyses showed that IL-1α, IL-1β and TNF-α have a high evolutionary conserved homology within the mammalian species.

III

Comparison of the Human and Canine Cytokines IL-1(α/β) and TNF-α to Orthologous Other Mammalians

Soller JT, Murua Escobar H, Willenbrock S, Janssen M, Eberle N, Bullerdiek J, Nolte I.

Journal of Heredity. 2007;98(5):485-90

Own contribution:

- Figure preparation
- Partial *in silico* analysis
- Partial manuscript drafting

Journal of Heredity Advance Access published June 15, 2007

Journal of Heredity
doi:10.1093/jhered/esm025

Comparison of the Human and Canine Cytokines *IL-1*(α/β) and *TNF*-α to Orthologous Other Mammalians

JAN T. SOLLER, HUGO MURUA. ESCOBAR, SASKIA WILLENBROCK, MIRIAM JANSSEN, NINA EBERLE, JÖRN BULLERDIEK, AND INGO NOLTE

From the Small Animal Clinic, University of Veterinary Medicine, Bischofsholer Damm 15, 30137 Hanover, Germany (Soller, Escobar, Willenbrock, Eberle, and Nolte); and the Centre for Human Genetics, University of Bremen, Leobener Strasse ZHG, 28359 Bremen, Germany (Soller, Escobar, Willenbrock, Janssen, and Bullerdiek).

Address correspondence to Dr. I. Nolte at the address above, or e-mail: inolte@klt.tiho-hannover.de.

Abstract

The cytokines interleukin-1 (IL-1α and IL-1β) and the tumor necrosis factor-α (TNF-α) both play a major role in the initiation and regulation of inflammation and immunity responses. Polymorphisms within the gene sequences of these cytokines *IL-1* and *TNF*-α have been proposed to play an important role in the pathogenesis of certain diseases. Affecting nearly every organ, various diseases, including some cancers, are described to be associated with an increased level of IL-1 and TNF-α proteins, for example, solid tumors, hematologic malignancies, malignant histiocytosis, autoimmune disorders, Alzheimer's disease, Parkinson's disease, sepsis, and rheumatoid arthritis. Regarding genetic backgrounds and pathways, numerous canine diseases show close similarities to their human counterparts. As a genetic model, the dog could be used to unravel the genetic mechanisms, for example, in particular the predispositions, the development, and progression of cancer and metabolic diseases. The identity comparison of gene and protein sequences of different species could be used to elucidate the structure and function of the genes and proteins by identifying the evolutionary conserved regions and domains. Herein we analyzed in detail the mRNA and protein structures and identities of the present known mammalian (human, canine, murine, rat, ovine, equine, feline, porcine, and bovine) *TNF*-α, *IL*-1α, and *IL-1*β mRNAs and proteins. Additionally, based on the canine genome sequence, we derived in silico the complete mRNA structures of the *IL-1*α and *IL-1*β mRNAs.

The cytokines interleukin-1 (IL-1α and IL-1β) and tumor necrosis factor-α (TNF-α) are primarily secreted by monocytes and macrophages and act as potent multifunctional cytokines in abundant signal transduction processes during immune response and inflammation, acting as proinflammatory proteins. These cytokines bind to cell-surface receptors inducing the activation of different transcription factors, for example, AP1, CREB, and NF-κB for regulation of immediate early genes. In detail, IL-1α and IL-1β will bind to membrane-bound receptor IL-1R1, whereas 2 distinct receptors TNF-R55 and TNF-R60 exist for TNF-α. Although both receptors for IL-1α and TNF-α are structurally unrelated, they operate both in a similar biological manner (Brockhaus et al. 1990; Eisenberg et al. 1991; Dinarello 1996).

In particular, NFκB-dependent signaling pathways play a key role for inflammatory responses caused by injury and infection stimuli. In mammals, 5 NF-κB proteins, RelA, RelB, c-Rel, NF-κB1, and NF-κB2 were described, which form homo- and heterodimer complexes in the cytoplasm. NF-κB proteins are inactivated by binding the inhibitory protein IκB. IL-1 and TNF-α are able to trigger phosphorylation and ubiquitinylation pathways to degrade the IκB protein having a releasing effect for NF-κB and thus inducing the transcription of several genes in the nucleus (for review see Beutler and Cerami 1989; Stylianou and Saklatvala 1998; Alberts et al. 2002).

*IL-1*α and *IL-1*β both belong to the same gene family of *Interleukin-1* and are translated as precursor proteins with a molecular weight of 31 kDa. The processing of the isoforms of proIL-1α and proIL-1β by cellular proteases results in a mature form of the protein of approximately 17 kDa (Dinarello 1996).

Intracellular proIL-1α is fully active and cleaved by Ca^{2+}-dependent membrane-associated cysteine proteases called calpains to IL-1α propiece (16 kDa), which then is able to bind to nuclear DNA, and to mature IL-1α, which is released to the extracellular compartment (Kobayashi et al. 1990; Dinarello 1996). IL-1α shows significant antitumor activity

on solid tumor cells in vitro and in vivo (Braunschweiger et al. 1988). It also has an effect on bone marrow cells to produce colony-stimulating factors (Bagby et al. 1986).

ProIL-β remains in the cytoplasm until it is cleaved by the cysteine proteinase IL-1β–converting enzyme to the IL-1β propiece (16 kDa) and the biologically active 17-kDa mature IL-1β protein. Either protein is able to bind the cell membrane or to be transported out of the cell (Dinarello 1996).

The TNF-α protein exists in 2 forms: a soluble form of 157 amino acids (aa) (17 kDa) cleaved at aa position 76 and 77 by ADAM17 and as a membrane-bound form of 233 aa (26 kDa). Additionally, it acts as a potent pyrogen when stimulated by IL-1. Also TNF-α can induce cell death of certain tumor cells (Beutler and Cerami 1989).

The human nucleotide sequences of the *IL-1*α and *IL-1*β genes contain 6 introns and 7 exons. The genes are located on HSA 2q14 (Furutani et al. 1986; Webb et al. 1986; Modi et al. 1988; Lafage et al. 1989). In humans, the *TNF*-α gene consists of 3 introns and 4 exons and spans approximately 3 kb and was mapped on HSA 6p21 (Nedwin et al. 1985; Spies et al. 1986).

Cytokines are considered to play a major role in the pathogenesis of several diseases.

Polymorphisms within the promoter and/or enhancer regions within the gene sequences of *IL-1*α/β and *TNF*-α are proposed to play a role in the development and pathogenesis of Alzheimer's disease and Parkinson's disease (Nicoll et al. 2000; McGeer PL and McGeer EG 2001; Mattila et al. 2002), as well as nonsmall cell lung cancer (Zienolddiny et al. 2004), tuberculosis (Correa et al. 2005), sepsis, and rheumatoid arthritis (Cox et al. 1999; Ruuls and Sedgwick 1999). Also the production of large quantities of IL-1 and TNF-α cytokines in T-cells are expected to be responsible for the development and progression of certain autoimmune and tumor diseases like in human the Langerhans' cell histiocytosis and the canine malignant histiocytosis (Ramsey et al. 1996; Egeler et al. 1999; Tazi et al. 2000; Affolter and Moore 2002; Arico 2006).

Some human and canine diseases show similarities, concerning the dysfunction of regulation of the immune system and inflammatory processes and the genetic pathways for the development of neoplastic diseases, for example, malignant histiocytosis (Ramsey et al. 1996; Affolter and Moore 2002). Comparative analyses of canine cytokine genes to the known gene information of other mammalians could be used to clarify the mechanisms of etiology and pathogenesis. The knowledge gained by the species comparison could help to evaluate the different species as appropriate models for research studies opening new aspects for experimental and therapeutic approaches.

In Figure 1A and B, the *IL-1*α, *IL-1*β, and *TNF*-α mRNA sequences of 7 mammalians currently present at the National Center for Biological Information (NCBI) database (October 2006) are shown in detail (including the present information on the coding sequences (CDS), 5′ untranslated regions [UTRs] and 3′UTRs). Additionally, we derived in silico the complete structures of the *IL-1*α and *IL-1*β mRNAs using the released canine genome sequence (Lindblad-Toh et al. 2005).

For CDS and protein identity analyses, we used the described sequences from human, dog, mouse, cat, pig, cattle, rat, horse, and sheep and deduced, if necessary, the corresponding parts for analysis. The in silico analysis were done using LASERGENE software programs (DNASTAR, Madison, WI).

The first publications of human and murine *IL-1*α gene sequences (NM_000575, NM_010554) were done at the middle of the 1980s. The human CDS is composed of 816 bp and 813 bp for the murine sequence (Furutani et al. 1985; Lomedico et al. 1984; March et al. 1985). Straubinger et al. characterized the canine (798 bp) and feline (813 bp) CDS and parts of 3′UTR for the *IL-1*α mRNAs (NM_001003157, AF047012) spanning exon 2–7, respectively. Two different splice variant transcripts of canine, feline, and porcine *IL-1*α were described to be found in total RNA from lipopolysaccharide-stimulated lung macrophages. One transcript was identified as a new mRNA splice variant of canine *IL-1*α missing the 175 bp of exon 5 (Straubinger et al. 1999). Due to the deletion of exon 5, the calpain cleavage site is lacking, and calpain is unable to cleave the precursor protein to the mature protein. In previous studies aimed at a single-nucleotide polymorphism screening analysis in canine cytokine mRNA transcripts of *IL-1*(α/β) and *TNF*-α, we cloned the *IL-1*α mRNAs adding new information on the 5′UTR (complete exon 1 and parts of exon 2) and additional parts for the 3′UTR (Soller et al. 2006). We also found both splice variants *IL-1a* (DQ923806) and the splice variant bearing the exon 5 deletion (EF068230): We analyzed them in detail and submitted them to the NCBI database completing the known information due to the fact that the sequences describing the splice variant were not submitted to the databases by the respective author. The genetic structure and organization of all compared *IL-1a* cytokines are highly conserved among the different mammalians. The detailed sequence comparisons (Figure 1A) showed that all cytokine transcripts of the different species with exception of the feline and ovine sequences are composed of equal number of 7 exons. The ovine and feline exceptions are the missing of the sequence information coding for exon 1, probably due to the transcripts have not been completely characterized up to date.

The identities of the canine *IL-1*α CDS (NM_001003157) to the CDS sequences of other species vary between mouse CDS (NM_008361) 43.9%, rat CDS (D00403) 69.3%, human CDS (NM_000575) 79.6%, horse CDS (U92480) 84.8%, and cat CDS (AF047012) 88.8% (Table 1). Respectively. the identities of the canine IL-1α protein sequence (ABJ51907) to the protein sequences of the other species vary between mouse protein (NP_034684) 57.1%, rat protein (BAA00306) 59.6%, human protein (NP_000566) 68.5%, horse protein (AAC39255) 79.3%, and cat protein (AAC03067) 82.7% (Table 1).

The IL-1α proteins of all mammalians show strong conservation of the predicted calpain cleavage site (-KP**RS**V-), located between the arginine residue at position 108 and the serine residue at position 109 of the canine protein. The average IL-1α protein size of the described mammalians is about 270 aa. The protein size range about 266 aa (dog,

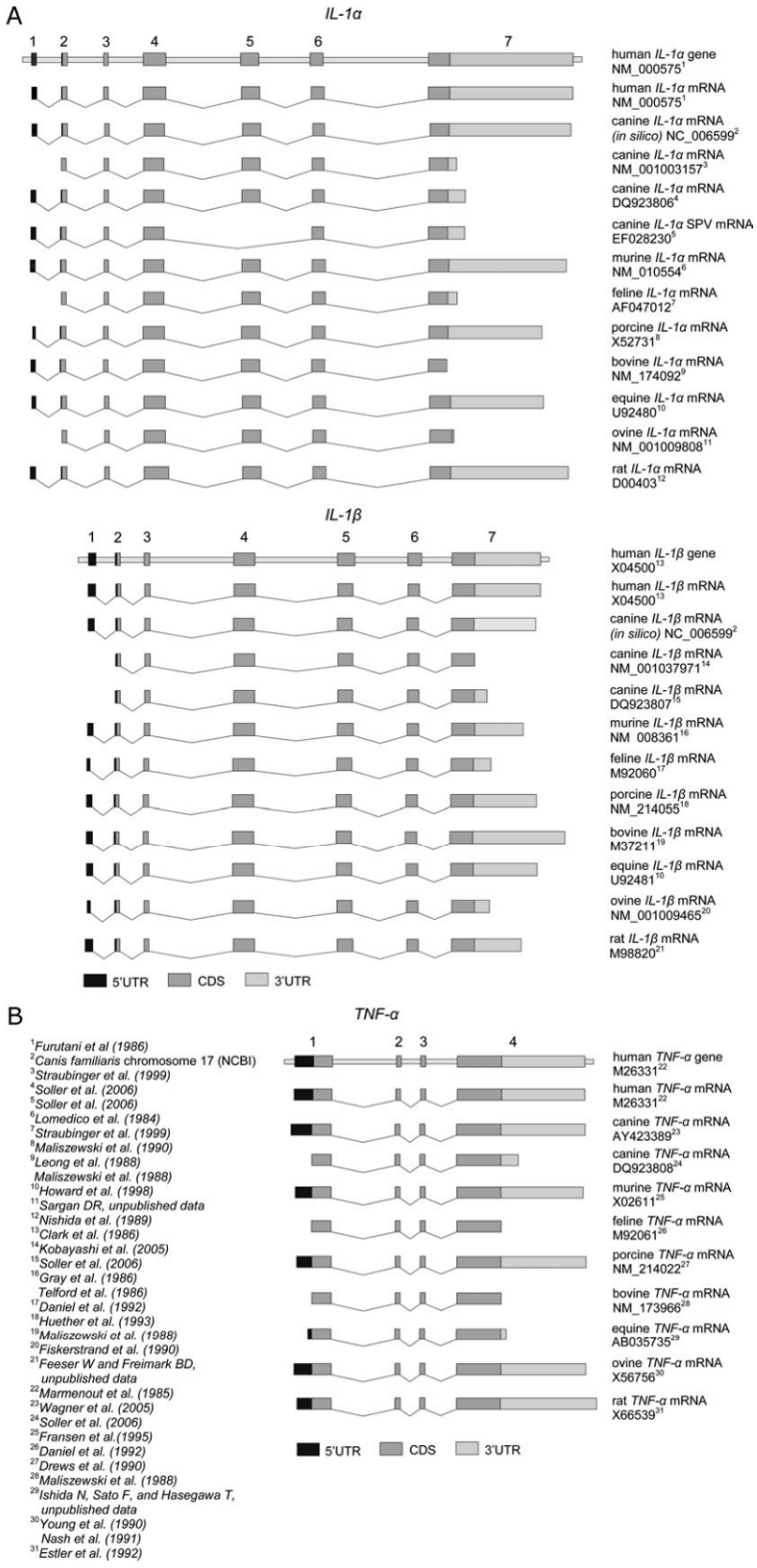

Figure 1. **(A)** Species comparison of *IL-1(α/β)* transcripts. The introns are scaled down by factor 0.4. **(B)** Species comparison of *TNF-α* transcripts.

Table 1. Cytokines IL-1 and TNF-α identity comparison (CDS and protein) of various species to canine transcripts and proteins; size in base pairs (bp) and amino acids (aa), and listed accession numbers

	Identity (%) to *Canis. familiaris*	
IL-1α	CDS 798 bp (DQ923806)	Protein 266 aa (ABJ51907)
Human (*Homo sapiens*) (NM_000575/NP_000566)	79.6 (816 bp)	68.5 (272 aa)
Mouse (*Mus musculus*) (NM_000575/NP_000566)	43.9 (813 bp)	57.1 (271 aa)
Cat (*Felis catus*) (AF047012/AAC03067)	88.8 (813 bp)	82.7 (271 aa)
Pig (*Sus scrofa*) (X52731/CAA36945)	81.8 (813 bp)	73.2 (271 aa)
Cattle (*Bos Taurus*) (NM_174092/NP_776517)	81.2 (807 bp)	75.1 (269 aa)
Horse (*Equus caballus*) (U92480/AAC39255)	84.8 (813 bp)	79.3 (268 aa)
Sheep (*Ovis aries*) (NM_001009808/NP_001009808)	81.0 (807 bp)	75.1 (266 aa)
Rat (*Rattus norvegicus*) (D00403/BAA00306)	69.3 (813 bp)	59.1 (268 aa)
IL-1β	CDS 801 bp (DQ923807)	Protein 267 aa (ABJ51908)
Human (*Homo sapiens*) (X04500/CAA28185)	76.4 (810 bp)	62.8 (270 aa)
Mouse (*Mus musculus*) (NM_008361/NP_032387)	71.7 (810 bp)	58.3 (270 aa)
Cat (*Felis catus*) (M92060/AAA30814)	83.8 (804 bp)	74.0 (268 aa)
Pig (*Sus scrofa*) (NM_214055/NP_999220)	76.3 (804 bp)	64.7 (268 aa)
Cattle (*Bos Taurus*) (M37211/AAA30584)	76.5 (801 bp)	62.5 (267 aa)
Horse (*Equus caballus*) (U92481/AAC39256)	79.5 (806 bp)	67.3 (266 aa)
Sheep (*Ovis aries*) (NM_001009465/NP_001009465)	75.5 (800 bp)	61.4 (261 aa)
Rat (*Rattus norvegicus*) (M98820/AAA41426)	70.3 (806 bp)	58.0 (263 aa)
TNF-α	CDS 702 bp (AY423389)	Protein 234 aa (AAR27885)
Human (*Homo sapiens*) (M26331/AAA36758)	90.8 (702 bp)	91.0 (234 aa)
Mouse (*Mus musculus*) (X02611/CAA26457)	80.4 (708 bp)	78.2 (236 aa)
Cat (*Felis catus*) (M92061/AAA30818)	93.3 (702 bp)	94.4 (234 aa)
Pig (*Sus scrofa*) (NM_214022/NP_999187)	85.5 (699 bp)	85.5 (233 aa)
Cattle (*Bos Taurus*) (NM_173966/NP_776391)	83.4 (705 bp)	78.7 (235 aa)
Horse (*Equus caballus*) (AB035735/BAA349)	89.3 (705 bp)	87.7 (233 aa)
Sheep (*Ovis aries*) (NM_001024860/NP_001020031)	83.9 (705 bp)	79.1 (233 aa)
Rat (*Rattus norvegicus*) (X66539/CAA47146)	79.7 (708 bp)	77.0 (234 aa)

sheep), 268 aa (horse, rat), 269 aa (cattle) to 271 aa (mouse, cat, pig), and 272 aa (human).

Correspondingly, the human (BC_008678) and the murine *IL-1*β (NM_008361) CDS and protein sequences (Auron et al. 1984; Gray et al. 1986; Telford et al. 1986) were analyzed by identity comparison and evaluated with the canine, feline, porcine, bovine, equine, ant rat sequences.

As described for *IL-1*α, we cloned the canine *IL-1*β mRNA, analyzed it in detail, and submitted it to the NCBI database adding new information on the 3′UTR to the present data. As shown in Figure 1A, again the genetic structure and organization of all compared *IL-1*β cytokine transcripts are highly conserved among the different analyzed mammalians. The detailed sequence data comparison (Figure 1A) showed that all analyzed mammalian cytokine transcripts, with the exception of the cloned canine sequences (NM_001037971 and DQ923807), are composed of equal number of 7 exons. The canine sequences (NM_001037971 and DQ923807) are missing the sequence information for the 5′UTR (exon 1) that have not been completely cloned until now. Taking into account the in silico-derived structure of the canine *IL-1*β (Figure 1A), the dog shows also 7 exons with a highly conserved structure to the compared species.

The CDS identities of the canine *IL-1*β (NM_001037971, DQ923807) to the sequences of the other mammalians vary between mouse CDS (NM_008361) 71.7%, human CDS (BC_008678) 76.4%, horse CDS (U92481) 79.3%, and cat CDS (M92060) 83.8% (Table 1). The identities of the canine IL-1β protein to the protein sequences of the other mammalians vary between mouse (NP_032387) 58.3%, human protein (CAA28185) 62.8%, horse protein (AAC39256) 67.3%, and cat protein (AAA30814) 74.0% (Table 1).

In the canine IL-1β protein, a β-strand motif at aa residue position 232–240 (-PNWYISTSQ-) is highly conserved in the other described mammalians human, mouse, rat, cat, pig, sheep, horse, and cattle. The IL-1β protein sizes of the different species vary between 267 aa (cattle, dog) and 270 aa (human).

The genetic structure and organization of all compared *TNF*-α cytokine transcripts are also highly conserved among the different species. The detailed sequence comparisons (Figure 1B) showed that all *TNF*-α transcripts of the different species are composed of 4 exons. All described sequences, with the exception of feline (M92061), bovine (NM_173966), and equine cDNAs (BAA88349), show the full mRNA sequences including the CDS, 5′UTR, and 3′UTRs. The feline, bovine, and equine sequences exceptions are the missing of the sequence information coding for the 5′UTRs and 3′UTRs, surely due to the missing complete characterization of the respective mRNA transcripts.

The highest identity values among the analyzed cytokines show the CDS and proteins of TNF-α. The canine CDS for

TNF-α (AY423389) shows identities from mouse CDS (X02611) 80.4%, sheep CDS (NM_001024860) 83.9%, pig CDS 85.5% (NM_214022), to human CDS 90.8% (M26331), and cat CDS 93.3% (M92061) (Table 1). Respectively, the identities of the canine TNF-α protein sequence (AAR27885) to the protein sequences of the other species vary between mouse protein (CAA26457) 78.2%, sheep protein (NP_001020031) 79.1%, pig protein (NP_999187) 85.5%, human protein (AAA36758) 91.0%, and cat protein (AAA30818) 94.4%. The TNF-α protein sizes vary between 233 aa (pig and sheep), 234 aa (human, dog, cat and rat) to 235 aa (cattle), and 236 aa (mouse).

The overall described cytokine identity values (Table 1) of the analyzed CDS and the derived proteins show a wide variance from 43.9% to 93.43% among the CDS and from 57.1% to 94.4% for the analyzed proteins.

The described mammalian cytokine transcript and protein comparison data emphasizes the relevance of structural comparative analysis of genes and proteins for the development of therapeutic strategies aimed at the development of therapeutic approaches targeting canine disorders. The observed overall cytokine identities are variable among the different species analyzed. In particular, the performed protein alignments of the cytokines IL-1 and TNF-α showed highly conserved protein regions and domains of the compared elements among the mammalian species. In spite of the observed high variability in terms of nucleotide sequence identity, the structure of the analyzed genes is highly conservative.

The described properties of the cytokine genes IL-1 and TNF-α and their described role in the development of tumor and metabolic diseases offer various possibilities for new approaches and applications and also for existing therapy concepts. The highly conserved structure of the cytokine proteins seen in mammalians allows knowledge transfer of already established experimental data and approaches from one mammalian species to another due to the fact that essential protein properties are comparable. It is to expect that future therapeutic approaches targeting cytokine-mediated diseases in humans and dogs will benefit from each other.

Acknowledgments

This research was supported by a grant of the Gesellschaft zur Förderung Kynologischer Forschung.

References

Affolter VK, Moore PF. 2002. Localized and disseminated histiocytic sarcoma of dendritic cell origin in dogs. Vet Pathol. 39:74–83.

Alberts B, Johnson A, Lewis J, Raff M, Roberts K, Walter P. 2002. Molecular biology of the cell. 4th ed. New York: Garland Science.

Arico M. 2006. Langerhans cell histiocytosis: too many cytokines, not enough gene regulation? Pediatr Blood Cancer. 47:118–119.

Auron PE, Webb AC, Rosenwasser LJ, Mucci SF, Rich A, Wolff SM, Dinarello CA. 1984. Nucleotide sequence of human monocyte interleukin 1 precursor cDNA. Proc Natl Acad Sci USA. 81:7907–7911.

Bagby GC Jr, Dinarello CA, Wallace P, Wagner C, Hefeneider S, McCall E. 1986. Interleukin 1 stimulates granulocyte macrophage colony-stimulating activity release by vascular endothelial cells. J Clin Invest. 78:1316–1323.

Beutler B, Cerami A. 1989. The biology of cachectin/TNF—a primary mediator of the host response. Annu Rev Immunol. 7:625–655.

Braunschweiger PG, Johnson CS, Kumar N, Ord V, Furmanski P. 1988. Antitumor effects of recombinant human interleukin 1 alpha in RIF-1 and Panc02 solid tumors. Cancer Res. 48:6011–6016.

Brockhaus M, Schoenfeld HJ, Schlaeger EJ, Hunziker W, Lesslauer W, Loetscher H. 1990. Identification of two types of tumor necrosis factor receptors on human cell lines by monoclonal antibodies. Proc Natl Acad Sci USA. 87:3127–3131.

Clark BD, Collins KL, Gandy MS, Webb AC, Auron PE. 1986. Genomic sequence for human prointerleukin 1 beta: possible evolution from a reverse transcribed prointerleukin 1 alpha gene. Nucleic Acids Res. 14: 7897–7914.

Correa PA, Gomez LM, Cadena J, Anaya JM. 2005. Autoimmunity and tuberculosis. Opposite association with TNF polymorphism. J Rheumatol. 32:219–224.

Cox A, Camp NJ, Cannings C, di Giovine FS, Dale M, Worthington J, John S, Ollier WER, Silman AJ, Duff GW. 1999. Combined sib-TDT and TDT provide evidence for linkage of the interleukin-1 gene cluster to erosive rheumatoid arthritis. Hum Mol Genet. 8:1707–1713.

Daniel SL, Legendre AM, Moore RN, Rouse BT. 1993. Isolation and functional studies on feline bone marrow derived macrophages. Vet Immunol Immunopathol. 36:107–122.

Dinarello CA. 1996. Biologic basis for interleukin-1 in disease. Blood. 87:2095–2147.

Drews RT, Coffee BW, Prestwood AK, McGraw RA. 1990. Gene sequence of porcine tumor necrosis factor alpha. Nucleic Acids Res. 18:5564.

Egeler RM, Favara BE, van Meurs M, Laman JD, Claassen E. 1999. Differential in situ cytokine profiles of Langerhans-like cells and T cells in Langerhans cell histiocytosis: abundant expression of cytokines relevant to disease and treatment. Blood. 94:4195–4201.

Eisenberg SP, Brewer MT, Verderber E, Heimdal P, Brandhuber BJ, Thompson RC. 1991. Interleukin 1 receptor antagonist is a member of the interleukin 1 gene family: evolution of a cytokine control mechanism. Proc Natl Acad Sci USA. 88:5232–5236.

Estler HC, Grewe M, Gaussling R, Pavlovic M, Decker K. 1992. Rat tumor necrosis factor-alpha. Transcription in rat Kupffer cells and in vitro post-translational processing based on a PCR-derived cDNA. Biol Chem Hoppe Seyler. 373:271–281.

Fiskerstrand C, Sargan D. 1990. Nucleotide sequence of ovine interleukin-1 beta. Nucleic Acids Res. 18:7165.

Fransen L, Muller R, Marmenout A, Tavernier J, Van der Heyden J, Kawashima E, Chollet A, Tizard R, Van Heuverswyn H, Van Vliet A, et al. 1985. Molecular cloning of mouse tumour necrosis factor cDNA and its eukaryotic expression. Nucleic Acids Res. 13:4417–4429.

Furutani Y, Notake M, Yamayoshi M, Yamagishi J, Nomura H, Ohue M, Furuta R, Fukui T, Yamada M, Nakamura S. 1985. Cloning and characterization of the cDNAs for human and rabbit interleukin-1 precursor. Nucleic Acids Res. 13:5869–5882.

Furutani Y, Notake M, Fukui T, Ohue M, Nomura H, Yamada M, Nakamura S. 1986. Complete nucleotide sequence of the gene for human interleukin 1 alpha. Nucleic Acids Res 14:3167–3179.

Gray PW, Glaister D, Chen E, Goeddel DV, Pennica D. 1986. Two interleukin 1 genes in the mouse: cloning and expression of the cDNA for murine interleukin 1 beta. J Immunol. 137:3644–3648.

Howard RD, McIlwraith CW, Trotter GW, Nyborg JK. 1998. Cloning of equine interleukin 1 alpha and equine interleukin 1 beta and determination of their full-length cDNA sequences. Am J Vet Res. 59:704–711.

Huether MJ, Lin G, Smith DM, Murtaugh MP, Molitor TW. 1993. Cloning, sequencing and regulation of an mRNA encoding porcine interleukin-1 beta. Gene. 129:285–289.

Kobayashi S, Baba H, Uchida K, Shimada S, Negoro K, Takeno K, Yayama T, Yamada S, Yoshizawa H. 2005. Localization and changes of intraneural inflammatory cytokines and inducible-nitric oxide induced by mechanical compression. J Orthop Res. 23:771–778.

Kobayashi Y, Yamamoto K, Saido T, Kawasaki H, Oppenheim JJ, Matsushima K. 1990. Identification of calcium-activated neutral protease as a processing enzyme of human interleukin 1 alpha. Proc Natl Acad Sci USA. 87:5548–5552.

Lafage M, Maroc N, Dubreuil P, de Waal Malefijt R, Pebusque MJ, Carcassonne Y, Mannoni P. 1989. The human interleukin-1 alpha gene is located on the long arm of chromosome 2 at band q13. Blood 73:104–107.

Leong SR, Flaggs GM, Lawman M, Gray PW. 1988. The nucleotide sequence for the cDNA of bovine interleukin-1 beta. Nucleic Acids Res. 16:9054.

Lindblad-Toh K, Wade CM, Mikkelsen TS, Karlsson EK, Jaffe DB, Kamal M, Clamp M, Chang JL, Kulbokas EJ III, Zody MC, et al. 2005. Genome sequence, comparative analysis and haplotype structure of the domestic dog. Nature. 438:803–819.

Lomedico PT, Gubler U, Hellmann CP, Dukovich M, Giri JG, Pan YC, Collier K, Semionow R, Chua AO, Mizel SB. 1984. Cloning and expression of murine interleukin-1 cDNA in Escherichia coli. Nature. 312:458–462.

Maliszewski CR, Baker PE, Schoenborn MA, Davis BS, Cosman D, Gillis S, Cerretti DP. 1988. Cloning, sequence and expression of bovine interleukin 1 alpha and interleukin 1 beta complementary DNAs. Mol Immunol. 25: 429–437.

Maliszewski CR, Renshaw BR, Schoenborn MA, Urban JF Jr, Baker PE. 1990. Porcine IL-1 alpha cDNA nucleotide sequence. Nucleic Acids Res. 18:4282.

Marmenout A, Fransen L, Tavernier J, Van der Heyden J, Tizard R, Kawashima E, Shaw A, Johnson MJ, Semon D, Muller R, et al. 1985. Molecular cloning and expression of human tumor necrosis factor and comparison with mouse tumor necrosis factor. Eur J Biochem. 152: 515–522.

March CJ, Mosley B, Larsen A, Cerretti DP, Braedt G, Price V, Gillis S, Henney CS, Kronheim SR, Grabstein K, et al. 1985. Cloning, sequence and expression of two distinct human interleukin-1 complementary DNAs. Nature. 315:641–647.

Mattila KM, Rinne JO, Lehtimaki T, Roytta M, Ahonen JP, Hurme M. 2002. Association of an interleukin 1B gene polymorphism (-511) with Parkinson's disease in Finnish patients. J Med Genet. 39:400–402.

McGeer PL, McGeer EG. 2001. Polymorphisms in inflammatory genes and the risk of Alzheimer disease. Arch Neurol. 58:1790–1792.

Modi WS, Masuda A, Yamada M, Oppenheim JJ, Matsushima K, O'Brien SJ. 1988. Chromosomal localization of the human interleukin 1 alpha (IL-1 alpha) gene. Genomics 2:310–314.

Nash AD, Barcham GJ, Brandon MR, Andrews AE. 1991. Molecular cloning, expression and characterization of ovine TNF alpha. Immunol Cell Biol. 69:273–283.

Nedwin GE, Naylor SL, Sakaguchi AY, Smith D, Jarrett-Nedwin J, Pennica D, Goeddel DV, Gray PW. 1985. Human lymphotoxin and tumor necrosis factor genes: structure, homology and chromosomal localization. Nucleic Acids Res. 13:6361–6373.

Nicoll JA, Mrak RE, Graham DI, Stewart J, Wilcock G, MacGowan S, Esiri MM, Murray LS, Dewar D, Love S, et al. 2000. Association of interleukin-1 gene polymorphisms with Alzheimer's disease. Ann Neurol. 47:365–368.

Nishida T, Nishino N, Takano M, Sekiguchi Y, Kawai K, Mizuno K, Nakai S, Masui Y, Hirai Y. 1989. Molecular cloning and expression of rat interleukin-1 alpha cDNA. J Biochem. 105:351–357.

Ramsey IK, McKay JS, Rudorf H, Dobson JM. 1996. Malignant histiocytosis in three Bernese mountain dogs. Vet Rec. 138:440–444.

Ruuls SR, Sedgwick JD. 1999. Unlinking tumor necrosis factor biology from the major histocompatibility complex: lessons from human genetics and animal models. Am J Hum Genet. 65:294–301.

Soller JT, Murua Escobar H, Janssen M, Fork M, Bullerdiek J, Nolte I. 2006. Cytokine genes single nucleotide polymorphism (SNP) screening analyses in canine malignant histiocytosis. Anticancer Res. 26:3417–3420.

Spies T, Morton CC, Nedospasov SA, Fiers W, Pious D, Strominger JL. 1986. Genes for the tumor necrosis factors alpha and beta are linked to the human major histocompatibility complex. Proc Natl Acad Sci USA. 83:8699–8702.

Straubinger AF, Viveiros MM, Straubinger RK. 1999. Identification of two transcripts of canine, feline, and porcine interleukin-1 alpha. Gene 236:273–280.

Stylianou E, Saklatvala J. 1998. Interleukin-1. Int J Biochem Cell Biol. 30: 1075–1079.

Tazi A, Soler P, Hance AJ. 2000. Adult pulmonary Langerhans' cell histiocytosis. Thorax. 55:405–416.

Telford JL, Macchia G, Massone A, Carinci V, Palla E, Melli M. 1986. The murine interleukin 1 beta gene: structure and evolution. Nucleic Acids Res. 14:9955–9963.

Wagner JL, Palti Y, DiDario D, Faraco J. 2005. Sequence of the canine major histocompatibility complex region containing non-classical class I genes. Tissue Antigens. 65:549–555.

Webb AC, Collins KL, Auron PE, Eddy RL, Nakai H, Byers MG, Haley LL, Henry WM, Shows TB. 1986. Interleukin-1 gene (IL1) assigned to long arm of human chromosome 2. Lymphokine Res 5:77–85.

Young AJ, Hay JB, Chan JY. 1990. Primary structure of ovine tumor necrosis factor alpha cDNA. Nucleic Acids Res. 18:6723.

Zienolddiny S, Ryberg D, Maggini V, Skaug V, Canzian F, Haugen A. 2004. Polymorphisms of the interleukin-1 beta gene are associated with increased risk of non-small cell lung cancer. Int J Cancer. 109:353–356.

Corresponding Editor: Steven Hannah

3.2. Improvement of in vitro transfection efficiencies using novel methods

In collaboration with the Laser Zentrum Hannover e.V. (LZH) within the CRC / TR37 and the Equine Clinic of the University of Veterinary Medicine Hannover two novel alternative transfection methods, fs-laser based opto-perforation and the application of positively charged AuNPs in combination with DNA, were established and enhanced. The transfection efficiencies and the cell toxicity effects of these novel methods were evaluated.

IV 'Quantified femtosecond laser based opto-perforation of living GFSHR-17 and MTH53 a cells.' **Baumgart *et al.*, Optics Express, 2008.**

Femtosecond laser-assisted opto-perforation of cells is a new method offering distinct advantages over the conventional transfection methods. Transfection using fs-laser pulses allows a highly specific, cell-type independent transfection with good cell viability after transfection and high transfection efficiencies. The cell membrane is exposed to a highly focussed fs-laser pulse leasing to the formation of a transient pore allowing diffusion of exogenous nucleic acids or other molecules into the cell.
In this work, the optimum parameters concerning cell viability, efficiency, and reproducibility were evaluated to get more insight into the mechanisms of fs-laser transfection. The changes of the membrane potential were measured by patch-clamp technique on eukaryotic GFSHR-17 granulosa cells allowing to estimate the extracellular and intracellular volume exchanged while an transient pore is induced and how long this pore remains opened. The measurements revealed that the relative volume exchanged is 0.4-fold of the total cell volume. Viability and efficiency measurements were performed with different irradiation times and pulse energies by propidium iodide (PI) re-staining of the perforated cells as the cell membrane impermeable PI only enters the cells which have lost their membrane integrity. The results showed that a good balance between viability and efficiency is achieved at an irradiation time of 40 ms and 3.6 million pulses with an energy of 0.9 nJ per pulse. With this parameters, 90 % viable and 70 % perforated cells could be found. Those parameters were used subsequently to proof the functionality of fs-laser transfected cells. Therefore, canine MTH53A cells were transfected with a HMGB1-GFP fusion protein expressing vector (pEGFP-C1-HMGB1) for nucleus specific labelling and the

corresponding pEGFP-C1 vector without insert expressing only the GFP protein for total cell labelling. Fluorescence of the expressed GFP was observed 24 h and 48 h after the opto-perforation showing a complete cell labelling at cells transfected with the pEGFP-C1 vector and while transfection with the pEGFP-C1-HMGB1 led to specific labelling of the nucleus with HMGB1-GFP. In total, 100 to 150 cells were targeted by fs-laser manipulation while 30 % of those cells were determined as GFP positive 48 h post-transfectional.

IV

Quantified femtosecond laser based opto-perforation of living GFSHR-17 and MTH53 a cells.

Baumgart J, Bintig W, Ngezahayo A, Willenbrock S, Murua Escobar H, Ertmer W, Lubatschowski H, Heisterkamp A.

Optics Express. 2008. 16(5):3021-31

Own contribution:

- Cultivation of MTH53A cells and supply
- Preparation and supply with cell culture media
- Plasmid preparation of pEGFP-C1 and pEGFP-HMGB1 expression vector
- Poly-L-lysine coating of glass-bottom-dishes

Quantified femtosecond laser based opto-perforation of living GFSHR-17 and MTH53a cells

J. Baumgart[1*], W. Bintig[2], A. Ngezahayo[2], S. Willenbrock[3], H. Murua Escobar[3], W. Ertmer[4], H. Lubatschowski[1], and A. Heisterkamp[1]

[1]*Laser Zentrum Hannover e.V., Hollerithallee 8, Hannover, Germany*
[2]*Institute of Biophysics, Leibniz University, Herrenhaeuserstr. 2, Hannover, Germany*
[3]*Small Animal Clinic, University of Veterinary Medicine, Bischofsholer Damm 15, Hannover, Germany*
[4]*Institute of Quantum Optics, Leibniz University, Welfengarten 1, Hannover, Germany*
[*]*Corresponding author:j.baumgart@lzh.de*

Abstract: Opto-perforation is an interesting alternative to conventional techniques for gene transfer into living cells. The cell membrane is perforated by femtosecond (fs) laser pulses, in order to induce an uptake of macromolecules e.g. DNA. In this study, we successfully transfected a canine cell line (MTH53a) with GFP vector or a vector coding for a GFP-*HMGB1* fusion protein. The transfected cells were observed 48 hours after treatment and they were not showing any signs of apoptosis or necrosis. Based on simultaneously measured membrane potential changes during the perforation, we were able to calculate and experimentally verify that the relative volume exchanged is 0.4 times the total cell volume. Thus, for first time a quantitative predication of the amount of uptaken molecules and therefore a quantification of the transfection is possible. Additionally, this method offers new high efficient possibilities for critical transfection approaches involving special cell types, e.g. primary and stem cells.

OCIS codes: (170.0170) Medical optics and biotechnology; (350.4855) Optical tweezers or optical manipulation; (320.7090) Ultrafast lasers; (999.9999) Optical transfection

References and links

1. M. Chalfie, Y. Tu, G. Euskirchen, W.W. Ward, D.C. Prasher, "Green fluorescent protein as a marker for gene expression," Science **263**, 802–805 (1994)
2. D.C. Prasher, V.K. Eckenrode, W.W. Ward, F.G. Prendergast, M.J. Cormier, "Primary structure of the Aequorea Victoria green-fluorescent preotein," Gene **111**, 229–233 (1992)
3. E. Tekle, R.D. Astumian, P.B. Chock, "Electroporation by Using Bipolar Oscillating Electric Field: An Improved Method for DNA Transfection of NIH 3T3 Cells," *Proc. Natl. Acad. Sci.* USA **88**, 4230–4234 (1991)
4. J.L. Stilwell, D.M. McCarty, A. Negishi, R. Superfine, R.J. Samulski, "Development anf Characterization of Novel Empty Adenovirus Capsids and Teir Impact on Cellular Gene Expression," J. Virol. 12881–12885 (2003)
5. W.S. Wold, K. Doronin, K. Toth, M. Kuppuswamy, D.L. Lichtenstein, A.E. Tollefson, "Immune responses to adenoviruses: viral evasion mechanisms and their implications for the clinic," Curr. Opin. Immunol. **11**, 380–386 (1999)
6. P. Menendez, L. Wang, M. Bhatia, "Genetic Manipulation of Human Embryonic stemm cells: A System to Study Early Human Development and Potential Therapeutic Applications," Curr. Gene Ther. **5**, 375–385 (2005)
7. U.K. Tirlapur, K. König, "Targeted transfection by femtosecond laser," Nature (London) **418**, 290–291 (2002)
8. D. Stevenson, B. Agate, X. Tsampoula, P. Fischer, C.T.A. Brown, W. Sibbett, A. Riches, F. Gunn-Moore, K. Dholakia, "Femtosecond optical transfection of cells: viability and efficiency," Opt. Express **14**, 7125–7133 (2006)

#91182 - $15.00 USD Received 2 Jan 2008; revised 15 Feb 2008; accepted 16 Feb 2008; published 20 Feb 2008

9. V. Kohli, J.P. Acker, A.Y. Elezzabi, "Reversible permeabilization using high-intensity femtosecond laser pulses: applications to biopreservation," Biotechnol. Bioeng. **92**, 7 (2005)
10. A. Vogel, J. Noack, G. Huettman, G. Paltauf, "Mechanisms of femtosecond laser nanosurgery of cells and tissues," Appl. Phys. B **81**, 1015–1047 (2005)
11. A. Ngezahayo, B. Altmann, H.-A. Kolb, "Regulation of Ion Fluxes, Cell Volume and Gap Junctional Coupling by cGMP in GFSHR-17 Granulosa Cells," J. Membrane Biol. **194**, 165–176 (2003)
12. M. Bustin, "Regulation of DNA-Dependent Activities by the Functional Motifs of the High-Mobility-Group Chromosomal Proteins," Mol. Cell. Biol. **19**, 5237–5246 (1999)
13. K. König, "Multophoton Microscopy in Life Sciences," J. Microscopy **200**, 2, 83–104 (2000)
14. O.P. Hamill, A. Marty, E. Neher, B. Sakmann, F.J. Sigworth, "Improved Patch-Clamp Techniques for High-Resolution Current Recording from Cells and Cell-Free Membrane Patches," Pflügers Arch. **391**, 85–100 (1981)
15. E. Neher, B. Sakmann, "Single-channel currents recorded from membrane of denervated frog muscle fibres," Nature (London) **260**, 799–802 (1976)
16. M. Numberger, A. Draguhn, *Patch-Clamp-Technik* (Spektrum Akademischer Verlag, 1996)
17. D. Goldman, "Potential, impedance, and rectification in membranes," J. Gen. Physiol. **27**, 37–60 (1943)

1. Introduction

DNA transfection is a central tool in cellular biology to study the effect of induced gene expression or negative gene regulation. For example gene transfer coding green fluorescent protein (GFP) fusion proteins [1, 2], allows to characterize the in vivo behavior and localization of these proteins, providing a central technique to understand the respective protein biology. Several methods were developed to introduce membrane impermeable molecules into the cells. Common methods are the use of viral vectors, chemical carriers and electroporation [3] to permeabilize the membrane so that the molecules can diffuse into the cell. However, the critical aspect in cell transfection remains the efficiency achieved, toxicity, and reproducibility depending on the characteristics of the used cells. Accordingly to this, primary cells are difficult to transfect using chemical reagents [4, 5]. Usage of electroporation might as well be limited because high electrical fields can induce irreversible cell damage to sensitive cells as primary cells and stem cells due to their limited cell population [6].

A novel alternative method avoiding the described problematics is the perforation of the membrane using fs-laser pulses [7, 8]. Whereas the whole membrane is perforated by electroporation, the fs-laser pulses are focused on a small region of the membrane less than one micrometer [9] in diameter. Due to the shortness of the laser pulses, almost no heating of the irradiated volume occurs as the applied pulse duration is shorter than the thermal conduction time. The manipulation induced by these pulses is limited to the focal volume, because the effect is based on multiphoton absorption [10] and therefore relies on very high photon densities. Thus, the perforation of the cell membrane by the fs-laser pulses does not damage the whole cell, affecting only a small volume of some femtoliters [8]. The opto-perforation technique allows a "single cell targeting" and hence provides a key advantage in respect to selectivity, when compared to standard transfection.

However, the optimum parameters in terms of viability of the cells after treatment, efficiency and reproducibility are still not well known and especially the basic mechanism of the process is not yet well understood. For example, at which time pores are created, for how long they remain open and which volume is exchanged during the perforation.

In this study we combined this method with the patch-clamp technique on GFSHR-17 granulosa cells to get more insight into the mechanisms of opto-perforation. The advantage of these cells was that we have determined the parameters, which could affect the membrane potential under whole-cell configuration, in previous experiments [11]. Thus the measurement of changes of the membrane potential allows to estimate the volume exchanged between the extracellular and the intracellular space during perforation relative to the cell volume (dilution factor) and gives an idea of the maximal life time of the induced transient pore. Additionally, the estima-

#91182 - $15.00 USD Received 2 Jan 2008; revised 15 Feb 2008; accepted 16 Feb 2008; published 20 Feb 2008

tion of the exchanged volume could be used to calculate the concentration of the internalized material e.g. DNA during perforation.

As proof of principle we opto-perforated canine mammary cells (MTH53a) and transfected them with a GFP vector or a vector coding for a GFP fusion protein with the architectural transcription factor *HMGB1* (GFP-*HMGB1*). Since previous experiments with MTH53a cells have shown that these cells are suitable for transfection and expression of GFP-*HMGB1* ([12]), they represent an advantageous model to study and compare transfection by opto-perforation with classical methods. The fs-laser based transfection resulted in either completely (GFP) or nucleus specific (GFP-*HMGB1*) fluorescing cells demonstrating the ability of the transfected cells to synthesis and process recombinant proteins.

2. Materials and methods

2.1. Laser system and microscope

The laser system used in this study is a tunable Ti:sapphire laser (Coherent, Chameleon) which generates ultrashort pulses of 140 *fs* at a repetition rate of 90 *MHz*. The accessible wavelength range is between 715 *nm* to 955 *nm* and the maximum pulse energy at 800 *nm* is 14 *nJ*. The pulse duration at the focus of the laser beam is about 210 *fs* due to dispersion in the optics, especially in the objective [13].

The laser beam is guided via a shutter (Thorlabs, SC10) and an attenuator to the microscope (Zeiss, Axiovert200) (Fig. 1). A 0.8-NA NIR water immersion objective (Zeiss, Achroplan) focuses the beam into the sample. The beam enters the tubus directly via a home built reflector cube without passing the UV lamp pathway, so that the fluorescence equipment can be used alternatively. A 0.8-NA NIR water immersion objective (*Carl Zeiss AG, Achroplan*) focuses the beam into the sample with a theoretical spot size of 600 *nm* at a central wavelength of 800 *nm*. The sample is placed in a chamber with a glass bottom having a thickness of 170 μm. Successful perforation of the cell membrane is observed by fluorescence visualized by a CCD-camera, concentration measurements were performed using an EM-CCD-camera (Andor Technology, iXon).

To allow the comparison of the different laser parameters as irradiation time and pulse energy, the irradiation time was regulated by a fast shutter between 30 *ms* and 60 *ms* with an accuracy

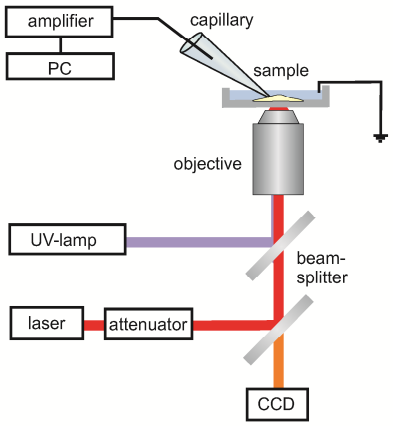

Fig. 1. (Color online) Schematic setup of the opto-perforation system.

#91182 - $15.00 USD Received 2 Jan 2008; revised 15 Feb 2008; accepted 16 Feb 2008; published 20 Feb 2008

of 1 *ms* and the pulse energy was changed by an attenuator consisting of a half waveplate and a polarizing beamsplitter cube. All experiments were realized at a central wavelength of 800 *nm*.

The imaging and manipulation program includes the manipulation tool for the nitrogen laser (Carl Zeiss AG, PALM), which was used to mark the manipulation area by cutting a rectangle into the glass cover slip. The microscope includes the fluorescence equipment, the UV lamp, the filters for propidium iodide (coupled to DNA) and for GFP, and the patch-clamp setup.

2.2. *Patch-clamp studies*

The membrane potential of the cells was measured by the patch-clamp technique [14] (Fig. 2) in current clamp modus using an amplifier (Axon Instruments, Axopatch-1D) and the computer interface (Instrutech Corporation).

The whole cell configuration was established on cells using a pipette-solution consisting of in mM: 100 K^+-Gluconat, 40 KCl, 10 Hepes (4-(2-hydroxyethyl)-1-piperazineethanesulfonic acid), 5 Na_2ATP, 1 Glucose, 1 $MgCl_2$, 5 EGTA (ethylene glycol tetraacetic acid), 0.25 cAMP (3'-5'-cyclic adenosine monophosphate), 0.5 cGMP (cyclic guanosine monophosphate), pH 7.4 and an osmolarity 295 ± 5. The patch electrode with the pipette-solution has a resistance of 10 $M\Omega$.

During the patch-clamp measurements the cells were maintained in NaCl-media containing in mM: 121 NaCl, 5 KCl, 0.8 $MgCl_2$, 1.8 $CaCl_2$, 6 $NaHCO_3$, 5.5 glucose, 25 HEPES, pH 7.4 and an osmolarity 295 ± 5.

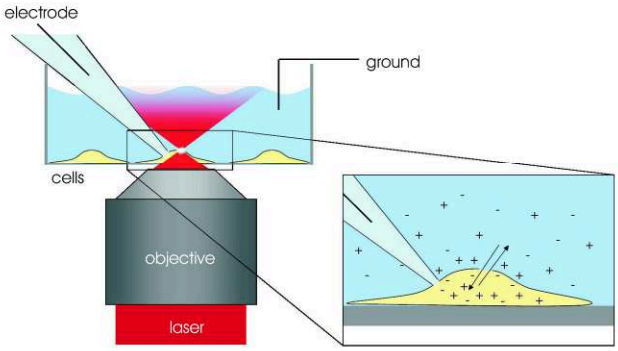

Fig. 2. (Color online) Sketch of simultaneous patch-clamp and opto-perforation of a living cell. The induced transient pore allows the diffusion of molecules through the membrane.

2.3. *Cell cultures and labeling of granulosa cells*

GFSHR-17 granulosa cells of rat were cultivated on cover slips using DMEM 8900 (Dulbecco's Modified Eagle Medium) supplemented with 5% fetal calf serum (FCS) and the antibiotics penicillin, streptomycin and partricin. For laser-manipulation, a cover slip with cells was transferred in a perfusion chamber containing 0.5 *ml* of NaCl-media and 100 to 1000 μM of lucifer yellow (LY) or 1.5 μM of propidium iodide (PI).

2.4. *Opto-perforation and viability control*

PI was dissolved in the media before manipulation. The laser was focussed onto the membrane of the cell to induce a transient pore and an uptake of the solution with the dye molecules by

#91182 - $15.00 USD Received 2 Jan 2008; revised 15 Feb 2008; accepted 16 Feb 2008; published 20 Feb 2008

diffusion. After treatment the cells were observed by fluorescence microscopy to verify the uptake of the dye and then washed with PBS and incubated in PBS for 90 minutes.

Then the viability of the treated cells was controlled by relabeling the sample with propidium iodide and comparing the fluorescence intensity before and after restaining. As the fluorescence intensity of the perforated cells is very low due to the small perforated area and the short interaction time of the laser, there should be an increase of fluorescence intensity in the cells with a damaged cell membrane which indicates the cells to be in a pathologic state.

2.5. Cell cultures of canine mammary cells and transfection by opto-perforation

Canine mammary cells MTH53a were cultivated in poly-L-lysine coated glass-bottom-dishes (MatTek) using M199 media (Gibco) supplemented with 20% FCS and penicillin and streptomycin. The demonstration of the principle of transfection using opto-perforation was performed either with 50 $\mu g/ml$ non-recombinant pEGFP-C1 vector plasmid (BD Bioscience Clontech) for total cell labeling or with 50 $\mu g/ml$ recombinant pEGFP-C1-*HMGB1* plasmid for nucleus specific labeling. The laser was focused onto the membrane to induce perforation. After treatment, the cells were washed with NaCl-media and incubated for 48 hours in the culture media. The uptake and expression of DNA was verified by fluorescence microscopy.

3. Results

3.1. Membrane potential measurement during opto-perforation by fs-laser pulses

During opto-perforation by fs-laser pulses neither shrinkage nor swelling of the cells under the present conditions were observed indicating that the cell volume was not affected. However, perforation of the membrane allows a bi-directional flux of solution into and out of the cells (Fig. 2). As long as the pore is open a volume exchange between the intracellular and extracellular space takes place. In the literature, a volume of some femtoliters is predicted [8]. For material e.g. DNA dissolved in the extracellular solution, the estimation of exchanged volume could give an indication of the concentration which can be achieved in the intracellular space after opto-perforation. Measurement of the change of membrane potential using the whole-cell configuration of the patch-clamp technique [14, 15, 16] allows to determine the exchanged volume in relation to the cell volume during opto-perforation. The verification of the uptake of molecules in these experiments was performed with PI and LY dissolved in the extracellular media. PI is only fluorescent when bound to DNA. Thus, it is not necessary to wash the sample for the fluorescence observation which could lead to the loss of the whole-cell configuration. LY offers the advantage that it could be also added to the patch pipette solution at a determined concentration. Measurement of the fluorescence of LY introduced into the cells after establishment of whole-cell with different concentration of LY in the pipette solution offered a calibration for fluorescence of LY introduced in the cells by opto-perforation. Thus allowing a verification of the theoretical calculated relative volume exchanged.

The resting membrane potential of granulosa cells was found to be about $-45\ mV$. Fs-laser irradiation divides two regimes of depolarization depending on the focusing of the laser relative to the membrane, characterized by the formation or absence of a visible gas bubble. This gas bubble is due to chemical and accumulative thermal effects, theoretically described as low density plasma regime at *MHz* repetition rate and pulse energies below the optical breakdown [10].

In both cases the membrane potential increases about 2 to 5 mV (Fig. 3(Λ)). The observed depolarization time Δt in both cases is some milliseconds longer than the laser irradiation time t.

$$\Delta t > t \tag{1}$$

#91182 - $15.00 USD Received 2 Jan 2008; revised 15 Feb 2008; accepted 16 Feb 2008; published 20 Feb 2008

While the cases showing no visible formation of the gas bubble were characterized by a slow potential repolarization, in the second case showing the gas bubble the depolarization was followed by a second step of a strong depolarization of 10 to 20 mV (Fig. 3(A) and 3(B)). After the manipulation, the potential repolarizes slowly or stays on the new level some mV above the initial value. The depolarization continues some milliseconds after the laser irradiation, as in the first case, $\Delta t > t$. After that, the cell repolarizes in some cases but slowly compared to the depolarization. The cases without bubble formation where only the first step of depolarization was achieved, no fluorescence was detectable whereas in the case of bubble formation an uptake of chromophores could be detected. Thus, the induced gas bubble can be used as indicator of perforation of the cell membrane and successful uptake of dye molecules.

3.2. Determination of the exchanged volume during opto-perforation

According to the Nernst and Goldman equations [17] (for constant dye-concentration in the media and constant cell volume) the relative exchanged cell volume can be calculated by the following equation:

$$\frac{\alpha}{V} = \frac{(1 - exp(-\Delta U_m F/RT)}{(1 - exp(U_m F/RT))} \tag{2}$$

where V is the cell volume, α the exchanged volume, R the gas constant, T the absolute temperature, F the Faraday constant, U_m the initial membrane potential and ΔU_m the change of membrane potential.

Knowing the membrane potential during laser irradiation, the relative exchanged cell volume can be calculated. With the mean value of 10 mV membrane potential depolarization, the relative exchanged volume α/V is about 0.4. For the GFSHR-17 granulosa cells with a diameter of 10 μm and a volume of 500 femtoliters (fl), the exchanged volume is 200 fl. At 600 μM dye concentration in the extracellular media, the intracellular dye concentration should be about 240 μM after opto-perforation.

These quantitative considerations were verified by measuring the fluorescence intensity of fs-laser induced uptake of LY by granulosa cells. Compared to PI, LY offers the advantage of a fluorescence independent on the binding to any other molecules and is therefore an excellent dye for concentration measurements. For calibration, fluorescence intensities were determined by introducing a defined LY concentration into the cell via the patch-clamp-pipette in whole-cell configuration, equilibration between the pipette-media and the cell was achieved after 15

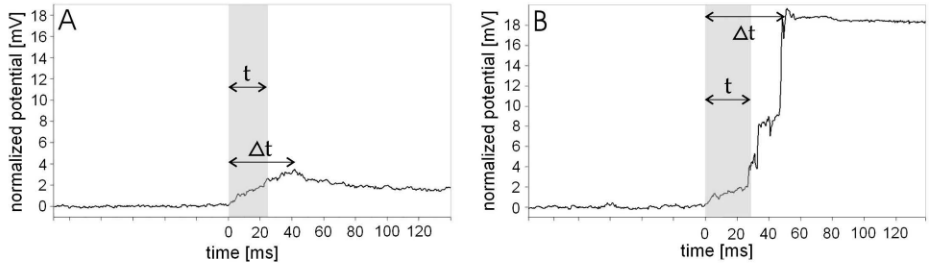

Fig. 3. The membrane potential of a granulosa cell during fs laser perforation. The laser pulse energy was 0.9 nJ. The grey bar represents the laser irradiation time t for the opto-perforation, Δt represents the maximum depolarization time. (A) There was no bubble formation during the treatment (n = 7); (B) a small gas bubble was created during the treatment (n = 4).

#91182 - $15.00 USD Received 2 Jan 2008; revised 15 Feb 2008; accepted 16 Feb 2008; published 20 Feb 2008

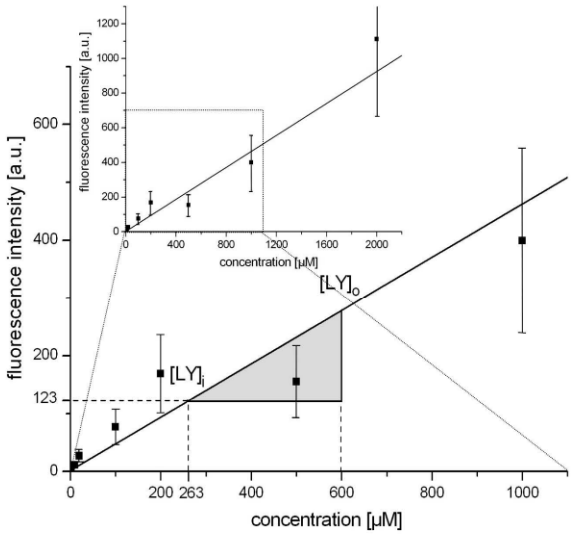

Fig. 4. The fluorescence intensity of LY introduced in cells at different concentrations via the patch-clamp pipette. The data points represent average standard deviation for at least 5 different cells for each concentration. The linear fit ($f(x) = 0.46x + 1.77$) was used to estimate the concentration of LY in the cells after opto-perforation induced uptake of the chromophor dissolved in the extracellular solution. The area of interest for the used extracellular concentrations during opto-perforation is zoomed out. As an example, to the extracellular LY concentration ($[\mathrm{LY}]_o$) of 600 μM corresponds an intracellular concentration ($[\mathrm{LY}]_i$) of 263 μM and a fluorescence intensity of 123 $a.u.$ (table 3.2) represented by the grey triangle.

minutes. The fluorescence can then be linked to the concentration as reference intensity.

The concentration of the LY in the pipette-media was chosen between 2 and 2000 μM. The fluorescence intensity increased linearly with increasing dye concentration (Fig. 4). The measured values fit well to the linear fit between 200 μM and 2 mM. At lower concentrations (2 and 10 μM) the fluorescence was to low to be clearly distinguished from the background.

We performed opto-perforation in presence of different concentrations of LY in the extracellular solution ($[LY]_o$). Since we assumed a relative volume exchange of 0.4, a dilution of LY by a factor of 2.5 in the cell was expected. The mean fluorescence intensity of the cells after laser-manipulation and after washing with NaCl-media was measured for an extracellular concentration of 1 mM, 600, 200, and 100 μM at standard laser parameters, 40 ms irradiation time and 0.9 nJ pulse energy (30 to 50 cells per concentration).

At a LY concentration of 1 mM in the extracellular media the calculation after equation (2) results in an intracellular concentration of 400 a.u. after opto-perforation. Following the reference curve for the concentration (Fig. 3), we expect a fluorescence intensity of 186 a.u. after perforation. We observed a mean intensity of 155 a.u. which leads to an intracellular concentration ($[LY]_i$) of 332 μM and a factor of exchanged media α/V of 0.33. For 600, 200, and 100 μM the corresponding factor of relative exchanged media α/V is 0.44, 0.35, and 0.37 respectively (table 3.2). The comparison of the theoretical and the measured values show that a quantitative estimation of the amount of material e.g. DNA which is taken up during

#91182 - $15.00 USD Received 2 Jan 2008; revised 15 Feb 2008; accepted 16 Feb 2008; published 20 Feb 2008

opto-perforation is possible. This represents to our knowledge the first attempt to quantify this parameter.

Table 1. Fluorescence intensity of LY measured in cells after application of opto-perforation in presence of different LY concentrations in the extracellular solution ($[LY]_o$). The values were reported on the calibration line (Fig. 4) to estimate the intracellular LY concentration ($[LY]_i$). The measured relative volume exchanged is given as $[LY]_i/[LY]_o$. The expected intracellular concentrations were calculated by assuming $\alpha/V = 0.4$. These values were reported to the calibration curve to obtain the expected fluorescence intensities. All measured values include $\pm$ standard deviation.

extracellular concentration $([LY]_o)$ $[\mu M]$	expected intracellular concentration $[\mu M]$ (with $\alpha/V = 0.4$)	measured intracellular concentration $([LY]_i)$ $[\mu M]$ (linear fit)	measured fluorescence intensity $[a.u.]$	relative exchanged volume α/V $([LY]_i/[LY]_o)$
1000	400	304 ± 91	142 ± 30	0.33 ± 0.10
600	240	263 ± 79	123 ± 37	0.44 ± 0.13
200	80	70 ± 21	34 ± 12	0.35 ± 0.10
100	40	37 ± 11	19 ± 6	0.37 ± 0.11

3.3. *Energy and irradiation time dependence of opto-perforation*

The energy deposited into the cells has to be as low as possible to avoid damage while the efficiency of the uptake of molecules increases at longer irradiation times and higher pulse energies. The viability of the cells strongly depends on the used pulse energy, the irradiation time of the laser beam and the position of the focal point relatively to the membrane. The visualization of the viability was performed by restaining the cells with propidium iodide. In cells whose membrane is damaged, the fluorescence intensity is higher after the restaining as the fluorophore is impermeable to the membrane and it can not enter the cells if the physiologic structure is intact after the treatment. Thus the dye highlights the cells that are in a pathologic state (Fig. 5).

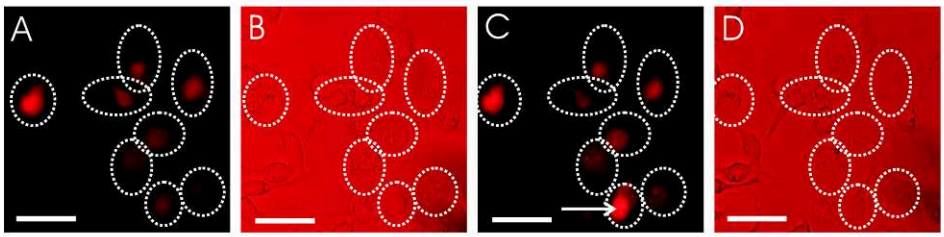

Fig. 5. (Color online) Opto-perforated granulosa cells in presence of PI. (A) Fluorescence image of granulosa cells growing on a cover slit during opto-perforation, the treated cells are highlighted by the dashed circles. 1.5 μM PI is solved in the media and the laser parameters were 0.9 nJ and 40 ms. All manipulated cells are fluorescent. (B) Bright field image of the same cells. C: Fluorescence image of the cells after 90 minutes incubation in PBS. The cells were re-stained with PI to verify the viability. The cell pointed out by the arrow is representative for a cell whose membrane is damaged and therefore still permeable for the fluorophore. D: Bright field image after the incubation time. Scale bars: 30 μm.

#91182 - $15.00 USD Received 2 Jan 2008; revised 15 Feb 2008; accepted 16 Feb 2008; published 20 Feb 2008

The parameters for the opto-perforation were chosen as follows. The central wavelength at 800 *nm*, a repetition rate of 90 *MHz* and pulse energies between 0.7 *nJ* and 1.1 *nJ* were used for the opto-perforation of the granulosa cells. The irradiation times were chosen between 30 *ms* and 60 *ms* (Fig. 6). The efficiency increased with the pulse energy and the irradiation time, while the viability observed 90 minutes after the treatment decreased. Every parameter combination was realized at 40 to 60 cells.

In the region of short irradiation time of 30 *ms* the viability of the cells is at up to 90% for pulse energies up to 0.9 *nJ*. For longer irradiation times as 60 *ms* and high pulse energy of 1.1 *nJ* the viability of the cells decreases to 40%.

In contrast, the efficiency of dye uptake is at 40% or lower for 30 *ms* irradiation time and pulse energies up to 1 *nJ*. The efficiency increases with increasing pulse energy and increasing irradiation time to 70% at 1.1 *nJ* and 60 *ms* (Fig. 6).

However, a good balance between viability and efficiency can be found at 40 *ms* irradiation time and thus 3.6 million pulses with an energy per pulse of 0.9 *nJ*. For these parameters, the viability is 90% and the efficiency 70%.

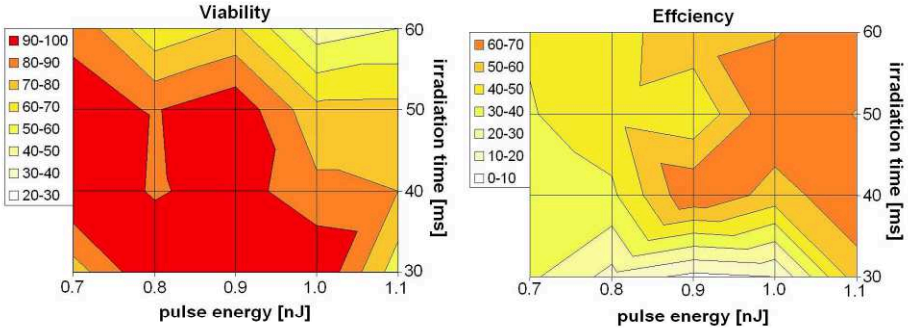

Fig. 6. (Color online) The viability of the cells (A) and the efficiency of the introduction of PI into the cells (B) dependent on the pulse energy and the irradiation time.

3.4. *Transfection of MTH53a cells by fs-laser pulses with pEGFP-C1 and pEGFP-C1-HMGB1 vectors*

The transfection of the canine mammary cells was performed at 40 *ms* irradiation time and thus 3.6 million pulses with an energy per pulse of 0.9 *nJ*, leading to a viability of the cells after treatment of about 90% and an efficiency of about 70%. The cells were treated either in presence of 50 $\mu g/ml$ non-recombinant pEGFP-C1 vector or recombinant pEGFP-C1-HMGB1 vector in the culture media. The fluorescence was observed 24 and 48 *h* after treatment allowing an expression and processing of the respective recombinant proteins. The cells transfected with pEGFP-C1 vector showed a labeling of the complete cell (Fig. 7) by the synthesized recombinant GFP proteins. The cells transfected with the pEGFP-C1-*HMGB1* vector showed a specific labeling of the nucleus (fig. 4B). These specific labeling shows that the cells are post transfected still able to synthesis the pEGFP-C1-*HMGB1* fusion protein and to transport the chromatin associated architectural transcription factor *HMGB1* to its native cellular localization in the nucleus.

#91182 - $15.00 USD Received 2 Jan 2008; revised 15 Feb 2008; accepted 16 Feb 2008; published 20 Feb 2008

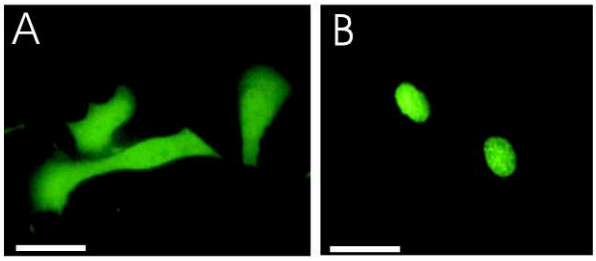

Fig. 7. (Color online) MTH53a cells transfected with either pEGFP-C1 or pEGFP-C1-*HMGB1* vectors. (A) Complete labelling of MTH53a cells by GFP. (B) Specific labelling of the MTH53a cell nucleus by pEGFP-C1-*HMGB1* fusion proteins. The opto-perforation was performed at a wavelength of 800 *nm*, a pulse energy of 0.9 *nJ* and an irradiation time of 40 *ms*. The images were taken 48 hours after the treatment. Scale bars: 20 μm.

4. Discussion and conclusion

Transfection of macromolecules represents a key technique in molecular biology. The methods currently applied e.g. viral vectors, chemical carriers, lipofection and electroporation face several critical problems in terms of the achieved efficiency, toxicity, and reproducibility. Although for multiple applications the systems used are sufficient, several experimental approaches require more sophisticated methods. Parameters like a defined amount of induced molecule intake, reduced cell damage and high transfection efficiency represent critical parameters when working with cell type requiring extremely high complexity handling e.g. stem cells. The used fs-laser based opto-perforation of cells allows a defined control of the described critical parameters. In detail the measurements of the cell membrane potential showed two different behaviors during opto-perforation.

As described previously the membrane potential increased in both cases instantaneously about 2 to 5 *mV* at all parameters. If no bubble was created fluorescence analysis using PI did not show an uptake of the fluorophore in contrast to the case of bubble formation showing a characteristic high PI uptake. The critical parameters for formation or non-formation of gas bubbles are combination of irradiation time, pulse energy, and position of the laser focus relatively to the membrane. It can therefore be assumed that without induced bubble formation no pore was formed in the membrane and the observed change in membrane potential is related to change of permeability of the membrane to ions which did not involve larger molecules such as chromophores. It is also possible that an inadequate focusing of the laser beam generated a very small pore which closed too quickly to allow an uptake of the molecules dissolved in the extracellular solution.

In the case of bubble formation, the potential depolarized first as described above and, as soon as the bubble was created, the potential increased by another 10 *mV* or more. After the manipulation, the membrane potential repolarized again or stayed at the same level but did not rise to 0 *mV* in most cases. These results show that there was an exchange of intra and extracellular media, especially when a bubble was induced which can be used as an indicator for successful opto-perforation. Additionally it can be concluded that the cell is still alive and it is able to repair the laser induced damage.

The maximum depolarization time ($\Delta t = 60$ *ms*) is longer than the irradiation time ($t = 30$ *ms*). Thus the induced pore seems to be open longer than the increasing time of the potential. By a change in membrane potential of 10 *mV*, the relative volume exchange between the cells and the extra cellular solution during opto-perforation was calculated to be about 0.4 times

#91182 - $15.00 USD Received 2 Jan 2008; revised 15 Feb 2008; accepted 16 Feb 2008; published 20 Feb 2008

the cell volume. At extracellular LY concentration of 1000, 600, 200, and 100 μM, a relative volume exchange α/V of respectively 0.33, 0.44, 0.35, and 0.37 were found. The theoretically estimated value is in perfect agreement with the average value experimentally obtained of about 0.37 (table 3.2), indicating that a quantitative estimation of the material taken up during opto-perforation is possible.

The uptake of fluorochromes by perforation of the membrane by fs laser pulses was optimized in the *MHz* regime using propidium iodide as fluorescent molecule. In the range between 0.7 *nJ* and 1.1 *nJ* pulse energy and irradiation times between 25 *ms* and 60 *ms*, the viability of the cells varies between 20% and 90%. In the same manner, the efficiency varies between 90% and 10%. As a very satisfactory result the viability of the cells is about 80% at a pulse energy of 0.9 *nJ* and an irradiation time of 40 *ms* yielding an efficiency of succeed membrane perforation of about 70%.

At these parameters, we successfully transfected canine mammary cells with non-recombinant pEGFP-C1 vector or recombinant pEGFP-C1-*IIMGB1* vector. This specific labeling shows that the fs-laser based transfection allows even to successfully transfect cells which are still able to synthesize and process recombinant proteins. For pEGFP-C1 or recombinant pEGFP-C1-*HMGB1* vector, 100 to 150 cells were targeted. 48 h after opto-perforation the expression of either gene was observed in about 30% of the targeted. The experiments with PI have shown that transfer of material and cell survival after opto-perforation is achieved in 70% of the targeted cells (Fig. 6). The observed difference may be related to different cellular behavior with respect to the introduced DNA. Further experiments should clarify this issue. The possibility of quantification could be used to calculate the number of DNA molecules taken up during opto-perforation. At an extracellular concentration of the pEGFP-*HMGB1* vector of 50 $\mu g/ml$, about 10 fg DNA molecules enter into the perforated cells during laser irradiation at a cell diameter of 10 μm.

The system established allows a controlled transfection including the possibility to determine the amount of uptake of molecules and thus allowing to regulate the amount of effector molecules transfected into the cell. Consequently this allows a gentle procedure for e.g. stem cell transfection opening new possibilities for stem cell based experimental and therapeutic approaches. Finally, the presented technique could also be applied for cell specific transfection in tissue (in situ) where various types of cells are present.

Acknowledgments

We would like to acknowledge Prof. Bernhard Keller (Georg-August University, Goettingen) for placing the patch-clamp setup to our disposal and BFI optilas for providing the EM-CCD camera. Parts of this work were funded by the German Research Foundation (DFG) (within the Transregio 37 and the excellence cluster REBIRTH).

#91182 - $15.00 USD Received 2 Jan 2008; revised 15 Feb 2008; accepted 16 Feb 2008; published 20 Feb 2008

V ‘Comparison of nanoparticle-mediated transfection methods for DNA expression plasmids: efficiency and cytotoxicity.’ **Durán & Willenbrock *et al*., Journal of Nanobiotechnology, 2011.**

In addition to the novel transfection method using fs-laser opto-perforation, nanoparticles have been taken into account as well as a new possibility for achieving enhanced transfection efficiencies. Gold nanoparticles (AuNP) are currently focussed in research. Herein, a new generation of stabiliser-free AuNP generated by pulsed laser ablation in liquids (PLAL) as recently attracted special interest.

The data concerning toxic potential of this new generation of PLAL-AuNP in combination with DNA expression vectors is still marginal. Therefore, in this study the transfection efficiency and cytotoxic effects of five different NP-mediated transfection protocols (two sizes of PLAL-AuNPs, one size of commercially available chemically generated AuNPs, two protocols with magnetic nanoparticles) was evaluated after transfection of MTH53A cells with two different eukaryotic vectors (vector backbone: pIRES-hrGFP II) leading to simultaneous but separate expression for a recombinant target protein (canine HMGB1 or equine IL-12) and the humanized renilla Green Fluorescent Protein (hrGFP). The results of the different protocols were compared to the efficiencies achieved by transfection with the conventional reagent FuGENE® HD (FHD). The efficiency analyses were carried out using fluorescence microscopy and GFP-based flow cytometry. The biological functionality of the expressed recombinant proteins was confirmed by immunofluorescence directed against canine HMGB1 and equine IL-12 after transfection. To assess the cell toxicity of each protocol, the cell proliferation was measured by BrdU incorporation and the percentage of PI positive cells was determined by flow cytometry.

The efficiency analyses revealed that the addition of PLAL-AuNPs increased the transfection efficiency significantly using the pIRES-hrGFP II-eIL-12 vector (FHD: 16 %; AuNP size 1: 28 %, AuNP size 2: 25 %) and the pIRES-hrGFP II-rHMGB1 vector (FHD: 31 %; PLAL-AuNP size 1: 46 %; PLAL-AuNP size 2: 50 %). The commercial available AuNP showed only an improvement of transfection efficiency for the pIRES-hrGFP II-*eIL-12* vector (28 %) whereas the efficiency was significantly lower at pIRES-hrGFP II-*rHMGB1* transfections (23 %) in comparison to the conventional FHD protocol (31 %). No significant cytotoxic effect could be observed at the application of PLAL-AuNP by PI staining and the cell proliferation

measurement whereas the commercially available AuNP induced a significant increase in the percentage of PI positive cells and a negative effect on cell proliferation. The two protocols using magnetic nanoparticles showed no significant improve in the transfection efficiency but resulted in the best tolerance concerning cell viability and proliferation.

The detection of protein expression via immunofluorescence after AuNP mediated pIRES-hrGFP II-*eIL-12* and pIRES-hrGFP II-*rHMGB1* transfection verified the functionality of the nuclear acting HMGB1 and the complex eIL-12 assembled of two separate subunits and the localisation of both recombinant proteins at their expected destination.

V

Comparison of nanoparticle-mediated transfection methods for DNA expression plasmids: efficiency and cytotoxicity.

Durán MC, Willenbrock S*, Barchanski A, Müller JM, Maiolini A, Soller JT, Barcikowski S, Nolte I, Feige K, Murua Escobar H.*

**equally contributed authorship*

Journal of Nanobiotechnology. 2011. 20;9:47

Own contribution:

- Participation in the expression vector design and construction, cell culture and transfection experiments, fluorescence and immunofluorescence microscopy analysis
- Partial drafting of the manuscript

Durán *et al. Journal of Nanobiotechnology* 2011, **9**:47
http://www.jnanobiotechnology.com/content/9/1/47

JOURNAL OF NANOBIOTECHNOLOGY

RESEARCH Open Access

Comparison of nanoparticle-mediated transfection methods for DNA expression plasmids: efficiency and cytotoxicity

María Carolina Durán[1†], Saskia Willenbrock[2†], Annette Barchanski[3], Jessika-M V Müller[1], Arianna Maiolini[2], Jan T Soller[4], Stephan Barcikowski[5], Ingo Nolte[2], Karsten Feige[1] and Hugo Murua Escobar[2*]

Abstract

Background: Reproducibly high transfection rates with low methodology-induced cytotoxic side effects are essential to attain the required effect on targeted cells when exogenous DNA is transfected. Different approaches and modifications such as the use of nanoparticles (NPs) are being evaluated to increase transfection efficiencies. Several studies have focused on the attained transfection efficiency after NP-mediated approaches. However, data comparing toxicity of these novel approaches with conventional methods is still rare.
Transfection efficiency and methodology-induced cytotoxicity were analysed after transfection with different NP-mediated and conventional approaches. Two eukaryotic DNA-expression-plasmids were used to transfect the mammalian cell line MTH53A applying six different transfection protocols: conventional transfection reagent (FuGENE HD, FHD), FHD in combination with two different sizes of stabilizer-free laser-generated AuNPs (PLAL-AuNPs_S1,_S2), FHD and commercially available AuNPs (Plano-AuNP), and two magnetic transfection protocols. 24 h post transfection efficiency of each protocol was analysed using fluorescence microscopy and GFP-based flow cytometry. Toxicity was assessed measuring cell proliferation and percentage of propidium iodide (PI%) positive cells. Expression of the respective recombinant proteins was evaluated by immunofluorescence.

Results: The addition of AuNPs to the transfection protocols significantly increased transfection efficiency in the pIRES-hrGFPII-*eIL-12* transfections (FHD: 16%; AuNPs mean: 28%), whereas the magnet-assisted protocols did not increase efficiency. Ligand-free PLAL-AuNPs had no significant cytotoxic effect, while the ligand-stabilized Plano-AuNPs induced a significant increase in the PI% and lower cell proliferation. For pIRES-hrGFPII-*rHMGB1* transfections significantly higher transfection efficiency was observed with PLAL-AuNPs (FHD: 31%; PLAL-AuNPs_S1: 46%; PLAL-AuNPs_S2: 50%), while the magnet-assisted transfection led to significantly lower efficiencies than the FHD protocol. With PLAL-AuNPs_S1 and _S2 the PI% was significantly higher, yet no consistent effect of these NPs on cell proliferation was observed. The magnet-assisted protocols were least effective, but did result in the lowest cytotoxic effect.

Conclusions: This study demonstrated that transfection efficiency of DNA-expression-plasmids was significantly improved by the addition of AuNPs. In some combinations the respective cytotoxicity was increased depending on the type of the applied AuNPs and the transfected DNA construct. Consequently, our results indicate that for routine use of these AuNPs the specific nanoparticle formulation and DNA construct combination has to be considered.

* Correspondence: Hugo.Murua.Escobar@tiho-hannover.de
† Contributed equally
[2]Small Animal Clinic and Research Cluster of Excellence "REBIRTH", University of Veterinary Medicine, Buenteweg 9, 30559 Hannover, Germany
Full list of author information is available at the end of the article

Background

Transfection of eukaryotic cells is a key technology in cell biology being used in several areas of basic and therapeutic research. The critical points in these experimental approaches are the achieved transfection efficiencies and the reproducibility of the performed experiments. Therefore, a stable high transfection rate with low methodology induced side effects in terms of toxicity would be desirable. Furthermore, the methods used should not interfere with the functionality of the delivered molecules such as large DNA expression plasmids or small RNAs such as siRNAs and miRNAs.

Currently, several non-viral transfection methods for eukaryotic cells are used to introduce membrane impermeable molecules into the cells. However, the efficiency, toxicity, and reproducibility, which may vary depending on the characteristics of the cells used, remain a crucial aspect in cell transfection. Consequently, various methods and modifications are currently being evaluated to increase efficiency and reduce toxicity. Thus, both novel laser-based transfection methods [1] as well as nanoparticle (NP) approaches have been evaluated in recent studies [2-4]. Considering the latter, gold Nanoparticles (AuNPs) are in the focus of intense research due to their chemical stability, electrodensity and -affinity to biomolecules such as DNA, when these AuNPs are charged [5]. However, the inherent characteristics of the applied NPs could induce different toxic effects on cells due to several factors such as particle number and size, surface dose, surface coatings, degree of agglomeration, surface charges on particles and method of particle synthesis as well as post-synthetic modifications. During or after most forms of NP synthesis, the generated NPs are modified to prevent aggregation or induce disaggregation. The surface modification and surface charge can have a major impact on the biological response to various particles, therefore, the particle specific surface modification and the agents are an important factor that must be considered when choosing particular NPs [6].

The valuable characteristics of AuNPs make them suitable to act as plasmid DNA carriers and transfection enhancers. Similarly, magnetic NPs loaded with the nucleic acid of interest are used to increase transfection efficiency by applying magnetic force to the DNA-NP complexes. These magnetic DNA-NP complexes are drawn towards the outer cell membrane via magnetic force and are subsequently taken up by the cell via endocytosis.

AuNPs can be generated using various methods, most of which rely on chemical reactions or gas pyrolysis, which carry the risk of agglomeration or contamination with impurities such as citrate and residual precursors like chloroauric acid [7].

Pulsed laser ablation in liquids (PLAL) has been reported to present advantages in NP generation such as low restriction for the choice of the source material allowing the generation of highly pure colloidal particles [8]. The generated pure AuNPs with the oxidation states Au^{+} and Au^{+3} were reported to have a unique surface chemistry and to be free of stabilizers, as a result of the chemical composition of the liquid media used during synthesis [8]. This inherent charge given to these AuNPs, without adding a special coating that could have a potential cytotoxic effect make these NPs interesting for DNA-binding and cell transfection. Previous studies demonstrated that unmodified, circular, negatively charged DNA molecules adsorb easily onto these positively charged NPs [2]. Moreover, the incubation of these AuNPs with plasmid DNA did not alter the uptake of the vector through the plasma membrane in presence of a transfection reagent, and showed no apparent effect on the biological activity of the produced recombinant protein [9]. However, although AuNP approaches have gained popularity, the data concerning the toxic potential of these particles is still marginal and the characterisation of the toxic potential of AuNPs in combination with complex DNA expression plasmids is mostly limited to model molecules.

Herein, we analysed the transfection efficiency and cytotoxicity of different NP-mediated transfection approaches after the transfection of a mammalian cell line with two different eukaryotic expression vectors encoding simultaneously for an expression protein (canine HMGB1 or equine IL-12) and the humanized renilla Green Fluorescent Protein (hrGFP). Results were compared to those obtained using a conventional standard transfection protocol (FuGENE HD, Roche, Mannheim, Germany).

Results

Transfection Efficiency

Fluorescence Microscopy

The uptake of plasmid DNA was primarily evaluated by comparing the GFP positive cells to the total quantity of cells showing blue DAPI fluorescence dye staining, thus attaining an estimate of the transfection efficiency. After 24 h incubation, the transfection process both with the plasmid DNA and with the transfection reagents alone did not induce major negative effects on the cells. An exception to this was the addition of the Plano-AuNP to the cells, where 24 h post-transfectional cells showed advanced apoptotic signs. The transfection efficiency of cells transfected with the Plano-AuNP, PLAL-AuNP Size 1 and Size 2 protocol was apparently higher than that achieved with the conventional FHD transfection reagent or with the magnetic transfection protocols (MATra-A, MA Lipofection) (Images not shown).

Flow cytometry analysis of GFP expression

The mean transfection efficiencies of the FHD transfection were 16.22% and 31.52% for pIRES-hrGFPII-*eIL-12* (Figure1; Table 1) and pIRES-hrGFPII-*rHMGB1* (Figure 2; Table 1), respectively.

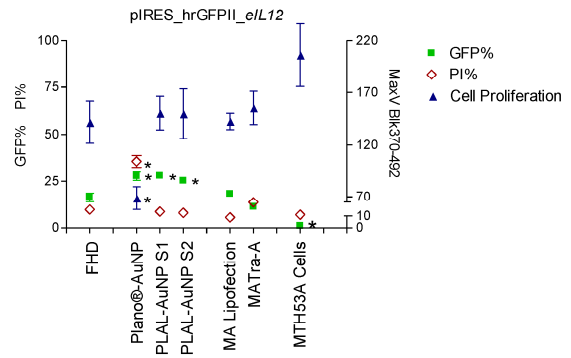

Figure 1 Transfection efficiency and toxicity of pIRES-hrGFPII-*eIL-12*. GFP- (■) and PI- (◊) positive cells 24 h after transfection with pIRES-hrGFPII-*eIL-12*. Mean cell proliferation (▲) (48 h and 72 h after transfection with pIRES-hrGFPII-*eIL-12*). Each bar represents a mean ± SD. * p ≤ 0.05.

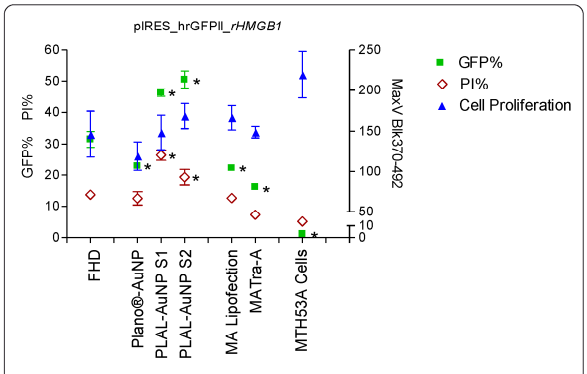

Figure 2 Transfection efficiency and toxicity of pIRES-hrGFP-*rHMGB1*. GFP- (■) and PI- (◊) positive cells 24 h after transfection with pIRES-hrGFP-*rHMGB1*. Mean cell proliferation (▲) (48 h and 72 h after transfection with pIRES-hrGFP-*rHMGB1*). Each bar represents a mean ± SD. * p ≤ 0.05.

When AuNPs (Plano-AuNP and PLAL-AuNPs Size 1 and 2) were added, transfection efficiencies were significantly increased for the pIRES-hrGFPII-*eIL-12* vector, reaching an almost two fold increase with PLAL-AuNPs Size 2 and Plano-AuNP (FHD: 16.22%; PLAL-AuNPs Size 2: 27.80%; Plano-AuNP: 28.01%; Figure 1; Table 1). For the pIRES-hrGFPII-*rHMGB1* vector a slighter but still significant increase was observed when PLAL-AuNPs Size 1 and 2 were applied (FHD: 31.52%, PLAL-AuNPs_S1: 46.33%, PLAL-AuNPs_S2: 50.56%; Figure 2; Table 1).

Toxicity Analyses

Flow cytometry analysis with propidium iodide staining

For the pIRES-hrGFPII-*eIL-12* vector the mean propidium iodide percentages (PI%) of each protocol were similar to those reached by the cells transfected with the conventional FHD protocol. An exception was the Plano-AuNP protocol, showing a three-fold increase of the mean PI% to 35.43% when compared to the FHD protocol (9.69%; Figure 1; Table 2).

Transfection of the pIRES-hrGFPII-*rHMGB1* vector with the different protocols resulted in significantly higher PI% using the PLAL-AuNPs_S1 and _S2. The PLAL-AuNPs_S1 (PI 26.45%) showed a PI% nearly twice that of the FHD protocol (13.75%; Figure 2; Table 2).

Proliferation Assay

The effect of the different transfection protocols on cell vitality was investigated by determining cell proliferative activity with a standard proliferation test (Cell Proliferation ELISA BrdU (colorimetric), Roche Diagnostics, Mannheim, Germany). The BrdU incorporation assayed 48 h after transfection was significantly reduced when pIRES-hrGFPII-*eIL-12* was transfected using the Plano-AuNP and the PLAL-AuNPs_S2 protocol. Seventy-two hours after transfection, a decreased BrdU incorporation was observed in the Plano-AuNP and in the FHD transfection protocols (Figure 1; Table 3). The pIRES-hrGFPII-*rHMGB1* transfections showed a significantly reduction in incorporation of BrdU 48 h after transfection using the PLAL-AuNPs_S1 protocol. Similar results were observed for the FHD and Plano-AuNP protocols 72 h post transfection (Figure 2; Table 3).

Table 1 Transfection efficiency

	pIRES-hrGFPII-*eIL-12*	pIRES-hrGFPII-*rHMGB1*
	GFP %	GFP %
FHD	16.22 ± 9.69	31.52 ± 4.33
Plano®-AuNP	27.80 ± 3.90 *	22.93 ± 0.98 *
LAG-AuNP S1	28.01 ± 1.97 *	46.33 ± 2.07 *
LAG-AuNP S2	25.41 ± 2.22 *	50.56 ± 4.71 *
MA Lipofection	18.11 ± 0.60	22.29 ± 1.36 *
MATra-A	11.33 ± 1.30	16.24 ± 1.25 *
MTH53A Cells	1.98 ± 0.17	1.15 ± 0.56 *

GFP positive cells 24 h after transfection with pIRES-hrGFPII-*eIL-12* or pIRES-hrGFP-*HMGB1*. Results are expressed as mean ± SD. * p ≤ 0.05.

Table 2 Transfection toxicity

	pIRES-hrGFPII-*eIL-12*	pIRES-hrGFPII-*rHMGB1*
	PI %	PI %
FHD	9.69 ± 2.92	13.75 ± 1.35
Plano®-AuNP	35.43 ± 5.53 *	12.56 ± 3.72
LAG-AuNP S1	8.65 ± 1.24	26.45 ± 2.93 *
LAG-AuNP S2	7.92 ± 0.49	19.37 ± 4.28 *
MA Lipofection	5.56 ± 1.43	12.67 ± 1.33
MATra-A	13.6 ± 3.74	7.25 ± 0.29
MTH53A Cells	1.14 ± 0.17	1.01 ± 0.28

PI positive cells 24 h after transfection with pIRES-hrGFPII-*eIL-12* or pIRES-hrGFP-*HMGB1*. Results are expressed as mean ± SD. * p ≤ 0.05.

Table 3 Cell proliferation after transfection

	pIRES-hrGFPII-*eIL-12*		pIRES-hrGFPII-*rHMGB1*	
	48 h	**72 h**	**48 h**	**72 h**
FHD	172.57 ± 53.44	111.06 ± 18.72*	201.13 ± 52.57	91.23 ± 1.04*
Plano®-AuNP	72.99 ± 39.32*	64.65 ± 14.19*	154.49 ± 28.71	83.81 ± 8.34*
LAG-AuNP S1	126.19 ± 41.31	174.86 ± 18.54	103.00 ± 21.84*	193.48 ± 14.05
LAG-AuNP S2	98.95 ± 25.09*	200.93 ± 7.52	140.53 ± 30.20	196.35 ± 15.79
MALipofection	132.24 ± 21.05	153.30 ± 12.38	153.17 ± 47.41	179.62 ± 24.20
MATra-A	165.15 ± 42.89	145.88 ± 40.31	143.72 ± 22.50	153.77 ± 13.07
MTH53A Cells	191.84 ± 25.75	188.01 ± 20.11	185.07 ± 21.15	178.11 ± 21.01

Cell proliferation 48 h and 72 h after transfection with pIRES-hrGFPII-*eIL-12* or pIRES-hrGFP-*HMGB1*. Results are expressed as mean absorbance values ± SD. * $p \leq 0.05$.

Protein Expression

Protein expression detection via immunofluorescence

Control cells showed only background staining, whereas cells transfected with pIRES-hrGFPII-*eIL-12* revealed a diffuse accumulation of eIL-12 protein in the cytoplasm and nuclei (Figure 3a-c). Cells transfected with pIRES-hrGFPII-*rHMGB1* showed a concentration of HMGB1 protein located in the nuclei (Figure 3d-f). Transfection of the cells with the pIRES-hrGFPII-*eIL-12* or the pIRES-hrGFPII-*rHMGB1* vector led to the expression of biological functional recombinant proteins localized in their final destination.

The transfections using both gold NP and Ma Lipofection protocols in combination with pIRES-hrGFPII-*rHMGB1* showed a HMGB1 protein expression similar to the FHD protocol (Figure 4).

Discussion

Advances in immunology and cancer research would benefit from improved transfection efficiencies, high reproducibility and low toxicity of the required transfection approach. High transfection efficiency for plasmid DNA delivery into cells is still an important issue in gene therapy. Thus, a number of different approaches have been used to increase efficiency [10-12]. Unfortunately, the majority of the studies involving transfection of mammalian cells with non-viral vectors primarily assess transfection efficiency, lacking toxicity data. Therefore, the present study compared several NP-mediated transfection protocols in which plasmid DNA vectors were transfected into a mammalian cell line and the transfection efficiency and cytotoxicity of each protocol was analysed after transfection.

The addition of AuNPs (PLAL-AuNPs_S1 and _S2 and Plano-AuNPs) to the pIRES-hrGFPII-*eIL-12* transfection protocols significantly increased transfection efficiency (FHD: 16%; AuNP transfection efficiency mean: 28%; p = 0.05). Compared to this, the magnet-assisted protocols did not improve the transfection efficiency of pIRES-hrGFPII-*eIL-12*, resulting in values similar to the FHD protocol. An increase of the transfection efficiency for the pIRES-hrGFPII-*rHMGB1* was only detectable with the PLAL-AuNPs (FHD: 31%; PLAL-AuNPs_S1: 46%; PLAL-AuNPs_S2: 50%; p = 0.05). As for pIRES-hrGFPII-*eIL-12*, with the recombinant pIRES-hrGFPII-*rHMGB1* vector no improvement of transfection efficiency was achieved through the use of the magnet-assisted transfection protocols. On the contrary, the efficiency was significantly lower when compared to the conventional FHD protocol.

Remarkably, the AuNP-mediated transfection efficiencies achieved in this study are higher than those reported by Schakowski *et al.* (2001) [12] in which a colon carcinoma cell line was transfected with minimal size gene transfer (MIDGE) vectors and corresponding plasmids (containing coding sequences for *eGFP* or human *IL-2*). Here, the transfection efficiency was up to 36% (MIDGE Vectors) and 33% (plasmid vectors) respectively [12]. A previous study by Petersen *et al.* (2009) [2] reported an apparent increase of the transfection rates when the biocompatibility of PLAL-AuNPs was analysed. The transfection reactions with plasmid DNA and PLAL-AuNPs of different hydrodynamic size classes (14, 24, 59 and 89 nm) showed transfection efficiencies ranging from 10 to 60%, reaching the highest efficiency using a NP size of 59 nm [2]. With regard to the many potential applications of these PLAL-AuNPs in the fields of research and therapy, the promising results described above indicated the necessity of analysing the definitive transfection efficiencies and the possible cytotoxicity of PLAL-AuNPs. Two of the former four PLAL-AuNPs size classes were selected for our experiments based on the results of Petersen *et al.* [2]. The chosen AuNP sizes should be considered relevant to the transfection outcome. The results of Chithrani *et al.* [13] showed that for mammalian cells (HeLa) the maximum uptake of spherical and rod-shaped AuNPs, in a size range of 10-100 nm (fully or partially modified by citric acid ligands), was reached with the 50 nm AuNPs (Feret diameter).

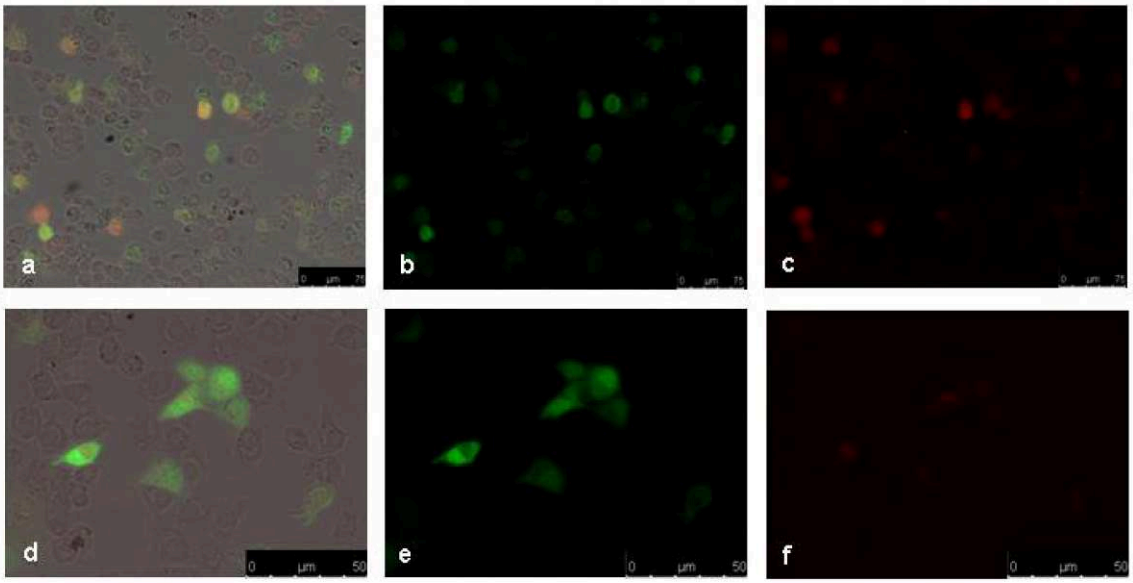

Figure 3 Immunofluorescence 24 h after transfection. pIRES-hrGFPII-*eIL-12* transfection with the FHD protocol, primary antibody goat IgG anti-p35 and a donkey anti-goat secondary antibody (Texas Red fluorochrome). (a) GFP and Red Fluorescence merged image, (b) GFP Fluorescence and (c) Red Fluorescence images. Scale bar 50 μm. pIRES-hrGFP-HMGB1 transfection with the FHD protocol, primary antibody mouse anti-HMGB1 and secondary antibody goat anti-mouse (Texas Red fluorochrome). (d) GFP and Red Fluorescence merged image, (e) GFP Fluorescence and (f) Red Fluorescence images. Scale bar 75 μm.

The transfection efficiencies for both expression vector constructs used in our study were similarly affected by the different protocols applied. The overall higher transfection efficiencies attained using the pIRES-hrGFPII-*rHMGB1* vector could be explained due to the different vector and insert sizes. The pIRES-hrGFPII-*rHMGB1* vector has a size of 5531 bp whereas pIRES-hrGFPII-*eIL-12* has a molecular length of 7709 bp. Such size mediated effects in transfections were studied by Yin *et al.* (2005) [14]. They demonstrated an inverse correlation between the construct size and the promoter/enhancer activity measured by the dual luciferase system in a transient transfection assay of mammalian cells. Larger plasmid or recombinant plasmid constructs resulted in lower transfection efficiencies than when smaller ones were used [14].

In the present study, in contrast to our expectation, the magnet-assisted protocols using magnetic nanoparticle-mediated DNA-uptake did not increase the transfection ratio of pIRES-hrGFPII-*eIL-12*, resulting in transfection efficiencies and PI% comparable to those achieved by the FHD protocol. When pIRES-hrGFPII-*rHMGB1* was transfected, the efficiency was significantly lower than that reached with the conventional FHD protocol, but with significantly lower toxicity results. A study by Bertram [3] suggested that the directed delivery of the cargo (e.g. DNA) towards the cells applying magnet-assisted transfection technology may increase the overall transfection efficiency depending on the cell type used. Although an improvement of the transfection efficiency could not be observed using the magnet-assisted protocol, it is important to highlight that as published by Renker *et al.* [15], in our study, when pIRES-hrGFPII-r*HMGB1* was transfected using the MATra-A transfection protocol, a significantly low PI% and a cell proliferation similar to non-transfected control cells was detected. This attribute of the MATra-A protocol should be taken into consideration when gentler transfection methods on sensitive cells are required.

The protein expression results for canine HMGB1 and eIL-12 show that the protein expression is sufficient. After transfection, the expression of simple proteins as GFP and the nuclear acting HMGB1 and of complex proteins consisting of two separate subunits as IL-12 is possible. Furthermore, the addition of NP or magnetic reagent to the pIRES-hrGFPII-r*HMGB1* transfections did not interfere with protein expression as shown in Figure 4.

Even though the use AuNPs improved the transfection efficiency achieved in this study, the required amount of reagent and type of enhancers (e.g. AuNPs) must be considered specifically for each cell type and vector in order to achieve an appropriate recombinant vector

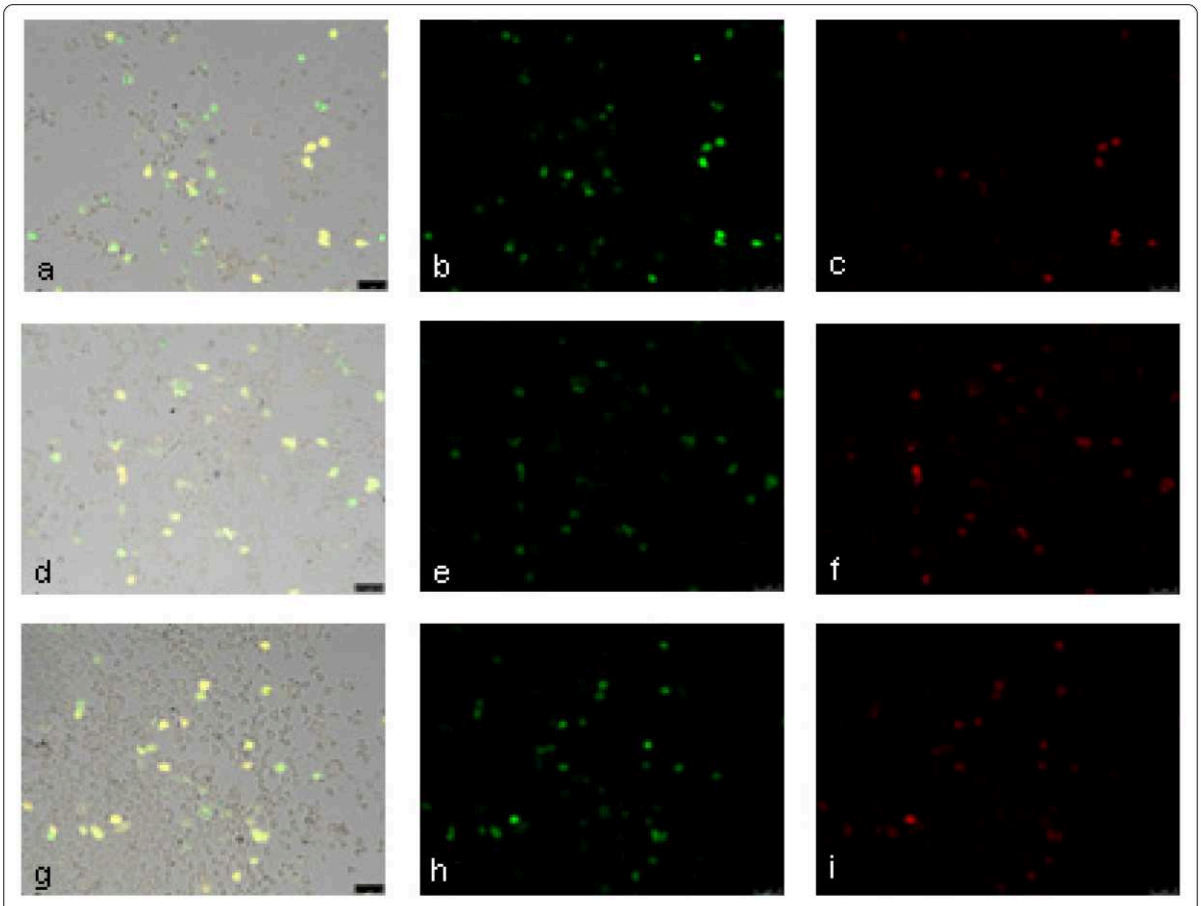

Figure 4 Immunofluorescence 24 h after NP-mediated transfection. pIRES-hrGFP-HMGB1 transfection with NP-mediated protocols. Plano-AuNP (a, b, c), PLAL-AuNP Size 2 (d, e, f), and MA Lipofection (g, h, i)). Primary antibody: mouse anti-HMGB; secondary antibody: goat anti-mouse (Texas Red fluorochrome). a, d, g: GFP and Red Fluorescence merged image; b, e, h: GFP Fluorescence and (c, f, i) Red Fluorescence images. Scale bar 75 μm.

expression without incurring cell toxicity. Despite the potential benefits of the AuNPs described, the safety of their use in biological organisms has to be evaluated in full. In this study, when the pIRES-hrGFPII-*eIL-12* vector was transfected, the addition of the ligand-free PLAL-AuNPs (S1 and S2) had no significant toxic effect on the cells. Nevertheless, when commercially purchased poly-L-lysine-coated colloidal gold NPs (Plano-AuNP) were applied, an increased PI% and decreased cell proliferation could be observed confirming a toxic effect of these particle formulations on cell vitality. For the pIRES-hrGFPII-*rHMGB1* transfections a significantly higher PI% was measured when PLAL-AuNPs (S1 and S2) were applied. This was not supported by the cell proliferation analysis where a NP-mediated toxic effect was observed neither 48 h nor 72 h after transfection.

The potential toxicity of AuNPs has been an issue in previous studies [4,16-18]. Recently, the uptake of ligand-free positively charged gold NPs during coincubation with a bovine cell line (GM7373) occurred apparently by diffusion [19]. At the same time, the assessment of cell morphology, membrane integrity, and apoptosis revealed no AuNP-related loss of cell vitality at gold concentrations of 25 μM or below, and no cytotoxic effect was observed in a proliferation assay after exposing low cell numbers to the same PLAL-AuNP concentrations [19]. Interestingly, cell proliferation was reduced when cells were coincubated with ligand-free gold NPs concentrations of 50 μM and above [19]. Although, AuNP cytotoxicity was not the aim of the study by Petersen *et al.* [2], they observed that the PLAL-AuNP application apparently had no cytotoxic effect, since normal cell density and appearance in all set ups was similar prior- and posttransfectional. In this context, Shukla *et al.* (2005) [20] concluded that chemically synthesized AuNPs (35 ± 7 Å in size, Feret diameter) are inert and nontoxic to the cells and that no stress-induced

secretion of proinflammatory cytokines as TNF-α and IL-1β by macrophage cells (RAW264.7) was detectable.

In our study, the average PI% of the transfected cells (12.3% for pIRES-hrGFPII-eIL-12; 13.9% for pIRES-hrGFPII-*rHMGB1*) can be compared with the 10-20% reported by Schakowski *et al.* [12] after the transfection of a colon carcinoma cell line with plasmid and MIDGE vectors. Regarding the size of NPs in relation to cell toxicity, Pernodet *et al.* (2006) [21] demonstrated that 13 nm AuNPs (Feret diameter) generate apoptosis and morphological deformation at 2-6 days in CF-31 human dermal fibroblast cells. Additionally, Pan *et al.* (2007) [16] reported that AuNPs with a diameter of 2 nm or less (Feret diameter) were cytotoxic for different cell lines (termed HeLa, SK-Mel28, L929 mouse fibroblasts and J774A1 mouse monocytic/macrophage cells), whereas 15 nm AuNPs were nontoxic to the cells. These NP size dependent results could be due to the larger surface area per unit mass of smaller sized NPs. Related to this, particle toxicology suggests that, for toxic particles generally, more particle surface equals more toxicity [6].

Interestingly, the significant toxicity we observed when using the 20 nm Plano-AuNP (with pIRES-hrGFPII-*eIL-12*) differs from the recent study by Brandenberger *et al.* [22]. They applied similar commercially available aqueous colloidal AuNPs, 15 nm in size and coated with poly-L-lysine. The AuNPs entered the cells, but no cytotoxic effects of these AuNPs were observed [22]. These results suggest that possibly the poly-L-lysine coating does not induce a direct toxic effect on cells, although impurities in the AuNP colloid formulations are supposed to increase the toxicity compared to pure AuNPs.

The results presented herein suggest that further use of each protocol should be evaluated under consideration of the transfection efficiency results together with the toxicity results. To do so, we subtracted the PI% from the total number of GFP positive cells (Figure 5). For the pIRES-hrGFPII-*eIL-12* transfections, this calculation showed that even though the Plano protocol generated almost the highest transfection efficiency, the outcome was not as good when considered in combination with the cell toxicity results. In contrast, the PLAL-AuNP_S1 protocol provided the best overall (combined) results. For the pIRES-hrGFPII-*rHMGB1* transfections the use of the PLAL-AuNPs_S2 protocol showed the highest efficiency and just a slightly increased toxicity, making this protocol the one with the best final outcome.

Hence, both test series (Figure 1 and 2, Table 1) indicate that AuNPs, in particular the physically made pure colloids, are able to significantly increase transfection efficiency and that a trade-off in cell vitality becomes significant in particular with the chemically made AuNPs. The residual nanoparticle ligands of these NPs may play an unintended, yet underestimated role in NP-mediated cellular uptake. However, further studies with different cell lines and expression vectors should be performed to be able to decide if the observed cytotoxic effects can be explained by simple NP cell intolerance or by incompatibility of the cells with the transfected recombinant vector or the expressed recombinant protein.

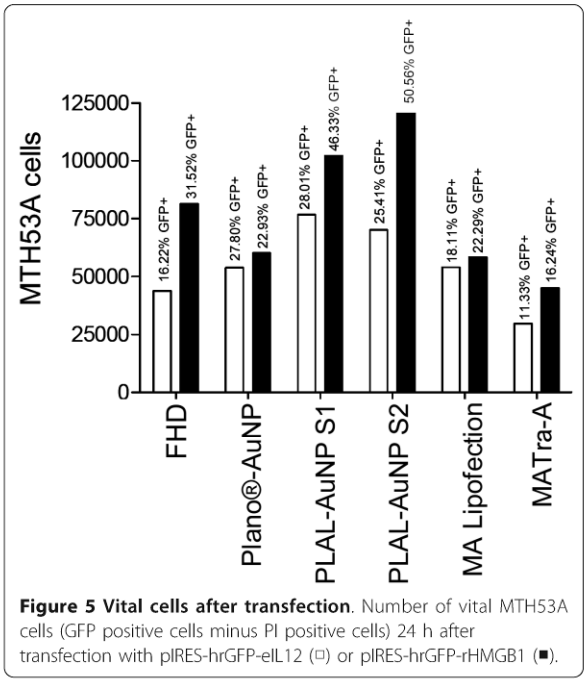

Figure 5 Vital cells after transfection. Number of vital MTH53A cells (GFP positive cells minus PI positive cells) 24 h after transfection with pIRES-hrGFP-eIL12 (□) or pIRES-hrGFP-rHMGB1 (■).

Conclusions

Transfection efficiency of plasmid DNA vectors can be significantly improved by the addition of ligand-free PLAL-AuNPs (29 nm and 52 nm in size) to conventional transfection reagents like FuGENE HD. Cell vitality was negatively affected mainly by the addition of chemically generated AuNPs (Plano-AuNPs), but also slightly by physically made AuNPs (PLAL-AuNPs_S1) resulting in increased cytotoxic effects and reduction of cell proliferation. Among the transfection methods investigated comparatively in this study, 29 nm AuNPs made by PLAL span the widest window in terms of high transfection efficiency with minimized trade-off in vitality.

Methods

Mammalian expression vectors

Two different mammalian expression vectors simultaneously encoding for an expression protein (canine HMGB1 (HMGB1) or equine IL-12 (eIL-12)) and the hrGFP were constructed. The expression of the inserted genes of interest can be assessed by the simultaneous but separate expression of hrGFP due to a bicistronic

expression cassette in the respective pIRES-*hrGFPII* plasmids used here. Accordingly, the successful transfection of the cells may be analysed using GFP-based fluorescence microscopy as well as flow cytometry. The used vectors differ in that, apart from the GFP, the HMGB1 vector encodes a single chain protein, while the IL-12 vector encodes a complex protein consisting of two different subunits which are posttranslationally processed by the cell to a joint complex. Thus, a successful assembling of recombinant IL-12 is dependent on the ability of the transfected cell to correctly process complex post-translational protein modifications.

PIRES-hrGFPII-eIL-12

DNA encoding for eIL-12 (Vetsuisse-Faculty, University of Zurich) was amplified by PCR (primer pair: NotI_IL-12_f 5'-CGGCGGCCGCATATGTGCCCGCCGCGC-3' (forward primer); NotI_IL-12_r 5'-CGGCGGCCGCAACTG-CAGGATACGG-3' (reverse primer)). The DNA contains the p35 and p40 IL-12 subunit cDNAs (p35: Acc. No. Y11129; p40: Acc. No. Y11130) separated by an IRES element, both IL-12 subunits are translated separately and then processed by the cell to a joint complex. The PCR products were separated on a 1.5% agarose gel, eluted using QIAquick Gel Extraction Kit (QIAGEN, Hilden, Germany), and cloned into the bicistronic pIRES-hrGFPII mammalian expression vector (Stratagene, La Jolla, CA, USA). Verification of the constructed plasmid was done by NotI restriction digest and sequencing.

PIRES-hrGFPII-rHMGB1

For construction of the pIRES-hrGFPII-*rHMGB1* expression plasmid, the canine *HMGB1* coding sequence (Acc. No. AY135519) without the terminal stop codon was inserted into the bicistronic pIRES-hrGFP II vector (Stratagene, La Jolla, CA, USA). Expression of the inserted HMGB1 coding sequence results in an HMGB1 fusion protein with a recombinant short 3 × FLAG peptide sequence at its C-terminal part (*rHMGB1*).

The following primer pair was used for PCR-amplification: EcoRI-B1-CFA-Fwd (5'-GGAATTCCACCATGGG-CAAAGGAGA-3'; forward primer) and NotI-B1-CFA-Rev/-TAA (5'-AAGAATGATGATGATGAAGCGGCC GCGC-3', reverse primer).

The amplified PCR product was separated on a 1.5% agarose gel, purified using QIAquick Gel Extraction Kit (QIAGEN, Hilden, Germany) and ligated into the pIRES-hrGFPII vector plasmid (Stratagene, La Jolla, CA). Verification of the constructed plasmid was done by NotI/EcoRI double restriction digest and sequencing.

Cell culture and in vitro transfection assays

The MTH53A canine mammary cell line used for the experiments was derived from epithelial healthy canine mammary tissue.

Eight hours prior to the transfection, 3×10^5 MTH53A cells were seeded in 6-well plates with 2 ml cell culture medium. The cells were grown as adherent cultures in a humidified atmosphere at 37°C and 5% CO_2 in complete medium 199 (medium 199; Invitrogen, Karlsruhe, Germany) supplemented with 10% heat-inactivated fetal calf serum (PAA Laboratories GmbH, Pasching, Austria), 200 U/ml penicillin and 200 ng/ml streptomycin (Biochrom AG, Berlin, Germany)).

For transfection the following different protocols were applied in triplicate

1) FHD: 5 μL of FuGENE HD (FHD, Roche, Mannheim, Germany) were added to 2 μg of pIRES-hrGFPII-*eIL-12* or pIRES-hrGFPII-*rHMGB1* at a total volume of 100 μL ddH_2O, incubated for 10 minutes at room temperature and added to the seeded cells.

2) Plano-AuNP (EM CGC20, 20 nm; Plano GmbH, Wetzlar, Germany): 20 μL of Plano-AuNP were incubated for 24 h at room temperature with 2 μg of pIRES-hrGFPII-*eIL-12* or pIRES-hrGFPII-*rHMGB1* at a total volume of 95 μL ddH_2O. For transfection 5 μL aliquots of FHD reagent (Roche, Mannheim, Germany) were added to 95 μL of the AuNP /vector suspension, incubated for 10 minutes at room temperature and added to cell cultures.

3) PLAL-AuNP size 1 (d50 = 28.5 nm and d90 = 43.4 nm hydrodynamic sizes; 14 ± 3 nm Feret diameter (Figure 6)) and size 2 (d50 = 52.4 nm and d90 = 78.6 nm hydrodynamic sizes; 41 ± 8 nm Feret diameter (Figure 6)): The PLAL-AuNP suspensions were sterilized by filtration through a 0.2 μm filter device (Millex-GV Sterilizing Filter Unit, Millipore, Billerica, USA). Subsequently, 20 μL of each sized AuNPs were incubated for 24 h at room temperature with 2 μg of pIRES-hrGFPII-*eIL-12* or pIRES-hrGFPII-*rHMGB1* at a total volume of 95 μL of ddH_2O. For transfection 5 μL aliquots of FHD reagent (Roche, Mannheim, Germany) were added to 95 μL of the AuNP /vector suspension, incubated for 10 minutes at room temperature and added to cell cultures.

3.1) Nanoparticle generation: AuNPs were generated by pulsed laser ablation in liquid (PLAL) [9]. The beam of a femtosecond laser system (Spitfire Pro, Spectra-Physics), delivering 120 fs laser pulses at a wavelength of 800 nm was focused with a 40 mm lens on a 99.99% pure gold target placed at the bottom of a Petri dish filled with 2 mL of ddH_2O. Pulse energy of 200 μJ at 5 kHz repetition rate was employed for 12 minutes of irradiation. The target position was set 4 mm or 2 mm below the determined focal point in air, in order to obtain colloidal suspensions containing AuNPs with mean hydrodynamic diameters of d_h = 29 nm (size 1) and d_h = 52 nm (size 2), respectively. The remaining small particles were removed by centrifugation. Characterisation of NP colloids was performed by

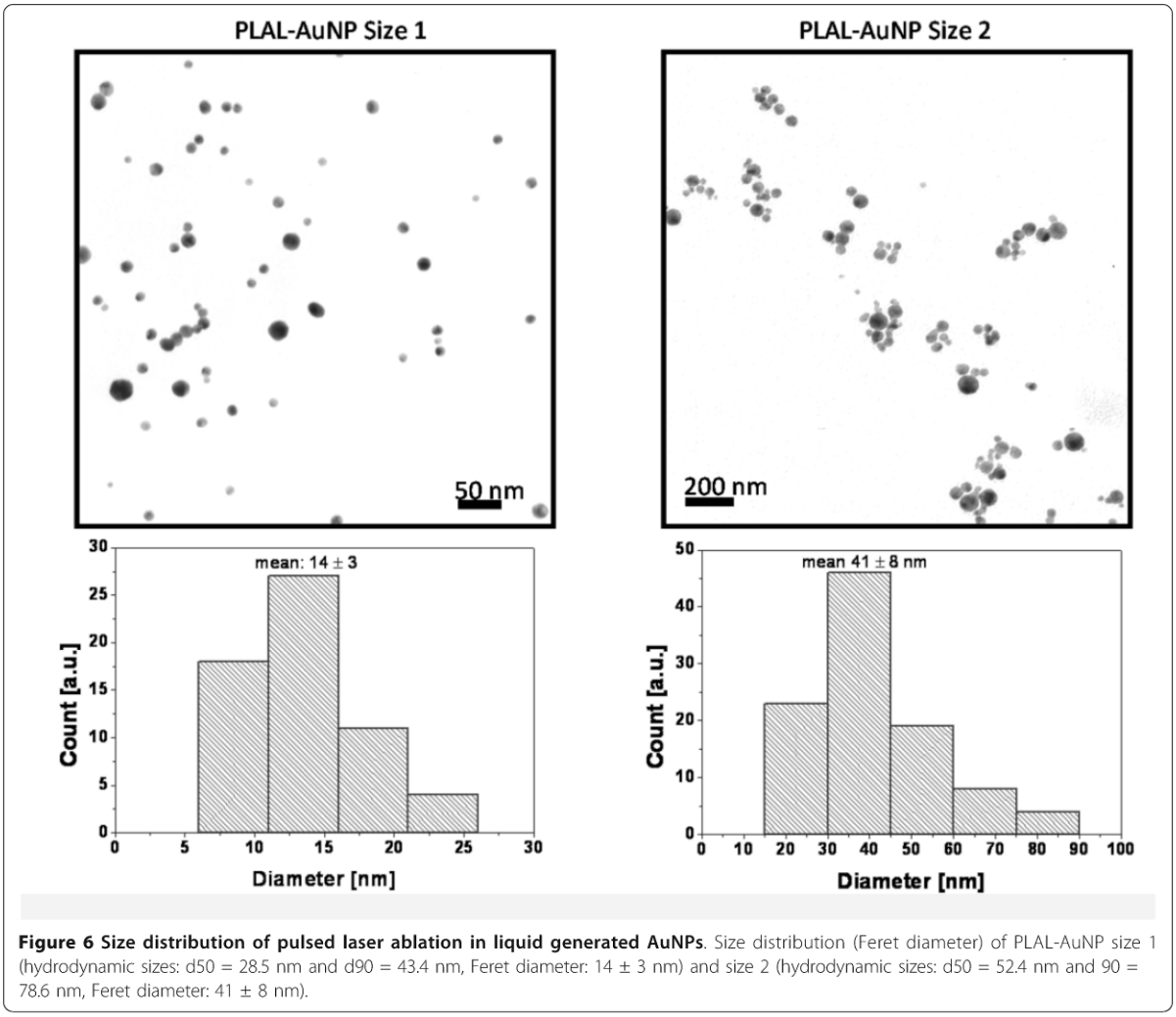

Figure 6 Size distribution of pulsed laser ablation in liquid generated AuNPs. Size distribution (Feret diameter) of PLAL-AuNP size 1 (hydrodynamic sizes: d50 = 28.5 nm and d90 = 43.4 nm, Feret diameter: 14 ± 3 nm) and size 2 (hydrodynamic sizes: d50 = 52.4 nm and 90 = 78.6 nm, Feret diameter: 41 ± 8 nm).

dynamic light scattering using a Malvern Zetasizer ZS and by UV-Vis spectroscopy using a Shimadzu 1650.

4) Magnet-assisted transfection: (MA Lipofection & MATra-A):

4.1) MA Lipofection: 5 μL of FHD (Roche, Mannheim, Germany) were added to 2 μg of pIRES-hrGFPII-*eIL-12* or pIRES-hrGFPII-*rHMGB1* to a total volume of 97 μL ddH_2O and incubated for 10 minutes at room temperature. Afterwards, 3 μL of MA Lipofection enhancer (PromoKine, Heidelberg, Germany) were added and incubated at room temperature for 15 minutes.

4.2) MATra-A: 3 μL of the magnetic reagent MATra-A (PromoKine, Heidelberg, Germany) were added to 2 μg of pIRES-hrGFPII-*eIL-12* or pIRES-hrGFPII-*rHMGB1* to a total volume of 97 μL of complete medium 199 (without FCS) and incubated for 15 minutes at room temperature.

For MATra-A and MA Lipofection, after final incubation, the 100 μL suspension was added to the cell cultures and each of the 6-well plates were placed on a magnetic plate at 37°C and 5% CO_2 for 15 minutes (Universal Magnet Plate; PromoKine, Heidelberg, Germany). Afterwards, the plate was removed.

After each transfection, cells were incubated for 24 hours in complete medium 199 at 37°C and 5% CO_2.

For each protocol the incubation of cells with the transfection reagents and without DNA was considered as the negative control.

The plasmid DNA uptake of pIRES-hrGFPII-*eIL-12* and pIRES-hrGFPII-*rHMGB1* was verified by fluorescence microscopy and measured by flow cytometry (FACSCalibur flow cytometer).

Each protocol was performed in triplicate.

Results are expressed as means.

Transfection Efficiency Analyses

Fluorescence Microscopy

Transfected cells were fixed in a 4% paraformaldehyde/PBS solution for 15 minutes at room temperature. After fixation 10 μL of Vectashield Mounting Medium with DAPI (4'-6-diamidino-2-phenylindol, Vector Laboratories, Burlingame, CA, USA) was applied for fluorescent visualization of nucleic DNA. Fluorescence microscopy was performed using an Axio Imager. Z1 fluorescence microscope (Carl Zeiss MicroImaging GmbH, Jena, Germany) and images were recorded using the AxioVision Software (Rel. 4.7). The hrGFP fluorescence was measured employing wavelength filter set 10 (Carl Zeiss MicroImaging, Goettingen, Germany), while DAPI fluorescence was measured employing wavelength filter set 2.

Flow cytometry

GFP expression of the transfected cells was analysed measuring green fluorescence by flow cytometry in order to determine the transfection efficiency of each protocol. Cells were trypsinized for 3-5 min, washed with PBS, resuspended in the medium, and measured with a FACScan flow cytometer (Becton, Dickinson and Company, Heidelberg, Germany). Fluorescence intensities were analysed with Cell Quest software (Becton, Dickinson and Company, Heidelberg, Germany). The percentage of positive cells was assessed comparing dot plot analysis of the transfected cells to cells incubated only with transfection reagent with or without the addition of NPs (depending of the protocol used).

Results are expressed as percentage of positive cells, as indicator for transfection efficiency.

The transfection efficiency results of each protocol were finally compared with those of the conventional FHD protocol.

Toxicity Analyses

Flow cytometry

Propidium iodide (PI) staining was used to identify the cell death percentage after transfection. Cells were trypsinized, resuspended in complete medium 199 and PI (5 μg/mL) was added. The cytometry analysis was performed using a FACSCalibur device (Becton, Dickinson and Company, Heidelberg, Germany) with Cell Quest software (Becton, Dickinson and Company, Heidelberg, Germany). Thereafter, the cells were assessed for PI florescence by dot plot analysis and compared to cells incubated only with transfection reagent with or without the addition of NPs (depending of the protocol used).

Results are expressed as percentage of positive cells

The toxicity results of each protocol were compared with those of the conventional FHD protocol.

Proliferation Assay

Proliferation of cells in response to each transfection protocol was evaluated using a colorimetric cell proliferation ELISA (Roche Applied Science, Mannheim, Germany) which measures the incorporation of 5-bromo-2-deoxyuridine (BrdU), a thymidine analogue, into DNA by ELISA using an anti-BrdU monoclonal antibody.

Eight hours prior to transfection, 1.5×10^4 MTH53A cells were placed in 96-well plates. Cells were grown at 37° C and 5% CO_2 in complete medium 199 (Invitrogen, Karlsruhe, Germany) supplemented with 10% heat-inactivated FCS (PAA Laboratories GmbH, Pasching, Austria), 200 U/ml penicillin and 200 ng/ml streptomycin (Biochrom AG, Berlin, Germany). Each protocol was performed in triplicate as explained above. The proliferation assay was carried out according to manufacturer's recommendations (Cell proliferation ELISA, colorimetric, Cat. No. 11647229001, Roche Applied Science, Mannheim, Germany). The reaction products were quantified by measuring the absorbance at 370 nm (reference wavelength 492 nm) using a scanning multiwell spectrophotometer equipped with the analysis software Gen 5 (Synergy HT multi-mode microplate reader, BioTek Instruments Inc., Bad Friedrichshall Germany). The absorbance results directly correlate to the amount of DNA synthesis and hereby to the number of proliferating cells.

Results are expressed as mean absorbance values

The proliferation results of each protocol were compared to those of non-transfected cells.

Protein Expression

To confirm biological functionality of the expressed proteins, immunofluorescence directed against eIL-12 and canine HMGB1 was performed after transfection.

Equine IL-12

The expression of eIL-12 was evaluated in MTH53A cells. Eight hours prior to transfection 3×10^5 MTH53A cells were seeded in 6-well plates. Cells were grown under standard conditions as described above. Transfection was performed as explained for the FHD protocol. Subsequently, 24 h after transfection cells were fixed in a 4% paraformaldehyde/PBS solution for 20 minutes at room temperature, permeabilized and blocked. Immunofluorescence was performed using a goat IgG anti-p35 polyclonal primary antibody (IL-12 p35, sc-1280, Santa Cruz Biotechnology, Inc.; Santa Cruz, CA, USA; dilution 1:40) and a donkey anti-goat secondary antibody (IgG-TR, sc-2783; Santa Cruz Biotechnology, Inc.; Santa Cruz, CA; dilution 1:180).

Fluorescence microscopy was carried out using a Leica DMI 6000 fluorescence microscope (Leica Microsystems GmbH, Wetzlar Germany).

Canine HMGB1

The expression of HMGB1 was also evaluated in MTH53A cells. Cells were prepared as described for the

eIL-12 expression. Twenty four hours after transfection with four different protocols (FHD, Plano-AuNP, PLAL-AuNP_S2 and Ma Lipofection), immunofluorescence was performed using an anti-HMGB1 mouse monoclonal antibody (HMGB1 antibody [HAP46.5], ab12029-100, Abcam, Cambridge, UK; 1:60) and a goat anti-mouse antibody (DyLight™ 549-TFP ester, Code Nr. 115-505-062, Jackson ImmunoResearch, West Grove, PA, USA; dilution 1:220). Fluorescence microscopy was also performed as described above.

Statistics

Results are presented as mean ± standard deviation. Statistical significance was determined using the 1-tailed Wilcoxon-Mann-Whitney test. Differences were considered statistically significant for $p \leq 0.05$.

Acknowledgements

The work was funded in part by the German Research Foundation within the excellence cluster REBIRTH. Further parts were funded by the collaborative research cluster Transregio 37 "Micro- und Nanosysteme in der Medizin".
MCD is being funded by a post-graduate DAAD (German Academic Exchange Service) /Conicyt (Chilean National Commission for Scientific and Technological Research) scholarship.

Author details

[1]Equine Clinic, University of Veterinary Medicine Hannover, Buenteweg 9, 30559 Hannover, Germany. [2]Small Animal Clinic and Research Cluster of Excellence "REBIRTH", University of Veterinary Medicine, Buenteweg 9, 30559 Hannover, Germany. [3]Laser Zentrum Hannover e.V., Hollerithallee 8, 30419 Hannover, Germany. [4]Institute of Veterinary Medicine, University of Goettingen, Burckhardtweg 2, 37077 Goettingen, Germany. [5]Institute of Technical Chemistry I, University of Duisburg Essen and Center for Nanointegration Duisburg-Essen (CeNIDE), Universitaetsstr. 5-7, 45141 Essen, Germany.

Authors' contributions

MCD carried out the construction of the expression vectors, the cell culture and DNA preparation, the transfections, the fluorescence and immunofluorescence microscopy analysis, the statistical analysis and the partial drafting of the manuscript. SW participated in the expression vector design and construction, in cell culture, fluorescence and immunofluorescence microscopy analysis and partial drafting of the manuscript. AB carried out the PLAL-AuNPs generation. AM assisted MCD in performing flow cytometry analysis. JM participated in the IL 12 vector design. JTS took part in the expression vector design and construction. SB performed the supervision of the PLAL-AuNPs generation. IN and KF, head of the Small Animal Clinic and the Equine Clinic, participated in the conception design of the study. HME carried out the principal study design, partial drafting and finalisation of the manuscript and the supervision of the molecular and cell biological work. All authors read and approved the final manuscript.

Competing interests

The authors declare that they have no competing interests.

Received: 21 June 2011 Accepted: 20 October 2011
Published: 20 October 2011

References

1. Baumgart J, Bintig W, Ngezahayo A, Willenbrock S, Murua Escobar H, Ertmer W, Lubatschowski H, Heisterkamp A: **Quantified femtosecond laser based opto-perforation of living GFSHR-17 and MTH53 a cells.** *Opt Express* 2008, **16**:3021-3031.
2. Petersen S, Soller JT, Wagner S, Richter A, Bullerdiek J, Nolte I, Barcikowski S, Murua Escobar H: **Co-transfection of plasmid DNA and laser-generated gold nanoparticles does not disturb the bioactivity of GFP-HMGB1 fusion protein.** *J Nanobiotechnology* 2009, **7**:6.
3. Bertram J: **MATra - Magnet Assisted Transfection: combining nanotechnology and magnetic forces to improve intracellular delivery of nucleic acids.** *Curr Pharm Biotechnol* 2006, **7**:277-285.
4. Ghosh P, Han G, De M, Kim CK, Rotello VM: **Gold nanoparticles in delivery applications.** *Adv Drug Deliv Rev* 2008, **60**:1307-1315.
5. Rosi NL, Giljohann DA, Thaxton CS, Lytton-Jean AK, Han MS, Mirkin CA: **Oligonucleotide-modified gold nanoparticles for intracellular gene regulation.** *Science* 2006, **312**:1027-1030.
6. Borm PJ, Robbins D, Haubold S, Kuhlbusch T, Fissan H, Donaldson K, Schins R, Stone V, Kreyling W, Lademann J, Krutmann J, Warheit D, Oberdorster E: **The potential risks of nanomaterials: a review carried out for ECETOC.** *Part Fibre Toxicol* 2006, **3**:11.
7. Dahl JA, Maddux BL, Hutchison JE: **Toward greener nanosynthesis.** *Chem Rev* 2007, **107**:2228-2269.
8. Sylvestre J, Poulin S, Kabashin AV, Sacher E, Meunier M, Luong JHT: **Surface Chemistry of Gold Nanoparticles Produced by Laser Ablation in Aqueous Media.** *J Phys Chem B* 2004, **108**:16864-16869.
9. Petersen S, Barcikowski S: **In Situ Bioconjugation: Single Step Approach to Tailored Nanoparticle-Bioconjugates by Ultrashort Pulsed Laser Ablation.** *Adv Funct Mater* 2009, **19**:1167-1172.
10. Luo D, Saltzman WM: **Enhancement of transfection by physical concentration of DNA at the cell surface.** *Nat Biotechnol* 2000, **18**:893-895.
11. Kamau SW, Hassa PO, Steitz B, Petri-Fink A, Hofmann H, Hofmann-Amtenbrink M, von Rechenberg B, Hottiger MO: **Enhancement of the efficiency of non-viral gene delivery by application of pulsed magnetic field.** *Nucleic Acids Res* 2006, **34**:e40.
12. Schakowski F, Gorschluter M, Junghans C, Schroff M, Buttgereit P, Ziske C, Schottker B, Konig-Merediz SA, Sauerbruch T, Wittig B, Schmidt-Wolf IG: **A novel minimal-size vector (MIDGE) improves transgene expression in colon carcinoma cells and avoids transfection of undesired DNA.** *Mol Ther* 2001, **3**:793-800.
13. Chithrani BD, Ghazani AA, Chan WC: **Determining the size and shape dependence of gold nanoparticle uptake into mammalian cells.** *Nano Lett* 2006, **6**:662-668.
14. Yin W, Xiang P, Li Q: **Investigations of the effect of DNA size in transient transfection assay using dual luciferase system.** *Anal Biochem* 2005, **346**:289-294.
15. Renker B, Diestel S, Ruonala M, Bertram J: **MATra ein Trojanisches Pferd fuer eine zellschonende Transfektion.** *BIOspektrum* 2010, 1-2.
16. Pan Y, Neuss S, Leifert A, Fischler M, Wen F, Simon U, Schmid G, Brandau W, Jahnen-Dechent W: **Size-dependent cytotoxicity of gold nanoparticles.** *Small* 2007, **3**:1941-1949.
17. Sperling RA, Rivera Gil P, Zhang F, Zanella M, Parak WJ: **Biological applications of gold nanoparticles.** *Chem Soc Rev* 2008, **37**:1896-1908.
18. Connor EE, Mwamuka J, Gole A, Murphy CJ, Wyatt MD: **Gold nanoparticles are taken up by human cells but do not cause acute cytotoxicity.** *Small* 2005, **1**:325-327.
19. Taylor U, Klein S, Petersen S, Kues W, Barcikowski S, Rath D: **Nonendosomal cellular uptake of ligand-free, positively charged gold nanoparticles.** *Cytometry A* **77**:439-446.
20. Shukla R, Bansal V, Chaudhary M, Basu A, Bhonde RR, Sastry M: **Biocompatibility of gold nanoparticles and their endocytotic fate inside the cellular compartment: a microscopic overview.** *Langmuir* 2005, **21**:10644-10654.
21. Pernodet N, Fang X, Sun Y, Bakhtina A, Ramakrishnan A, Sokolov J, Ulman A, Rafailovich M: **Adverse effects of citrate/gold nanoparticles on human dermal fibroblasts.** *Small* 2006, **2**:766-773.
22. Brandenberger C, Rothen-Rutishauser B, Muhlfeld C, Schmid O, Ferron GA, Maier KL, Gehr P, Lenz AG: **Effects and uptake of gold nanoparticles deposited at the air-liquid interface of a human epithelial airway model.** *Toxicol Appl Pharmacol* **242**:56-65.

doi:10.1186/1477-3155-9-47
Cite this article as: Durán *et al.*: Comparison of nanoparticle-mediated transfection methods for DNA expression plasmids: efficiency and cytotoxicity. *Journal of Nanobiotechnology* 2011 **9**:47.

3.3. Functional analysis of modified cells

After efficient transfection of the desired cell types, the functionality of the introduced DNA expression plasmids needs to be characterised. An analysis of the cellular responses of target cells to e.g. cytokines or other stimulating agents such as synthetic CpG-oligonucleotides (CpG-ODN) is necessary. Especially the protein secretion potential, viability and growth behaviour of these cells needs to be investigated in detail after stimulation.

In the following publications, the characterisation of the HMGB1 secretion potential by modified canine mammary cells expressing recombinant HMGB1, and the cell proliferative response of canine B-cell lymphoma cells to stimulation with CpG-ODN DSP30 combined with IL-2 are described.

VI ‘TNF-α induced secretion of HMGB1 from non-immune canine mammary epithelial cells (MTH53A).’ **Willenbrock *et al.*, Cytokine, 2012.**

The HMGB1 DNA expression vectors constructed in this study were used to serve as basis for the immunotherapeutic approach, which was followed within the CRC / TR37. This project aimed at the enhancement of anti-tumour responses of the host immune system by secretion of HMGB1 from genetically engineered dendritic cells. A crucial point to realize this approach is the ability of the modified cells to actively secrete the recombinant expressed HMGB1 at the targeted location time-dependently. This can be implemented by stimulation of the cells with ‘early’ proinflammatory cytokines such as TNF-α, IFN-γ, and IL-1β or bacterial LPS.

The biofunctionality of the constructed vectors was assessed as a proof of principle in the canine non-neoplastic mammary cell line MTH53A due to good availability of these cells. As MTH53A cells are usually HMGB1-non-secreting, this cell line was appropriate for evaluating the HMGB1 secretion potential in response to cytokine stimulation.

The two recombinant bicistronic *HMGB1* expression vector constructs carrying the *hrGFP* gene and the canine *HMGB1* CDS encode either for an unmodified recombinant HMGB1 or an HMGB1 fusion protein with a short 3x FLAG peptide sequence located C-terminally. The HMGB1+FLAG variant was built to allow the discrimination between recombinant and endogenous expressed HMGB1 via Western blotting. Expression of both bicistronic vectors leads to a simultaneous but

separate synthesis of recombinant HMGB1 and hrGFP allowing the verification of successful plasmid DNA uptake by visualisation of green fluorescence.

After transfection, the release kinetics of MTH53A cells expressing recombinant HMGB1 were analysed by stimulation with the proinflammatory cytokines TNF-α and IFN-γ in a time-dependent manner (6, 24, 48 h). The secretion of HMGB1 into the cultivation medium was analysed via Western blotting and quantified with an HMGB1-ELISA. In addition, live cell laser scanning multiphoton microscopy was performed over a time spam of 50 h on transfected MTH53A cells expressing a recombinant HMGB1-GFP fusion protein in order to visualise the release of this HMGB1-GFP protein under TNF-α stimulating conditions.

The transfection of both bicistronic vector constructs resulted in the expression of biofunctional recombinant HMGB1. The active release of recombinant HMGB1 protein was clearly detectable with a time peak of 24 h after stimulation with TNF-α while IFN-γ showed to have only small effects on HMGB1 secretion. Quantification of HMGB1 by ELISA confirmed the findings gained by Western blotting leading to the highest secretion of HMGB1 after 24 h of TNF-α application. By live cell microscopy diffuse cell membrane structure changes, but no clear secretion of recombinant HMGB1-GFP was visualisable starting at 29 h and ending at 42.5 h after TNF-α stimulation.

VI

TNF-α induced secretion of HMGB1 from non-immune canine mammary epithelial cells (MTH53A).

Willenbrock S, Braun O, Baumgart J, Lange S, Junghanss C, Heisterkamp A, Nolte I, Bullerdiek J, Murua Escobar H.

Cytokine. 2012. 57(2):210-20

Own contribution:

- All experimental work including:
  - pIRES-hrGFPII plasmid construction
  - Cell culture, transfection and sample preparation
  - Fluorescense microscopy
  - Anti-HMGB1 Western blot and enzyme-linked immunosorbent assay (ELISA)
  - Cytokine stimulation of MTH53A cells
  - Cell preparation for live-cell imaging
  - Cell viablity staining
- Drafting of the manuscript

Cytokine 57 (2012) 210–220

Contents lists available at SciVerse ScienceDirect

Cytokine

journal homepage: www.elsevier.com/locate/issn/10434666

TNF-α induced secretion of HMGB1 from non-immune canine mammary epithelial cells (MTH53A)

Saskia Willenbrock [a,b], Olga Braun [b], Judith Baumgart [c], Sandra Lange [d], Christian Junghanss [d], Alexander Heisterkamp [e], Ingo Nolte [a], Jörn Bullerdiek [a,b], Hugo Murua Escobar [a,*]

[a] Small Animal Clinic and Research Cluster of Excellence "REBIRTH", University of Veterinary Medicine Hannover, Buenteweg 9, D-30559 Hannover, Germany
[b] Centre for Human Genetics, University of Bremen, Leobener Strasse ZHG, D-28359 Bremen, Germany
[c] Laser Zentrum Hannover e.V. and Research Cluster of Excellence "REBIRTH", Hollerithallee 8, D-30419 Hannover, Germany
[d] Division of Medicine, Dept. of Haematology/Oncology, University of Rostock, Ernst-Heydemann-Straße 6, D-18057 Rostock, Germany
[e] Institute for Applied Optics, Friedrich-Schiller-University Jena, Froebelstieg 1, D-07743 Jena, Germany

ARTICLE INFO

Article history:
Received 9 August 2010
Received in revised form 7 November 2011
Accepted 9 November 2011
Available online 6 December 2011

Keywords:
HMGB1
Secretion
Cytokines
Tumor
Canis familiaris

ABSTRACT

Background: Mammary neoplasias are one of the most frequent and spontaneously occurring malignancies in dogs and humans. Due to the similar anatomy of the mammary gland in both species, the dog has become an important animal model for this cancer entity. In human breast carcinomas, the overexpression of a protein named high-mobility group box 1 (HMGB1) was reported. Cells of the immune system were described to release HMGB1 actively exerting cytokine function. Thereby it is involved in the immune system activation, tissue repair, and cell migration. Passive release of HMGB1 by necrotic cells at sites of tissue damage or in necrotic hypoxic regions of tumors induces cellular responses e.g. release of proinflammatory cytokines leading to elevated inflammatory response and neo-vascularization of necrotic tumor areas.
Herein we investigated if a time-dependent stimulation with the separately applied proinflammatory cytokines TNF-α and IFN-γ can cause secretion of HMGB1 in a non-immune related HMGB1-non-secreting epithelial canine mammary cell line (MTH53A) derived from non-neoplastic tissue.
Methods: The canine cell line was transfected with recombinant HMGB1 bicistronic expression vectors and stimulated after transfection with the respective cytokine independently for 6, 24 and 48 h. HMGB1 protein detection was performed by Western blot analysis and quantified a by enzyme-linked immunosorbent assay. Live cell laser scanning multiphoton microscopy of MTH53A cells expressing a HMGB1–GFP fusion protein was performed in order to examine, if secretion of HMGB1 under cytokine stimulating conditions is also visible by fluorescence imaging.
Results: The observed HMGB1 release kinetics showed a clearly time-dependent manner with a peak release 24 h after TNF-α stimulation, while stimulation with IFN-γ had only small effects on the HMGB1 release. Multiphoton HMGB1 live cell microscopy showed diffuse cell membrane structure changes 29 h after cytokine-stimulation but no clear secretion of HMGB1–GFP after TNF-α stimulation was visible.
Conclusion: Our results demonstrate that non-immune HMGB1-non-secreting cells of epithelial origin derived from mammary non-neoplastic tissue can be induced to release HMGB1 by single cytokine application. This indicates that tumor and surrounding tissue can be stimulated by tumor present inflammatory and necrotic cytokines to release HMGB1 acting as neo-vascularizing factor thus promoting tumor growth.

1. Introduction

Human and canine mammary tumors are one of the most frequent malignancies in females. In both species they present similar patterns of tumor progression and metastasis [1]. Thereby, the dog has become an important animal model for cancer due to the fact that tumors in dogs are naturally occurring in contrast to the commonly used rodent animal model systems with induced tumors [2]. Accordingly, several distinct naturally occurring canine cancers

* Corresponding author. Tel.: +49 511 953 6382; fax: +49 511 953 6204.
E-mail addresses: saskia.willenbrock@tiho-hannover.de (S. Willenbrock), olga.braun@mail.uni-oldenburg.de (O. Braun), j.baumgart@lzh.de (J. Baumgart), sandra.lange@med.uni-rostock.de (S. Lange), christian.junghanss@med.uni-rostock.de (C. Junghanss), a.heisterkamp@uni-jena.de (A. Heisterkamp), inolte@tiho-hannover.de (I. Nolte), bullerd@uni-bremen.de (J. Bullerdiek), hescobar@tiho-hannover.de (H. Murua Escobar).

1043-4666/$ - see front matter © 2011 Elsevier Ltd. All rights reserved.
doi:10.1016/j.cyto.2011.11.011

were reported to show similar biological behavior when compared to their human counterpart e.g. mammary carcinomas, osteosarcomas or lung carcinomas [3,4]. In case of mammary gland tumors a clear age and hormone dependency has been shown in dogs as well as in humans [5,6]. The anatomy of the mammary gland in both species is very similar, making the dog an excellent model to reveal mechanisms of the respective tumor biology and to evaluate therapeutic approaches providing benefit to both species.

One protein strongly associated with breast cancer in dogs and humans is the high-mobility group box protein 1 (HMGB1; syn. amphoterin or HMG-1). This protein has an amino acid sequence identity of 100% amongst the two species [7]. Therefore it provides an interesting aspect in terms of comparative oncology.

HMGB1 was reported to be higher expressed in primary human breast carcinomas in comparison to normal breast tissue [8,9]. Analysis of HMGB1 transcripts by Northern blot hybridization identified a strong intertumoral variation of *HMGB1* expression among breast cancer samples [9].

HMGB1 was initially described as an ubiquitous expressed non-histone nuclear protein belonging to the HMG-protein-superfamily [10,11]. Later on, HMGB1 was discovered to exert two main fields of activity depending on the cellular localization. Intracellular HMGB1 plays a role as DNA-binding protein to sustain nucleosome structure [12], acts as architectural transcription factor regulating gene expression by bending promoter DNA regions [13] and modulates activity of steroid hormone receptors [14].

Besides the nuclear function, HMGB1 can be passively or actively released into the extracellular space acting there as a proinflammatory cytokine. Passive liberation of HMGB1 is caused by necrotic or damaged cells [15,16]. In contrast, cells that undergo apoptosis do not secrete HMGB1 as the protein stays tightly associated to the chromatin [15]. HMGB1 is actively secreted by activated cells of the immune system such as monocytes, macrophages, pituicytes, dendritic cells and natural killer cells [17–21]. Those cells release HMGB1 in response to inflammatory stimuli causing cellular responses like inflammation, sepsis, development of acute lung injury as well as stimulation of cytokine expression and secretion [17,18,22,23]. In macrophage cell cultures, HMGB1 is found to be released as a "late" appearing inflammatory mediator in a delayed manner 8–20 h after bacterial infection or following stimulation with endotoxin or "early" cytokines (tumor necrosis factor-alpha (TNF-α), interleukin-1 beta (IL-1β), interleukin-6 (IL-6), interferon-gamma (IFN-γ)) [22,24–26].

In addition to immune-related cells, adenocarcinoma derived tumor cell lines (HCT 116, WiDr, Caco-2) were also reported to secrete HMGB1 spontaneously without exogenous stimuli or in a polarized fashion after cytokine-mix stimulation [27–29]. Liu et al. were able to induce HMGB1 secretion in primary mouse intestinal epithelial cells (IEC) after stimulation with a mixture of different cytokines [29]. Fujii et al. recently demonstrated that also co-treatment with chemical factors (deoxycholic acid and azoxymethane) leads to accelerated secretion of HMGB1 in IEC-6 cells [30].

However, the relationship between HMGB1-release and time-dependently stimulation with the separately applied inflammatory cytokines TNF-α und IFN-γ in a mammary epithelial cell line has not been studied so far.

The effect of extracellular HMGB1 is mediated by interaction with the receptor for advanced glycation end products (RAGE) [31] and/or the Toll-like receptors (TLR)-2, and -4 [32,33]. Signaling via Toll-like receptors enables cells of the innate immune system to respond to various exogenous and endogenous stimuli causing cell activation and transcription of proinflammatory cytokines [34]. In the setting of cancer, the HMGB1/RAGE ligand/receptor complex is supposed to regulate proliferation, migration and metastasis of tumor cells [31,35,36].

Due to the high mitotic rate of the tumor cells and the existence of unsystematic tumor vessel architecture, hypoxia can be observed in large numbers of solid tumors [37] leading to the formation of necrotic areas with passively released HMGB1 [38]. In this scenario HMGB1 is supposed to play a key role in the promotion of the tumor growth by mediating angiogenic effects through increasing the expression of angiogenesis-related cytokines and growth factors [38,39]. Besides necrotic tumor cells, activated tumor-associated macrophages have the function to release HMGB1 actively as response to hypoxia or cytokines (e.g. TNF-α or IL-1β) and also by HMGB1 itself due to autostimulation [17,18,22,23].

The mediation of HMGB1 signaling between non-tumorigenic cells like e.g. epithelial cells and the tumor cells in case of breast cancer is supposed to be arranged by specialized activated tumor stroma [40].

Therefore, we hypothesized in the described context of tumor development and progression if also non-transformed HMGB1-non-secreting epithelial cells transfected with recombinant HMGB1 bicistronic expression vectors can be stimulated by time-dependent separate application of the proinflammatory cytokines TNF-α and IFN-γ to start active HMGB1 secretion.

To prove this, we chose a non-neoplastic HMGB1-non-secreting MTH53A canine mammary cell line of epithelial origin for our experiments with regard to the previously described advantages of the canine animal model resembling human neoplasias.

We were able to detect a clear secretion of recombinant HMGB1 from TNF-α stimulated MTH53A cells by HMGB1–Western blotting and quantified the amount of released HMGB1 by enzymelinked immunosorbent assay (ELISA). To confirm the results gained by Western blotting and HMGB1-ELISA, we performed multiphoton live cell microscopy on transfected HMGB1–GFP expressing MTH53A cells under TNF-α stimulating condition to visualize the secretion of HMGB1.

2. Materials and methods

2.1. pIRES-hrGFPII plasmid construction

Two variants of recombinant pIRES-hrGFP II (Stratagene, La Jolla, CA) vector constructs were generated, carrying the *hrGFP* gene (pIREShrGFP) and the gene of interest.

The bicistronic expression cassette of the different constructed vectors permits the simultaneous but separate expression of the inserted genes of interest and of *hrGFP* showing successful transfection of the cells with the respective vector by green fluorescence.

The first variant contains the canine *HMGB1* coding sequence (GenBank ID: AY135519.1) without the terminal stop codon resulting in an HMGB1 fusion protein with a recombinant short 3×FLAG peptide sequence at its C-terminal part (pIRES-hrGFP II-*rHMGB1* + FLAG) to differentiate via immunohistochemistry between endogenous and expressed recombinant HMGB1 protein (rHMGB1 + FLAG). The second construct contains the complete HMGB1 coding sequence, including the terminal TAA stop codon (pIRES-hrGFP II-*rHMGB1*). This vector variant was constructed to make sure that the 3×FLAG-tail has no effect on the function of the recombinant HMGB1 (rHMGB1) protein.

The following primer pairs were used for polymerase chain reaction (PCR) to amplify the corresponding sequences: EcoRI-B1-CFA-FWD (5′- GGAATTCCACCATGGGCAAAGGAGA-3′; forward primer for rHMGB1 + FLAG and rHMGB1), NotI-B1-CFA-REV (5′-GCGCGGCCGCTTATTCATCATCATC-3′, reverse primer rHMGB1), NotI-B1-CFA-Rev/-TAA (5′-AAGAATGATGATGATGAAGCGGCCGCG C-3′, reverse primer rHMGB1 + FLAG). The amplified PCR products were separated on a 1.5% agarose gel, eluted using QIAquick Gel

Extraction Kit (QIAGEN, Hilden, Germany) and ligated into the pIRES-hrGFP II vector plasmid (Stratagene, La Jolla, CA). Verification of the constructed plasmids was done by NotI/EcoRI double restriction digest and sequencing.

2.2. Cell culture, transfection and sample preparation

The MTH53A canine mammary cell line, derived from epithelial healthy canine mammary tissue, was established at the Centre for Human Genetics, University of Bremen, Bremen, Germany. The cells were cultivated in medium 199 (Gibco, Karlsruhe, Gemany) supplemented with 20% heat-inactivated fetal calf serum (PAA Laboratories GmbH, Coelbe, Germany), 200 U/ml (U; unit) penicillin and 200 ng/ml streptomycin (Biochrom AG, Berlin, Germany).

The transient transfection assays were performed in 6-well plates with approximately 400,000 cells per well and 2 ml medium. pIRES-hrGFP II vector constructs (2 μg) were transfected into MTH53A cells according to the manufacturer's instructions using 3 μl FuGeneHD (Roche, Mannheim, Germany) in 100 μl H_2O. The transfected MTH53A cells (tMTH53A) were incubated for 48 h in culture medium and fixed with phosphate-buffered formaldehyde (4%, pH 7.4, 10 min). The nuclei were stained using Vectashield Mounting Medium with DAPI (4′-6-diamidino-2-phenylindol, Vector Laboratories, Burlingame, CA, USA) and the uptake of plasmid DNA was verified by fluorescence microscopy using an Axioskop microscope (Carl Zeiss, Oberkochen, Germany).

For Western blot analysis, 48 h after transfection the cell-conditioned medium was harvested and the adherent MTH53A cells were lysed using cell lysis buffer (50 mM Tris, pH 7.8, 150 mM NaCl, 1% Nonidet P-40). Cellular debris was removed by centrifugation for 10 min at 1000*g* and the supernatants were collected.

2.3. Induction of HMGB1 release by cytokine stimulation

Approximately 400,000 MTH53A cells were plated in 6-wells and transfected as described above in Section 2.2 with the pIRES-hrGFPII-*rHMGB1* + FLAG vector construct to differentiate between the recombinant HMGB1 (rHMGB1 + FLAG) and endogenous HMGB1 (eHMGB1). To induce the release of HMGB1 the cells were stimulated 24 h after transfection with 50 ng/ml canine TNF-α (R&D Systems, Minneapolis, USA) or 100 U/ml canine IFN-γ (R&D Systems, Minneapolis, USA) for different time periods (6, 24, 48 h) at 37 °C and 5% CO_2. After incubation the conditioned medium and the MTH53A cells were harvested as described for immunochemical assays.

2.4. Cell viability staining

Viability of 24 h TNF-α or IFN-γ tMTH53A and MTH53A stimulated cells was assessed by Trypan blue exclusion (Invitrogen, Carlsbad, USA), which detects cells undergoing necrosis.

It is generally known that TNF-α stimulation can induce apoptosis in a variety of cell types [41]. To verify if incubation with TNF-α or IFN-γ may lead to apoptosis or necrosis and thus possibly to a release of HMGB1, double staining with annexin V-PE/propidium iodide (PI) was performed using the Annexin V-PE Apoptosis Detection Kit (PromoCell GmbH, Heidelberg, Germany). This assay distinguishes between apoptotic and necrotic cells.

A number of approximately 400,000 MTH53A cells was seeded in 1-well Falcon CultureSlides (Becton, Dickinson and Company, Heidelberg, Germany), transfected with pIRES-hrGFPII-*rHMGB1* + FLAG and treated with TNF-α or IFN-γ for 6, 24, and 48 h as described in Section 2.3. After incubation, the culture medium was replaced by 500 μl 1× Annexin V binding buffer.

For detection of phosphatidyl serine exposure on the external leaflet of the plasma membrane during apoptosis, Annexin V-PE reagent was added showing orange-red staining. Necrotic cell detection was performed by adding propidium iodide (PromoCell GmbH, Heidelberg, Germany) in a concentration of 30 μM. PI is a nucleic acid intercalator passing only through disturbed cell membranes staining the nuclei of necrotic cells with a light red fluorescence.

The cells were incubated for 15 min at room temperature in the dark, washed twice with 1x phosphate-buffered saline after incubation and fixed for 10 min using 4% phosphate-buffered formaldehyde (pH 7.4). The cells were analyzed by fluorescence microscopy using an Axioskop microscope with a rhodamine filter (Carl Zeiss, Oberkochen, Germany).

2.5. Immunochemical assays: Western blot analysis and HMGB1 enzyme-linked immunosorbent assay (ELISA)

The presence of recombinant and endogenous HMGB1 in the harvested cell-conditioned medium or in lysed MTH53A cells was assayed before and after cytokine treatment by Western blotting analysis and quantified using the HMGB1 ELISA Kit II (Shino-Test Corporation, Kanagawa, Japan).

For Western blot analysis equal volumes of the harvested samples were heated for 5 min at 95 °C in reducing sample buffer, fractioned by sodiumdodecylsulfate–polyacrylamide gel electrophoresis (SDS–PAGE) (4% stacking gel, 12% running gel) and transferred to a polyvinylidene difluorid membrane with 0.2 μM pore size (PALL Corporation, New York, USA) in order to examine recombinant HMGB1 protein expression. Membranes were probed using a 1:5000 dilution of primary HMGB1 antibody [HAP46.5] (Abcam plc, Cambridge, UK) and 1:10,000 dilution of goat anti mouse IgG (H&L):HRP (AbD Serotec, Martinsried/Planegg, Germany) secondary antibody (HRP; horseradish peroxidase). To exclusively detect recombinant rHMGB1 + FLAG protein, we used a monoclonal ANTI-FLAG® M2-Peroxidase (HRP) antibody (Sigma–Aldrich, St. Louis, USA) in a dilution of 1:10,000. Visualization was done by chemiluminescence using 3.3′-diaminobenzidine (DAB) substrate (Sigma–Aldrich, St. Louis, USA). To determine the HMGB1 level in the cell-conditioned medium and MTH53A cell lysates after cytokine stimulation the Shino-Test HMGB1 ELISA Kit II was used according to the manufacturer's instructions.

The samples were concentrated before ELISA-application from 200 to 450 μl lysate and 500 μl medium to 20 μl end volume via 10 kDa (kilo Dalton) Roti-Spin Midi-10 columns (Carl Roth GmbH, Karlsruhe, Germany). The absorbance of the performed ELISA was read at 455 nm in a Synergy HT multi-detection microplate reader (BioTek Instruments GmbH, Bad Friedrichshall, Germany) using KC4 software (Kineticalc for Windows, version 3.4, BioTek Instruments GmbH). The levels of HMGB1 were calculated with reference to standard curves of purified recombinant HMGB1 at various dilutions (1.25, 2.5, 5.0, 10.0, 20.0, 40.0, 80.0 ng/ml) and in consideration of the concentrations factors.

2.6. HMGB1–GFP live cell imaging using laser scanning microscopy

For HMGB1 live cell imaging the protein coding sequence of the canine HMGB1 was amplified by PCR using the following primer pair: EcoRI-B1-CFA-FWD (5′-CGGAATTCCACCATGGGCAAAGGAG A-3′, forward primer) and KpnI-B1-CFA-REV (5′- GATGATGATGA ATAAGGTACCGC-3′, reverse primer). The obtained PCR products were separated on a 1.5% agarose gel, recovered with QIAquick Gel Extraction Kit (QIAGEN, Hilden, Germany), ligated in pEGFP-C1 vector plasmid (BD Bioscience Clontech) and sequenced for verification. The canine MTH53A mammary cells were cultivated in glass-bottom-dishes (MatTek Corporation, Ashland, USA) using M199 media (Gibco, Karlsruhe, Gemany) supplemented with 20% heat-inactivated fetal calf serum (PAA Laboratories GmbH, Coelbe,

Germany) and 200 U/ml penicillin and 200 ng/ml streptomycin (Biochrom AG, Berlin, Germany) and transfected using 3 μl FuGeneHD reagent (Roche, Mannheim, Germany) and 2 μg pEGFP-HMGB1 vector construct in 100 μl H_2O according to the manufacturer's instructions. Twenty-four hours after transfection the cells were stimulated with 50 ng/ml canine TNF-α (R&D Systems, Minneapolis, USA) for induction of HMGB1 release. Live cell imaging was performed for 50 h on an uniquely modified multiphoton laser scanning system (Zeiss Axiovert S100) consisting of a femtosecond-laser system (Chameleon Ultra II, Coherent Inc., tunable wavelength 690–1040 nm; fs, femtosecond, 10^{-15} s) and a custom built scanning and detection module. Used parameters: 37 °C, 5% CO_2, 900 nm wavelength, 2.71 V amplifier voltage, 8 mW (80 megahertz) pulse energy. Images were recorded in 30 μm 3D-stacks with 1.5 μm layer distance and 256 × 256 pixel resolution every 30 min.

3. Results and discussion

During the last years HMGB1 has become an interesting molecular target in oncology due to the described pro-angiogenetic activity [39,42] as well as the involvement in cell proliferation and metastasis [31,35,36]. As previously reported, the expression of HMGB1 is strongly associated with mammary cancer, but the involvement of HMGB1 in its cytokine function is still not completely uncovered.

Therefore, we investigated if HMGB1-secretion is inducible by time-dependent TNF-α and IFN-γ stimulation in a non-immune related HMGB1-non-secreting transfected canine non-neoplastic mammary cell line of epithelial origin (MTH53A) overexpressing recombinant HMGB1.

3.1. Fluorescence analysis and verification of transfected canine MTH53A cells

Prior cytokine stimulation the transient transfection of MTH53A cells with the two constructed recombinant HMGB1 bicistronic expression vectors (pIRES-hrGFP II-*rHMGB1* + FLAG and pIRES-hrGFP II-*rHMGB1*) was carried out. The uptake of plasmid DNA and expression of hrGFP was evaluated by fluorescence microscopy 24 h after transfection.

As shown in Fig. 1, the canine MTH53A cell line was transfected with FuGeneHD transfection reagent using pIRES-hrGFP II-*rHMGB1* + FLAG (Fig. 1a and d), pIRES-hrGFP II-*rHMGB1* (Fig. 1b and e) and pIRES-hrGFP II (Fig. 1c and f) plasmid without insert, used as positive control. No particular changes in the morphology and growing behavior of the transfected cells carrying the different expression vector constructs (Fig. 1a–f) could be observed. The transfected cells showed green fluorescence in the cytoplasm due to hrGFP expression. In case of transfection with pIRES-hrGFP II-*rHMGB1* + FLAG or pIRES-hrGFP II-*rHMGB1* this implicates successful expression of recombinant HMGB1 (rHMGB1 + FLAG (1a), and rHMGB1 (1b)). A transfection efficiency of approximately 20% was achieved in all transfection experiments.

Direct detection of recombinant HMGB1 by fluorescence microscopy is not possible due to the bicistronic vector. Thus, the HMGB1 detection was carried out subsequently by Western blot analysis of the harvested cell lysates and cell-conditioned media (Figs. 2 and 3).

3.2. Unstimulated transfected MTH53A cells do not release HMGB1

The Western blot analyses were performed to investigate the HMGB1 release potential in unstimulated pIRES-hrGFP II-*rHMGB1* or pIRES-hrGFP II-*rHMGB1* + FLAG transfected canine MTH53A cells, expressing rHMGB1 or rHMGB1 + FLAG in large quantity.

3.2.1. Anti-HMGB1 Western blot

Fig. 2a displays a representative Western blot using anti-HMGB1 antibody [HAP46.5] showing the presence of endogenous and inducible expression of rHMGB1 and rHMGB1 + FLAG. Recombinant commercially available His-tagged HMGB1 with a molecular mass of 31 kDa was used as positive control (Fig. 2a, lane 2). The samples analyzed by Western blotting were used in unconcentrated condition directly after harvesting.

The analyzed cell lysate of pIRES-hrGFP II-*rHMGB1* transfected MTH53A cells (Fig. 2a, lane 7) and the corresponding control (Fig. 2a, lane 1) showed one clear signal at a molecular mass of less

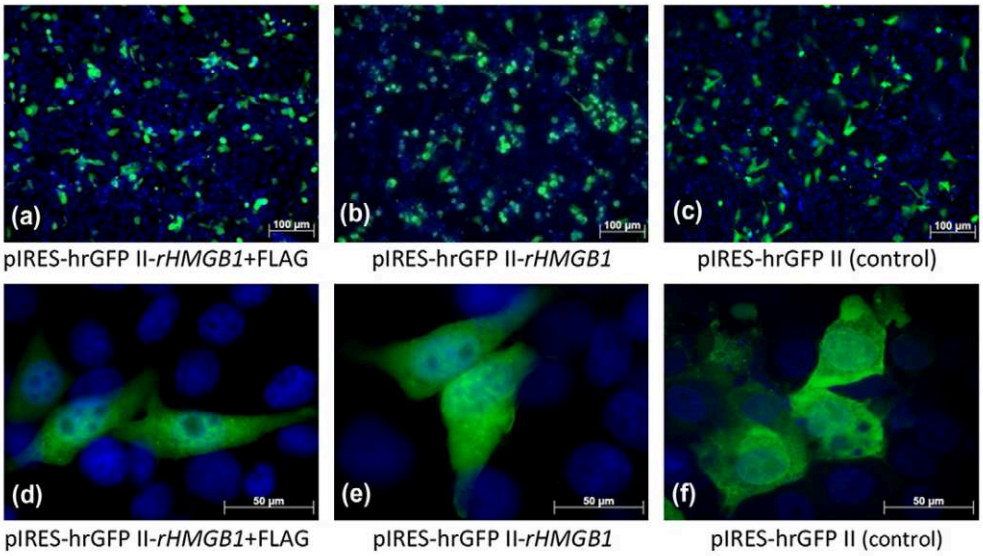

Fig. 1. Fluorescence analysis. Fluorescence analysis of (a) pIRES-hrGFPII-*rHMGB1* + FLAG, (b) pIRES-hrGFPII-*rHMGB1*, and (c) pIRES-hrGFPII expression in canine MTH53A mammary cell line; each 24 h after transfection. DAPI fluorescent staining of cell nuclei, merged GFP and DAPI images at 100-fold magnification. (d) pIRES-hrGFPII-*rHMGB1* + FLAG, (e) pIRES-hrGFPII-*rHMGB1*, and (f) pIRES-hrGFPII expression, merged GFP and DAPI images at 400-fold magnification.

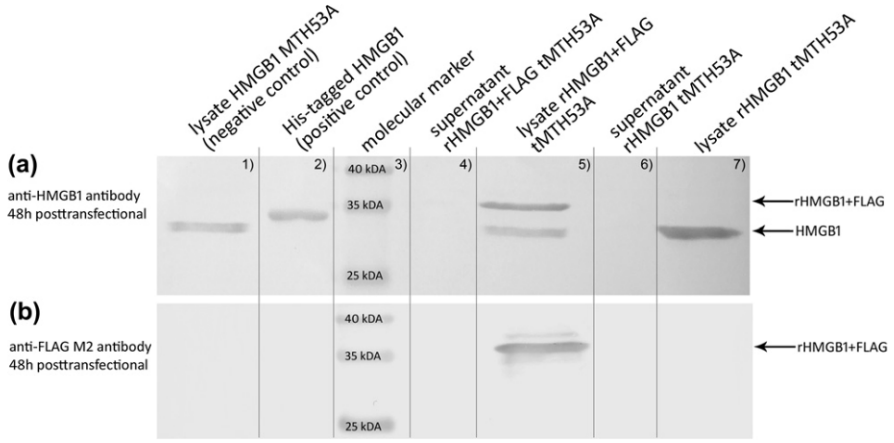

Fig. 2. Western blot analysis (cells w/o cytokine stimulation). Expression of HMGB1 and rHMGB1 + FLAG in untransfected (MTH53A) and transfected MTH53A (tMTH53A) cells w/o cytokine stimulation was analyzed. Transfection of MTH53A cells was performed with 3 μl FuGene HD reagent and 2 μg recombinant pIRES-hrGFPII-*rHMGB1* + FLAG (rHMGB1 + FLAG) and pIRES-hrGFPII-*rHMGB1* (rHMGB1) expression vector, respectively. For Western blot analysis, 48 h after transfection the cell-conditioned medium was harvested and the adherent MTH53A cells were lysed. Commercially available polyhistidine (His)-tagged HMGB1 was used during all Western blot analyses for verification. (a) Western blot using anti-HMGB1 antibody (HAP46.5). In all analyzed cell lysates eHMGB1 and/or rHMGB1 and rHMGB1 + FLAG, respectively, was detectable. No HMGB1 release in the cell-conditioned media could be observed w/o cytokine stimulation. (b) Western blot analysis with anti-FLAG M2 antibody for specific detection of the rHMGB1 + FLAG protein variant. As expected, solely a signal for rHMGB1 + FLAG is present at the cell lysate of MTH53A cells transfected with the pIRES-hrGFPII-*rHMGB1* + FLAG expression vector and no extracellular located HMGB1 or rHMGB1 + FLAG in the respective cell-conditioned medium is detectable.

than 35 kDa matching to eHMGB1 (Fig. 2a, lane 1) and/or unmodified rHMGB1 (Fig. 2a, lane 7). Due to same protein sizes of eHMGB1 and unmodified rHMGB1 only one signal was detectable in the lysate of tMTH53A cells expressing the recombinant unmodified HMGB1 (Fig. 2a, lane 7). The experimentally determined protein mass for HMGB1 differed from the calculated mass of 25 kDa because of commonly known post-translational modifications. As shown in the literature, HMGB1 has an experimental determined protein size of approx. 30 kDa [43,44].

The cell lysate of tMTH53A cells expressing rHMGB1 + FLAG (Fig. 2a, lane 5) showed two signals with more intensive staining of the upper protein band. The signal with the lower molecular weight equated to eHMGB1. Thus, the signal with the higher molecular mass of approx. 35 kDa detected the rHMGB1 + FLAG. Although the theoretical calculated molecular mass of FLAG-tagged HMGB1 is about 28 kDa, the differing experimentally determined molecular mass can be explained as previously described for unmodified HMGB1.

Summarizing, a detection of eHMGB1, rHMGB1 and rHMGB1 + FLAG in the analyzed cell lysates was possible using the anti-HMGB1 antibody. In contrast, the corresponding cell culture media of tMTH53A cells expressing rHMGB1 or rHMGB1 + FLAG showed no signals for HMGB1 (Fig. 2a, lanes 4 and 6).

3.2.2. Anti-FLAG Western blot

To prove the expression of rHMGB1 + FLAG, we performed Western blot analyses using an anti-FLAG M2 antibody for exclusive FLAG-tag detection (Fig. 2b). The cell lysate of tMTH53A cells expressing rHMGB1 + FLAG (Fig. 2b, lane 5) showed just one signal with a molecular mass of 35 kDa equivalent to the detected rHMGB1 + FLAG represented in Fig. 2a (lane 5). HMGB1 protein without FLAG-tag modification was not detectable by Western blotting in the other analyzed cell lysates (Fig. 2b, lanes 1 and 7) because the anti-FLAG M2 antibody exclusively detects proteins modified by FLAG-tag. In the corresponding analyzed culture media (Fig. 2b, lanes 4 and 6) no signals for rHMGB1 + FLAG were detectable.

The gained Western blot results demonstrate the possibility to differentiate between FLAG-tagged and untagged HMGB1 because of the differing molecular weight. Therefore, we exclusively used the pIRES-hrGFP II-*rHMGB1* + FLAG (rHMGB1 + FLAG) expression vector and the anti-HMGB1 antibody for detection of rHMGB1 + FLAG and unmodified endogenous HMGB1 in the following experiments.

3.2.3. Anti-HMGB1 and anti-FLAG Western blot conclusions

The anti-HMGB1 and anti-FLAG Western blot analyses indicated that pIRES-hrGFP II-*rHMGB1* or pIRES-hrGFP II-*rHMGB1* + FLAG transfected MTH53A non-neoplastic cells do not secrete HMGB1 w/o (without) cytokine stimulation. In contrast, non-immune related cells as the already mentioned HMGB1 over-expressing human colon carcinoma derived tumor cell lines are known to be HMGB1-secreting spontaneously without exogenous stimuli [27,28].

Due to the fact that MTH53A cells are not spontaneously secreting HMGB1, we wanted to induce the secretion of HMGB1 by cytokine stimulation. As previously described, secretion of HMGB1 is inducible by different stimuli as lipopolysaccharides or single and combined cytokines in different cell types in a dose- and time-dependent manner whereas the cytokines TNF-α and IFN-γ appear to be most effective [17–20,22,24–27,45]. Concerning dosage and time of incubation for activation of highest HMGB1 secretion different findings ranging for stimulation with TNF-α from 6 to 72 h at concentrations of 5–100 ng/ml and for IFN-γ from 5 to 100 U/ml) were reported [22,24,27].

We followed these results regarding the selection of the incubation parameters time and dose for TNF-α and IFN-γ.

3.3. Effect of TNF-α and IFN-γ stimulation on HMGB1 release by MTH53A cells

The aim was to evaluate the potential role of the proinflammatory cytokines TNF-α and IFN-γ to stimulate HMGB1 secretion in non-immune related non-neoplastic MTH53A cells. Therefore, MTH53A and pIRES-hrGFP II-*rHMGB1* + FLAG tMTH53A were stimulated independently by addition of the canine cytokines in a time-dependent manner (6, 24 and 48 h).

The cell lysates and cell-conditioned media of the stimulated cells were subsequently assayed by Western blot. Analyses of all cell lysates (Fig. 3a, c and e) detected signals for either eHMGB1

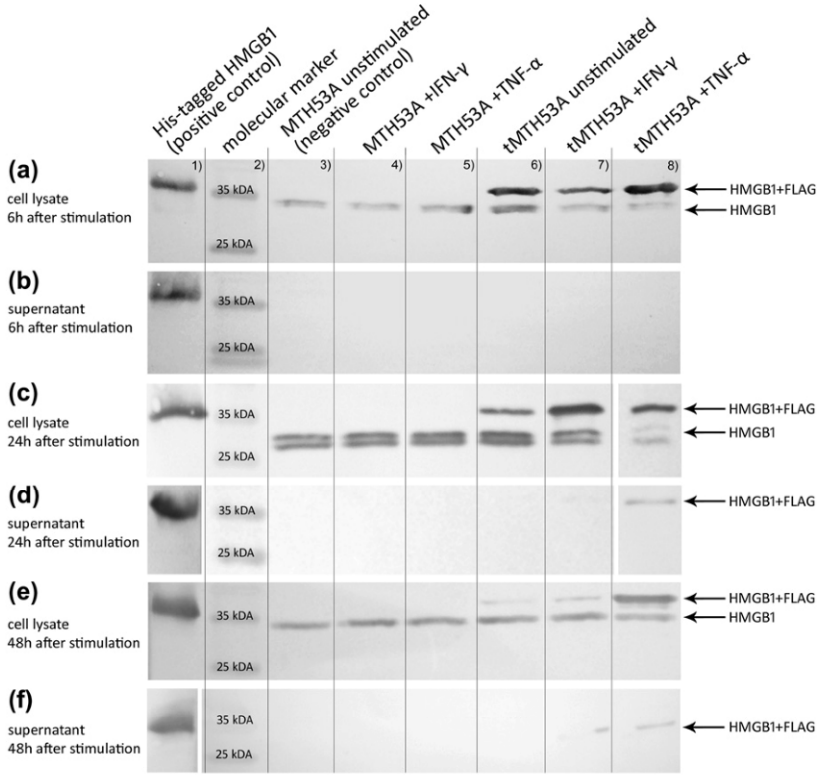

Fig. 3. Western blot analysis (cytokine-stimulated cells). Expression and secretion of eHMGB1 and rHMGB1 + FLAG in cytokine-stimulated MTH53A and tMTH53A (pIRES-hrGFPII-*rHMGB1* + FLAG transfected) cells analyzed by Western blotting. 24 h after transfection cytokine stimulation was done with TNF-α and IFN-γ. For Western blot analysis 6, 24, and 48 h after stimulation the cell-conditioned media were harvested and the adherent MTH53A and tMTH53A cells were lysed. The Western blotting experiments were performed with anti-HMGB1 antibody (HAP46.5) detecting eHMGB1 and rHMGB1 + FLAG. Commercially available His-tagged HMGB1 was carried along all Western blots for verification. (a, c and e) In all of the analyzed cell lysates eHMGB1 and rHMGB1 + FLAG was detectable showing continuously higher amounts of rHMGB1 + FLAG (upper band at approximately 35 kDa) in comparison to eHMGB1 (lower band). (b) No released eHMGB1 or rHMGB1 + FLAG was detectable in the media of the cytokine-stimulated cells after an incubation period of 6 h. (d) rHMGB1 + FLAG secretion, but no release of eHMGB1, was detectable in the conditioned medium of tMTH53A cells incubated for 24 h with TNF-α. The supernatant of untransfected MTH53A cells showed no secretion of eHMGB1. Incubation for 24 h with IFN-γ induced a weak secretion of rHMGB1 + FLAG but no release of eHMGB1. (f) rHMGB1 + FLAG secretion after stimulation for 48 h with TNF-α could be observed. As seen in D, no release of eHMGB1 as well was detectable in the conditioned media of tMTH53A cells incubated for 48 h with TNF-α. Stimulation for 48 h with IFN-γ resulted in a slightly higher secretion of rHMGB1 + FLAG compared to IFN-γ stimulation for 24 h. Matching to the 24 h incubation period no eHMGB1 was released after 48 h of IFN-γ stimulation. (c and d) Cell lysate and supernatant of transfected MTH53A cells under 24 h stimulation with TNF-α (tMTH53A + TNF-α) were interchanged during Western blot analysis. For a better overview the two samples were exchanged accordingly here. (d and f) The positive control (His-tagged HMGB1) was originally applied on the left side of the displayed Western blot. For a better overview the position of this sample was switched to the right side of the figure.

(lanes 3, 4 and 5) or rHMGB1 + FLAG in addition to the eHMGB1 (lanes 6, 7 and 8) comparable to the experimentally determined protein sizes described in Section 3.2 (Fig. 2a and b, lanes 1, 5 and 7).

The eHMGB1 doublet band appearance displayed in Fig. 3c (lanes 3–8) shows two molecularly different forms of the protein. This is an infrequently phenomenon with still not clearly elucidated reason as shown in different studies [46,47]. HMGB1 doublet bands can be explained by the presence of isoforms occurring due to differing acetylation states depending on the activation state of a cell taking diverse roles in inflammatory disorders [48]. Additionally, mass spectroscopy analysis by Li et al. revealed that the lower band of HMGB1 shows a form with a partially degraded C-terminus but with the same functionality as full length HMGB1 [49].

3.3.1. Analysis of TNF-α stimulated cells

The Western blots performed on conditioned media of MTH53A and tMTH53A cells 6 h after stimulation with TNF-α (Fig. 3b, lanes 3–5) showed no signals for eHMGB1 or rHMGB1 + FLAG. Apparently, the incubation time of 6 h is insufficient for an effective induction of active HMGB1 secretion in MTH53A and tMTH53A cells.

Focusing on the analyses of the cell-conditioned media after TNF-α stimulation (Fig. 3c and d, lanes 5 and 8), the highest secretion level of HMGB1 was detectable after 24 h. A clear signal for rHMGB1 + FLAG (Fig. 3d, lane 8), but no eHMGB1 was visualizable (Fig. 3d, lanes 3–8).

Forty-eight hours after TNF-α stimulation rHMGB1 + FLAG is also present, but in a slightly reduced level (Fig. 3f). This indicates that an extended TNF-α stimulation time does not evoke increased HMGB1 secretion. Reduced extracellular HMGB1 level might be explained by proteolytic degradation. It is known that mammary epithelial cells have the ability to express the plasminogen activator system which is implicated in tissue remodeling [50]. Parkkinen et al. revealed in 1991 that the lysine-rich HMGB1 protein serves as substrate for plasminogen and tissue plasminogen activator (t-PA) resulting in degradation of HMGB1 [51].

Transfected MTH53A cells stimulated for 24 and 48 h with TNF-a should also have the ability to secrete eHMGB1. However, a release of the endogenous protein was not detectable in the examined cell-conditioned media. This can probably be explained by protein levels below the Western blot detection limit or the previously described degradation of the protein.

Regarding to the released rHMGB1 + FLAG protein, our results agree with the findings of Wang et al. [22] which signify that

HMGB1 is released by macrophages in highest levels after TNF-α stimulation for 18–24 h. Moreover, our results are confirmed by findings of Liu et al. [29], showing an increased time-dependent secretion of HMGB1 by CaCo-2 epithelial cells after stimulation with a mixture of cytokines (TNF-α, IL-1β and IFN-γ).

Differing from the mentioned previous studies, we were able to induce HMGB1 secretion by single TNF-α stimulation in the non-neoplastic epithelial cell line MTH53A.

3.3.2. Analysis of IFN-γ stimulated cells

The Western blot analyses of MTH53A and tMTH53A cells stimulated for 6 h with IFN-γ showed no release of HMGB1 (Fig. 3b, lanes 6–8) which can be explained as discussed for the 6 h TNF-α stimulation. After an incubation period of 24 h with IFN-γ the secretion of rHMGB1 + FLAG (Fig. 3d, lane 7) was also inducible, but in an obviously reduced amount in comparison to 24 h of TNF-α stimulation. The secretion of rHMGB1 + FLAG stimulated by IFN-γ increased after 48 h (Fig. 3f, lane 7), but no release of eHMGB1 was detectable. Our obtained findings act in accordance with the results of Rendon-Mitchell et al. [24], who showed time-dependently increasing HMGB1 levels in the culture medium of macrophage cell cultures with peak levels after 32 h of IFN-γ stimulation.

3.3.3. Analysis of untransfected cytokine stimulated cells

The analysis of the conditioned media of untransfected cytokine stimulated MTH53A cells (Fig. 3b, d and f, lanes 3–5) showed no release of eHMGB1. Theoretically those cells as well as tMTH53A cells should be able to secrete HMGB1.

A comparison of HMGB1 RNA expression levels of untransfected MTH53A cells w/o cytokine stimulation to the expression found in a canine pleomorphic mammary adenoma cell line (ZMTH3) showed an approx. 3.8 higher *HMGB1* expression in the neoplastic ZMTH3 cell line (unpublished data of relative real-time PCR analysis quantifying *HMGB1* in relation to the canine endogenous control [*GUSB* = beta-glucuronidase]). Consequently, it is likely that the endogenous HMGB1 protein level in MTH53A cells is low at conditions w/o cytokine stimulation.

In case of untransfected cytokine stimulated MTH53A cells, potentially the amount of secreted HMGB1 might be too low to be detected sufficiently by Western blot analyses in contrast to the highly expressed recombinant HMGB1 + FLAG protein. To avoid the problem of the detection limit, all samples were concentrated for ELISA quantification as stated later on (see Section 3.5.).

The levels of released eHMGB1 might be located below the Western blotting detection limit but effectual enough promoting tumor growth due to the known fact that secreted HMGB1 induces a positive feedback loop mediated by inflammatory cytokines stimulating new cells in an autocrine/paracrine manner to release HMGB1 [52,53].

3.4. Cell viability staining: TNF-α or IFN-γ stimulation does not induce necrosis or apoptosis in MTH53A cells

HMGB1 also can be released in a passive way by necrotic cell death [15,16]. We excluded this possibility by performing Trypan blue viability tests with TNF-α and IFN-γ stimulated tMTH53A cells showing a viability ratio of 90–95%.

Moreover, TNF-α stimulation can induce apoptosis in different types of cells [41] leading in the stage of secondary necrosis to passive release of HMGB1. To exclude the induction of apoptosis and/or necrosis by TNF-α or IFN-γ stimulation in MTH53A and tMTH53A cells, annexin V-PE/PI staining was performed.

The results of the double staining showed no detectable increase of annexin V and PI positive cells after cytokine stimulation with TNF-α or IFN-γ compared to the untreated control cells (untransfected cytokine-stimulated cells, transfected cells w/o cytokine treatment, respectively; data not shown). Merely a time-dependent slight increase of annexin V labeled and PI stained cells was observable after 6, 24 and 48 h of incubation in cytokine-treated and the corresponding control experiments. One reason for the marginal increase of labeled cells might be the continuous cultivation from 6 to 48 h. Altogether, the comparison of all experiments showed no excessive annexin v or PI staining in GFP-fluorescent cells after 48 versus 6 h of incubation (data not shown).

Thus, it is excludable that the detection of HMGB1-release in the Western blot analyzed cytokine-stimulated supernatants is caused by apoptotic or necrotic cell death.

3.5. Quantification of HMGB1 release using HMGB1-ELISA Kit II

HMGB1 detection by Western blot allows only a qualitative estimation. Due to the detection limit of this method, low concentrations of e.g. extracellular HMGB1 in cell culture supernatants can barely be visualized. Therefore, a specific HMGB1-ELISA was performed subsequently after Western blotting to quantify the amount of released and intracellular HMGB1 in the Western blot analyzed samples.

It must be noted, that the ELISA-test is unable to distinguish between eHMGB1 and rHMGB1 + FLAG due to the use of a specific anti-HMGB1 antibody. Thus, the total amount of HMGB1, including eHMGB1 and rHMGB1 + FLAG, was quantified by the HMGB1-ELISA.

Assuming that the unverifiable HMGB1 secretion in the Western blot analyzed supernatants (see Fig. 3b, d and f) might also be non-detectable by HMGB1-ELISA, we concentrated the cell-conditioned media preliminary to ELISA-application. The cell lysates were also concentrated by the same factor as the conditioned media for corresponding comparability and to maintain extracellular and intracellular HMGB1 in the same relation.

3.5.1. HMGB1 concentration calculation

Analysis of the measured ELISA absorbance values (data not shown) showed actually no need for cell lysate concentration because the values consistently exceeded the standard curve values showing high content of HMGB1 in the analyzed cell lysates. For example, the absorbance measured at tMTH53A lysate stimulated for 6 h with TNF-α was approx. 4.0 in comparison to the measured absorbance of 1.0 for the highest standard value.

However, to determine the HMGB1 protein concentrations, the amount of HMGB1 was calculated by extrapolation.

In consideration of the concentration factors, the calculation of the HMGB1 amounts resulted in altered concentrations of less than 80 ng/ml (Fig. 4), ranging in fact from approx. 30 ng/ml (lysate MTH53A, 6 h + IFN-γ) to 50 ng/ml (lysate tMTH53A, 48 h + TNF-α).

Theoretically, the expected HMGB1-concentrations of the concentrated cell lysates should exceed the highest standard curve value due to the fact that the determined sample absorbance values were considerably higher than the values building the standard curve. The unexpected calculated data can probably be explained by a saturation effect achieved due to the concentration of the samples containing excessive HMGB1 amounts.

To investigate these results in detail, some cell lysates and conditioned media (e.g. 24 h TNF-α stimulated tMTH53A) were also assayed in unconcentrated condition by HMGB1-ELISA resulting also in absorbance values exceeding the highest standard curve value. Therefore, the HMGB1 concentrations were also calculated by extrapolation showing approx. 210 ng/ml HMGB1 in the cell lysate and 251 ng/ml HMGB1 in the conditioned media of 24 h TNF-α stimulated tMTH53A cells (complete data not shown). These results suggest that the HMGB1 ELISA is saturated at concentrations of approx. 250 ng/ml HMGB1.

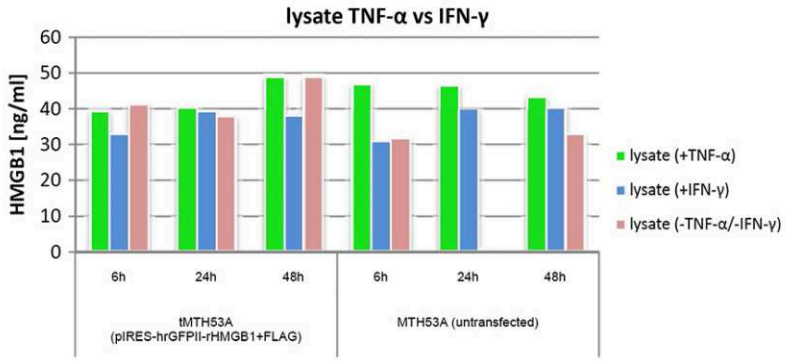

Fig. 4. HMGB1 quantification in cell lysates using HMGB1-ELISA. Detection of intracellular HMGB1 concentrations in cell lysates after 6, 24 and 48 h of TNF-α or IFN-γ stimulation using HMGB1-ELISA. The cell lysates of MTH53A, tMTH53A, and additionally, MTH53A w/o (without) cytokine stimulation (-TNF-α/-IFN-γ) were examined. In the cell lysate of MTH53A cells, incubated for 24 h w/o cytokines showed a concentration of less than 1 ng/ml HMGB1 and was excluded from the analysis. Comparison of all cell lysates showed HMGB1 concentrations ranging from 30 to 50 ng/ml.

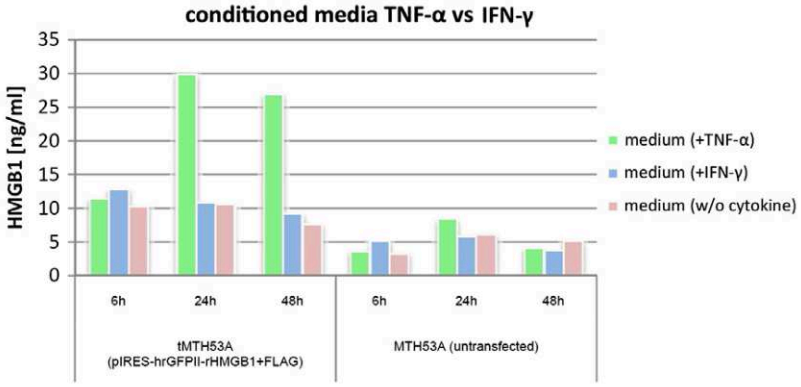

Fig. 5. HMGB1 quantification in cell-conditioned media using HMGB1-ELISA. Detection of secreted HMGB1 in cell-conditioned media after 6, 24 and 48 h of TNF-α or IFN-γ stimulation using HMGB1-ELISA. Concentrated media of MTH53A, tMTH53A, and additionally, MTH53A w/o cytokine stimulation were examined. In the conditioned media of tMTH53A cells, incubated for 24 h with TNF-α, the HMGB1 concentration of 30 ng/ml is about 3-fold as high as the corresponding controls (TNF-α stimulated MTH53A: 8 ng/ml HMGB1; tMTH53A w/o cytokine treatment: 10 ng/ml HMGB1). After 48 h of TNF-α treatment the level of HMGB1 is still elevated (27 ng/ml) in comparison to the corresponding controls. Stimulation with IFN-γ showed no significant effects on the secretion of HMGB1.

The complex calculation of the HMGB1 concentrations can be summarized by the conclusion that the calculated ELISA-data for the conditioned media (Fig. 5) are coherent and confirm the results achieved by Western blotting (Fig. 3) concerning TNF-α stimulation even though the HMGB1 threshold for the concentrated samples should be presumably higher than in unconcentrated condition.

3.5.2. Quantification of HMGB1 after TNF-α stimulation

We were able to detect a clearly elevated level of HMGB1 in the conditioned media of tMTH53A cells by stimulation with TNF-α in a time-dependent manner (Fig. 5). A stimulation with TNF-α for 24 h resulted in concentrations of 30 ng/ml HMGB1 in the culture media (Fig. 5), whereas the HMGB1 level was low after 6 h of TNF-α stimulation (11 ng/ml). This coincides with the fact that HMGB1 is released highest by macrophages after TNF-α stimulation for 18–24 h [18,22]. The data of the 48 h TNF-α stimulation experiments as well confirm the results received by Western blotting. In the assayed conditioned medium continuously elevated HMGB1 levels were detectable (27 ng/ml, 48 h) with slightly decreasing tendency in comparison to 24 h TNF-α stimulation. As expected, analysis of the corresponding controls led to determination of low HMGB1 levels (untransfected TNF-α stimulated MTH53A: 8 ng/ml HMGB1, tMTH53A w/o cytokine treatment: 10 ng/ml HMGB1).

3.5.3. Quantification of HMGB1 after IFN-γ stimulation

The ELISA results of 6, 24 and 48 h IFN-γ stimulated MTH53A and tMTH53A showed no elevated HMGB1-secretion. However, a slight increase of extracellular HMGB1 after 6 h IFN-γ stimulation on transfected MTH53A cells with a quantified concentration of 13 ng/ml HMGB1 could be observed in comparison to the corresponding controls (MTH53A + IFN-γ: 5 ng/ml, and tMTH53A w/o IFN-γ: 10 ng/ml). The results of the Western blot analyses, showing low release of rHMGB1 + FLAG after 24 and 48 h of IFN-γ stimulation, could not be confirmed by ELISA, probably due to protein loss during the concentration of the cell-conditioned media.

3.5.4. ELISA conclusions

The ELISA results displayed in Fig. 5 suggest that the stimulation of HMGB1 secretion is inducible by TNF-α, but not IFN-γ.

While it is generally known that IFN-γ and TNF-α act synergistically leading to induction of numerous biological processes, the induction of HMGB1 secretion in the scenario of IFN-γ acting in the presence of TNF-α was also reported [22,24,29]. Although the combination of different cytokines induces active HMGB1 secretion in different types of cells very effectively, a critical point is the fact that combined application of IFN-γ and TNF-α can lead to apoptosis. Sagoo et al. treated mouse corneal endothelial cells with various combinations of proinflammatory cytokines (TNF-α, IL-1β, IL-1α and IFN-γ). They revealed that combined inflammatory

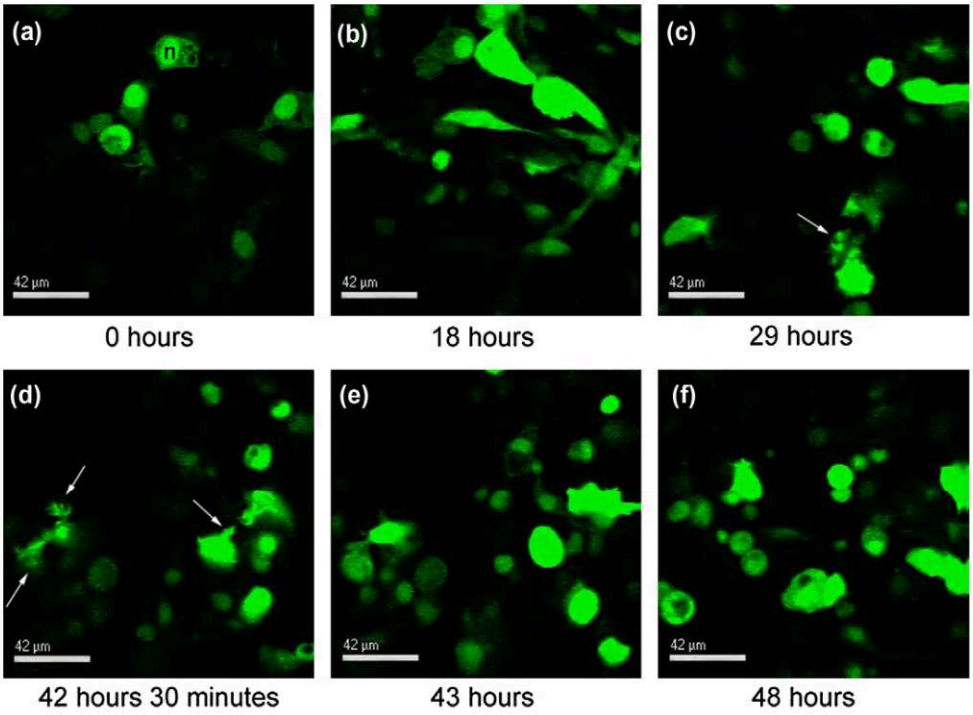

Fig. 6. HMGB1–GFP live cell imaging. Multiphoton microscopy live cell imaging analyses of TNF-α stimulated MTH53A cells at incubation times of 0–48 h. Twenty-four hours before TNF-α stimulation, MTH53A cells were transfected with the pEGFP-HMGB1 vector construct. Single images are shown at 0 h (a), 18 h (b), 29 h (c), 42 h and a half (d), 43 h (e) and 48 h (f) after TNF-α stimulation. HMGB1 was observed staining strongly the nuclei (n, nucleus) and less intensive the cytoplasm of successfully transfected cells. In the course of the incubation time, a more intensive staining of the cytoplasm visible by green fluorescence is detectable. No HMGB1–GFP secretion after TNF-α stimulation was observable spanning from 0 to 48 h. Merely irregular cell membrane structures occurred between 29 and 43 h as indicated by white arrows. Bar 42 µm.

cytokine stimulation led to a synergistic induction of apoptosis with IFN-γ and TNF-α as the major players [54]. Additionally, a study by Suk et al. showed that the combination of IFN-γ and TNF-α, but neither cytokine alone, induced classical caspase-dependent apoptosis in insulinoma and pancreatic islet cells [55].

Summarizing all Western blot and HMGB1-ELISA results, we were able to demonstrate that single stimulation with TNF-α specifically mediates active secretion of HMGB1 in a time-dependent manner by tMTH53A canine mammary epithelial cells. Additionally, the performed annexin V-PE/PI double staining (data not shown) verified, that stimulation with IFN-γ and especially TNF-α does not induce apoptosis or necrosis.

3.6. Laser microscopy: HMGB1–GFP live cell imaging

To examine if active secretion of HMGB1 under cytokine stimulating conditions can be visualized, TNF-α stimulated tMTH53A cells expressing an HMGB1–GFP fusion protein were observed by laser scanning live cell multi-photon imaging.

The live cell imaging of canine HMGB1 protein secretion is shown in Fig. 6a–f in selected single images at 0 h (starting point), 18, 29, and 42.5 h under TNF-α stimulating condition. Successfully transfected MTH53A cells with strongly GFP-stained nuclei, less intensive stained cytoplasm, and clear cell membrane shapes are visible at the stimulation starting point (24 h after transfection, Fig. 6a). After 18 h of incubation with TNF-α more intensive staining of the cytoplasm is detectable. This can be explained by translocation of HMGB1–GFP from the nucleus to the cytoplasm as a result of the TNF-α stimulation (Fig. 6b) and is visible by green fluorescence with varying intensity from cell to cell.

The transfected cells start to form irregular cell membrane structures (indicated by arrows) beginning at 29 h of TNF-α stimulation, and ending at 42.5 h (Fig. 6c and d). A regression of these structures was observed between 43 and 48 h (Fig. 6e and f). Subsequently defined cell membrane shapes were regained. The meaning of the detected irregular cell structures is unclear, but obviously the TNF-α stimulation of HMGB1–GFP expressing tMTH53A cells showed an effect on the cell morphology.

Active secretion of HMGB1 was described by Gardella et al. [56] via non-classical pathway involving exocytosis of specific vesicles related to lysosomes. However, our results of the performed live cell imaging by laser scanning microscopy detected no vesicle-like structures.

Numerous reports showed the visualization of active HMGB1 externalization using fixed or lysed cells by various methods e.g. cell fractionation, fluorescence microscopy with immunofluorescence staining, immunohistochemistry, or immunochemical assays as Western blot and ELISA. Though, the herein attempted *in vivo* visualization of TNF-α stimulated HMGB1–GFP release via laser scanning microscopy live cell imaging represents the first step to reveal the secretion-involved mechanisms *in vivo* avoiding an immunostaining.

4. Conclusions

Regarding to the fact that only certain cells [17–20,26–28] are able to release HMGB1, our results show, that it is also possible to stimulate active time-dependent HMGB1 secretion by TNF-α application from a non-neoplastic canine non-immune related cell line of epithelial origin. As discussed in the literature, the crosstalk between non-tumorigenic epithelial cells and tumor cells might be basically mediated by the tumor surrounding stroma [40]. The tumor stroma participates in the induction or promotion of oncogenesis [57] and a reciprocal relationship between epithelial cells and

stroma in normal tissue could be reported [58]. In case of cancer, an activated, specialized stroma was observed, which contains abundance of inflammatory and activated cells passing signals as secreted cytokines, growth factors and chemokines to neighboring cells [59].

Concerning tumor biology, those findings indicate, that not exclusively necrotic cells, tumor cells or activated immune-system cells show release of HMGB1. The ability of epithelial cells to active secretion of HMGB1, if activated by inflammatory cytokines like TNF-α, results in excessive levels of extracellular HMGB1. This causes prolonged inflammation and tumor growth because HMGB1 acts as dose-dependent neo-vascularizing factor [39,42]. As mentioned before, mamma carcinomas of dog and human have resembling naturally occurring tumor mechanisms as spontaneously development, and similarities in histology, biology and phenotype [3,4]. This suggests that tumor development and progression are very similar and the dog may be a useful large animal model which is transferable to man helping to reveal the characteristics of tumor biology and to establish therapeutic and preclinical studies for tumor treatment.

Conflict of interest

The authors declare that they have no competing interests.

Acknowledgements

This work was funded by the German Research Foundation (DFG) within the SFB/TransRegio 37 (Micro- and Nanosystems in Medicine) and supported by the Research Cluster of Excellence "REBIRTH".

References

[1] MacEwen EG, Patnaik AK, Harvey HJ, Panko WB. Estrogen receptors in canine mammary tumors. Cancer Res 1982;42:2255–9.
[2] Khanna C, Hunter K. Modeling metastasis in vivo. Carcinogenesis 2005;26:513–23.
[3] Withrow SJ, MacEwen EG. Clinical veterinary oncology. Philadelphia (USA): Lippincott Williams & Wilkins; 1989.
[4] MacEwen EG. Spontaneous tumors in dogs and cats: models for the study of cancer biology and treatment. Cancer Metastasis Rev 1990;9:125–36.
[5] Nolte I, Nolte M. Praxis der onkologie bei hund und katze. Stuttgart: Enke Verlag; 2000.
[6] Withrow SJ, MacEwen EG. Small animal clinical oncology. Philadelphia, USA: W.B. Saunders Co.; 2001.
[7] Murua Escobar H, Meyer B, Richter A, Becker K, Flohr AM, Bullerdiek J, et al. Molecular characterization of the canine HMGB1. Cytogenet Genome Res 2003;101:33–8.
[8] Brezniceanu ML, Volp K, Bosser S, Solbach C, Lichter P, Joos S, et al. HMGB1 inhibits cell death in yeast and mammalian cells and is abundantly expressed in human breast carcinoma. FASEB J 2003;17:1295–7.
[9] Flohr AM, Rogalla P, Meiboom M, Borrmann L, Krohn M, Thode-Halle B, et al. Variation of HMGB1 expression in breast cancer. Anticancer Res 2001;21:3881–5.
[10] Walker JM, Goodwin GH, Johns EW, Wietzes P, Gaastra W. A comparison of the amino-terminal sequences of two calf-thymus chromatin non-histone proteins. Int J Pept Protein Res 1977;9:220–3.
[11] Bustin M. Revised nomenclature for high mobility group (HMG) chromosomal proteins. Trends Biochem Sci 2001;26:152–3.
[12] Wolffe AP. Architectural transcription factors. Science 1994;264:1100–1.
[13] Bustin M. Regulation of DNA-dependent activities by the functional motifs of the high-mobility-group chromosomal proteins. Mol Cell Biol 1999;19:5237–46.
[14] Onate SA, Prendergast P, Wagner JP, Nissen M, Reeves R, Pettijohn DE, et al. The DNA-bending protein HMG-1 enhances progesterone receptor binding to its target DNA sequences. Mol Cell Biol 1994;14:3376–91.
[15] Scaffidi P, Misteli T, Bianchi ME. Release of chromatin protein HMGB1 by necrotic cells triggers inflammation. Nature 2002;418:191–5.
[16] Andersson U, Tracey KJ. HMGB1 as a mediator of necrosis-induced inflammation and a therapeutic target in arthritis. Rheum Dis Clin North Am 2004;30:627–37. xi.
[17] Andersson U, Wang H, Palmblad K, Aveberger AC, Bloom O, Erlandsson-Harris H, et al. High mobility group 1 protein (HMG-1) stimulates proinflammatory cytokine synthesis in human monocytes. J Exp Med 2000;192:565–70.
[18] Wang H, Vishnubhakat JM, Bloom O, Zhang M, Ombrellino M, Sama A, et al. Proinflammatory cytokines (tumor necrosis factor and interleukin 1) stimulate release of high mobility group protein-1 by pituicytes. Surgery 1999;126:389–92.
[19] Lotze MT, Tracey KJ. High-mobility group box 1 protein (HMGB1): nuclear weapon in the immune arsenal. Nat Rev Immunol 2005;5:331–42.
[20] Semino C, Angelini G, Poggi A, Rubartelli A. NK/iDC interaction results in IL-18 secretion by DCs at the synaptic cleft followed by NK cell activation and release of the DC maturation factor HMGB1. Blood 2005;106:609–16.
[21] Kawahara K, Biswas KK, Unoshima M, Ito T, Kikuchi K, Morimoto Y, et al. C-reactive protein induces high-mobility group box-1 protein release through activation of p38MAPK in macrophage RAW264.7 cells. Cardiovasc Pathol 2008;17:129–38.
[22] Wang H, Bloom O, Zhang M, Vishnubhakat JM, Ombrellino M, Che J, et al. HMG-1 as a late mediator of endotoxin lethality in mice. Science 1999;285:248–51.
[23] Abraham E, Arcaroli J, Carmody A, Wang H, Tracey KJ. HMG-1 as a mediator of acute lung inflammation. J Immunol 2000;165:2950–4.
[24] Rendon-Mitchell B, Ochani M, Li J, Han J, Wang H, Yang H, et al. IFN-gamma induces high mobility group box 1 protein release partly through a TNF-dependent mechanism. J Immunol 2003;170:3890–7.
[25] Ulloa L, Batliwalla FM, Andersson U, Gregersen PK, Tracey KJ. High mobility group box chromosomal protein 1 as a nuclear protein, cytokine, and potential therapeutic target in arthritis. Arthritis Rheum 2003;48:876–81.
[26] Yang H, Ochani M, Li J, Qiang X, Tanovic M, Harris HE, et al. Reversing established sepsis with antagonists of endogenous high-mobility group box 1. Proc Natl Acad Sci USA 2004;101:296–301.
[27] Wahamaa H, Vallerskog T, Qin S, Lunderius C, LaRosa G, Andersson U, et al. HMGB1-secreting capacity of multiple cell lineages revealed by a novel HMGB1 ELISPOT assay. J Leukoc Biol 2007;81:129–36.
[28] Kuniyasu H, Yano S, Sasaki T, Sasahira T, Sone S, Ohmori H. Colon cancer cell-derived high mobility group 1/amphoterin induces growth inhibition and apoptosis in macrophages. Am J Pathol 2005;166:751–60.
[29] Liu S, Stolz DB, Sappington PL, Macias CA, Killeen ME, Tenhunen JJ, et al. HMGB1 is secreted by immunostimulated enterocytes and contributes to cytomix-induced hyperpermeability of Caco-2 monolayers. Am J Physiol Cell Physiol 2006;290:C990–9.
[30] Fujii K, Luo Y, Sasahira T, Denda A, Ohmori H, Kuniyasu H. Co-treatment with deoxycholic acid and azoxymethane accelerates secretion of HMGB1 in IEC6 intestinal epithelial cells. Cell Prolif 2009;42:701–9.
[31] Hori O, Brett J, Slattery T, Cao R, Zhang J, Chen JX, et al. The receptor for advanced glycation end products (RAGE) is a cellular binding site for amphoterin. Mediation of neurite outgrowth and co-expression of rage and amphoterin in the developing nervous system. J Biol Chem 1995;270:25752–61.
[32] Park JS, Svetkauskaite D, He Q, Kim JY, Strassheim D, Ishizaka A, et al. Involvement of toll-like receptors 2 and 4 in cellular activation by high mobility group box 1 protein. J Biol Chem 2004;279:7370–7.
[33] Yu M, Wang H, Ding A, Golenbock DT, Latz E, Czura CJ, et al. HMGB1 signals through toll-like receptor (TLR) 4 and TLR2. Shock 2006;26:174–9.
[34] Aderem A, Ulevitch RJ. Toll-like receptors in the induction of the innate immune response. Nature 2000;406:782–7.
[35] Taguchi A, Blood DC, del Toro G, Canet A, Lee DC, Qu W, et al. Blockade of RAGE-amphoterin signalling suppresses tumour growth and metastases. Nature 2000;405:354–60.
[36] Huttunen HJ, Rauvala H. Amphoterin as an extracellular regulator of cell motility: from discovery to disease. J Intern Med 2004;255:351–66.
[37] Helmlinger G, Netti PA, Lichtenbeld HC, Melder RJ, Jain RK. Solid stress inhibits the growth of multicellular tumor spheroids. Nat Biotechnol 1997;15:778–83.
[38] Zhang CL, Shu MG, Qi HW, Li LW. Inhibition of tumor angiogenesis by HMGB1 A box peptide. Med Hypotheses 2008;70:343–5.
[39] Schlueter C, Weber H, Meyer B, Rogalla P, Roser K, Hauke S, et al. Angiogenetic signaling through hypoxia: HMGB1: an angiogenetic switch molecule. Am J Pathol 2005;166:1259–63.
[40] Tlsty TD, Coussens LM. Tumor stroma and regulation of cancer development. Annu Rev Pathol 2006;1:119–50.
[41] Laster SM, Wood JG, Gooding LR. Tumor necrosis factor can induce both apoptic and necrotic forms of cell lysis. J Immunol 1988;141:2629–34.
[42] Mitola S, Belleri M, Urbinati C, Coltrini D, Sparatore B, Pedrazzi M, et al. Cutting edge: extracellular high mobility group box-1 protein is a proangiogenic cytokine. J Immunol 2006;176:12–5.
[43] Dumitriu IE, Baruah P, Manfredi AA, Bianchi ME, Rovere-Querini P. HMGB1: guiding immunity from within. Trends Immunol 2005;26:381–7.
[44] Yang H, Wang H, Tracey KJ. HMG-1 rediscovered as a cytokine. Shock 2001;15:247–53.
[45] Kalinina N, Agrotis A, Antropova Y, DiVitto G, Kanellakis P, Kostolias G, et al. Increased expression of the DNA-binding cytokine HMGB1 in human atherosclerotic lesions: role of activated macrophages and cytokines. Arterioscler Thromb Vasc Biol 2004;24:2320–5.
[46] Ulloa L, Ochani M, Yang H, Tanovic M, Halperin D, Yang R, et al. Ethyl pyruvate prevents lethality in mice with established lethal sepsis and systemic inflammation. Proc Natl Acad Sci USA 2002;99:12351–6.
[47] Zamora R, Grishin A, Wong C, Boyle P, Wang J, Hackam D, et al. High-mobility group box 1 protein is an inflammatory mediator in necrotizing enterocolitis: protective effect of the macrophage deactivator semapimod. Am J Physiol Gastrointest Liver Physiol 2005;289:G643–52.

[48] Ulloa L, Messmer D. High-mobility group box 1 (HMGB1) protein: friend and foe. Cytokine Growth Factor Rev 2006;17:189–201.
[49] Li J, Wang H, Mason JM, Levine J, Yu M, Ulloa L, et al. Recombinant HMGB1 with cytokine-stimulating activity. J Immunol Methods 2004;289:211–23.
[50] Ossowski L, Biegel D, Reich E. Mammary plasminogen activator: correlation with involution, hormonal modulation and comparison between normal and neoplastic tissue. Cell 1979;16:929–40.
[51] Parkkinen J, Rauvala H. Interactions of plasminogen and tissue plasminogen activator (t-PA) with amphoterin. Enhancement of t-PA-catalyzed plasminogen activation by amphoterin. J Biol Chem 1991;266:16730–5.
[52] Campana L, Bosurgi L, Rovere-Querini P. HMGB1: a two-headed signal regulating tumor progression and immunity. Curr Opin Immunol 2008;20:518–23.
[53] van Beijnum JR, Buurman WA, Griffioen AW. Convergence and amplification of toll-like receptor (TLR) and receptor for advanced glycation end products (RAGE) signaling pathways via high mobility group B1 (HMGB1). Angiogenesis 2008;11:91–9.
[54] Sagoo P, Chan G, Larkin DF, George AJ. Inflammatory cytokines induce apoptosis of corneal endothelium through nitric oxide. Invest Ophthalmol Vis Sci 2004;45:3964–73.
[55] Suk K, Kim S, Kim YH, Kim KA, Chang I, Yagita H, et al. IFN-gamma/TNF-alpha synergism as the final effector in autoimmune diabetes: a key role for STAT1/IFN regulatory factor-1 pathway in pancreatic beta cell death. J Immunol 2001;166:4481–9.
[56] Gardella S, Andrei C, Ferrera D, Lotti LV, Torrisi MR, Bianchi ME, et al. The nuclear protein HMGB1 is secreted by monocytes via a non-classical, vesicle-mediated secretory pathway. EMBO Rep 2002;3:995–1001.
[57] Sharma M, Beck AH, Webster JA, Espinosa I, Montgomery K, Varma S, et al. Analysis of stromal signatures in the tumor microenvironment of ductal carcinoma in situ. Breast Cancer Res Treat 2009.
[58] Bhowmick NA, Moses HL. Tumor–stroma interactions. Curr Opin Genet Dev 2005;15:97–101.
[59] Coussens LM, Werb Z. Inflammation and cancer. Nature 2002;420:860–7.

VII ‘Cytogenetic Analysis of CpG-Oligonucleotide DSP30 plus Interleukin-2-Stimulated Canine B-Cell Lymphoma Cells Reveals the Loss of One X Chromosome as the Sole Abnormality.’ **Reimann-Berg *et al.*, Cytogenetic and Genome Research, 2011.**

In the fields of vaccination and immunomodulation, various CpG-ODN are in focus as immunotherapeutic agents due to their potential to induce humoral immune responses or to enhance the proliferation of cells. In this study, stimulation with the CpG-ODN DSP30 in combination IL-2 was utilised to generate a higher mitotic rate in usually slowly growing canine lymphoid cell cultures. Two short-term cultures of a thoracic fluid aspirate taken from a female 7 year old Retriever diagnosed with high-grade B-cell lymphoma were set up. One culture was set up in non-stimulative standard RPMI medium with 20 % FCS, L-glutamine and antibiotics. The other culture was prepared with the addition of DSP30 and IL-2 to the standard RPMI medium.

The stimulation with DSP30 and IL-2 resulted in the generation of an adequate number of metaphases for cytogenetic analyses. The karyotyping of the thoracic fluid aspirate revealed the loss of one X chromosome as sole cytogenetic deviation.

VII

Cytogenetic Analysis of CpG-Oligonucleotide DSP30 plus Interleukin-2-Stimulated Canine B-Cell Lymphoma Cells Reveals the Loss of One X Chromosome as the Sole Abnormality.

Reimann-Berg N, Murua Escobar H, Kiefer Y, Mischke R, Willenbrock S, Eberle N, Nolte I, Bullerdiek J.

Cytogenetic and Genome Research. 2011. 135(1):79-82.

Own contribution:

- Sampling
- Partial manuscript drafting

Short Report

Cytogenetic and Genome Research

Cytogenet Genome Res 2011;135:79–82
DOI: 10.1159/000330126

Accepted: May 31, 2011
by K. Reed
Published online: July 28, 2011

Cytogenetic Analysis of CpG-Oligonucleotide DSP30 plus Interleukin-2-Stimulated Canine B-Cell Lymphoma Cells Reveals the Loss of One X Chromosome as the Sole Abnormality

N. Reimann-Berg[a, b] H. Murua Escobar[a] Y. Kiefer[b] R. Mischke[a]
S. Willenbrock[a, b] N. Eberle[a] I. Nolte[a] J. Bullerdiek[a, b]

[a]Small Animal Clinic and Research Cluster REBIRTH, University of Veterinary Medicine Hannover, Hannover, and
[b]Center for Human Genetics, University of Bremen, Bremen, Germany

Key Words
Animal model · Canine B-cell lymphoma · DSP30 · IL-2 · Monosomy X

Abstract
Human and canine lymphoid neoplasms are characterized by non-random cytogenetic abnormalities. However, due to the low mitotic activity of the B cells, cytogenetic analyses of B-cell lymphoid proliferations are difficult to perform. In the present study we stimulated canine B-cell lymphoma cells with the immunostimulatory CpG-oligonucleotide DSP30 in combination with interleukin-2 (IL-2) and obtained an adequate number of metaphases. Cytogenetic analyses revealed the loss of one X chromosome as the sole cytogenetic aberration. Chromosome analysis of the corresponding blood showed a normal female karyotype. Monosomy X as the sole clonal chromosomal abnormality is found in human hematopoietic malignancies as well, thus the dog may serve as a promising animal model.

The importance of non-random cytogenetic abnormalities in human leukemia and lymphoma has been recognized for more than 40 years. The World Health Organization classification of the hematopoietic and lymphoid tissues considers cytogenetic analysis to be an essential element of the diagnostic evaluation of neoplastic diseases and incorporates cytogenetic findings into the definition of a number of subtypes [Swerdlow et al., 2008]. There are several reports about cytogenetic analyses of canine lymphoid neoplasms, demonstrating that lymphomas in dogs are characterized by non-random cytogenetic abnormalities as well [Hahn et al., 1994; Winkler et al., 2005; Breen and Modiano, 2008; Devitt et al., 2009]. Conventional cytogenetic analyses of B-cell lymphoid proliferations are difficult to perform due to a low mitotic activity of the B cells in general. Therefore, mitogen stimulation of B cells is required to gain a sufficient number of metaphases for analyses. For human chronic lymphatic leukemia (CLL) and B-cell lymphoid neoplasms, the immunostimulatory CpG-oligonucleotide DSP30 in combination with interleukin-2 (IL-2) has been reported to be an easy and efficient stimulus for metaphase generation [Decker et al., 2000; Haferlach et al., 2007; Struski et al., 2009].

KARGER

Fax +41 61 306 12 34
E-Mail karger@karger.ch
www.karger.com

1424–8581/11/1351–0079$38.00/0

Accessible online at:
www.karger.com/cgr

Dr. Nicola Reimann-Berg
Small Animal Clinic, University of Veterinary Medicine Hannover
Bünteweg 9
DE–30559 Hannover (Germany)
Tel. +49 511 953 6382, E-Mail nicola.reimann-berg@tiho-hannover.de

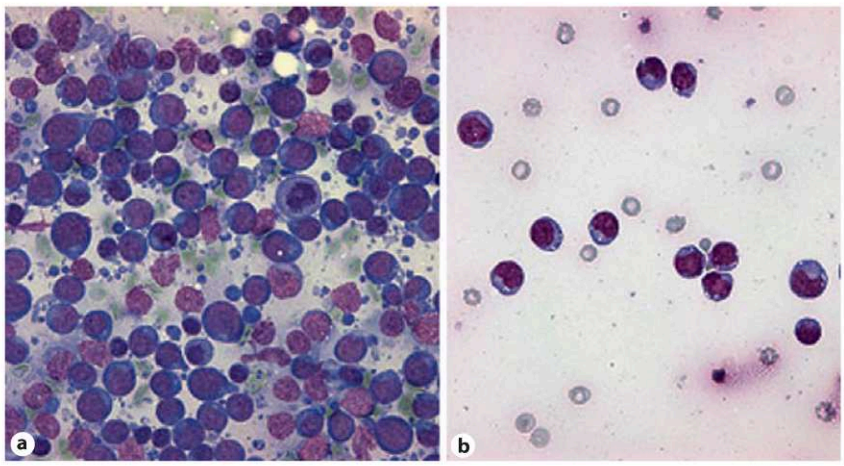

Fig. 1. Results of the histological examination of cells from the canine B-cell lymphoma. **a** Fine needle aspirate of the sternal lymph node containing more than 80% centroblasts indicating a high-grade lymphoma (Pappenheim stain, 400×). **b** Direct smear of the thoracic effusion of the patient indicating the high cellularity consisting predominantly of lymphoblasts (Pappenheim stain, 400×).

Herein, we present a case of a high-grade lymphoma in a female dog, showing the loss of one X chromosome in all analyzed metaphases of the lymphoma. Stimulation of the lymphoid cell cultures with DSP30 plus IL-2 resulted in an adequate number of metaphases. Control analysis of the corresponding blood revealed a normal female karyotype in all analyzed metaphases.

Case Report and Methods

The dog (Retriever, 7 years, female) was presented at the Small Animal Clinic, Veterinary University of Hannover, and the clinical examination showed a moderately enlargement of the peripheral lymph nodes, swollen warm mammary glands of the left side, and an increased body temperature. Radiation examination of the thorax revealed a pleural effusion. Fine needle aspirates from different lymph nodes (sternal, inguinal, sublumbal), liver, spleen, bone marrow, mammary gland, and thoracic fluid were taken. Histological examination of the aspirates from the lymph nodes revealed the existence of more than 80% lymphoid blasts (centroblastic type), consistent with the diagnosis of a high-grade lymphoma (fig. 1a). Significant amounts of lymphoma cells were also present in fine needle aspirates of the liver and spleen, whereas the examination of a bone marrow aspirate revealed only individual lymphoma cells. The thoracic fluid contained a high cell number (94,300/μl) with 80% lymphoblasts, i.e. a typical picture of a lymphoma-associated effusion (fig. 1b). Aspirates of the lymph nodes were immunophenotyped via flow cytometry according to the protocol described by Culmsee and Nolte [2002], resulting in the confirmation of the diagnosis of a B-cell lymphoma.

For chromosome analyses, 2 short-term cultures from the thoracic fluid aspirate were set up in RPMI 1640 (PAN Biotech GmbH, Aidenbach, Germany) supplemented with 20% fetal calf serum, L-glutamine, and antibiotics (Invitrogen, Karlsruhe, Germany). One culture was set up with the medium alone (1 ml cell suspension ad 5 ml medium); for the other culture the CpG-oligonucleotide DSP30 (1 μmol/l; TIBMolBiol, Berlin, Germany) and IL-2 (100 U/ml, PAN Biotech GmbH) were used for stimulation. The blood cells (1 ml whole blood) were cultured in 10 ml Chromosome B medium with phytohaemagglutinin (Biochrom, Berlin, Germany). The cultures were incubated in 5% CO_2 at 37°C for 72 h. For chromosome preparation, Colcemid (Biochrom) was added at a final concentration of 0.1 μg/ml for 2 h before harvesting. Subsequently, the cells were incubated for 20 min in 0.05 M KCl and finally fixed with methanol/glacial acetic acid (3:1). The suspension was then dropped on ice-cold slides and dried for 5 days at 37°C followed by GTG-banding which was performed as previously described [Reimann-Berg et al., 2011]. Results were processed and recorded with BandView, 6.0, MultiSpecies, Applied Spectral Imaging, Israel. Karyotype description followed the nomenclature proposed by Reimann et al. [1996].

Results and Discussion

In case of the short-term cultures of the lymphoma cells, we were able to receive a moderate amount of metaphases for the stimulated culture, whereas the preparation of the unstimulated cells showed no metaphases. The chromosome preparation of the PHA-stimulated whole-blood cultures showed many metaphases. For both, the lymphoma cells and the blood cells, a total of 20 metaphases were analyzed. In case of the lymphoma cells, an aberrant karyotype 77,X,–X was found in all analyzed metaphases (fig. 2a, c). However, the blood cells were characterized by a normal female karyotype 78,XX (fig. 2b).

This is the first report presenting a canine B-cell lymphoma with a monosomy X as the sole cytogenetic deviation. For human hematopoietic diseases, monosomy X as

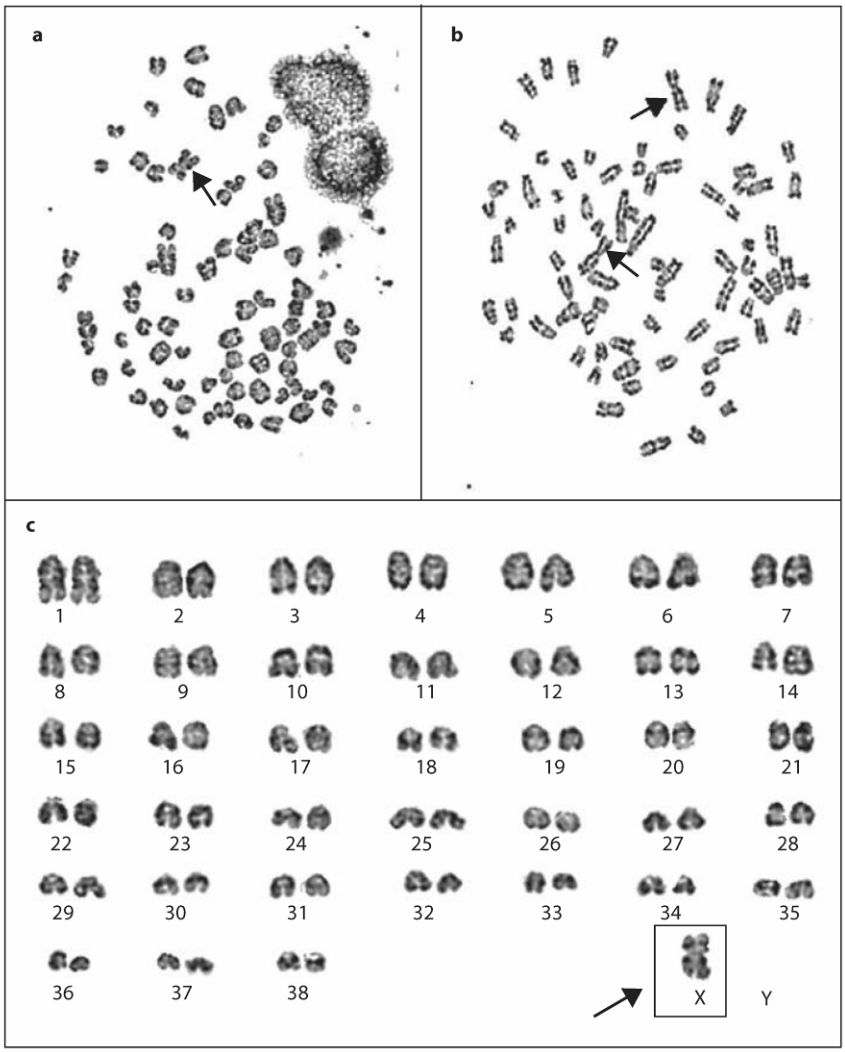

Fig. 2. Results of chromosome analyses of cells from the canine B-cell lymphoma (DSP30 plus IL-2-stimulated culture from the aspirate taken from the thoracic effusion) and the corresponding blood cultures. **a** Lymphoma: metaphase spread after GTG-banding. The arrow indicates the X chromosome. **b** Blood: metaphase spread after GTG-banding. The arrows indicate both X chromosomes. **c** Lymphoma: corresponding karyotype (77,X,–X) of metaphase (**a**). The arrow indicates monosomy X.

the sole cytogenetic abnormality has been predominantly reported for myelodysplastic disorders [Abruzzese et al., 1997]. However, the loss of one X chromosome as the only aberration is also found in acute lymphoblastic leukemia [Bueno et al., 1999]. Thus, monosomy X is observed in human as well as in canine hematopoietic diseases. Increasingly, the dog proves to be a promising animal model for the study of human tumor diseases. Recent results of cytogenetic investigations of canine prostate tumors underline the significance of polysomy 13 in the development of prostate cancer [Reimann-Berg et al., 2011]. Canine chromosome 13 shares high homology with human chromosome 8q [Breen et al., 1999]. This chromosomal region has been reported to be involved in growth and progression of human prostate cancer [Steiner et al., 2002]. Thus, a conserved area on canine chromosome 13 and human chromosome 8 is involved in tumorigenesis in both species.

In the present report we were able to show that the immunostimulatory CpG-oligonucleotide DSP30 in combination with IL-2 generates a higher mitotic rate in canine lymphoid cell cultures. Taken together, the capability of generating a sufficient number of metaphases for cytogenetic analyses of canine hematopoietic disorders simplifies cytogenetic investigations which might help to understand the significance of X chromosome loss as the only karyotype anomaly in canine as well as in human hematopoietic and lymphoid diseases.

References

Abruzzese E, Rao PN, Slatkoff M, Cruz J, Powell BL, et al: Monosomy X as a recurring sole cytogenetic abnormality associated with myelodysplastic diseases. Cancer Genet Cytogenet 93:140–146 (1997).

Breen M, Modiano JF: Evolutionarily conserved cytogenetic changes in hematological malignancies of dogs and humans – man and his best friend share more than companionship. Chromosome Res 16:145–154 (2008).

Breen M, Thomas R, Binns MM, Carter NP, Langford CF: Reciprocal chromosome painting reveals detailed regions of conserved synteny between the karyotypes of the domestic dog *(Canis familiaris)* and human. Genomics 61:145–155 (1999).

Bueno JL, Watson A, Dainton MG, Hughes DM, Killick S, et al: Monosomy X as the sole cytogenetic abnormality in acute lymphoblastic leukemia: a report of two new patients. Leuk Lymphoma 32:381–384 (1999).

Culmsee K, Nolte I: Flow cytometry and its application in small animal oncology. Methods Cell Sci 24:49–54 (2002).

Decker T, Schneller F, Kronschnabl M, Dechow T, Lipford GB, et al: Immunostimulatory CpG-oligonucleotides induce functional high affinity IL-2 receptors on B-CLL cells: costimulation with IL-2 results in a highly immunogenic phenotype. Exp Hematol 28: 558–568 (2000).

Devitt JJ, Maranon DG, Ehrhart EJ, Bachand AM, Lana SE, et al: Correlations between numerical chromosomal aberrations in the tumor and peripheral blood in canine lymphoma. Cytogenet Genome Res 124:12–18 (2009).

Haferlach C, Dicker F, Schnittger S, Kern W, Haferlach T: Comprehensive genetic characterization of CLL: a study on 506 cases analysed with chromosome banding analysis, interphase FISH, IgV(H) status and immunophenotyping. Leukemia 21:2442–2451 (2007).

Hahn KA, Richardson RC, Hahn EA, Chrisman CL: Diagnostic and prognostic importance of chromosomal aberrations identified in 61 dogs with lymphosarcoma. Vet Pathol 31: 528–540 (1994).

Reimann N, Bartnitzke S, Bullerdiek J, Schmitz U, Rogalla P, et al: An extended nomenclature of the canine karyotype. Cytogenet Cell Genet 73:140–144 (1996).

Reimann-Berg N, Willenbrock S, Murua Escobar H, Eberle N, Gerhauser I, et al: Two new cases of polysomy 13 in canine prostate cancer. Cytogenet Genome Res 132:16–21 (2011).

Steiner T, Junker K, Burkhardt F, Braunsdorf A, Janitzky V, et al: Gain in chromosome 8q correlates with early progression in hormonal treated prostate cancer. Eur Urol 41:167–171 (2002).

Struski S, Gervais C, Helias C, Herbrecht R, Audhuy B, et al: Stimulation of B-cell lymphoproliferations with CpG-oligonucleotide DSP30 plus IL-2 is more effective than with TPA to detect clonal abnormalities. Leukemia 23:617–619 (2009).

Swerdlow SH, Campo E, Harris NL, Jaffe ES, Pileri SA, et al: WHO Classification of Tumours of the Haematopoetic and Lymphoid Tissues (IARC, Lion, 2008).

Winkler S, Murua Escobar H, Reimann-Berg N, Bullerdiek J, Nolte I: Cytogenetic investigations in four canine lymphomas. Anticancer Res 25:3995–3998 (2005).

3.4. In vivo imaging of cells

To establish approaches targeting at cancer immunotherapy using modified cells, reliable and well-tolerated techniques for non-invasive tracking and imaging of the migration of administered cells *in vivo* are needed. Therefore, two different strategies implementing specific *in vivo* detection were followed within this thesis being also of significant value for further development of the immunotherapeutic approach followed within the CRC/TR37.

VIII ‘Generation of recombinant antibody fragments that target canine dendritic cells by phage display technology.’ **Fitting *et al*., Veterinary Comparative Oncology, 2011.**

The use of autologous modulated DCs for cancer immunotherapy leading to the induction of specific anti-tumour responses is currently of great interest in research. The success of these therapeutic approaches is dependent on the effectiveness of the cells to migrate to their final destination, where immune responses are induced. In humans, DC specific antibodies are used to localise and quantify the applied DCs in the organism, but the availability of such antibodies is limited for dogs.
Therefore, in this study highly specific single-chain variable fragment (scFV) antibodies specifically binding to canine DCs were generated and characterised by phage display technology. A stringent subtractive three-step panning strategy was carried out beginning with a negative selection on canine PBMCs and followed by positive selection on canine DC membrane fragments. Between each panning round the selection pressure was increased by enhancing the stringency of washing conditions and reduced antigen concentrations. The enrichment for a phage population specifically binding canine DCs was documented in polyclonal phage ELISA. The monoclonal phage verification by ELISA and sequencing revealed a total of eight unique clones. Two of those clones were selected for further characterisation showing a six- and 20-fold affinity to canine DCs respectively in comparison to canine PBMCs. The two identified scFV clones were expressed as soluble periplasmic proteins and a scFV ELISA was performed subsequently to confirm the two clones as highly specific binding to functional canine DC membrane fragments.

VIII

Generation of recombinant antibody fragments that target canine dendritic cells by phage display technology.

Fitting J, Killian D, Junghanss C, Willenbrock S, Murua Escobar H, Lange S, Nolte I, Barth S, Tur MK.

Veterinary Comparative Oncology*. 2011. 9(3):183-95*

Own contribution:

- Partial manuscript drafting
- Partial cell culture handling

Veterinary and Comparative Oncology

Original Article

DOI: 10.1111/j.1476-5829.2010.00246.x

Generation of recombinant antibody fragments that target canine dendritic cells by phage display technology

J. Fitting[1], D. Killian[2], C. Junghanss[2], S. Willenbrock[3], H. Murua Escobar[3], S. Lange[2], I. Nolte[3], S. Barth[1,4,*] and M. K. Tur[1,*]

[1]Experimental Medicine and Immunotherapy, Department of Applied Medical Engineering, Helmholtz Institute for Biomedical Engineering, University Hospital RWTH Aachen, Aachen, Germany
[2]Department of Medicine, Division of Hematology/Oncology, University of Rostock, Rostock, Germany
[3]Clinic of Small Animals, University of Veterinary Medicine Hannover, Hannover, Germany
[4]Department of Pharmaceutical Product Development, Fraunhofer Institute for Molecular Biology and Applied Ecology, Aachen, Germany

Abstract

One of the main goals in cancer immunotherapy is the efficient activation of the host immune system against tumour cells. Dendritic cells (DCs) can induce specific anti-tumour immune responses in both experimental animal models and humans. However, most preclinical studies using small animal models show only limited correlation with studies carried out in clinical settings, whereas laboratory dogs naturally develop tumours that are biologically and histopathologically similar to their human counterparts. Here, we describe the generation and characterization of recombinant antibodies against canine DCs, isolated using the Tomlinson phage display system. We successfully isolated highly specific single-chain variable fragment (scFv) antibodies in a sequential three-step panning strategy involving depletion on canine peripheral blood mononuclear cells followed by positive selection on native canine DCs. This provides the basis for an antibody-based method for the immunological detection and manipulation of DCs and for monitoring antigen-specific immune responses.

Keywords
cancer, dendritic cells, dogs, phage display technology, scFv antibody

Correspondence address:
Dr. Mehmet Kemal Tur
Experimental Medicine and Immunotherapy
Department of Applied Medical Engineering
Helmholtz Institute for Biomedical Engineering
University Hospital RWTH Aachen
Pauwelsstr. 20
52074 Aachen, Germany
e-mail:
tur@hia.rwth-aachen.de

Introduction

Cancer is a leading cause of death in humans and their companion animals. The disease is becoming more prevalent, with up to 27 million new human cases expected in the next 40 years and 17.5 million cancer-related deaths predicted based on projected increases in the size and average age of the human population.[1] Dogs are genetically, anatomically and physiologically very similar to humans and this extends to the manifestation of cancer, including presentation, biological behaviour and response to conventional therapies.[2] Additionally, dogs share close vicinity to their owner and can therefore be seen as sentinel animal for environmental influences.[3,4] Accordingly, therapeutic targets and protocols evaluated in humans have been successfully adapted for dogs and vice versa.[5]

In both species, the immune system plays a fundamental role in cancer development and progression[5] and can recognize, control and eliminate aberrant cells, a process known as immunosurveillance.[6] As part of the innate immune system, dendritic cells (DCs) play a crucial role in this surveillance process, activating and co-ordinating the adaptive immune system.[7] Immature DCs are activated by stimuli such as pro-inflammatory mediators which prompt them to undergo terminal maturation. The mature DCs

*These authors contributed equally to this work.

can then initiate primary and secondary B-cell and cytotoxic T-cell (CTL) responses by presenting target antigens via major histocompatibility complex (MHC) class I and II proteins on the cell surface, leading to protective immunity against inflammatory diseases and cancer.[7] This efficient presentation of tumour antigens for CTL priming has generated considerable interest in the use of autologous DCs as fundamental targets and tools for cancer vaccination. A number of strategies involving the use of modulated DCs for the induction of specific anti-tumour immune responses have been evaluated in the laboratory and the clinic, such as the use of DCs loaded with inactivated cancer cells or antigenic tumour fragments, although a favourable clinical response was observed in only a few patients.[8,9] Significant progress in DC-based adoptive immunotherapy therefore requires the ability to monitor and quantify DCs in secondary lymphoid organs. In humans, this is facilitated by the availability of DC-specific antibodies that allow the use of optical labelling techniques for observation, but no such antibodies are currently available for use in dogs.

Here, we report the use of phage display technology to isolate scFv antibodies that bind specifically to canine DCs. This provides the basis for the development of a novel tool for the immunological detection, characterization and quantification of DCs in canine tissue, which is the first step towards the development of improved DC-based vaccination strategies.

Materials and methods

Phage display libraries, bacterial strains and helper phage

The human single-fold scFv libraries I+J (Tomlinson I+J) with side-chain diversity (either DVT or NNK encoded), including *Escherichia coli* strains TG1 [*K12 Δ(lac-proAB) supE thi hsdD5/F′ traD36 proA*$^{+}$*B lacI*^{q} *lacZΔM15*] for the production of phage-displayed antibody fragments and HB2151 [*K12 ara Δ(lac-proAB) thi/F′ proA*$^{+}$*B lacI*^{q} *lacZΔM15*] for the expression of soluble antibody fragments, were obtained from the Medical Research Council (MRC) Centre for Protein Engineering (Cambridge, United Kingdom). Polyvalent or monovalent phage particles were produced after superinfecting phagemid-containing TG1 bacteria with the M13KO7ΔpIII hyperphage (PROGEN Biotechnik GmbH, Heidelberg, Germany) or the M13KO7 helper phage (New England Biolabs GmbH, Frankfurt am Main, Germany), respectively. *E. coli* XL-1 blue MR supercompetent cells [*Δ(mcrA)183 Δ(mcrCB-hsdSMR-mrr)173 endA1 supE44 thi-1 recA1 gyrA96 relA1 lac*; Stratagene, Heidelberg, Germany] were used for the cloning, maintenance and propagation of plasmids.

Animals

Four normal and healthy Beagle dogs (Harlan, Borchen, Germany) of both sexes at a median age of 19 months (range from 7 to 31 months) functioned as intermediate donors for bone marrow samples. All animal experiments were approved by the review board of the state Mecklenburg-Vorpommern (Landesamt für Landwirtschaft, Lebensmittelsicherheit und Fischerei MV, Rostock, Germany).

Bone marrow collection

For bone marrow aspiration dogs were anaesthetized with a combination of Ketamine 10% (Veterinaria AG, Pfäffikon, Switzerland) and Xylazine 2% (Rompun; Bayer HealthCare, Leverkusen, Germany) i.v. at a dose of 0.1 mL kg^{-1} body weight, respectively. Metamizole 2.5 mg (Novaminsulfon 2.5 mg; ratiopharm, Ulm, Germany) were administered i.v. for analgesia. Canine bone marrow was aspirated from the femur, tibia and/or ilia crest of each animal with a Biosystem 15Gx 7 cm bone marrow biopsy needle (Gallini Medical Devices, Montava, Italy) into heparinized 20-mL syringes (280 U heparin per syringe) to achieve a total target volume of 80–100 mL.

Generation of canine DCs

CD34^{+} hematopoietic stem cells were isolated by Ficoll density gradient centrifugation followed by magnetic cell sorting (autoMACS™) using a mouse anti-canine CD34^{+} phycoerythrin-conjugated monoclonal antibody (Clone 1H6; AbD Serotec, Düsseldorf, Germany) and anti-PE MicroBeads (Miltenyi Biotec, Bergisch Gladbach,

Germany). DCs were produced from $CD34^+$ cells as described[10] with the following modifications. Cells were seeded into 48-well culture plates (Greiner Bio-One, Essen, Germany) at a density of 2.5×10^5/well and cultured in IMDM medium containing 10% sterile filtered dog serum, 5% fetal bovine serum (FBS; PAA, Cölbe, Germany), 1% penicillin/streptomycin, 1% non-essential amino acids, 1% sodium pyruvate, 10 ng mL^{-1} rhTNF-α (R&D, Minneapolis, MN, USA), 200 ng mL^{-1} rhFLT3L (kindly provided by Amgen, Thousand Oaks, CA, USA) and 40 ng mL^{-1} hGM-CSF (Bayer, Pittsburgh, PA, USA), and were incubated at 37 °C, 5% CO_2 and 95% humidity for 5 days. The medium was reconditioned every other day at a 1:1 ratio for up to 14 days. DCs were harvested between days 11 and 14 based on the development of dendrites and their characteristic phenotype as determined by flow cytometry.

Flow cytometric analysis

Cell purity was determined using a FACScan™ Flow Cytometer and CellQuest™ software (BD Bioscience, Heidelberg, Germany). The following monoclonal antibodies were used to label the positive fraction of the $CD34^+$ hematopoietic stem cell population after sorting: phycoerythrin-conjugated mouse anti-canine $CD34^+$ (Clone 1H6; AbD Serotec), mouse anti-canine CD11c (Clone CA11.6A; AbD Serotec) in combination with PE-conjugated F(ab′)2 rabbit anti-mouse immunoglobulin G (IgG):RPE (BZL04182; BIOZOL, Eching, Germany) and FITC-conjugated rat anti-canine MHCII (AbD Serotec). The same antibodies were used for post-harvest flow cytometric analysis to characterize the canine DCs. Canine DCs were defined as CD34 negative, CD11c positive and MHCII positive as described.[10,11] Staining was carried out according to the manufacturer's protocols.

Cell-membrane antigen preparation

Functional membranes from canine cells were prepared using a combination of sonication and fractionated ultracentrifugation as described[12] with the following modifications. Briefly, 1×10^7 cells were suspended and washed three times in phosphate-buffered saline (PBS, pH 7.4). The cell pellet was suspended in 10 mL ice-cold homogenization buffer (320 mM sucrose, 25 mM Tris–HCl, pH 7.4, plus one Protease-Inhibitor Cocktail Tablet Complete™/50 mL) and incubated on ice for 10 min. The cells were then sonicated on ice, 2×1 min at 20% intensity and 2×1 min at 30% intensity. Crude cell debris was pelleted at $1000 \times g$ for 12 min at 4 °C and the supernatant was transferred to a fresh tube and ultracentrifuged at $100\,000 \times g$ for 30 min at 4 °C. The supernatant was removed and the membrane fraction pellet was taken up in 10 mL resuspension buffer (50 mM Tris–HCl, pH 7.4) and centrifuged again under the same conditions. Finally, the membrane fraction pellet was suspended in PBS (1.2 mL per 10^7 cells), aliquoted and stored at −80 °C for cryoconservation. Canine peripheral blood mononuclear cell (cPBMC) membrane fragments were prepared by isolating the mononuclear cell population from canine full blood using Ficoll reagent (GE Healthcare, München, Germany) and using the process described above for DCs.

Phage library preparation

The two Tomlinson phage libraries I+J (diversified with DVT or NNK triplets) were prepared separately for panning as previously described.[13] Briefly, an aliquot of *E. coli* TG1, harbouring the library, was added to 25 mL 2× TY (16 g L^{-1} tryptone, 10 g L^{-1} yeast extract, 5 g L^{-1} NaCl) containing 100 µg mL^{-1} ampicillin and 1% (w/v) glucose, and was cultured with agitation (250 r.p.m.) at 37 °C until the OD_{600} (optical density at 600 nm) reached 0.4. We then added 1×10^{10} helper phage to 5 mL of the culture (ratio of infectious virus particles to cells ≥20) in a fresh 50-mL tube and incubated the mixture at 37 °C for 30 min without agitation, then for 30 min with agitation to allow infection. The helper phage infected cells were centrifuged at $4120 \times g$, 4 °C for 5 min, and the pellet was resuspended in 25 mL 2× TY containing 100 µg mL^{-1} ampicillin, 50 µg mL^{-1} kanamycin and 0.25 mM isopropyl β-D-1-thiogalactopyranoside (IPTG) followed by incubation at 30 °C overnight with agitation. The overnight culture was centrifuged at $4120 \times g$ for

30 min at 4 °C to remove any bacterial debris and the supernatant was transferred to fresh 50-mL tubes. The phage particles were precipitated by adding 0.2 volumes of ice-cold PEG/NaCl (20% polyethylene glycol 6000, 2.5 M NaCl) for 1 h on ice, slewing occasionally, and then pelleted by centrifugation at 12 000 × *g* for 30 min at 4 °C. The supernatant was removed and the phage pellet was resuspended in 1 mL PBS, transferred to an Eppendorf tube and centrifuged at 13 000 × *g* for 1 min in a bench-top centrifuge to remove any remaining bacterial debris. The supernatant was aliquoted and maintained at 4 °C for short-term storage or at −80 °C for preservation.

A small aliquot was used to produce a dilution series from 10^{-2} to 10^{-14} in 100 µL PBS, and these were each added to 900 µL of TG1 culture in mid-logarithmic growth phase and incubated at 37 °C for 30 min to allow infection. Bacteria were spread on lysogeny broth (LB) agar plates containing ampicillin and glucose (10 g L^{-1} tryptone, 10 g L^{-1} NaCl, 5 g L^{-1} yeast extract, 15 g L^{-1} agar containing 100 µg mL^{-1} ampicillin and 1% glucose) and incubated overnight at 37 °C. The number of applied phage particles (input titre) was determined using the equation $[N^{\circ}_{col}/(DF \times V_{plate})] \times [(V_{TG1}/V_{phage}) + 1] = \text{cfu mL}^{-1}$, where N°_{col} is the number of colonies, DF is the dilution factor of the phage suspension, V_{plate} is the volume of suspension spread on the plate, V_{TG1} is the volume of TG1 culture for infection and V_{phage} is the volume of diluted phage suspension (cfu refers to colony forming units).

Subtractive selection of phage antibody libraries

For the following panning procedure the freshly precipitated phage suspension was blocked for 2 h at 21 °C with 2% MPBS (PBS containing 2% dried skimmed milk powder). A 96-well MaxiSorp™ microtitre plate (Nalge Nunc International, Roskilde, Denmark) was coated with 100 µL canine PBMC membrane fragments as the depletion antigen and 100 µL canine DC membrane fragments as the selection antigen one day prior to panning round and was stored at 4 °C. The plates were washed three times with PBS and blocked with 200 µL 2% MPBS per well, incubating for 2 h at 21 °C with agitation. After washing, approximately 10^{12} pre-blocked scFv-displaying phage particles were transferred to the wells containing immobilized and pre-blocked depletion antigen and were incubated for 1 h at 21 °C with agitation (400 r.p.m.). The supernatant was transferred to wells coated with the selection antigen and incubated as above.

The supernatant containing non-bound scFv-phage antibodies was removed and non-specifically bound phage particles were washed away with 0.05% PBST (PBS containing 0.05% Tween-20). Specifically bound phage antibodies were then eluted by a pH shift using 200 µL 0.2 M glycine–HCl buffer (pH 2.2) per well for 10 min with agitation. The phage eluate was neutralized with 500 µL 1 M Tris–HCl (pH 7.5) and transferred to 14 mL of TG1 culture in mid-logarithmic growth phase ($OD_{600} = 0.4$), and the mixture was incubated at 37 °C for 30 min without agitation and then for 30 min with agitation (250 r.p.m.) to facilitate infection. Additionally, 200 µL of the TG1 culture were added to the microtitre plate wells coated with the selection antigen and the aliquots were pooled with the major culture after infection.

The bacteria were centrifuged at 4500 × *g* for 5 min at 4 °C, resuspended in 600 µL 2× TY and plated out on LB agar plates containing ampicillin and glucose as above. The plates were incubated overnight at 37 °C and colonies were scrapped off with 1.5 mL 2× TY containing 15% glycerol for cryopreservation. The number of phage antibodies eluted after each panning round (output) was calculated based on the number of colonies formed after re-infection of a dilution series of the phage particles in TG1 according to the equation for the input titre shown above. After each selection, the output titre was divided by the input titre to determine the enrichment factor (EF) for DC-specific phage antibodies. The phages precipitated in the first selection round were prepared using polyvalent scFvs displaying hyperphage (M13KO7ΔpIII), whereas those precipitated in the second and third rounds were precipitated as monovalent scFvs displaying helper phage (M13KO7).

Phage ELISAs

Polyclonal and monoclonal phage ELISAs (enzyme-linked immunosorbent assays) were carried out using a HRP/anti-M13 monoclonal mouse secondary antibody (GE Healthcare, München, Germany) and 2,2′-azino-bis(3-ethylbenzothiazoline-6-sulfonic acid) (ABTS) as the peroxidase substrate (Roche Diagnostics GmbH, Mannheim, Germany).

Polyvalent phage particles from each panning round and from the unselected initial phage library J were rescued with PEG/NaCl and suspended in PBS as described above. The phage solution was adjusted to a final concentration of 10^{12} cfu mL^{-1} and blocked for 2 h at 21 °C with agitation. A 96-well MaxiSorp™ microtitre plate was coated overnight at 4 °C with a 1:100 dilution of canine DC and PBMC membrane fragments in PBS. The plate was washed three times with PBS, blocked to prevent non-specific binding of phage and immunoglobulins for 2 h at 21 °C with 200 µL 2% MPBS per well and washed again as described above. Meanwhile, the polyclonal phage suspensions were blocked for 2 h at 21 °C with 2% MPBS in a 1:10 ratio. Afterwards, 100 µL of the pre-blocked phage were transferred in triplicate to the corresponding coated well and incubated for 1 h at 21 °C with agitation at 400 r.p.m. The plate was washed three times with 0.05% PBST and the specifically bound phage particles were detected using the HRP-conjugated anti-M13 antibody (100 µL/well) in a dilution of 1:5000 in 2% MPBS using the same incubation conditions as above. After three washes with 0.05% PBST, 100 µL of freshly prepared ABTS substrate were added to each well and incubated in the dark as described above. The absorbance was determined at three time points (15, 30 and 60 min after the addition of ABTS) at OD_{405nm} with reference at OD_{490nm} in a Tecan reader.

In order to confirm antigen recognition of single clones, individual phage antibodies were prepared from single phagemid-containing TG1 colonies selected by panning. A dilution series from 10^{-4} to 10^{-8} of bacteria after the third selection round were plated out on LB agar plates containing ampicillin and incubated overnight at 37 °C. Individual colonies were transferred into 150 µL 2× TY medium containing 100 µg mL^{-1} ampicillin and 1% glucose in a sterile 96-well microtitre master plate and grown overnight at 37 °C. A small inoculum of the overnight culture was transferred to a fresh 96-microtitre induction plate into 200 µL 2× TY with 100 µg mL^{-1} ampicillin and 1% glucose per well by using a 96-well transfer device and incubated for 2 h at 37 °C with agitation until the OD_{600} reached 0.4. Glycerol (final concentration 15%) was added to the master plate for cryopreservation, and the plate was stored at −80 °C. The production of individual scFv-displaying phage particles was initiated on the induction plate by adding 25 µL 2× TY containing 100 µg mL^{-1} ampicillin, 1% glucose and 10^9 helper phage to each culture in mid-logarithmic growth phase, and incubating at 37 °C for 30 min without agitation and 30 min with agitation at 200 r.p.m. to allow infection. The culture was centrifuged at 1800 × *g* for 10 min, 4 °C, and the supernatant was removed. Each pellet was resuspended in 200 µL 2× TY with 100 µg mL^{-1} ampicillin, 50 µg mL^{-1} kanamycin and 0.25 mM IPTG for overnight incubation at 30 °C. After centrifugation, supernatant containing the scFv-presenting phage was blocked for 2 h with 2% MPBS in a 1:1 ratio. In parallel, overnight-coated MaxiSorb™ 96-well microtitre plates with immobilized canine DC and PBMC membrane fragments were also blocked as described above, washed three times with PBS and the pre-blocked phage antibodies were transferred in triplicate to the appropriate antigen-coated wells. The phage suspension was incubated for 1 h at 21 °C with agitation at 400 r.p.m. Non-bound phage antibodies were eliminated by washing three times with 0.05% PBST. Phage antibody fragments binding specifically to DCs were detected with the HRP-anti-M13 antibody and ABTS as the substrate, as described above for the polyclonal phage ELISA.

Sequence analysis

Plasmid vectors were prepared using the NucleoSpin Plasmid kit (Macherey-Nagel, Düren, Germany). The scFv sequence was amplified by PCR using GoTaq Hot Start Polymerase (Promega, Madison, WI, USA) and primers LMB3 (5′-CAG GAA ACA GCT ATG AC-3′) and fdseq1 (5′-GAA TTT TCT GTA TGA GG-3′) were designed and

synthesized by Invitrogen (Darmstadt, Germany). An initial denaturation step of 95 °C for 3 min was followed by 25 cycles of 1 min at 95 °C, 45 s at 50 °C and 2 min at 72 °C and a final extension cycle of 10 min at 72 °C. PCR products were analysed by 1% agarose gel electrophoresis and the scFv cDNA fragment was isolated using the QIAquick gel extraction kit (Qiagen, Hilden, Germany). The scFv fragments were sequenced by eurofins MWG Operon (MWG, Ebersberg, Germany) using the primer set described above and analysed using Vector NTI Advance 10 Sequence Analysis Software (Invitrogen).

Bioinformatic analysis of antibody variable regions

The sequenced clones were compared using Vector NTI AlignX algorithm (Invitrogen). Unique sequences were then analysed with V-BASE (http://vbase.mrc-cpe.cam.ac.uk/) and IgBLAST (http://www.ncbi.nlm.nih.gov/blast/Blast.cgi) using the Kabat numbering system to determine framework and complementary determining regions (CDR) of the variable heavy (V_H) and variable light (V_L) chains.

Site-directed mutagenesis

The scFv clones were found to contain an amber termination codon (TAG) within the CDR. Site-directed mutagenesis was therefore used to convert this nonsense codon to a sense codon specifying glutamine (CAG). Primers were designed using the QuickChange™ method (Stratagene) according to the manufacturer's Primer Design Program (http://www.stratagene.com/sdmdesigner/default.aspx). The following primers were used for B8: forward primer B8mut_sense (5′-G GAG TGG GTC TCA AGT ATT ACT AAG CAG GGT GTT CAT AC-3′) and reverse primer B8mut_antisense (5′-GT ATG AAC ACC CTG CTT AGT AAT ACT TGA GAC CCA CTC C-3′). The following primers were used for G11: forward primer G11mut_sense (5′-G GTC TCA ACG ATT AGG GAT CAG GGT CTT CAT ACA ACT TAC GC-3′) and reverse primer G11mut_antisense (5′-GC GTA AGT TGT ATG AAG ACC CTG ATC CCT AAT CGT TGA GAC C-3′). Site-directed mutagenesis was carried out using 50 ng of vector DNA. Mutated clones were repaired by combination of proofreading PCR (Pfu DNA Polymerase; Fermentas GmbH, St. Leon-Rot, Germany) and digestion with restriction endonuclease DpnI (Stratagene) in two separate reactions according to the manufacturer's instructions. Mutated DNAs were verified by sequencing.

Soluble scFv antibody production

The mutated scFv phagemid clones were introduced into chemically competent HB2151 cells for the expression of soluble scFv antibodies. The cells were spread out in a dilution series from 10^{-2} to 10^{-6} on LB agar plates with ampicillin and incubated overnight at 37 °C. Individual colonies were transferred to 150 µL 2× TY containing 100 µg mL^{-1} ampicillin and 1% glucose in a sterile 96-well microtitre plate and incubated overnight at 37 °C with agitation at 200 r.p.m. A small inoculum from each well was transferred to a second 96-well plate, into 200 µL 2× TY containing 100 µg mL^{-1} ampicillin and 0.1% glucose, using a 96-well transfer device, and the plate was incubated for 3 h at 37 °C with agitation until the OD_{600} reached 0.9. Protein expression was initiated by the addition of 25 µL 2× TY containing 100 µg mL^{-1} ampicillin and 9 mM IPTG to a final concentration of 1 mM, and the plate was incubated overnight at 30 °C with agitation. The plate was centrifuged at 1800 × *g* for 10 min at 4 °C and the supernatant was removed. Periplasmic fractions containing the scFv were prepared from bacterial pellets by osmotic shock. Each pellet was suspended in 40 µL 1× TES buffer (50 mM Tris, 1 mM EDTA, pH 8.0, 20% sucrose) and incubated for 30 min at 37 °C with agitation at 200 r.p.m. Each suspension was then supplemented with 60 µL 0.2× TES buffer and incubated as above before centrifugation at 1800 × *g* for 10 min to pellet bacterial debris. An aliquot of the supernatant was taken for evaluation by 12% SDS–PAGE (sodium dodecyl sulphate–polyacrylamide gel electrophoresis), Western blot and scFv-ELISA.

ELISA with soluble scFv

The scFv proteins were blocked with 2% MPBS (1:1 ratio) for 2 h at 21 °C. A 96-well MaxiSorp™ microtitre plate was coated with a 1:100 dilution of

canine DC and PBMC membrane fragments and incubated overnight at 4 °C. The coated plate was washed three times with PBS and blocked with 200 µL 2% MPBS for 2 h at 21 °C with agitation at 400 r.p.m. The coated plate was then washed three times with PBS and the pre-blocked scFvs were added and incubated for 1 h at 21 °C with agitation. After washing with 0.05% PBST, specifically bound scFv antibody fragments were detected with a monoclonal mouse anti-polyHistidine antibody (Sigma-Aldrich, München, Germany; diluted 1:2000 in 2% MPBS) and a HRP-conjugated monoclonal goat anti-mouse IgG(H+L) antibody (Vector Laboratories, Peterborough, United Kingdom; diluted 1:5000 in 2% MPBS). After three washes with 0.05% PBST, 100 µL of freshly prepared ABTS substrate solution were added to each well and the absorbance was measured as described above.

SDS–PAGE and Western blot

Protein samples were boiled at 95 °C for 5 min with loading buffer and fractionated by 12% SDS–PAGE prior to detection with Coomassie Brilliant Blue R-250 and quantification by AIDA (see below) and the Bradford assay (Bio-Rad, München, Germany), with bovine serum albumin standards. Proteins were transferred to a nitrocellulose membrane at 200 V for 1 h at 4 °C. The membrane was blocked with 2% MPBS for 2 h, washed three times with PBST, and incubated with monoclonal mouse anti-polyHistidine (1:2000) and subsequently with HRP-labeled monoclonal goat anti-mouse IgG(H+L) (1:5000) before visualization with 3,3′-diaminobenzidine (DAB, Sigma-Aldrich).

Data analysis

Quantitative analysis of soluble scFv proteins was carried out using AIDA image analyzer 4.27 software (Raytest, Straubenhardt, Germany) after digital scanning of Coomassie-stained SDS-polyacrylamide gels. Statistical analysis was carried out with GraphPad Prism software (GraphPad, La Jolla, CA, USA). Data were quoted as mean ± standard deviation (SD). A two-tailed *t*-test was used to determine the significance of independent experiments. The criterion $P < 0.05$ was considered significant.

Results

Generation of canine DCs

The differentiated DC population was harvested after an average cultivation period of 12.5 days and analysed for characteristic cell surface markers in flow cytometry using the antibody set-up as described above. The population of interest could be distinguished visually in terms of their spherical shape and the typical dendrites as well as in FACS, owing to their lack of staining with CD34, and positive staining with CD11c and MHCII. Enriched DCs with a mean recovery rate of 104.5% (in relation to the initial $CD34^+$ population) and a mean purity of 79.24% (range 71.67–89.27%) were used for subsequent cell-membrane antigen preparation. The diminutive amount of $CD34^+$ undifferentiated cells (mean 3.2%) was minimal and intermittent-appearing fibroblast could be removed by their plastic adherence.

Subtractive cell panning strategy

Canine DC-specific recombinant antibody fragments were obtained from the human naive scFv Tomlinson library J, with a complexity of 1.2×10^8 different inserts, which approximates the complexity of the human B-cell immune system.[14] The variable regions of the heavy (V_H) and light (V_L) antibody chains, separated by a flexible 15-amino-acid glycine-serine linker (L), are encoded by the phagemid vector pIT2 and are under the transcriptional control of the lactose promoter (*lac* pro) and terminator (*lac* term) sequences. The cassette also includes a bacterial leader peptide sequence (*pel*B) that directs the recombinant protein into the periplasmic space. After helper phage infection with either M13KO7 or M13KO7ΔpIII, scFv sequences upstream of the amber stop codon are displayed as an scFv-pIII fusion protein on the phage particle if a suppressor strain such as TG1 is used, whereas the use of a non-suppressor strain such as HB2151 allows the expression of soluble scFvs bearing a His_6-Myc tag (Fig. 1A).

Phage particles displaying scFvs were subjected to three rounds of panning, starting with a negative selection (depletion) on canine PBMCs to remove scFvs that recognized cell surface antigens

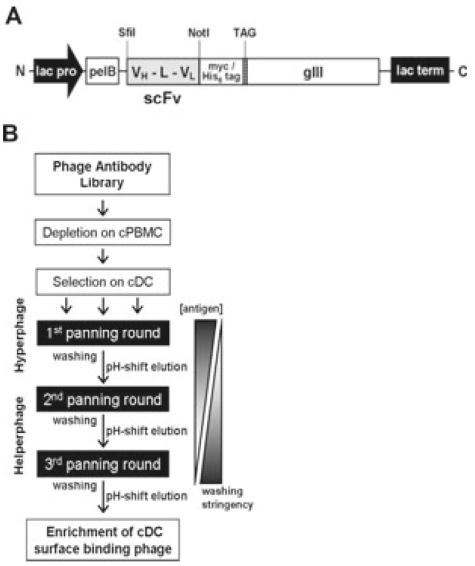

Figure 1. Phage display selection scheme for the identification of phage particles with high affinity and specificity for canine dendritic cells (cDCs). (A) Schematic diagram of the pIT2 phagemid-derived expression cassette, which contains a *lac* promoter (lac pro) and *pel*B leader sequence upstream of the scFv insert, and a downstream His_6-Myc tag, amber termination codon, the gene encoding the pIII phage coat protein and a *lac* terminator (lac term). (B) Flow chart of the subtractive solid-phase panning strategy. Each panning round began with a depletion step, in which phage particles were incubated with cPBMC membrane fragments prior to positive selection on immobilized cDC membrane fragments. Non-specific binders were washed away, whereas bound scFv-phage antibodies were eluted by pH shift and prepared for the subsequent panning round. The selection pressure was increased over successive panning rounds to isolate high-affinity binders by reducing the antigen concentration ([antigen]) and increasing the stringency of washing conditions. Furthermore, polyvalent phages (hyperphage) were used in the first panning round but monovalent phage particles (helper phage) were used in the subsequent rounds.

common to canine blood cells. There followed the positive selection on canine DCs to enrich for specific binders. The selection pressure was increased between rounds by reducing the antigen concentration and increasing the wash stringency (Fig. 1B).

Enrichment of specific phage particles

Enrichment for DC-specific phage particles was monitored by calculating the EF. The second panning round achieved approximately four-fold enrichment (EF_{2nd}/EF_{1st}), whereas the third round achieved 143-fold enrichment (EF_{3rd}/EF_{2nd}) (Table 1). In addition, specific enrichment was monitored by polyclonal phage ELISA carried out on immobilized canine DC membrane fragments, by evaluating the binding activity of the phage pool after each selection step. The ELISA absorbance signal measured after the second selection round was approximately 5.6-fold higher than the background signal of the unselected naive phage library J, whereas the signal after the third round had increased to 9.3-fold higher than background (Fig. 2). All ELISAs were carried out with the appropriate negative controls including the omission of the target antigen, the selected phage pool and a combination of both.

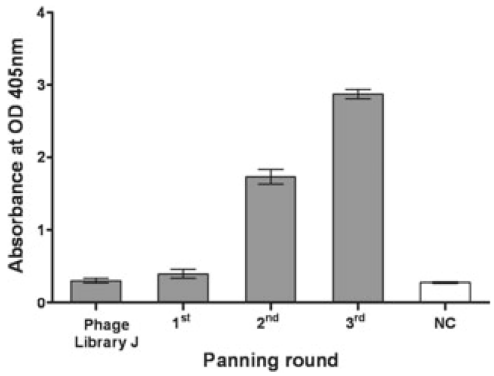

Figure 2. Selective enrichment of scFv-phage particles by subtractive panning illustrated using a polyclonal phage ELISA. Polyclonal phage particles (10^{10} cfu mL^{-1}) from each panning round were added to immobilized canine DC membrane fractions to determine their binding activity. The nonselected phage pool (Phage Library J) displays the naive antigen reactivity. ELISA background controls (NC) included the omission of the target antigen, the selected phage pool and a combination of both.

Table 1. Enrichment of phage particles specifically binding to canine DCs

Helperphage	Panning round	Antigen dilution	Input	Output	EF	Relative enrichment
M13KO7ΔpIII	First	Undiluted	4.3×10^{11}	4×10^{4}	9.3×10^{-8}	—
M13KO7	Second	1/10	2.09×10^{12}	7.8×10^{5}	3.73×10^{-7}	4×
M13KO7	Third	1/50	5.6×10^{10}	7.47×10^{5}	1.33×10^{-5}	143×

Identification of unique binders

We randomly picked 240 individual clones after the third selection round and transferred the colonies into 96-well microtitre plates for small-scale phage production and screening against canine DC membrane fragments by monoclonal phage ELISA. In parallel, we screened the same clones for unwanted binding activity against canine PBMCs and plastic microtitre surfaces (background signal). Absorbance values four-fold higher than the highest background signal were considered indicative of positive binders, and those 10-fold higher or more were considered indicative of high-affinity binders. Hyperphage-prepared clones (polyvalent display) revealed 56 positive binders, 23 with high-affinity binding activity. Equivalent ELISAs using the monovalent display helper phage M13KO7 identified 21 positive binders, eight of which were high-affinity binders. The inserts from all the ELISA-positive clones were amplified by PCR and sequenced, revealing that all clones carried a correctly sized insert approximately 975 bp in length (data not shown). Sequencing revealed a total of eight unique clones, two of which were selected for further characterization. These were designated as B8 (accession number HM560963) and G11 (accession number HM560964). Clones B8 and G11, respectively, showed 6- and 20-fold higher affinities for canine DC cells than negative controls (Fig. 3).

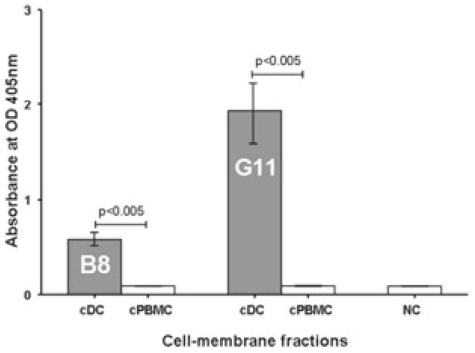

Figure 3. Binding activity of unique scFv-phage antibodies visualized in a monoclonal phage ELISA. Unique phage particles (10^{11} cfu mL^{-1}) of clones B8 and G11 were applied to immobilized canine dendritic cell (cDC) and cPBMC membrane fragments. Horizontal bars denote statistically significant differences ($P < 0.005$) between specific binding to the selection antigen (cDC) and cross-reactivity to the depletion antigen (cPBMC). Vertical bars represent SDs of three replicates.

Sequence analysis and site-directed mutagenesis

Comparison of the B8 and G11 sequence revealed that V_H and V_L CDRs 2 and 3 showed the greatest sequence variation, and both incorporated an amber termination codon (TAG) in the V_H CDR2 region (from NNK randomization), which yields a full-length scFv when using the TG1 suppressor strain. However, for the production of soluble scFvs it is necessary to use a non-suppressor strain such as HB2151, where the amber codon, mentioned earlier, would result in truncation and the production of a non-functional protein. Therefore, the amber stop codon was successfully mutated from TAG to CAG (specifying glutamine, indicated in bold italic letters) using site-directed mutagenesis (Table 2). The product was digested with DpnI to remove the methylated DNA template (target sequence: 5′-Gm^6ATC-3′) allowing the selective digestion of the parenteral vector DNA. Back-mutated phagemid clones were introduced into chemically competent *E. coli* HB2151 cells for the small-scale production of soluble scFv proteins.

Production of soluble scFvs from pIT2 phagemids

Individual HB2151 colonies were transferred to 96-well microtitre plates for scFv expression. After IPTG induction, the periplasmatic fractions were isolated by osmotic shock and analysed for scFv expression by SDS–PAGE and Western blot (Fig. 4A). Gels stained with Coomassie Brilliant Blue R-250 revealed a strong band at 29 kDa, the anticipated molecular weight of the recombinant scFv, and this band matched the position of the only signal the Western blot revealed by a monoclonal antibody specific for the His-tag. The scFv represented approximately 40% of the total protein, allowing direct use of protein extracts for scFv-ELISA. Both clones produced a significant absorbance signal ($P < 0.005$) compared to the negative controls in scFv-ELISA, although the higher background signal of the secondary and tertiary detection antibodies made scFv

Table 2. Primary sequence of amino acids in the variable regions of heavy and light chain

	Variable heavy chain (V_H)			Variable light chain (V_L)		
Clone	CDR1	CDR2	CDR3	CDR1	CDR2	CDR3
B8	SYAMS	SITK***Q***GVHTSYADSVKGR	GLRM	RASQSISSYLN	AASLLQS	QQMVKPPMTFGQ
G11	SYAMS	TIRD***Q***GLHTTYADSVKGR	GARV	RASQSISSYLN	HASSLQS	QQGVKSPATFGQ

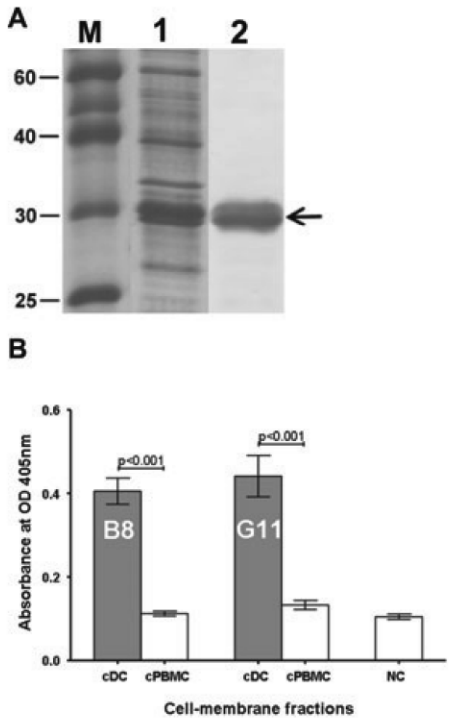

Figure 4. Expression and binding activity of soluble scFv proteins. (A) Coomassie-stained SDS-polyacrylamide gel (1) and the corresponding Western blot (2). Lysates from *E. coli* HB2151 cells transfected with pIT2-scFv after the induction of protein expression were separated and transferred to a nitrocellulose membrane, and recombinant proteins were detected with antibodies binding to the His-tag. Molecular weight markers (M) are shown on the left. (B) ELISAs showing the binding specificity of the selected scFv antibody fragments towards membrane fragments from canine dendritic cells (cDCs) and cPBMCs. Horizontal bars denote statistically significant differences ($P < 0.005$) between specific binding to the selection antigen (cDC) and cross-reactivity to the depletion antigen (cPBMC). Vertical bars represent SDs of three replicates. Negative controls (NC) include the background signal of the secondary antibody and the signal from non-transfected bacteria.

detection more difficult to achieve. Optimization of the experimental conditions revealed a low but significant ($P < 0.001$) binding signal for the soluble scFvs (Fig. 4B).

Discussion

Tumour cells express aberrant antigens that can be recognized by the host lymphocyte population and therefore such antigens are potential targets for cancer immunotherapy.[15] The CTL response is the most important response available for the host to control the growth of antigenic tumour cells, providing protection against the establishment of tumours and the means to reject tumours that are already established.[16] DCs are dedicated antigen-presenting cells and they are a critical component in both the induction and regulation of lymphocyte-mediated immune responses.[17] Several mechanisms for the uptake of extracellular material enable DCs to present antigens from virtually any type of pathogen. The uptake of antigens at infection sites causes DCs to mature and to be directed to the draining lymphoid tissues, leading them to peripheral lymph nodes where immune responses are generated. In the lymph nodes, mature DCs act as powerful activators of antigen-specific primary T- and B-cell responses, inducing memory cells and breaking immunological tolerance against tumours.[18]

Currently, the most popular approach in cancer immunotherapy is to immunize cancer patients with autologous, patient-derived DCs loaded with tumour antigens *ex vivo*. During this adoptive immunotherapeutic approach, DCs must migrate into the lymph nodes and interact with antigen-specific T- and B-cells.[8] Although recent preclinical trials of DC-based vaccines have achieved encouraging results, only a small number of injected exogenous DCs eventually reach the peripheral lymph nodes.[19] Therefore, reliable and selective monitoring of the migration behaviour of injected DCs might provide a better insight into ongoing vaccination protocols, despite the highly complex and cost-intensive techniques applied in such an individualized therapy.

In this study, we present *in vitro* data concerning the generation of specific scFv antibodies to canine DCs, which will facilitate immunodetection and enhanced immune modulation activity during adoptive cellular immunotherapy. Our major findings can be summarized as follows: (1) functional membrane fractions from canine DCs and PBMCs were prepared by a combination of sonication and fractionated ultracentrifugation, which is consistent with the previously published data[12,20]; (2) specific enrichment for a phage population that binds specifically to canine DCs was achieved after three rounds of subtractive panning using canine DC and PBMC membrane fractions as documented in polyclonal phage ELISA; (3) monoclonal phage verification was performed and sequence analysis identified eight unique scFv clones; (4) two scFv clones, B8 and G11, were expressed as soluble periplasmic proteins and canine DC-specific binding activity was confirmed by scFv-ELISA.

Present technologies for the non-invasive monitoring of static and migrating DCs *in vivo* are limited.[21] Typically, cell migration must be monitored in 'snapshots' obtained using classical radioactively labeled scintigraphic imaging methods.[22] A variety of novel approaches for the *in vivo* analysis of DCs could be used in the clinic, including optical imaging (fluorescence, luminescence) and nuclear magnetic resonance (NMR) techniques.[23] The direct visualization of DC migration in patients undergoing adoptive immunotherapy would allow the efficacy of the treatment to be monitored from the early treatment states, and once optimal conditions (e.g. administration route) are defined, then the treatment could be refined and improved. DC-specific antibodies might allow the direct visualization of DC migration in immunological tissues, which has not been achieved efficiently.

Using a semi-synthetic human phage display library, we isolated recombinant antibody fragments directed to biologically active canine DCs which were derived from $CD34^+$ hematopoietic stem cells. The differentiated DC cell population was highly enriched, containing only a negligible number (3.2%) of undifferentiated $CD34^+$ cells. Intermittent-appearing fibroblasts were removed by adhesion to tissue culture plastic. In order to select the highest-affinity DC-specific scFvs, we switched from polyvalent display in the first panning round to monovalent display in the subsequent panning rounds,[24] at the same time reducing the target membrane antigen concentration while increasing the washing stringency.[25] We used a subtractive selection approach[26] to eliminate phage particles showing irrelevant or non-specific binding to canine PBMCs.

The semi-synthetic library introduced an additional factor for consideration, which was the presence of an amber termination codon (TAG) in the V_H CDR2 region of all DC-specific scFvs. The Tomlinson J library comprises random NNK nucleotide triplets at defined positions within the antibody variable region to maximize the side-chain diversity.[27] According to the IUPAC nomenclature, NNK encodes all naturally occurring amino acids as well as specifying the amber codon, the latter having a theoretical inclusion probability of approximately 3%.[28] However, amber mutants have a considerable growth advantage and are more efficiently propagated over variants that carry intact antibody cDNAs resulting in selective enrichment in evolutionarily based selection libraries.[29–31] Phage display using the *E. coli* suppressor strain TG1 allows the amber codon to be mistranslated as glutamine and does not interfere with the initial panning and phage screening process. However, the production of soluble scFvs in non-suppressor strains would result in truncation and the production of a non-functional protein. Therefore, site-directed mutagenesis was carried out to change the amber codon to CAG (glutamine) and specific binding activity was confirmed for scFvs produced in non-suppressing bacteria.

In summary, we used a stringent subtractive panning strategy to generate recombinant antibody fragments from a naive phage display library that are highly specific for canine DCs. The selection strategy we used suggests that the isolated antibodies bind with high affinity to canine DCs and can therefore be used for the specific detection and manipulation of DCs during the development of immunotherapeutic approaches.

Acknowledgments

This work was funded by the German Research Foundation (DFG), Sonderforschungsbereich Transregio 37 (SFB TR 37), sub-project A2. The authors declare no conflicts of interest.

References

1. Garcia MJA, Ward EM, Center MM, Hao Y, Siegel RI and Thun MJ. *Global Cancer Facts and Figures.* Available at: http://www.cancer.org/acs/groups/content/@nho/documents/document/globalfactsandfigures2007rev2p.pdf.
2. Paoloni MC and Khanna C. Comparative oncology today. *The Veterinary Clinics of North America. Small Animal Practice* 2007; **37**: 1023–1032; v.
3. Andrade FH, Figueiroa FC, Bersano PR, Bissacot DZ and Rocha NS. Malignant mammary tumor in female dogs: environmental contaminants. *Diagnostic Pathology* 2010; **5**: 45.
4. Bukowski JA, Wartenberg D and Goldschmidt M. Environmental causes for sinonasal cancers in pet dogs, and their usefulness as sentinels of indoor cancer risk. *Journal of Toxicology and Environental Health Part A* 1998; **54**: 579–591.
5. Khanna C, Lindblad-Toh K, Vail D, London C, Bergman P, Barber L, Breen M, Kitchell B, McNeil E, Modiano JF, Niemi S, Comstock KE, Ostrander E, Westmoreland S and Withrow S. The dog as a cancer model. *Nature Biotechnology* 2006; **24**: 1065–1066.
6. Bergman PJ. Anticancer vaccines. *The Veterinary Clinics of North America. Small Animal Practice* 2007; **37**: 1111–1119; vi–vii.
7. Steinman RM, Hawiger D and Nussenzweig MC. Tolerogenic dendritic cells. *Annual Review of Immunology* 2003; **21**: 685–711.
8. Banchereau J and Palucka AK. Dendritic cells as therapeutic vaccines against cancer. *Nature Reviews. Immunology* 2005; **5**: 296–306.
9. Aarntzen EH, Figdor CG, Adema GJ, Punt CJ and de Vries IJ. Dendritic cell vaccination and immune monitoring. *Cancer Immunology, Immunotherapy* 2008; **57**: 1559–1568.
10. Hagglund HG, McSweeney PA, Mathioudakis G, Bruno B, Georges GE, Gass MJ, Moore P, Sale GE, Storb R and Nash RA. Ex vivo expansion of canine dendritic cells from CD34+ bone marrow progenitor cells. *Transplantation* 2000; **70**: 1437–1442.
11. Altmann S, Lange S, Pommerencke J, Murua Escobar H, Bullerdiek J, Nolte I, Freund M and Junghanss C. High Mobility Group Box 1-Protein expression in canine haematopoietic cells and influence on canine peripheral blood mononuclear cell proliferative activity. *Veterinary Immunology and Immunopathology* 2008; **126**: 367–372.
12. Tur MK, Rothe A, Huhn M, Goerres U, Klimka A Stocker M, Engert A, Fischer R, Finner R and Barth S. A novel approach for immunization, screening and characterization of selected scFv libraries using membrane fractions of tumor cells. *International Journal of Molecular Medicine* 2003; **11**: 523–527.
13. Tur MK, Sasse S, Stocker M, Djabelkhir K, Huhn M, Matthey B, Gottstein C, Pfitzner T, Engert A and Barth S. An anti-GD2 single chain Fv selected by phage display and fused to Pseudomonas exotoxin A develops specific cytotoxic activity against neuroblastoma derived cell lines. *International Journal of Molecular Medicine* 2001; **8**: 579–584.
14. MRC. http://www.lifesciences.sourcebioscience.com/media/143421/tomlinsonij.pdf (accessed June 2010).
15. Rouas-Freiss N, Moreau P, Ferrone S and Carosella ED. HLA-G proteins in cancer: do they provide tumor cells with an escape mechanism? *Cancer Research* 2005; **65**: 10139–10144.
16. Hamai A, Benlalam H, Meslin F, Hasmim M, Carre T, Akalay I, Janji B, Berchem G, Noman MZ and Chouaib S. Immune surveillance of human cancer: if the cytotoxic T-lymphocytes play the music, does the tumoral system call the tune? *Tissue Antigens* 2010; **75**: 1–8.
17. Ilett EJ, Prestwich RJ and Melcher AA. The evolving role of dendritic cells in cancer therapy. *Expert Opinion on Biological Therapy* 2010; **10**: 369–379.
18. Martin-Fontecha A, Lanzavecchia A and Sallusto F. Dendritic cell migration to peripheral lymph nodes. *Handbook of Experimental Pharmacology* 2009; **188**: 31–49.
19. Verdijk P, Aarntzen EH, Punt CJ, de Vries IJ and Figdor CG. Maximizing dendritic cell migration in cancer immunotherapy. *Expert Opinion on Biological Therapy* 2008; **8**: 865–874.
20. Tur MK, Huhn M, Sasse S, Engert A and Barth S. Selection of scFv phages on intact cells under low pH conditions leads to a significant loss of insert-free phages. *Biotechniques* 2001; **30**: 404–408.
21. Akins EJ and Dubey P. Noninvasive imaging of cell-mediated therapy for treatment of cancer. *Journal of Nuclear Medicine* 2008; **49**(Suppl. 2): 180S–195S.
22. De Vries IJ, Krooshoop DJ, Scharenborg NM, Lesterhuis WJ, Diepstra JH, Van Muijen GN, Strijk

SP, Ruers TJ, Boerman OC, Oyen WJG, Adema GA, Punt CJ and Figdor CG. Effective migration of antigen-pulsed dendritic cells to lymph nodes in melanoma patients is determined by their maturation state. *Cancer Research* 2003; **63**: 12–17.

23. Kiessling F. Noninvasive cell tracking. *Handbook of Experimental Pharmacology* 2008; **185/2**: 305–321.
24. Bratkovic T. Progress in phage display: evolution of the technique and its applications. *Cellular and Molecular Life Sciences* 2009; **67**: 749–767.
25. Nielsen U and Marks J. Affinity maturation of phage antibodies. In: *Phage Display A Practical Approach,* edn, Clackson T and Lowman H, eds., Oxford, Oxford University Press, 2004; **266**: 309–311.
26. Eisenhardt SU, Schwarz M, Bassler N and Peter K. Subtractive single-chain antibody (scFv) phage-display: tailoring phage-display for high specificity against function-specific conformations of cell membrane molecules. *Nature Protocols* 2007; **2**: 3063–3073.
27. Braunagel M. Construction of semisynthetic antibody libraries. *Methods in Molecular Biology* 2003; **207**: 123–132.
28. Cwirla SE, Peters EA, Barrett RW and Dower WJ. Peptides on phage: a vast library of peptides for identifying ligands. *Proceedings of the National Academy of Sciences of the United States of America* 1990; **87**: 6378–6382.
29. Marcus WD, Wang H, Lohr D, Sierks MR and Lindsay SM. Isolation of an scFv targeting BRG1 using phage display with characterization by AFM. *Biochemical and Biophysical Research Communications* 2006; **342**: 1123–1129.
30. Beekwilder J, Rakonjac J, Jongsma M and Bosch D. A phagemid vector using the E. coli phage shock promoter facilitates phage display of toxic proteins. *Gene* 1999; **228**: 23–31.
31. Hust M, Meysing M, Schirrmann T, Selke M, Meens J Gerlach GF, and Dubel S. Enrichment of open reading frames presented on bacteriophage M13 using hyperphage. *Biotechniques* 2006; **41**: 335–342.

IX ‘*In vivo* MRI of Intraspinally Injected SPIO-labelled Human CD34+ Cells in a Transgenic Mouse Model of ALS.’ **Willenbrock *et al*., In Vivo. 2012.**

An alternative to the *in vivo* detection of cells with specific antibodies is the unspecific cell-labelling using MRI detectable SPIO nanoparticles causing strong T2* specific signal extinctions. Due to their high biocompatibility and low cellular toxicity, by now different types of SPIOs with varying sizes and surface modifications are widely used for labelling diverse types of cells.

Purpose of this study was the establishment of a non-invasive modality for cell tracking of intraspinally transplanted CD34+ human umbilical cord blood stem cells (hUCBCs) in a transgenic ALS mouse model closely mimicking the neurodegenerative disease as it occurs in humans.

The cell labelling was performed with the commercially FDA-approved SPIO-contrast agent ENDOREM® on MTH53A cells as proof-of-principle and subsequently on hUCBCs. The tracking efficiency of the labelled cells was determined *in vitro* for MTH53A and for hUCBCs *in vitro* and *in vivo* by 1.0 and 7.0 T MRI. The *in vitro* experiments were carried out in agar gel phantoms loaded with different numbers of SPIO-labelled cells.

The *in vitro* detection limit with 1.0 T was determined at 100,000 MTH53A cells and 250,000 hUCBCs while at 7.0 T 25,000 MTH53A cells were visible. Based on these results, in the *in vivo* imaging experiment 100,000 labelled hUCBCs were intraspinally injected into the mouse model and scanned with 7.0 T at day 0 and 4. The injected cells were clearly detectable at day 0 and also at day 4 a signal with the same intensity was present, but no cell migration could be visualised.

IX

***In vivo* MRI of Intraspinally Injected SPIO-labelled Human CD34+ Cells in a Transgenic Mouse Model of ALS.**

Willenbrock S, Knippenberg S, Meier M, Hass R, Wefstaedt P, Nolte I, Murua Escobar H, Petri S.

IN VIVO. *2012. 26(1):31-8*

Own contribution:

- Cultivation of canine MTH53A cells
- *In vitro* SPIO labeling of canine MTH53A and CD34+ hUCBCs
- Cell viability and Prussian blue staining
- Agar gel phantom construction for *in vitro* MRI scans
- Assistance during *in vitro* MRI scans
- MRI data analysis
- Partial manuscript drafting

in vivo *26*: 31-38 (2012)

In Vivo MRI of Intraspinally Injected SPIO-labelled Human CD34+ Cells in a Transgenic Mouse Model of ALS

S. WILLENBROCK[1], S. KNIPPENBERG[2], M. MEIER[3], R. HASS[4], P. WEFSTAEDT[1], I. NOLTE[1], H. MURUA ESCOBAR[1] and S. PETRI[2]

[1]*Small Animal Clinic and Research Cluster of Excellence 'REBIRTH', University of Veterinary Medicine Hannover, Hannover, Germany;*
[2]*Department of Neurology, Hannover Medical School, Hannover, Germany;*
[3]*Institute of Laboratory Animal Science and Research Cluster of Excellence 'REBIRTH' (AG36), Hannover Medical School, Hannover, Germany;*
[4]*Laboratory of Biochemistry and Tumor Biology, Gynecology Research Unit, Department of Obstetrics and Gynecology, Hannover Medical School, Hannover, Germany*

Abstract. *Background/Aim: Administration of stem cells is a promising novel approach for treatment of neurodegenerative diseases. For in vivo monitoring of transplanted cells, non-invasive imaging modalities are needed. In this study we determined the tracking efficiency of a superparamagnetic iron oxide (SPIO)-labelled canine cell line (MTH53A) in vitro as well as the human CD34+ umbilical cord blood stem cells (hUCBCs) in vitro and in vivo efficiency by magnetic resonance imaging (MRI). Materials and Methods: SPIO-labelled MTH53A cells and hUCBCs were scanned in agar gel phantoms at 1.0 T or 7.0 T. For in vivo detection, 100,000 labelled hUCBCs were injected into the spinal cord of a transgenic amyotrophic lateral sclerosis (ALS) mouse and scanned at 7.0 T. Results: In vitro, 100,000 MTH53A cells and 250,000 hUCBCs were visible at 1.0 T. Scanning with 7.0 T revealed 25,000 detectable MTH53A cells. In vivo, 7.0 T MRI showed clear signals of 100,000 implanted cells. Conclusion: MRI combined with SPIO nanoparticles provides valuable potential for non-invasive, non-toxic in vivo tracking of cells implanted into the spinal cord.*

Cellular therapies represent a novel approach for the treatment of a variety of neurodegenerative diseases including amyotrophic lateral sclerosis (ALS). ALS is the most common adult motor neuron disorder characterized by progressive degeneration of motor neurons in the brainstem, the primary motor cortex and the spinal cord, with a mean survival of about three to five years (1). To date, the causes of ALS are still undefined and effective therapeutic strategies are lacking (2-4). While the majority of ALS cases (>90%) are sporadic, mutations in the superoxide dismutase I (*SOD1*) gene were detected as a genetic cause of familial ALS (5). This led to the generation of the most commonly used and best characterized mouse model of ALS. SOD1-G93A mice overexpress human mutant SOD1 closely mimicing human ALS (6, 7).

Transplantation of stem or progenitor cells is being evaluated with the purpose of either replacing lost or dysfunctional neurons, or creating a neuroprotective environment for degenerating neurons, *e.g.* by secretion of trophic factors and/or anti-inflammatory effects (8, 9). In spite of a large number of *in vivo* studies in transgenic animal models, it is still not sufficiently understood how many cells transplanted into the central nervous system migrate and differentiate. Moreover, for translation into clinical trials, the development of safe *in vivo* imaging methods to monitor the fate of transplanted cells is urgently needed (8, 9).

Different types of cells, such as embryonic stem cells, neural stem cells, bone marrow cells and umbilical cord blood cells, are suitable for cellular therapy of neurodegenerative diseases (9). Among these cell types, adult stem cells from human umbilical cord blood (hUCBCs) are discussed as being preferable due to their non-fetal origin, ethical innocuousness, low immunogenic potential, and easy availability (10). While bone marrow-derived cells and hUCBCs have already been shown to have therapeutic potential in the mouse model of ALS (11-13) and have even been applied in some human ALS patients (14, 15), suitable non-invasive, non-toxic *in vivo* imaging methods to better

Correspondence to: PD Dr. rer. nat. H. Murua Escobar, Small Animal Clinic, University for Veterinary Medicine, Buenteweg 9, D-30559 Hannover, Germany. Tel: +49 05119536382, Fax: +49 05119536204, e-mail: hescobar@tiho-hannover.de

Key Words: In vivo imaging, cell transplantation, ALS, SPIO, umbilical cord blood stem cells, MRI, tracking, MTH53A cells, SOD1-ALS mouse, CD34+.

0258-851X/2012 $2.00+.40

in vivo 26: 31-38 (2012)

understand the fate and migration of transplanted cells are lacking. In this context, magnetic resonance imaging (MRI) appears to be a promising clinically transferable tool, with high spatial resolution, a long effective imaging window, and fine signal intensity (16). In order to detect transplanted cells by MRI, the cells must be labelled with an effective contrast agent. Due to their low toxicity and high biocompatibility, different types of superparamagnetic iron oxide (SPIO) nanoparticles with strong T2* specific signal extinctions are widely used for labelling of different stem cell types (16-22).

Human umbilical cord mesenchymal stem cells (hUC-MSCs) labelled with the FDA-approved SPIO-particle Feridex have been assessed *in vitro* and *in vivo* after transplantation into the dorsal spinal cord of Sprague-Dawley rats by MRI using a 1.5 T scanner in a study by Hu *et al.* (23). A study by Delalat *et al.* (24) examined the *in vivo* migratory capacity of hUCBCs and human mesenchymal stem cells (MSCs) isolated from bone marrow labelled with the FDA-approved SPIO-contrast agent Endorem. These cell populations were transplanted into Balb/c mice by tail vein injection and detected by histopathology using Prussian blue (PB) staining, but not by MRI (24). Endorem is widely used as MRI contrast agent and can be easily incorporated by endocytosis. In contrast to other SPIO particles, the uptake of Endorem does not require transfection agents, which may reduce the viability of cells (25).

For the first time, we have specifically evaluated the tracking efficiency of Endorem-labelled CD34$^+$ hUCBCs *in vitro* and *in vivo* by MRI after intraspinal injection in a transgenic mouse model of ALS.

Materials and Methods

Cultivation of canine MTH53A cells. The canine mammary epithelial cell line MTH53A was chosen due to its unlimited availability to perform the 'proof of concept' for determination of the lowest detectable SPIO-labelled cell numbers *via* 1.0 T and 7.0 T MRI *ex vivo* in an agar gel matrix. The MTH53A canine mammary cell line, derived from healthy canine mammary epithelial tissue, was established at the Centre for Human Genetics, University of Bremen, Bremen, Germany. MTH53A cells were grown at 37˚C and 5% CO_2 in 199 medium (Gibco, Karlsruhe, Gemany) supplemented with 10% heat-inactivated foetal calf serum (PAA Laboratories GmbH, Coelbe, Germany), 200 U/ml penicillin and 200 ng/ml streptomycin (Biochrom AG, Berlin, Germany).

Isolation and ex vivo expansion of CD34$^+$ hUCBCs. Isolation of CD34$^+$ cells was performed by magnetic antibody cell sorting (MACS) from human umbilical cord blood. Thus, cord blood was obtained from healthy pregnant women with non-complicated pregnancies at spontaneous term-deliveries (38-40 weeks of gestation) or by Caesarean section after informed written consent, respectively, as approved by the Institutional Review Board, project #3037 on June 17th, 2006. The cord blood was immediately transferred into EDTA-containing monovettes on ice and separated *via* Ficoll density gradient centrifugation. Following removal of the lymphocyte interphase, further separation was performed *via* the CD34$^+$-associated MACS technology according to the manufacturer's instructions (Miltenyi GmbH, Bergisch Gladbach, Germany). The isolated population was analyzed for appropriate CD34$^+$ hematopoietic stem cell enrichment by flow cytometry. Thereafter, the separated primary stem cell population was cultured and expanded in the presence of Iscove's Modified Dulbecco's Medium (IMDM; Biochrom AG, Berlin, Germany), 10% FCS (PAA Laboratories GmbH, Coelbe, Germany), 1% Pen/Strep (Biochrom AG), Stem Cell Factor (SCF), Interleukin-3 (IL-3), Interleukin-6 (IL-6), FMS-like tyrosine kinase 3 (FLT-3) (all growth factors and cytokines were purchased from PeproTech GmbH, Hamburg, Germany) at 5% CO_2 and 37˚C for 7 to 14 days with a medium change every third day. Before surgery, the expanded cells (hereafter termed hUCBCs) were washed twice with a 0.9% (w/v) sodium chloride solution and resuspended at a density of 100,000 cells/µl.

In vitro SPIO cell labelling. Cell labelling was performed with the commercially available SPIO suspension ENDOREM® (Guerbet S.A., Roissy, France). This infusion suspension contains particles with an approximate size of 80 to 150 nm and has a total iron content of 11.2 mg/ml.

A total of 5×10^6 MTH53A cells or CD34$^+$ hUCBCs was seeded in a 25 cm^2 cell culture flask with 5 ml of the respective cultivation medium. For labelling, 41.15 µl SPIO suspension (=130 pg iron oxide nanoparticles/cell) was added to the seeded cells followed by an overnight incubation at 37˚C in 5% CO_2. After SPIO incubation, the viability of the labelled cells and unlabelled cells as controls was assessed by trypan blue staining.

Prussian blue staining. After SPIO labelling, cells were fixed with 4% paraformaldehyde, washed with 1× Phosphate Buffered Saline (PBS; Biochrom AG, Berlin, Germany) and incubated with a 1:1 solution of 5% potassium ferrocyanide and 5% hydrochloric acid for 30 min. The ferric iron (iron(III) oxide; Fe_2O_3) of the intracellular SPIO particles reacts with potassium ferrocyanide to form ferric ferrocyanide (=Prussian blue), a water-insoluble, blue precipitate. A final washing step with 1× PBS was performed before visualization of the internalized particles was carried out under light microscopy.

Agar gel phantom construction. For *ex vivo* MRI detection of SPIO-labelled cells, 250 ml of a hand-warm bubble-free 1% agar (Carl Roth GmbH & Co. KG, Karlsruhe, Germany) solution (in dH_2O) were prepared and put into an empty pipette tip box (Greiner Bio-One, Frickenhausen, Germany). For generation of sample wells, an unskirted 96-well PCR plate (Eppendorf AG, Hamburg, Germany) was placed onto the surface of the liquid agar solution. After polymerisation of the agar, the 96 well-plate was removed and the sample wells were ready for cell loading.

The SPIO-labelled cells were trypsinized after incubation with SPIOs and the cell number was determined. Defined numbers of cells were aliquoted into 1.5 ml cups (Eppendorf AG, Hamburg, Germany) as indicated in the results. The aliquoted cells were centrifuged for 10 min at 1,000 rpm (room temperature), the supernatant was discarded and the pellet was resuspended in 30 µl of hand-warm 4% gelatine (AppliChem, Darmstadt, Germany)/dH2O solution. The cell-gelatine mixture was pipetted into the wells of the agar gel phantom and air bubbles were removed. The phantom was cooled at 4˚C until the gelatine was solidified. As controls, additionally to unlabelled cells, 1.0 µl or 1.5 µl SPIO solution (1.0 T MRI and 7.0 T MRI, respectively) and 30 µl culture medium were

prepared by mixing 30 μl of the 4% gelatine solution and loading the samples into the wells of the agar gel phantom. Finally, to embed the loaded samples evenly in the agar phantom, the top was covered with 1% agar gel solution. After polymerisation, the construct was stored at 4˚C until MRI analysis.

In vivo experiment. *In vivo* imaging of SPIO-labelled hUCBCs was performed in a transgenic mutant SOD1-ALS mouse. The G93A-ALS mouse model (B6SJL-Tg(SOD1-G93A)1Gur/J) is bred and maintained at the animal facility of Hannover Medical School. The animal experiment in this study has been approved by the Niedersächsisches Landesamt für Verbraucherschutz und Lebensmittelsicherheit (LAVES, Oldenburg) (AZ 06/1128).

SPIO-labelled cells were trypsinised, washed twice in PBS (Biochrom AG, Berlin, Germany) and the cell density was adjusted to 100,000 cells/ml. A centrifugation step was performed at 1,000 rpm for 10 min, at room temperature, to pellet the cells and the supernatant was discarded. To remove residual cell culture medium, the cell pellet was resuspended in sterile 1× PBS (Biochrom AG, Berlin, Germany) and centrifuged again. After a second PBS washing step, the cell pellet was resuspended in an adequate volume of sterile PBS to prepare a solution of 100,000 cells/ml.

For surgery, the animal was anaesthetized by a combination of ketamine (0.1 ml/100 g, 100 mg/kg), xylazine 2% (0.01 ml/100g, 2 mg/kg) and midazolame (0.05 ml/100 g, 0.5 mg/kg), prepared under sterile conditions with 0.9% sodium chloride. Anaesthesia was administered intraperitoneally, adjusted to the body weight (0.1 ml/10 g) and lasted 60 min as controlled by the toe and eyelid reflex. An area of 3×2 cm on the back of the animal was disinfected and shaved. Eye ointment protected the eyes against dehydration. The animal was fixed in ventral position by tape and the skin was disclosed longitudinally. Laminectomy was performed at vertebral bodies Th12/L1 with sharp scissors to expose the spinal cord at level L1-L4. For better visibility, the backbone adjacent to the exposed spinal cord was fixed with a clamp, which again was fixed in a stereotactic frame. A Hamilton syringe with an elongated glass capillary on top (50-80 μm diameter) was used for injection. The syringe was filled with 0.9% sodium chloride before 1 μl stem cell solution (*i.e.* 100,000 cells in 0.9% sodium chloride) was administered into the lumbar region of the spinal cord. The syringe was clamped into the arm of the stereotactic frame and inserted 1 mm in the ventral direction from the dorsal surface of the spinal cord, followed by slow injection of the cells over a period of three minutes. After a period of an additional two minutes, the syringe was removed slowly to prevent reflux of inserted cells. After wound closure, the animal received a single dose of carprofene (5 mg/kg subcutaneously) and metamizole *via* drinking water (200 mg/kg/day) for 3 post-surgical days for analgesia.

In vitro MRI. The scans of the prepared agar gel phantom, loaded with SPIO-labelled cells and respective controls, were performed in a clinical whole-body MR imaging system at 1.0 T (Magnetom Expert, Siemens Healthcare, Erlangen, Germany) and a Bruker Pharmascan 70/16 7.0 T MR-tomograph for small laboratory animals (Bruker BioSpin MRI GmbH, Ettlingen, Germany).

For 1.0 T analysis, a T2*-weighted gradient echo flash 2-D sequence with a repetition time (TR) of 800 ms and an echo time (TE) of 26.0 ms, slice thickness of 2.0 mm, flip angle (FA) of 20˚, field of view (FoV) of 201×230, 168×256 and two repetitions was used and the data analysis was carried out by dicomPACS version 5.2 (Oehm and Rehbein, Rostock, Germany).

To scan the agar gel phantom in the 7.0 T MRI, an 8 cm volume resonator designed for MRI analysis of rats was used. The agar gel phantom was trimmed with a scalpel to fit into the 8 cm volume resonator. The parameters for the 7.0 T scan were as follows: T2*-weighted flash 2D sequence, TR/TE=200/20, slice thickness 2.0 mm, FA=90˚, one repetition.

Data were analysed using ImageJ, version 1.41 (NIH, Bethesda, MD, USA) extended by the Bruker Opener plugin version 2008/04/22 (Fraunhofer Institute for Biomedical Engineering, St. Ingbert, Germany).

In vivo MRI. *In vivo* MRI was performed on a 7.0 T Bruker Pharmascan 70/16 (Bruker Biospin) equipped with a 6 cm volume resonator using Paravision 5.0. The mouse was anaesthetized with isoflurane during the MRI scans. The body temperature was kept at approximately 37˚C using a temperature control unit (Small Animal Instruments, Stony Brook, NY, USA). A T2* multi-gradient echo (MGE) with the following parameters was used: TR=1500 ms, TE=9 ms, FA=30˚, slice thickness=1 mm.

The G93A-ALS mouse was scanned at day 0 (injection day) and day 4 to detect the injected SPIO-labelled cells and to analyse if cell migration could be visualized.

Results

1.0 T and 7.0 T MRI scans of ex vivo agar gel phantoms. MTH53A cells were used for the proof of concept experiments. The 1.0 T MRI scan of SPIO-labelled canine MTH53A cells embedded in the agar gel phantom revealed a cell detection limit of 1×10^5 labelled cells due to SPIO-induced T2*-specific signal extinctions (Figure 1A). The respective negative controls (medium alone and unlabelled cells) showed no signal extinction and the positive controls with 1.0 and 1.5 μl Endorem® showed strong signal extinctions.

To examine the cellular detection limit at higher field strength, an agar gel phantom with SPIO-labelled MTH53A cells was scanned with 7.0 T MRI (Figure 1B). Medium and unlabelled cells as negative controls exhibited no signals. The positive control with 1.0 μl Endorem® demonstrated a strong T2*-specific signal extinction. The 7.0 T MRI scan revealed a cell detection limit of 2.5×10^4 labelled cells in comparison to the detection limit of 1×10^5 labelled cells at 1.0 T field strength.

1.0 T MRI analysis of SPIO-labelled $CD34^+$ hUCBCs in the agar gel phantom detected a minimal limit of 2.5×10^5 labelled cells, while controls (medium and unlabelled cells) were undetectable (Figure 2). The positive controls (1.0 and 1.5 μl Endorem®) showed signal extinctions as observed in the agar gel phantom with SPIO-labelled MTH53A cells.

In vitro cell labelling, viability and Prussian blue staining. Trypan blue staining was performed directly after the respective labelling reaction. All labelled and unlabelled cells had a viability of nearly 98% (data not shown). After staining with Prussian blue, an accumulation of iron in the cytosol of SPIO labelled cells was detected, indicating that the cells were successfully labelled for MRI tracking (Figure 3A and B).

in vivo *26*: 31-38 (2012)

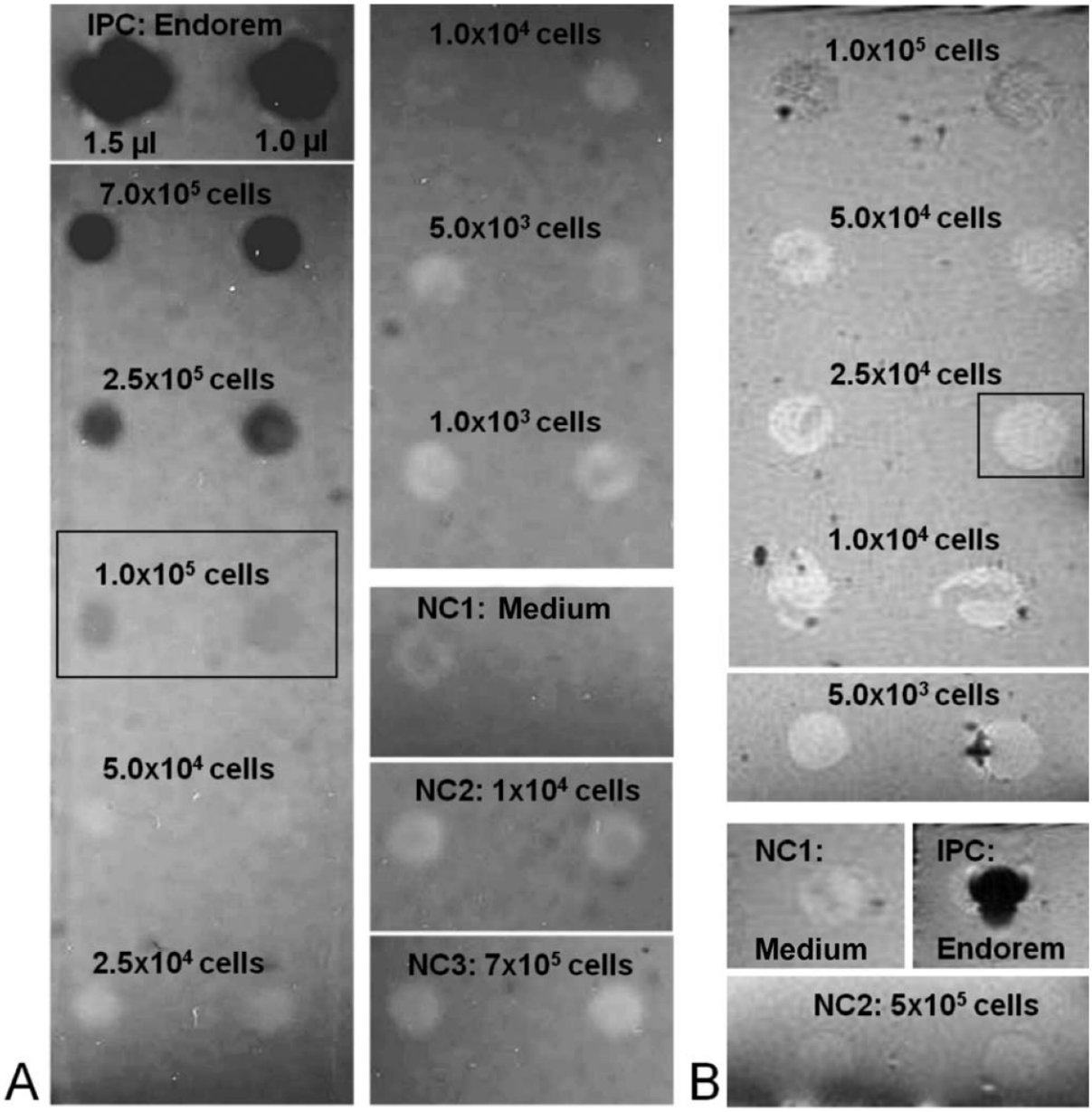

Figure 1. *Ex vivo agar gel phantom detection of superparamagnetic iron oxide (SPIO) labelled canine MTH53A cells by 1.0 and 7.0 T magnet resonance imaging (MRI). A: 1.0 T MRI showing embedded numbers of MTH53A cells. IPC, Positive control (1.0 and 1.5 µl Endorem solution); NC1, cell culture medium; NC2, 1×10^4 unlabelled cells; NC3, 7×10^5 unlabelled cells. Detection limit of SPIO-labelled cells was determined as 1×10^5 by 1.0 T MRI. The negative controls NC1, NC2 and NC3 show no signals. The positive control IPC shows strong signal extinction. B: 7.0 T MRI showing embedded numbers of MTH53A cells. IPC, Positive control (1.0 µl Endorem solution); NC1, cell culture medium; NC2, 5×10^5 unlabelled cells. The controls show the expected signals corresponding to Figure 2A. Detection limit of SPIO-labelled cells was determined as 2.5×10^4 by 7.0 T MRI.*

In vivo 7.0 T MRI scan. For *in vivo* MRI detection of 1×10^5 SPIO-labelled intraspinally injected $CD34^+$ hUCBCs, the G93A-ALS mouse was scanned at day 0 (injection day) and day 4 to analyse if cell migration could be visualized. At day 0, the injected 1×10^5 SPIO-labelled cells were clearly detectable due to the SPIO-induced signal extinctions at 7.0 T (Figure 4A). After 4 days, the signal was still clearly detectable, but no migration of the cells was observed (Figure 4B).

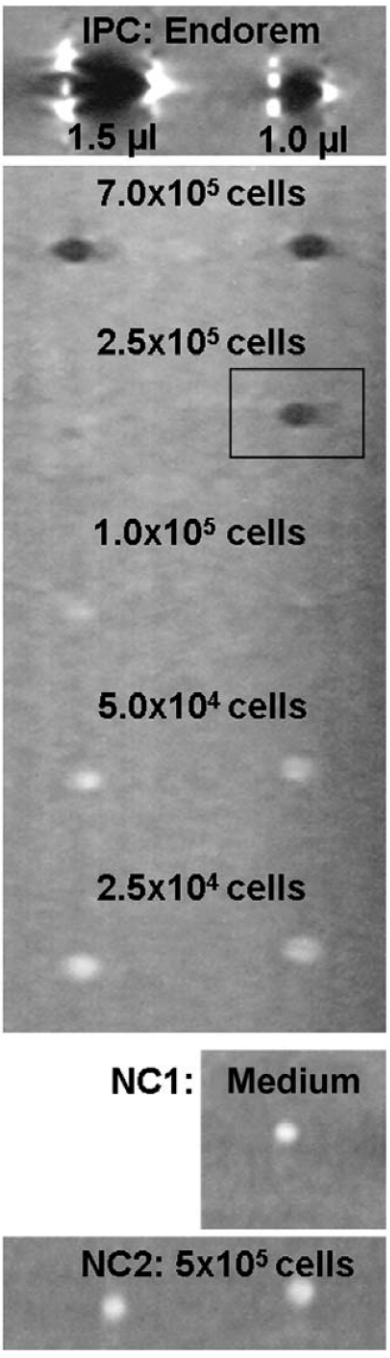

Figure 2. *Ex vivo agar gel phantom detection of superparamagnetic iron oxide (SPIO)-labelled human umbilical cord blood stem cells (hUCBCs) by 1.0 T magnet resonance imaging (MRI). The imaging shows the embedded numbers of hUCB cells. IPC, Positive control (1.0 and 1.5 µl Endorem solution); NC1, cell culture medium, NC2, 5×10^5 unlabelled cells. Detection limit of SPIO-labelled cells was determined as 2.5×10^5 by 1.0 T MRI. The negative controls NC1 and NC2 show no signals. The positive control IPC shows strong signal extinction.*

Discussion

In the present study, the feasibility of SPIO-labelling of canine mammary epithelial cells and of hUCBCs and their subsequent *in vitro* and *in vivo* detection by MRI was assessed. Transplantation of stem or progenitor cells into the CNS is being widely investigated as a novel therapeutic option for a variety of neurological disorders including stroke, spinal cord injury and neurodegenerative diseases such as Parkinson's disease and ALS (9, 26-28). Adult stem cells such as the $CD34^+$ population of hUCBCs, represent promising candidates for cell therapies in general due to their availability, ethical innocuousness, low tumorigenity and high differentiation potential (8).

We have previously shown that intraspinal injection of hUCBCs into the spinal cord prolongs survival, delays deterioration of motor function and prevents motor neuron loss and astrocytosis in mutant *SOD1* transgenic mice (13). However, little is known about the long-term differentiation and migration of transplanted stem cells. In experimental studies on transgenic rodent ALS models, different methods for detection of transplanted cells, such as hUCBCs or other types of stem cells, are used. The use of fluorescence-labelled cells (29), specific mRNA expression measurement (10, 29, 30), and immunohistological analysis of dissected sacrificed animals at different time intervals (10, 11, 30) are commonly used techniques. For successful translation into clinical trials, it will however be mandatory to establish non-invasive imaging protocols to better understand potential mechanisms of action of cellular therapies.

We have now developed a protocol for successful *in vivo* detection by MRI of SPIO-labelled hUCBCs after transplantation into the spinal cord. As the SPIO-labelling efficiency is dependent on the cell type under use, the detection limit of the target cell type was first verified *in vitro* by scanning agar gel phantoms loaded with SPIO-labelled cells. We determined the lowest detectable cell number of our SPIO-labelled proof-of-concept cell line MTH53SA by 1.0 T and 7.0 T MRI in order to assess the visualization potential of SPIO cell-labelling in general and to examine if the field strength is inversely proportional to the detectable SPIO-labelled cell number. The lowest detectable number of SPIO-MTH53A cells was determined to be 1×10^5 with 1.0 T (Figure 1A) and 2.5×10^4 with 7.0 T field strength (Figure 1B). As a 4-fold smaller cell number was detectable at 7.0 T, the comparison of the *in vitro* 1.0 T and 7.0 T data indicates that the field strength is not directly inversely proportional to the detectable cell number. These data were used as basic concept for hUCBC-labelling and MRI.

Due to the fact that a minimum of 2.5×10^5 SPIO-labelled hUCBCs was clearly detectable at 1.0 T field strength (Figure 2), the 7.0 T *in vitro* MR scan of the agar gel phantom was omitted and a cell number of 1×10^5 implanted hUCBCs was

in vivo *26*: 31-38 (2012)

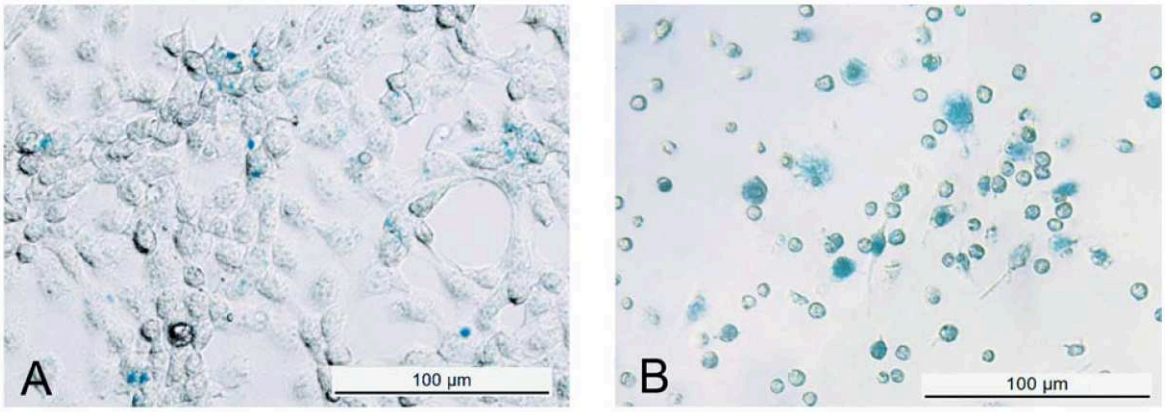

Figure 3. *Prussian blue staining of superparamagnetic iron oxide (SPIO)-labelled canine MTH53A cells (A) and CD34+ human umbilical cord blood stem cells (B), showing positively labelled cells (blue staining) with accumulated iron in the cytosol.*

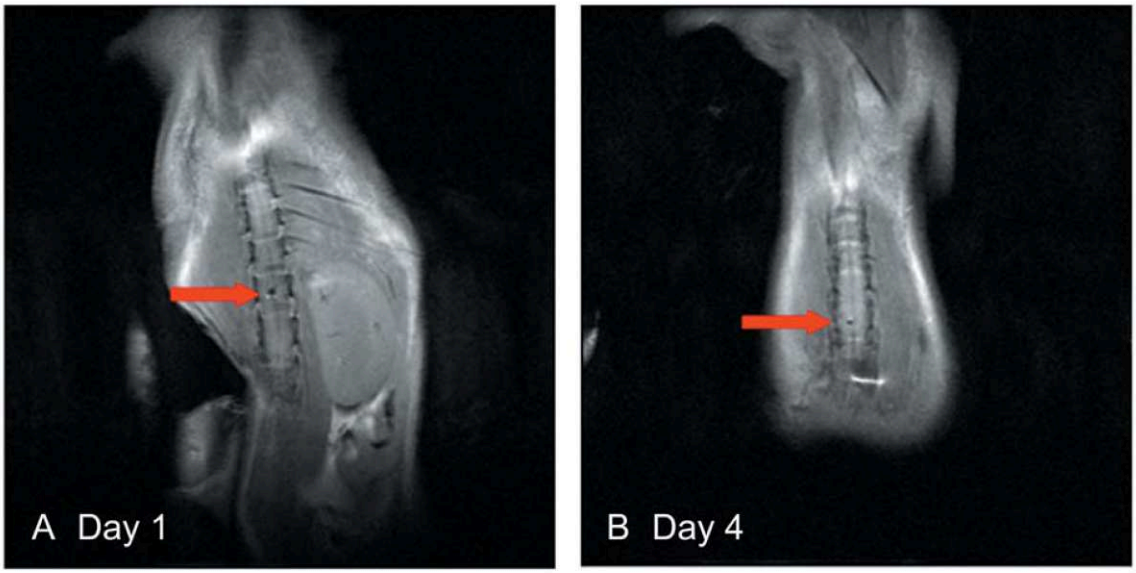

Figure 4. *In vivo 7.0 T magnet resonance imaging (MRI) scan. Detection of 1×10^5 SPIO-labelled intraspinally injected hUCB cells in a G93A-ALS mouse. In vivo scans were performed at day 0 (injection day) and day 4. The cells are clearly detectable (arrow), showing the SPIO-induced T2*-specific signal extinctions at the injection site (Figure 4A). Four days post-injection, the signal is still clearly detectable at the injection site (Figure 4B).*

set for 7.0 T *in vivo* imaging. Taken into account the difference in field strength from 1.0 T to 7.0 T and the thereby available higher resolution at 7.0 T, the detection of 1×10^5 hUCBCs *in vivo* was to be expected due to the fact that 2.5×10^5 hUCBCs are clearly visible at 1.0 T in the agar gel phantom (Figure 2).

Prior to MRI, Prussian blue staining was performed to verify SPIO cell labelling. Figure 3A and B show positively stained MTH53A cells and hUCBCs with accumulated iron in the cytosol. The blue staining demonstrates that the labelling was successful.

Numerous reports are available on *in vivo* tracking of iron oxide nanoparticle-labelled stem and progenitor cells in cell therapy for various diseases (20, 22, 23, 31-34), but only few studies recently investigated the detection of transplanted SPIO-labelled stem cells in the spinal cord of rodent models, which differed in the used cell type, SPIO particles and MR field strength. On this context, Dunning *et al*. imaged 5X104 implanted SPIO-labelled Schwann cells and olfactory ensheathing cells after transplantation into focal areas of demyelination in adult rat spinal cords with a 9.4 T MR

imager (35). In comparison to our results generated with a lower field strength of 7.0 T, twice the number of implanted cells (1×10^5) and with regard to the different section planes, we achieved similar intensities of T2-weighted SPIO-induced hypointense signal extinctions.

Another study by Hu *et al*. examined the fate of 5×10^4 SPIO-labelled hUC MSCs after transplantation into focal areas in adult rat spinal cord (23). Signal extinctions were detectable for up to 14 days using a 1.5 T MR imager and a T2-weighted protocol, but no migration of the implanted cells was observable. Regarding signal intensity, the results by Hu *et al*. are in agreement with our finding although lower field strength and half the cell number was used. The signal extinction area of our implanted SPIO-labelled hUCBCs appears somewhat sharper due to the higher field strength MRI with 7.0 T. It should be noted that the labelling efficiency depends on the targeted cell type and the labelling time. The type of superparamagnetic iron oxide nanoparticles used for cell labelling and the MRI sequences are also relevant (36). This might explain why imaging of a lower number of SPIO labelled cells can cause more intensive signal extinctions.

MRI of SPIO-labelled cells in the spinal cord of rodents was also performed by Jendelova *et al*. (18). In this study, the migration of 2×10^6 intravenously-injected rat bone marrow stromal cells into the injured spinal cord of Wistar rats in a 4.7 T Bruker tomographer was examined. SPIO-labelled cells were clearly detectable in the spinal cord. Due to the fact that in their study the injection was intravenous and not intraspinal, no information about the number of the imaged cells can be given and a comparison of their data to ours concerning implanted cell numbers is not possible.

To summarize, we were able to successfully detect 1×10^5 SPIO-labelled intraspinally injected hUCBCs *in vivo* in a transgenic mouse model of ALS by 7.0 T MRI for the first time. No migration of the injected cells in the form of signal reduction or dislocation was observed along the spinal cord, but a persistent signal was detectable after four days (Figure 4B). Possibly the length of time of four days was not sufficient to monitor cell migration. To investigate this in detail, a longer observation time might be required. In reference to the studies of Dunning *et al*. (35) and Jendelova *et al*. (18), a time period of two to four weeks could be adequate. In addition to this, a stimulation of the transplanted cells with special mobilization factors might also improve cell migration.

The major limitation of this study is the dependency of the cell detection limit in relation to the MR field strength. At present, visualization at the single-cell level by 7.0 T MRI is unlikely and will rather require alternative *in vivo* imaging techniques such as intravital microscopy. *In vivo* monitoring of cell-cell interactions will, however, be of interest mainly for basic science-related questions. For cellular therapy in animal models and its translation into clinical application, administration of large cell numbers will be required so that the detection limit of MRI does not consist a problem in this context.

Due to the non-invasive character of MRI studies, the nanoparticle-based cell detection further allows to study cell behaviour in single individuals at different stages significantly reducing intra-individual variance and the total number of requested animals.

Further studies could also include a canine model with spontaneously occurring ALS due to an *SOD1* missense mutation. In dogs, this spontaneously occurring form of ALS is named degenerative myelopathy. The development of therapeutic options is already of considerable interest for dogs as patients. Moreover, in comparison to the mouse model of ALS, canine degenerative myelopathy closely reflects the human disease regarding the anatomy of the nervous system and the disease course. We therefore now intend to perform further studies using SPIO-labelled canine and human $CD34^+$ cells in mice and dogs over longer time intervals to evaluate the long-term behaviour of intraspinally transplanted cells with respect to signal intensity and cell migration. Ultimately, these data will provide a basis for developing valuable tools for the monitoring of clinical trials assessing the benefit of cell transplantation in humans.

References

1 Mitsumoto H, Chad DA and Pioro EP: Amyotrophic lateral sclerosis. F.A. Davis Company, Philadelphia, pp. 22-23, 1998.
2 Bruijn LI, Miller TM and Cleveland DW: Unraveling the mechanisms involved in motor neuron degeneration in ALS. Annu Rev Neurosci *27*: 723-749, 2004.
3 Pasinelli P and Brown RH: Molecular biology of amyotrophic lateral sclerosis: insights from genetics. Nat Rev Neurosci *7*: 710-723, 2006.
4 de Carvalho M and Swash M: Amyotrophic lateral sclerosis: an update. Curr Opin Neurol, 2011.
5 Rosen DR, Siddique T, Patterson D, Figlewicz DA, Sapp P, Hentati A, Donaldson D, Goto J, O'Regan JP, Deng HX, Rahmani Z, Krizus A, McKenna-Yasek D, Cayabyab A, Gaston SM, Berger R, Tanzi RE, Halperin JJ, Herzfeldt B, Van den Bergh R, Hung WY, Bird T, Deng G, Mulder DW, Smyth C, Laing NG, Soriano E, Pericak-Vance MA, Haines J, Rouleau GA, Gusella JS, Horvitz RH and Brown RH Jr.: Mutations in Cu/Zn superoxide dismutase gene are associated with familial amyotrophic lateral sclerosis. Nature *362*: 59-62, 1993.
6 Gurney ME, Pu H, Chiu AY, Dal Canto MC, Polchow CY, Alexander DD, Caliendo J, Hentati A, Kwon YW, Deng HX, Chen W, Zhai P, Sufit RL and Siddique T: Motor neuron degeneration in mice that express a human Cu,Zn superoxide dismutase mutation. Science *264*: 1772-1775, 1994.
7 Gurney ME: Transgenic-mouse model of amyotrophic lateral sclerosis. N Engl J Med *331*: 1721-1722, 1994.
8 Silani V, Cova L, Corbo M, Ciammola A and Polli E: Stem-cell therapy for amyotrophic lateral sclerosis. Lancet *364*: 200-202, 2004.

9 Hedlund E, Hefferan MP, Marsala M and Isacson O: Cell therapy and stem cells in animal models of motor neuron disorders. Eur J Neurosci *26*: 1721-1737, 2007.

10 Garbuzova-Davis S, Willing AE, Zigova T, Saporta S, Justen EB, Lane JC, Hudson JE, Chen N, Davis CD and Sanberg PR: Intravenous administration of human umbilical cord blood cells in a mouse model of amyotrophic lateral sclerosis: distribution, migration, and differentiation. J Hematother Stem Cell Res *12*: 255-270, 2003.

11 Vercelli A, Mereuta OM, Garbossa D, Muraca G, Mareschi K, Rustichelli D, Ferrero I, Mazzini L, Madon E and Fagioli F: Human mesenchymal stem cell transplantation extends survival, improves motor performance and decreases neuroinflammation in mouse model of amyotrophic lateral sclerosis. Neurobiol Dis *31*: 395-405, 2008.

12 Cabanes C, Bonilla S, Tabares L and Martinez S: Neuroprotective effect of adult hematopoietic stem cells in a mouse model of motoneuron degeneration. Neurobiol Dis *26*: 408-418, 2007.

13 Knippenberg S, Thau N, Schwabe K, Dengler R, Schambach A, Hass R and Petri S: Intraspinal injection of human umbilical cord blood-derived cells is neuroprotective in a transgenic mouse model of amyotrophic lateral sclerosis. Neurodeg Diseases, in press, 2011.

14 Mazzini L, Ferrero I, Luparello V, Rustichelli D, Gunetti M, Mareschi K, Testa L, Stecco A, Tarletti R, Miglioretti M, Fava E, Nasuelli N, Cisari C, Massara M, Vercelli R, Oggioni GD, Carriero A, Cantello R, Monaco F and Fagioli F: Mesenchymal stem cell transplantation in amyotrophic lateral sclerosis: A Phase I clinical trial. Exp Neurol *223*: 229-237, 2010.

15 Cordes AL, Jahn K, Hass R, Schwabe K, Weissinger EM, Ganser A, Gotz F, Dengler R, Krauss JK and Petri S: Intramedullary spinal cord implantation of human CD34(+) umbilical cord-derived cells in ALS. Amyotroph Lateral Scler, 2011.

16 Ju S, Teng G, Zhang Y, Ma M, Chen F and Ni Y: *In vitro* labeling and MRI of mesenchymal stem cells from human umbilical cord blood. Magn Reson Imaging *24*: 611-617, 2006.

17 Hoehn M, Kustermann E, Blunk J, Wiedermann D, Trapp T, Wecker S, Focking M, Arnold H, Hescheler J, Fleischmann BK, Schwindt W and Buhrle C: Monitoring of implanted stem cell migration *in vivo*: a highly resolved *in vivo* magnetic resonance imaging investigation of experimental stroke in rat. Proc Natl Acad Sci USA *99*: 16267-16272, 2002.

18 Jendelova P, Herynek V, Urdzikova L, Glogarova K, Kroupova J, Andersson B, Bryja V, Burian M, Hajek M and Sykova E: Magnetic resonance tracking of transplanted bone marrow and embryonic stem cells labeled by iron oxide nanoparticles in rat brain and spinal cord. J Neurosci Res *76*: 232-243, 2004.

19 Sykova E and Jendelova P: Magnetic resonance tracking of implanted adult and embryonic stem cells in injured brain and spinal cord. Ann N Y Acad Sci *1049*: 146-160, 2005.

20 Niemeyer M, Oostendorp RA, Kremer M, Hippauf S, Jacobs VR, Baurecht H, Ludwig G, Piontek G, Bekker-Ruz V, Timmer S, Rummeny EJ, Kiechle M and Beer AJ: Non-invasive tracking of human haemopoietic CD34(+) stem cells *in vivo* in immunodeficient mice by using magnetic resonance imaging. Eur Radiol *20*: 2184-2193, 2010.

21 Chen R, Yu H, Jia ZY, Yao QL and Teng GJ: Efficient nano iron particle-labeling and noninvasive MR imaging of mouse bone marrow-derived endothelial progenitor cells. Int J Nanomedicine *6*: 511-519, 2011.

22 Ma GS, Qi CM, Liu NF, Shen CX, Chen Z, Liu XJ, Hu YP, Zhang XL, Teng GJ, Ju SH, Ma M and Tang YL: Efficiently tracking of stem cells *in vivo* using different kinds of superparamagnetic iron oxide in swine with myocardial infarction. Chin Med J (Engl) *124*: 1199-1204, 2011.

23 Hu SL, Zhang JQ, Hu X, Hu R, Luo HS, Li F, Xia YZ, Li JT, Lin JK, Zhu G and Feng H: *In vitro* labeling of human umbilical cord mesenchymal stem cells with superparamagnetic iron oxide nanoparticles. J Cell Biochem *108*: 529-535, 2009.

24 Delalat B, Pourfathollah AA, Soleimani M, Mozdarani H, Ghaemi SR, Movassaghpour AA and Kaviani S: Isolation and *ex vivo* expansion of human umbilical cord blood-derived $CD34^+$ stem cells and their cotransplantation with or without mesenchymal stem cells. Hematology *14*: 125-132, 2009.

25 Arbab AS, Yocum GT, Wilson LB, Parwana A, Jordan EK, Kalish H and Frank JA: Comparison of transfection agents in forming complexes with ferumoxides, cell labeling efficiency, and cellular viability. Mol Imaging *3*: 24-32, 2004.

26 Gowing G and Svendsen CN: Stem Cell Transplantation for Motor Neuron Disease: Current Approaches and Future Perspectives. Neurotherapeutics *8(4)*: 591-606, 2011.

27 Lepore AC and Maragakis NJ: Stem cell transplantation for spinal cord neurodegeneration. Methods Mol Biol *793*: 479-493, 2011.

28 Bjorklund A: Cell therapy for Parkinson's disease: problems and prospects. Novartis Found Symp *265*: 174-186; discussion 187, 204-211, 2005.

29 Ende N, Weinstein F, Chen R and Ende M: Human umbilical cord blood effect on sod mice (amyotrophic lateral sclerosis). Life Sci *67*: 53-59, 2000.

30 Garbuzova-Davis S, Sanberg CD, Kuzmin-Nichols N, Willing AE, Gemma C, Bickford PC, Miller C, Rossi R and Sanberg PR: Human umbilical cord blood treatment in a mouse model of ALS: optimization of cell dose. PLoS One *3*: e2494, 2008.

31 Bulte JW, Duncan ID and Frank JA: *In vivo* magnetic resonance tracking of magnetically labeled cells after transplantation. J Cereb Blood Flow Metab *22*: 899-907, 2002.

32 Hoehn M, Kustermann E, Blunk J, Wiedermann D, Trapp T, Wecker S, Focking M, Arnold H, Hescheler J, Fleischmann BK, Schwindt W and Buhrle C: Monitoring of implanted stem cell migration *in vivo*: a highly resolved *in vivo* magnetic resonance imaging investigation of experimental stroke in rat. Proc Natl Acad Sci USA *99*: 16267-16272, 2002.

33 Ruhparwar A, Ghodsizad A, Niehaus M, Bara C, Lotz J, Voelkel T, Makoui M, Martin U, Wolf F, Gams E, Klein M and Haverich A: Clinically applicable 7-Tesla magnetic resonance visualization of transplanted human adult stem cells labeled with CliniMACS nanoparticles. Thorac Cardiovasc Surg *54*: 447-451, 2006.

34 Cao AH, Shi HJ, Zhang Y and Teng GJ: *In vivo* tracking of dual-labeled mesenchymal stem cells homing into the injured common carotid artery. Anat Rec (Hoboken) *292*: 1677-1683, 2009.

35 Dunning MD, Lakatos A, Loizou L, Kettunen M, ffrench-Constant C, Brindle KM and Franklin RJ: Superparamagnetic iron oxide-labeled Schwann cells and olfactory ensheathing cells can be traced *in vivo* by magnetic resonance imaging and retain functional properties after transplantation into the CNS. J Neurosci *24*: 9799-9810, 2004.

36 Liu W and Frank JA: Detection and quantification of magnetically labeled cells by cellular MRI. Eur J Radiol *70*: 258-264, 2009.

Received October 12, 2011
Revised November 14, 2011
Accepted November 15, 2011

4. Discussion

4.1. Structural and functional characterisation of HMGB1 and RAGE genes, proteins and associated cytokines

Two targets focussed in this thesis are the HMGB1 and RAGE genes and proteins. The structural characterisation of the canine HMGB1 and RAGE was carried out previously by Murua Escobar *et al*. in 2003 for *HMGB1* [24] and in 2006 for *RAGE* [25] showing for HMGB1 100 % protein identity to its human counterpart, whereas the comparison of the canine RAGE protein revealed a total of 77.6 % identity to the human RAGE. In detail, the comparison of the ligand-binding RAGE V-domain showed an identity of 85.7 %. The high similarity of the human and canine RAGE/HMGB1 complex allows the establishment of therapeutic approaches for the dog as animal model, which can also be used for translational oncology research in humans [24, 25].

HMGB1, initially known to be a nuclear protein, is also described to exert extracellular function acting mainly as a ligand for RAGE and the Toll-like receptors -2, -4, and -9 [58, 59, 100, 102]. Interaction of HMGB1 with RAGE is reported to play a crucial role in the pathogenesis of various diseases, immune responses, inflammation processes and cancer progression [118, 122, 127, 131, 150, 151, 163, 166, 170, 177, 232]. Besides the full-length RAGE, nearly 20 naturally occurring splicing variants of the receptor with either C-terminal or N-terminal truncations were identified [136-140, reviewed in 143]. The soluble C-terminal truncated RAGE forms are acting extracellular as decoy receptors for HMGB1 displacing the membrane located full-length protein [146], while the N-terminally truncated forms are not able to bind ligands without the Ig V-domain. In general, the diverse variants of RAGE are discussed to act as mechanisms for receptor regulation by competitive inhibition [reviewed in 148, 149].

As described in the results section, (see: 3.1., publication I), Sterenczak *et al*. (2009) [233] were able to describe 14 *RAGE* splice variants in different tissues and cancer cell lines, which were not yet discovered in any species. In addition, four new splice variants were detected in human cell lines. Two groups of *RAGE* isoforms were classified. The first group encoded for full-length or the soluble *RAGE*, the second group included N-terminally truncated proteins lacking the capacity to bind ligands. The coding sequences of the second group are recurrently characterised by

insertions of intron 1 resulting in protein variants which have lost their function as competitive inhibitor due to the missing V-domain, or the CDS encodes for a nonsense protein. A similar variant with an intron 1 insertion was identified in 2003 by Yonekura *et al*. [138] in human endothelial cells and pericytes showing that those types of variants are also present in human non-neoplastic tissues. The data generated by Sterenczak *et al*. confirm and complement the findings by Yonekura *et al*. providing information on the expression of intron 1 insertion variants and other *RAGE* isoforms in human neoplastic samples as well as in canine non-neoplastic tissues, tumour samples, and cancer cell lines.

Additionally, the expression ratio between the *RAGE* intron 1 variants and the ligand-binding *RAGE* transcripts was quantified in the study by Sterenczak *et al*. in the canine non-neoplastic tissue, tumour samples and the cell lines showing expression of both forms in all samples. In detail, the healthy tissues of lung, testis, and thyroid gland showed a higher amount of the ligand-binding transcripts compared to the *RAGE* intron 1 variants. In contrast, the majority of the examined tumour samples and tumour cell lines showed a greater quantity of N-terminally truncated *RAGE* intron 1 transcripts. The putative protein of this splice variant would result in a truncated transmembrane RAGE lacking the ligand-binding V-domain. The human intron 1 variant is discussed to be non-translated and considered to be targeted to nonsense-mediated decay (NMD), as it failed to produce an immunoreactive band in Western blot analyses [143, 147, 234]. This theory might also be valid for the canine intron 1 variants and needs to be confirmed on protein level. During the performed study in 2009, the detection of RAGE proteins in the dog was challenging due to the lack of specific antibodies. Recently, antibodies detecting specifically the canine RAGE [235] as well as an ELISA for quantification of canine sRAGE (Supplier: Shanghai BlueGene Biotech Co. Ltd.) are available, and offer new possibilities for characterisation of canine RAGE expression on protein level.

The exact biological role of the diverse soluble and membrane bound RAGE variants in humans and dogs remains still to be elucidated in detail. Recent studies reported that deregulations of the naturally occurring functional RAGE isoform are associated with RAGE mediated diseases in humans. Especially circulating soluble RAGE levels in human serum are in the current focus of RAGE research. Soluble RAGE was detected in human serum in a strong correlation with the pathologic state of various RAGE-related diseases [reviewed in 143, 148, 236, and 237].

In terms of cancer, the expression of endogenous sRAGE was firstly shown to be a suitable prognostic tumour marker for the classification of the malignancy of chondrosarcomas [238]. Other studies reported that soluble RAGE is inversely associated with human breast [239], lung [240], liver [241], pancreatic [242] and colon cancer [243] and may contribute to disease progression.

In general, RAGE splicing seems to be more complex than initially expected due to the presence of the wide range of structurally different RAGE splicing variants found in humans, rodents, as well as in dogs [233]. The findings of the present study contribute to understand the complexity in which deregulation or aberration of the splice variants play a role in the pathogenesis of RAGE-mediated diseases [233].

As previously described, deregulations of RAGE and HMGB1 were found in various human cancer types [reviewed in 165, 180], but HMGB1 and RAGE expression analyses in canine tissues and especially neoplasias are still rare [24, 25, 94].

As lymphoma is a commonly occurring neoplasia in dogs and resembles the human disease closely, during the work on this thesis the expression of HMGB1 and RAGE was analysed for potential deregulations in 23 canine lymphomas and control samples of healthy dogs. The analysis revealed a highly significant up-regulation of HMGB1 in all lymphoma samples in comparison to the samples of healthy dogs whereas the expression of RAGE was not significantly different in comparison to the controls [244] (see: results section 3.2., publication II). The findings concerning HMGB1 expression are consistent with the results generated in a previous study by Meyer *et al.* in which high HMGB1 levels in human NHL were reported [96]. In addition, high levels of HMGB1 in serum of lymphoma bearing dogs were detected [97].

Up to now, besides the herein presented study by Sterenczak *et al*. (2010) [244], RAGE expression analysis in lymphoma was only carried out in one study using multi-tumour tissue microarray (TMA) technology detecting merely a borderline positive staining against specific RAGE [181]. Although this result was not further discussed by the authors, it seems to be consistent with the findings by Sterenczak *et al*. indicating low levels of RAGE in lymphoma [244].

HMGB1 signalling is not solely mediated via RAGE, but also by binding to TLR receptors such as TLR-2 and TLR-4 [58, 59, 101]. Thus, TLRs should also be considered regarding lymphoma development and progression, especially in the context of tumour angiogenesis and the existent linking to the increased expression

of the vascular endothelial growth factor (VEGF) in lymphoma cells [180, 244-246]. The expression or overexpression of TLR receptors found in different tumour types underlines this assumption [247]. Genotyping of DNA from human lymphoma cases detected polymorphisms in the TLR-2 and TLR-4 genes which were hypothesised to increase the risk of follicular lymphoma and mucosa-associated lymphoid tissue lymphoma respectively [248]. Expression analyses revealed that TLR-2 is strongly expressed in human diffuse large B-cell lymphoma and peripheral T-cell lymphoma, whereas TLR-4 expression was only up-regulated in the latter one [249]. TLR-4 was also found to be overexpressed in mantle cell lymphoma [250]. The involvement of TLR receptors in the pathogenesis of lymphoma in dogs has not yet been examined and remains to be elucidated.

In conclusion, the overexpression of *HMGB1* in canine lymphoma strongly supports the assumption that similar mechanisms might be involved in the progression of the disease as they are existent in humans.

In terms of structural and functional basic research on the canine *HMGB1* and *RAGE* genes, the characterisation of canine cytokines being involved in the signal transduction of HMGB1-mediated effects is also fundamental for understanding the involvement in pathogenic processes.

HMGB1 in its cytokine function plays a major role in the induction of immune system reactions by activation of cells and initiation of inflammatory responses. Immune cells like monocytes, macrophages and DCs, but also other cell types, have been reported to secrete HMGB1 actively triggered by LPS or classical 'early' response proinflammatory cytokines such as TNF-α, IL-1β or IFN-γ [55, 72, 75, 82-85, 251, 252]. In turn, HMGB1 itself has the capacity to induce the cellular release of proinflammatory cytokines including TNF-α, IL-1α, IL-1β, IL-6, IL-8, IFN-γ and the chemokines MIP-1α (macrophage inflammatory protein), MIP-1β and MIP-2 [55, 58, 72, 253, 254].

Especially TNF-α, IL-1α and IL-1β are generally described play a pivotal role as potent multifunctional proinflammatory cytokines in signal transduction processes during host immune response and inflammation [255]. In dogs, the same key cytokines might also be involved in the initiation and regulation of inflammation and immunity responses [255]. To examine cell stimulatory effects of cytokines like the previously mentioned, approaches with those proteins need to be carried out. For cell stimulation experiments, mainly recombinant proteins are used. At the beginning of

this thesis, the availability of recombinant canine cytokines was poor in contrast to the recombinant human and murine analogues. Therefore, an *in silico* identity comparison of the canine *TNF-α, IL-1α* and *IL-1β* mRNAs to several presently known sequences of other mammalian species (human, canine, murine, rat, ovine, equine, feline, porcine, and bovine) was carried out by Soller *et al*. (2007) to identify potential cross-reactivity between species [255] (see: results section 3.1., publication III).
The analyses revealed a highly conserved homology for all analysed cytokines concerning their functional domains and sequence motifs amongst the mammalian species included in this study. In particular, the highest identities were found between dog and human on protein level, with TNF-α showing an especially high similarity index of 91 %. The properties of the analysed cytokines are of significant value for the development of *in vitro* and *in vivo* stimulatory experiments with canine cells and can also contribute to the establishment of preclinical therapeutic approaches. At present, canine recombinant TNF-α, IL-1α and IL-1β are commercially available, but still limited to purchase just at a small number of companies and quite expensive in contrast to the human and murine counterparts. Thus, especially the information concerning the high identity of canine and human TNF-α is valuable for conducting canine cell stimulation analyses with the same efficiency in large experimental setups and within standard cell differentiations as e.g. the *ex vivo* expansion of canine DCs from canine CD34+ haematopoietic stem cells (HSC), but with much lower expenses.

4.2. Improvement of in vitro transfection efficiencies using novel methods

Besides the proinflammatory and tumour progressing abilities, HMGB1 in its role as cytokine is also described to mediate immunomodulatory effects such as triggering immune responses and initiation of reparative processes [182-184, 256]. A delicate balance of HMGB1 seems herein to be the key for the mediation of beneficial to pathological effects [182, 184]. The advantageous immune system activating properties of HMGB1 may be used to establish novel therapeutic strategies in terms of cancer immunotherapy.
During this thesis, such an approach was followed within an interdisciplinary project. A vaccination strategy with recombinant HMGB1-secreting genetically engineered DCs for induction of enhanced host anti-tumour immune responses in the dog as model organism was aimed herein. As previously described, the highly efficient transfection of canine haematopoietic stem cells with *HMGB1* expression plasmids was a crucial point within this approach. Standard methods are coming to the limits at

distinct cell types like stem or primary cells resulting in unsatisfactory transfection efficiencies of cell toxicity. Consequently, new methods showing high efficiencies and reduced cell toxicity effects are needed for cells being difficult to transfect.

The principle of the femtosecond (fs)-laser based opto-perforation as alternative method for transfection offers distinct advantages. With this method the selective targeting of different types of single cells without addition of chemical reagents while maintaining high transfection efficiency and cell viability is possible. The fs-laser operates without contact, thus sterile conditions are present during the transfection procedure.

Firstly, the fs-laser transfection was described by Tirlapur *et al*. in 2002 [207], but reliable data concerning the efficiency and viability were just generated in the year 2006 by Stevenson *et al*. using Chinese hamster ovary (CHO) cells [208]. The average transfection efficiencies using a pEGFPN2 plasmid encoding for GFP were found to be 50 ± 10 % while the overall corrected cellular viability was 70 ± 8 % after transfection [208]. However, the optimum parameters in terms of cell viability after treatment, efficiency and reproducibility were not characterised in detail. Furthermore, the basic mechanism of the perforation process (lifetime of created pores, volume exchange during perforation) was not well understood at this time. Therefore, the study by Baumgart *et al*. (2008) investigated these issues [257] (see: results section 3.2., publication IV). Of main interest for the forthcoming of molecular therapeutic approaches such as followed within this thesis, is the successful transfection of cells with DNA expression plasmids. As proof of principle, canine MTH53A cells were transfected by Baumgart *et al.* with either non-recombinant pEGFP-C1 vector or a recombinant variant encoding for an EGFP-HMGB1 fusion protein for nucleus specific labelling. The fs-laser transfection parameters were optimised aiming at a good balance between viability and efficiency. With those parameters 30 % EGFP or EGFP-HMGB1 positive cells were detectable 48 hours after transfection. The localisation of the recombinant EGFP-HMGB1 in the nucleus of successfully transfected cells showed nicely, that the fs-laser opto-perforation does not impair the biofunctionality of the introduced DNA plasmids. These results demonstrate that the expression of more complex proteins than EGFP and specific targeting of the recombinant proteins to their final destination is possible with this method. The efficiencies gained with the newly established parameters were lower in comparison

to the results by Stevenson *et al*. [208], but with a higher viability rate of 90 % being significant for the subsequent transfection of more sensitive primary cell types.
The improvement of the fs-laser opto-perforation carried out by Baumgart *et al*. shows that a highly specific single cell targeting for transfection is possible [257]. However, the method is limited by its rather low throughput because the laser focus needs to be aligned by the operating person to every single cell.
In this context, different approaches targeting at the automation of this process to generate higher a throughput are currently ongoing. One promising approach based on the previous findings is the gold nanoparticle (AuNP)-mediated lasertransfection [258-264]. This method uses ultrashort laserpulses, which are not as strongly focussed as in the opto-perforation method. The transient permeabilisation of the cell membrane is attained by the plasmonic effects which occur due to the interaction of AuNPs and laser radiation [260]. This novel method allows a simultaneous high-throughput transfection of multiple adherent as well as floating cells [259, 260]. Currently, high perforation efficiencies can be achieved for introduction of small molecules such as fluorescent dyes and fluorescent dextranes with sizes of 10 to 2000 kDa into mammalian cells [260, 263, 264].
An alternative novel transfection method using AuNPs differing in terms of the fabrication technique to the particles used in the previously described AuNP-mediated laser transfection was also carried out within this thesis in collaboration with the Equine Clinic of the University of Veterinary Medicine Hannover. Herein, a new generation of positively charged AuNPs was used, which were generated by pulsed laser ablation in liquids (PLAL) without addition of any stabilising agents. PLAL-AuNPs were shown to easily attract biomolecules such as single stranded DNA oligonucleotides [265]. First data indicated that mammalian cells can be efficiently transfected with DNA expression vectors in the presence of different sizes of PLAL-AuNP without disturbing the bioactivity of the introduced DNA [216]. Although the transfection efficiency was improved by adding AuNP to standard transfection protocols and a biofunctionality of the transfected DNA was given, information about the toxic potential of these particles in combination with DNA expression plasmids were lacking [216]. Therefore, the transfection efficiencies and methodology-induced cytotoxic side effects of PLAL-AuNP-mediated transfection in comparison to other NP-mediated and conventional methods were analysed within this thesis in the collaborative publication of Durán and Willenbrock *et al.* (2011) [266]

(see: results section 3.2., publication V). The transfection efficiency of two DNA expression plasmids with different sizes (pIRES-hrGFP II-*rHMGB1*: 5531 bp; pIRES-hrGFP II-*eIL12*: 7709 bp) was significantly increased by the addition of the physically produced PLAL-AuNP in comparison to conventional protocols, while the AuNPs added did not interfere with the biosynthesis of the recombinant proteins. Variations in the efficiencies using the same transfection protocol with different expression vectors could be explained by the inverse correlation between the construct size and the cellular uptake of DNA [267-269]. Although the PLAL-AuNP protocols showed the highest transfection outcome, also slightly increased cytotoxic effects and reduction of cell proliferation were observed. To clarify if the observed cytotoxic effects are caused by intolerance to the used AuNPs or to the expression products of the transfected recombinant expression vector constructs, further studies with different cell lines and expression vectors should be performed.

In conclusion, the addition of PLAL-AuNP aiming at the improvement of the achievable transfection efficiency provides an interesting novel tool for DNA transfection approaches in general. Nevertheless, as stated before, considering the observed AuNP induced side effects, the attainable enhancement on transfection efficiency should critically be evaluated for the respective target cell type and vector construct.

4.3. Functional analysis of modified cells

Various types of cells including monocytes, activated macrophages, mature dendritic cells, and natural killer cells [55, 73, 74, 192] are capable to secrete HMGB1 actively, which in turn stimulates proinflammatory cytokine synthesis [62, 72]. In general, active HMGB1 release was shown to occur in a delayed manner ranging from 8 to 20 hours following most effective stimulation with LPS, TNF-α or IL-1β, [55, 62, 75].

To establish an immunotherapeutic approach on the immunostimulating beneficial effects of HMGB1, the functionality of recombinant HMGB1 expression vector constructs needs to be characterised after transfection of the targeted cell types. Further, a detailed analysis of the release kinetics of the desired recombinant HMGB1 protein from the genetically engineered cells in response to certain stimuli is essential in order to achieve a directed release of HMGB1 at the targeted destination. The functionality of two bicistronic *HMGB1* expression vector construct variants was therefore verified by transfection of the canine mammary epithelial cell line MTH53A within this thesis by Willenbrock *et al*. (2012b) (see: results section 3.3., publication

VI) [270]. In the following, the HMGB1 secretion potential and the release kinetics of transfected recombinant HMGB1 expressing canine mammary cells were assessed after stimulation with TNF-α or IFN-γ by Western blot and quantified with an HMGB1 ELISA. The biofunctionality of both bicistronic vectors was successfully demonstrated by fluorescence microscopy and Western blotting resulting in the expression of hrGFP and recombinant HMGB1. These results were essential for the subsequent cytokine stimulation experiments with TNF-α or IFN-γ. Unstimulated transfected MTH53A cells were shown not to secrete HMGB1 spontaneously, whereas a clearly time-dependent release kinetic of recombinant HMGB1 into the cell culture medium could be demonstrated upon stimulation with TNF-α. The peak release was observed after 24 hours. A shorter stimulation time of 6 hours seems to be insufficient for an effective induction of active HMGB1 secretion from MTH53A cells. In comparison to the 24 hour TNF-α stimulation results, a slightly reduced level of HMGB1 was detectable after 48 hours which indicates that an extended stimulation with TNF-α does not induce an increased HMGB1 secretion. The reduction of extracellular HMGB1 after 48 hours might be explained by proteolytic degradation. HMGB1 was shown to be rapidly degraded by plasmin due to its lysine-rich structure [271] and plasmin is known to be present in mammary epithelial cells [272]. Thus, this theory might also be applied to the mammary epithelial cell line MTH53A.

The stimulation with IFN-γ showed to have only small effects on HMGB1 secretion after 24 hours with a slight increase after 48 hours. A study by Rendon-Mitchell *et al*. showed similar results in which peak levels of HMGB1 were observed after 32 hours in the culture medium of macrophage cultures after IFN-γ application. The reduced efficiency of IFN-γ to induce HMGB1 release may be explained by the partial regulation of IFN-γ through a TNF-α dependent mechanism [251].

To confirm that the induced HMGB1 release was specific and not due to cell death, cell viability staining was performed at which no increase of dead cells was detectable after cytokine stimulation in comparison to untreated controls. By the cell viability staining a necrotic or apoptotic effect caused by excessive levels of extracellular HMGB1 was also excluded.

In conclusion, the findings gained within this study show that mammalian cells transfected with *HMGB1* expression vectors can be stimulated with TNF-α in a time-dependent manner to actively release recombinant HMGB1 [270]. Further, the HMGB1 release kinetics are in agreement with previous reports which signify that

HMGB1 is secreted at highest levels after 18-24 hours of TNF-α stimulation [55, 75, 84]. This delayed HMGB1 release opens a time window of approx. 24 hours leaving an extended scope for the implementation of immunotherapeutic approaches using e.g. HMGB1 transfected DCs such as targeted within the CRC / TR37. The release kinetics of HMGB1 from such genetically engineered DCs need to be carefully characterised as well. HMGB1 is known to mediate its proinflammatory effect by activating the release of 'early' cytokines [55, 72, 253]. Thus, the release profile of those cytokines also needs to be focussed in immunotherapeutic approaches. Recently, this can be easily performed for dogs as well due to the availability of the 'MILLIPLEX MAP Canine Cytokine / Chemokine Magnetic Bead Panel' (EMD Millipore Corp., Billerica, MA, USA) detecting 13 different key cytokines simultaneously in one sample based on the Luminex® xMAP® platform (Luminex Corporation, Austin, TX, USA). Another point, which may be drawn closer into consideration, is the fact that HMGB1 underlies posttranslational modifications like e.g. the oxidative state of HMGB1 that modulates its activity [69]. It is necessary to be investigated if recombinant HMGB1 expressing cells are capable to secrete the recombinant protein in the proinflammatory acting reduced form, or if it is possible that the cells release oxidised HMGB1 which was described to be rather tolerogenic [69].

Besides cytokines, other effector molecules such as synthetic oligodeoxynucleotides containing the cytosine-phosphate-guanine (CpG) motif (CpG-ODN) provide the opportunity to stimulate cellular responses in a number of different mammals [273]. By binding to TLR-9 [109], CpGs have been shown to trigger strong immune system responses by direct stimulation of B-cells [274-276], induction of maturation and differentiation of DCs [277], NK cell toxicity [278], and secretion of proinflammatory cytokines [279]. Owing to the described immunomodulatory effects, CpG-ODN may be useful as non-specific immune system stimulating adjuvant serving as a therapeutic tool for tumour therapy, or in the modulation of allergic and infective responses [273]. The stimulative effect of particular CpG-ODNs can also be used for enhancing the mitotic activity of B-cells. For instance, the CpG-ODN DSP30 in combination with IL-2 has been reported to be an easy and efficient mitotic stimulus allowing e.g. to detect clonal abnormalities in human chronic lymphatic leukaemia (CLL) and B-cell lymphoid neoplasms [280-282].

Based on this information, within the study of Reimann-Berg *et al.* (2011) stimulation with the CpG-ODN DSP30 in combination IL-2 was used to achieve a higher mitotic rate in usually slowly growing canine lymphoid cell cultures (see: results section 3.3., publication VII) [283]. The stimulation showed that the human CpG-ODN DSP30 in combination with IL-2 also induces proliferative responses of canine lymphoid cell cultures by the generation of an adequate number of metaphases. The cytogenetic analyses revealed a monosomy of the X chromosome in all analysed metaphases. This clonal chromosome abnormality is also present in human malignancies [284, 285]. Thus, the haematopoietic disorders in dogs may help to understand the significance of such chromosomal abnormalities in humans.

In general, the CpG-ODN sequence motifs are considered to vary among mammalian species for induction of cellular responses [286, 287]. For example, DSP30 was reported to be poor in activating murine immune cells (Bauer 1999), but seems to be effective in dogs as demonstrated by Reimann-Berg *et al*. [283]. So far, the research concerning the identification of effective canine CpGs is still rare. Merely some human CpG-ODN sequences were reported to induce lymphocyte proliferation of canine spleen and lymph node cells in contrast to a control GpC ODN [273], and a specific CpG-ODN was identified to induce Th1 cytokines in canine PBMCs [286]. In conclusion, the potential application of CpG-ODN, for example as adjuvant immunotherapy, may also be valuable in veterinary medicine and for translational research in humans, but the specific identification of effective CpG-ODNs in canines is necessary [286].

4.4. In vivo imaging of cells

To implement cancer immunotherapeutic approaches using unmodified or modified cells such as gene-modified DCs to enhance immune responses, not only the functional analysis of the cells before implantation, but also the *in vivo* migration behaviour of the transplanted cells and their homing to the desired destination in the organism needs to be clarified. Therefore, well-tolerated, reliable techniques for non-invasive *in vivo* tracking over long time periods are needed. As previously mentioned, two different strategies for specific *in vivo* detection were followed during the work on this thesis in collaborative work packages contributing to the development of a cancer vaccine approach.

The first strategy followed the utilisation of highly specific antibodies for targeting canine DCs *in vivo*. Due to the fact that the availability of such antibodies is limited in

dogs, recombinant single-chain variable fragment (scFV) antibodies specifically binding to canine DCs were successfully isolated by phage display technology within the study by Fitting *et al*. (2011) (see: results section 3.4., publication VIII) [288]. These antibodies provide a basis for the development of new techniques for immunological detection, characterisation and quantification of canine DCs due to the fact that present technologies for the non-invasive monitoring of DCs *in vivo* are limited [288, reviewed in 289]. The localisation and function of immune cells at the desired destination are up to now prevalently determined by classical non-invasive radioactive labelled scintigraphic imaging [198]. Other invasive methods such as biopsies and *ex vivo* cell functionality analysis allow only one 'snap shot' per time and location, but lacking to adequately reflect the distribution of the implanted cells in all physical dimensions [reviewed in 289, and 290]. In contrast, the non-invasive *in vivo* visualisation of cell migration would allow monitoring the therapy efficacy directly. Besides the classical imaging techniques, various novel *in vivo* imaging approaches with minimal toxicities are presently developed and improved, such as optical fluorescence and bioluminescence imaging or MRI [289]. Prospectively, the use of specific antibodies such as isolated by Fitting *et al*. [288], coupled e.g. with fluorescent dyes or near-infrared (NIR; 700-900 nm) fluorescent semiconductor quantum dots (QD), might be used for effective labelling of DCs *in vivo* by systemic administration at the desired time points. QD are recently discussed as an alternative to organic fluorescent dyes to be useful for long-term tracking of live cells *in vitro* due to their bright fluorescence, narrow emission, broad ultraviolet (UV) excitation, and high photostability [291-294]. However, QD with a cadmium selenide (CdSe) core were found to be significantly cytotoxic under certain conditions. The cytotoxic effect is caused by the release of free cadmium-ions from the QD cores during long-time UV light exposure in primary hepatocytes [294]. Therefore, the toxic potential of QD in *in vivo* applications must be critically evaluated. Nevertheless, tracking of tumour cells in mice using QD-conjugated specific antibodies against cancer biomarkers was successful, but *in vivo* imaging with QD cannot be scaled up directly to larger organisms due to limited optical signal penetration depth [reviewed in 295]. In this context, first encouraging results concerning the detection and diagnosis in patients with breast cancer using non-invasive NIR optical imaging devices instead of UV light were shown [reviewed in 295, and 296, 297].

The second *in vivo* imaging strategy is based upon unspecific cell-labelling with biocompatible superparamagnetic iron oxide (SPIO) nanoparticles and detection via MRI. Within this study, the feasibility of SPIO-labelling of MTH53A cells as proof of principle and of CD34+ human umbilical cord blood stem cells (hUCBCs) and their subsequent *in vitro* and *in vivo* MRI detection was assessed by Willenbrock *et al*. (2012a). The study revealed that the *in vitro* MRI detection limit at 1.0 T field strength was higher for SPIO-labelled MTH53A cells than for hUCBCs (see: results section 3.4., publication IX) [298]. This might be explained by a larger cell surface size of MTH53A cells leading to a higher possibility of SPIO-uptake by MTH53A cells in comparison to hUCBCs. When comparing the 1.0 and 7.0 T *in vitro* data, a four-fold smaller number of labelled MTH53A cells was detectable at 7.0 T. This indicates that the filed strength seems to be not directly inversely proportional to the detectable cell number. The *in vivo* data showed a clear signal for 100,000 SPIO-labelled implanted hUCBCs, while at day four after transplantation into the spinal cord a signal with the same intensity, but no cell migration could be observed. Possibly, the duration time of four days for *in vivo* imaging was not sufficient to monitor migration of cells. Thus, a longer time period of e.g. two to four weeks as reported in similar studies might be adequate [299, 300]. Additionally, stimulation of hUCBCs with factors improving cell migration such as G-CSF (granulocyte colony-stimulating factor) [301-303], AMD3100 [303], CXCL12 (Chemokine (C-X-C motif) ligand 12) [304] or HMGB1 [66, 305] might also improve cell migration along the spinal cord.

In general, the dependency of the cell detection limit in correlation to the MR field strength is a limitation within this study. The visualisation at single-cell level is presently not possible by 7.0 T MRI in combination with SPIOs. However, due to the fact that cellular therapy in animal models and humans requires the administration of large cell numbers, the detection limit does not represent a problem within this context. The present study was actually carried out to establish a non-invasive modality for *in vivo* imaging of intraspinally injected hUCBCs in a transgenic ALS mouse model which mimics the human neurodegenerative disease in large parts. Nevertheless, the generated data can also be transferred to other settings such as cell-based cancer immunotherapeutic approaches, where *in vivo* monitoring of implanted cells is indispensable. In this context, tracking of SPIO-labelled DCs via MRI was reported to be realisable [226-231, 306-309], but there is more room for

further improvement due to the present availability of novel, more powerful magnetic iron oxide nanoparticles and MR scanners with increased field strengths.

In conclusion, MRI as a clinical standard technique in combination with the commercially FDA-approved SPIO-contrast agent ENDOREM® provides valuable potential for non-toxic, non-invasive *in vivo* tracking of implanted cells in the murine model system. These data provide a basis to the future development of valuable *in vivo* cell monitoring tools for clinical trials assessing the benefit of cell transplantation human and veterinary medicine as well.

In summary, within this thesis basic research on canine HMGB1, RAGE and associated cytokines revealed conserved molecular homologies and compareable expression patterns as seen in humans. This underlines the postulated high similarty of the involved tumour mechanisms allowing thereby a comparable prediction of responses to therapeutic agents in dogs and humans. In addition, the herein presented collaborative interdisciplinary work allowed the establishment of innovative methodical approaches contributing to the development of translational therapeutic strategies targeting at neoplasias in dogs as patients, whilst also offering benefit for human medicine.

5. Summary

Cancer is a leading cause of death worldwide although extensive research in human cancer medicine is carried out. To develop and improve anticancer therapies, the mechanisms involved in the genesis and metastasis of tumours need to be elucidated. Herein, also the characterisation of the structure and function of cancer related genes and proteins is essential. In terms of cancer, the dog is one of the companion animals being considered as an invaluable model system in addition to the popular rodent model. Several canine neoplasias have been described to share striking similarities with humans and therefore are assumed to represent appropriate models for the corresponding human diseases. The spontaneous development of tumours in the context of an intact immune system in dogs offers new prospects for cancer immunotherapy in contrast to immunocompromised rodent models. Thus, basic research on tumour-associated genes provides valuable information for analysis of the comparative tumour biology between humans and dogs, and for the transferability of therapeutic approaches.

Within this thesis, the molecular structure and function of the cancer-related genes and proteins HMGB1, RAGE, IL-1α, IL-1β, and TNF-α were analysed. The characterisation of human and canine RAGE splicing variants revealed highly conserved molecular similarities in both species. An expression analysis of *HMGB1* and *RAGE* in canine lymphoma showed similar expression patterns as observed in humans. An *in silico* analysis of the canine cytokines IL-1α, IL-1β, and TNF-α also identified conserved sequence homologies in comparison to other mammals.

Besides basic research on cancer-related genes, parts of this thesis were conducted to support the development of a cell-based cancer immunotherapy vaccination strategy with genetically engineered recombinant HMGB1-secreting canine DCs in dogs. Within this project, opto-perforation using a femtosecond-laser for selective transfection was developed being also applicable for sensitive cell types. Additionally, another transfection method was established based on the application of a new type of laser-generated positively charged gold nanoparticles showing good efficiencies in a mammalian cell line. Furthermore, the functionality of different *HMGB1* vectors and expression of the respective recombinant proteins were analysed. Subsequently, the time-dependent secretion of recombinant HMGB1 from generally HMGB1-non-secreting mammary epithelial cells was induced by TNF-α stimulation. In the context

of cell stimulation, the potential of a CpG-ODN combined with IL-2 was investigated on canine B-cell lymphoma cells revealing an increased proliferative response.
To monitor the fate of transplanted cells such as DC-vaccines non-invasively *in vivo*, more safely methods in comparison to the commonly used standard techniques are needed. Thus, the last part of this thesis presents the generation of antibody fragments targeting specifically canine DCs and improved cell tracking of SPIO-labelled cells via MRI, which can be used alternatively to follow cells *in vivo*.
In summary, within this thesis the different fields of research allowed to establish innovative methods contributing to the development of therapeutic approaches targeting at neoplasias in dogs as patients, but also providing benefit for human medicine in terms of the dog as model organism.

6. Zusammenfassung

Tumorerkrankungen sind weltweit eine der häufigsten Todesursachen. Daher wird intensive wissenschaftliche und klinische Forschung zur Entwicklung von Therapien betrieben. Um tumortherapeutische Ansätze entwickeln und verbessern zu können, müssen grundlegende Mechanismen aufgeklärt werden, die an der Entstehung und Metastasierung von Tumoren beteiligt sind. Hierbei spielt unter anderem die Charakterisierung der Struktur und Funktion von Genen sowie Proteinen eine wesentliche Rolle, die mit der Entstehung von Tumoren in Verbindung gebracht werden. Neben den klassischen Nagermodellen hat der Hund ein besonderes Interesse als Modelltier in der Humanmedizin erlangt, da viele canine Neoplasien auffallende Ähnlichkeiten zu denen des Menschen besitzen. Dabei bietet die spontane Entstehung von Tumoren in der Umgebung eines intakten Immunsystems bei Hunden neue Perspektiven für die Tumorimmuntherapie im Vergleich zu Nagermodellen, wobei vornehmlich immunsupprimierte Tiere verwendet werden. Somit liefert die Grundlagenforschung an tumorassoziierten Genen wertvolle Informationen zur Untersuchung der vergleichenden Tumorbiologie von Mensch und Hund und zur Übertragbarkeit von Therapieansätzen.

Im Rahmen dieser Promotionsarbeit wurden die molekulare Struktur und Funktion der tumorassoziierten HMGB1, RAGE, IL-1α, IL-1β und TNF-α Gene und Proteine des Hundes analysiert. Die Charakterisierung von humanen und caninen *RAGE* Spleißvarianten zeigte hochkonservierte molekulare Homologien in beiden Spezies. Die Analyse der Expression von *HMGB1* und *RAGE* in caninen Lymphomen ließ ähnliche Expressionsmuster wie beim Menschen erkennen. Weiterhin wurden *in silico* Analysen an den caninen Zytokinen IL-1α, IL-1β und TNF-α durchgeführt. Es zeigten sich hierbei stark konservierte Sequenzhomologien im Vergleich zu anderen Säugetieren.

Neben der Erforschung grundlegender Genfunktionen trugen Teile dieser Arbeit zur Entwicklung einer genetisch modifizierten HMGB1-sezernierenden caninen DC-Vakzine zur Tumorimmuntherapie bei Hunden bei. Im Rahmen dieses Projektes wurde die neuartige Methode der Optoperforation mit einem Femtosekundenlaser zur selektiven Transfektion entwickelt, welche sich aufgrund der rein physikalischen Durchführung auch für sensitive Zelltypen eignet. Zusätzlich wurde ein weiteres Transfektionsverfahren etabliert, welches auf der Anwendung neuartiger

lasergenerierter Goldnanopartikel basiert und hohe Effizienzen in einer Säugerzelllinie zeigte. Weiterhin wurden die Funktionalität unterschiedlicher HMGB1-Vektoren und die Expression der jeweiligen rekombinanten Proteine analysiert. Anschließend wurde die zeitabhängige Sezernierung von rekombinantem HMGB1 aus einer caninen Mammaepithel-Zelllinie durch TNF-α Stimulation induziert. Ferner wurden canine primäre Lymphomzellen durch Applikation eines CpG-ODN in Kombination mit IL-2 zu einer erhöhten proliferativen Antwort angeregt.

Um das Verbleiben von transplantierten Zellen wie z.B. DC-Vakzinen *in vivo* mit nicht-invasiven Methoden zu untersuchen, wird intensiv an sichereren und sensitiveren Nachweisverfahren gearbeitet. In diesem Zusammenhang wurde im letzten Teil dieser Arbeit an der Generierung hochspezifischer Antikörperfragmente zur Detektion von caninen DCs gearbeitet. Weiterhin wurde die *in vivo* Migrationsdetektion von SPIO-markierten Zellen mittels MRT verbessert.

Die im Rahmen dieser Arbeit erzielten Ergebnisse tragen einerseits dazu bei, innovative Ansätze zur Tumortherapie bei Hunden in der Veterinärmedizin zu etablieren. Andererseits können die gewonnenen Erkenntnisse aufgrund der hohen Ähnlichkeit von Neoplasien bei Mensch und Hund einen wertvollen Beitrag zur Entwicklung vorklinischer Studien in der Humanmedizin liefern.

7. Selected list of publications

7.1. Peer-Reviewed papers

Durán MC, Willenbrock S, Müller JMV, Nolte I, Feige K, Murua Escobar H: *Establishment and evaluation of a bead-based Luminex assay allowing simultaneous quantification of equine IL-12 and IFN-alpha*. Anticancer research, submitted (2013).

Durán MC, Willenbrock S, Carlson R, Feige K, Nolte I, Murua Escobar H: *Enhanced protocol for CD14+ cell enrichment from equine peripheral blood via anti human CD14 mAb and automated magnetic activated cell sorting.* Equine Veterinary Journal 2012, Ms. No. EVJ-SC-12-002, accepted for publication.

Sterenczak KA, Meier M, Glage S, Meyer M, Willenbrock S, Wefstaedt P, Dorsch M, Bullerdiek J, Murua Escobar H, Hedrich H, Nolte I: *Longitudinal MRI contrast enhanced monitoring of early tumour development with manganese chloride (MnCl2) and superparamagnetic iron oxide nanoparticles (SPIOs) in a CT1258 based in vivo model of prostate cancer*. BMC cancer 2012, 12:284.

Rütgen BC*, Willenbrock S*, Reimann-Berg N, Walter I, Fuchs-Baumgartinger A, Wagner S, Kovacic B, Essler SE, Schwendenwein I, Nolte I, Saalmüller A, Murua Escobar H: *Authentication of primordial characteristics of the CLBL-1 cell line prove the integrity of a canine B-cell lymphoma in a murine in vivo model.* PLoSOne 2012, 7(6). *equally contributed authorship

Willenbrock S, Braun O, Baumgart J, Lange S, Junghanss C, Heisterkamp A, Nolte I, Bullerdiek J, Murua Escobar H: *TNF-alpha induced secretion of HMGB1 from non-immune canine mammary epithelial cells (MTH53A)*. Cytokine 2012b, 57(2):210-20.

Willenbrock S, Knippenberg S, Meier M, Hass R, Wefstaedt P, Nolte I, Murua Escobar H, Petri S: *In vivo MRI of intraspinally injected SPIO-labelled human CD34+ cells in a transgenic mouse model of ALS*. IN VIVO 2012a, 26(1):31-8.

*Durán MC, *Willenbrock S, Barchanski A, Muller JM, Maiolini A, Soller JT, Barcikowski S, Nolte I, Feige K, Murua Escobar H, authorship ec: *Comparison of nanoparticle-mediated transfection methods for DNA expression plasmids: efficiency and cytotoxicity*. Journal of nanobiotechnology 2011, 9:47. *equally contributed authorship.

Fitting J, Killian D, Junghanss C, Willenbrock S, Murua Escobar H, Lange S, Nolte I, Barth S, Tur MK: *Generation of recombinant antibody fragments that target canine dendritic cells by phage display technology*. Veterinary and comparative oncology 2011, 9(3):183-95.

Reimann-Berg N, Murua Escobar H, Kiefer Y, Mischke R, Willenbrock S, Eberle N, Nolte I, Bullerdiek J: *Cytogenetic analysis of CpG-oligonucleotide DSP30 plus Interleukin-2-Stimulated canine B-Cell lymphoma cells reveals the loss of one X Chromosome as the sole abnormality*. Cytogenetic and genome research 2011, 135(1):79-82.

Reimann-Berg N, Willenbrock S, Murua Escobar H, Eberle N, Gerhauser I, Mischke R, Bullerdiek J, Nolte I: *Two new cases of polysomy 13 in canine prostate cancer*. Cytogenetic and genome research 2010, 132(1-2):16-21.

Sterenczak KA, Joetzke AE, Willenbrock S, Eberle N, Lange S, Junghanss C, Nolte I, Bullerdiek J, Simon D, Murua Escobar H: *High-mobility group B1 (HMGB1) and receptor for advanced glycation end-products (RAGE) expression in canine lymphoma*. Anticancer research 2010, 30(12):5043-8.

Sterenczak KA, Willenbrock S, Barann M, Klemke M, Soller JT, Eberle N, Nolte I, Bullerdiek J, Murua Escobar H: *Cloning, characterisation, and comparative quantitative expression analyses of receptor for advanced glycation end products (RAGE) transcript forms*. Gene 2009, 434(1-2):35-42.

Fork MA, Murua Escobar H, Soller JT, Sterenczak KA, Willenbrock S, Winkler S, Dorsch M, Reimann-Berg N, Hedrich HJ, Bullerdiek J, Nolte I: *Establishing an in vivo model of canine prostate carcinoma using the new cell line CT1258*. BMC cancer 2008, 8:240.

Beuing C, Soller JT, Muth M, Wagner S, Dolf G, Schelling C, Richter A, Willenbrock S, Reimann-Berg N, Winkler S, Nolte I, Bullerdiek J, Murua Escobar H: *Genomic characterisation, chromosomal assignment and in vivo localisation of the canine high mobility group A1 (HMGA1) gene*. BMC genetics 2008, 9:49.

Baumgart J, Bintig W, Ngezahayo A, Willenbrock S, Murua Escobar H, Ertmer W, Lubatschowski H, Heisterkamp A: *Quantified femtosecond laser based opto perforation of living GFSHR-17 and MTH53 a cells*. Optics express 2008, 16(5):3021-31.

Soller JT, Murua-Escobar H, Willenbrock S, Janssen M, Eberle N, Bullerdiek J, Nolte I: *Comparison of the human and canine cytokines IL-1(alpha/beta) and TNF-alpha to orthologous other mammalians*. J Hered 2007, 98(5):485-90.

7.2. Published abstracts

7.2.1. Oral presentations

16th ECVIM-CA Congress. The European College of Veterinary Internal Medicine - Companion Animals. 14. - 16.09.2006, Amsterdam, Netherlands. Murua Escobar H, Soller JT, Willenbrock S, Sterenczak S, Sperveslage JD, Schlüter C, Winkler S, Bullerdiek J, Nolte I. *Recombinant Tools to Block the CANINE HMGB1-RAGE Complex*. In: Conference Proceedings of the 16th ECVIM-CA Congress, p. 194, No 183.
This presentation was given on behalf of PD Dr. Murua Escobar.

European Life Scientist Organisation Conference (ELSO). 03.09.2007, Dresden, Germany. Rowiak GmbH Workshop 'Nanodissection using ultrashort laserpulses'.
Willenbrock S: *HMG Protein induced effects and possible applications*.
This presentation was given on behalf of PD Dr. Murua Escobar.

18. Jahrestagung der FG „Innere Medizin und klinische Labordiagnostik" der DVG (InnLab). 06.-07.02.2010, Hannover, Germany. Willenbrock S, Braun O, Lange S, Junghanss C, Nolte I, Bullerdiek J, Murua Escobar H. *Cytokine-stimulated release of high mobility group box 1 (HMGB1) protein in a mammary cell line of epithelial origin.*

European Society of Veterinary Oncology (ESVONC) Annual Congress 2011. 23.03. - 27.03.2011, Glasgow, Scotland, UK. Willenbrock S, Knippenberg S, Petri S, Nolte I, Murua Escobar H. *Nanoparticle-based labelling of canine cells for in vivo detection.* In: Proceedings of the European Society of Veterinary Oncology 2011.

2nd World Veterinary Cancer Congress (WVCC). 01.03. – 03.03.2012, Paris, France. Willenbrock S, Reimann-Berg N, Eberle N, Bullerdiek J, Nolte I, Murua Escobar H. *Establishment of a new canine prostate carcinoma cell line with complex karyotype changes involving polysomy 13.* In: Proceedings of the 2nd WVCC 2012, p. 44.

Veterinary Cancer Society Annual Conference. 18.10. - 21.10. 2012, Las Vegas, Nevada, USA. Willenbrock S, Rütgen BC, Reimann-Berg N, Wagner S, Kovacic B, Essler SE, Schwendenwein I, Nolte I, Saalmüller A, Murua Escobar H. *Chromosomal stability and proliferative response of a canine B cell lymphoma cell line after inoculation in a murine in vivo model.* In: Proceedings of the Veterinary Cancer Society 2012, p. 94.

7.2.2. Poster presentations

25th American College of Veterinary Internal Medicine Conference (ACVIM). 05.06. - 09.06.2007, Seattle, USA. Willenbrock S, Murua Escobar H, Soller JT, Sterenczak KA, Winkler S, Bullerdiek J, Nolte I. *Construction of a soluble RAGE variant for competitive blocking of the canine HMGB1-RAGE complex*. In: Proceedings: American College of Veterinary Internal Medicine Conference 2007, p. 814, No. 176.

4th International Conference: Advances in canine and feline genomics and inherited diseases. 21.05. - 25.05.2008, Saint Malo, France. Reimann-Berg N, Murua Escobar H, Bullerdiek J, Nolte I. *Klinefelter Syndrome in a dog with a testicular Tumor.* In: Program and Abstract Book: 4th International Conference: Advances in canine and feline genomics and inherited diseases, p. 121, No. 53.
This poster was presented in on behalf of Dr. Reimann-Berg.

Veterinary Cancer Society Annual Conference. 29.10. - 1.11. 2010, San Diego, California, USA. Willenbrock S, Braun O, Lange S, Junghanss C, Bullerdiek J, Nolte I, Murua Escobar H: *Cytokine-stimulated Release of HIGH Mobility Group Box 1 (HMGB1) Protein in a Canine Non-Neoplastic Mammary Cell Line.* In: Proceedings of the Veterinary Cancer Society 2010, p. 171.

8. Abbreviations

aa	Amino acid(s)
Acc. No.	Accession number
AGEs	Advanced glycation end products
ALS	Amyotrophic lateral sclerosis
AMD3100	CXCR4 antagonist; syn. Plerixafor
APC	Antigen presenting cell
AuNP	Gold nanoparticle
bp	Base pair(s)
BrdU	5-bromo-2-deoxyuridine
CD	Cluster of differentiation
cDNA	DNA complementary to RNA
CDS	Coding sequence(s)
CdSe	Ccadmium selenide
CFA	*Canis familiaris*
CGH	Comparative genomic hybridisation
CHO cells	Chinese hamster ovary cells
CLL	Chronic lymphatic leukaemia
cm	Centimetre
CNA	Copy number aberrations
CpG	Short single-stranded synthetic DNA molecules with cytosine-phosphodiester-guanine sequence motifs
CRC	Collaborate research cluster
C-terminal	Carboxy-terminal
Cys	Cysteine
CXCL12	Chemokine (C-X-C motif) ligand 12; syn. SDF-1 (stromal cell derived factor-1)
DAB	3.3'-diaminobenzidine
DAPI	4'-6-diamidino-2-phenylindole
DC	Dendritic cell
DFG	Deutsche Forschungsgemeinschaft / German Research Foundation
DNA	Deoxyribonucleic acid

DSP30	A specific CpG-ODN
E. coli	*Escherichia coli*
ED	Extracellular domain
ELISA	Enzyme linked immunosorbent assay
FA	Flip angle
FCS	Fetal calf serum
FDA	Food and Drug Administration
FHD	FuGENE® HD; transfection reagent
FoV	Field of view
fs	Femtosecond
G-CSF	Granulocyte colony-stimulating factor
GFP	Green fluorescent protein
EGFP	Enhanced green fluorescent protein
hrGFP	Humanized renilla green fluorescent protein
GUSB	Beta-glucuronidase
h	Hours
HMG	High mobility group
HMGB1	High mobility group protein B1
rHMGB1	Recombinant HMGB1
eHMGB1	Endogenous HMGB1
HRP	Horseradish peroxidase
HSC	Haematopoietic stem cells
hUCBCs	Human umbilical cord blood stem cells
IFN-γ	Interferone gamma
IgG	Immunoglobulin G
IL	Interleukin
IL-12	Interleukin-12
IL-1α	Interleukin-1alpha
IL-1β	Interleukin-1beta
IL-2	Interleukin-2
IL-6	Interleukin-6
IRES	Internal ribosomal entry site
kDa	Kilo Dalton
Laser	Light Amplification by Stimulated Emission of Radiation

LPS	Lipopolysaccharides
LZH	Laser Zentrum Hannover e.V.
MAP kinase	Mitogen activated protein kinase
MATra	Magnet-assisted transfection
mg	Milligram
MGE	Multi-gradient echo
min	Minute
MIP	Macrophage inflammatory protein
ml	Millilitre
µl	Microlitre
µm	Micrometre
mM	Millimolar
MRI	Magnet resonance imaging
mRNA	Messenger ribonucleic acid
mW	Milliwatt
NCBI	National Center for Biotechnology Information
NFκB	Nuclear factor-kappa B
ng	Nanogram
NHL	Non-Hodgkin's lymphoma
NIR	Near-infrared
nJ	Nanojoule
nm	Nanometre
NMD	Nonsense-mediated decay
NP	Nanoparticle
N-terminal	Amino-terminal
ODN	Oligodeoxynucleotides
P	p-value
PAGE	Polyacrylamide gel electrophoresis
PBMC	Peripheral blood mononuclear cell
PBS	Phosphate buffered saline
PCR	Polymerase chain reaction
PE	Phycoerythrin
pEGFP-C1	Plasmid encoding enhanced green fluorescent protein
pg	Picogram

PI	Propidium iodide
PLAL	Pulsed laser ablation in liquids
pRb	Retinoblastoma protein
PVDF	Polyvinylidene difluorid
QD	Quantum dots
RAGE	Receptor for advanced glycation end products
RNA	Ribonucleic acid
RPM	Revolutions per minute
scFV	Single-chain variable fragment
SDS	Sodium dodecyl sulphate
SNP	Single nucleotid polymorphism
SOD1	Superoxide dismutase 1
SPIO	Superparamagnetic iron oxide
sRAGE	Soluble RAGE variant(s)
T	Tesla
TE	Echo time
TLR	Toll-like receptor
TMA	Tissue microarray
TM	Transmembrane domain
TNF-α	Tumour necrosis factor-alpha
TR	Repetition time
TR37	Transregio 37
TREM-1	Rriggering receptor expressed on myeloid cells-1
U	Unit
UV	Ultraviolet
WHO	World Health Organization

9. References

[1] Ferlay J, Shin HR, Bray F, Forman D, Mathers C, Parkin DM: *Estimates of worldwide burden of cancer in 2008: GLOBOCAN 2008*. Int J Cancer 2008, 127(12):2893-917.

[2] Ott JJ, Ullrich A, Mascarenhas M, Stevens GA: *Global cancer incidence and mortality caused by behavior and infection*. Journal of public health (Oxford, England) 2010, 33(2):223-33.

[3] Khleif SN, Curt GA: *Animal Models in Developmental Therapeutics*. In: *Cancer Medicine (5th ed).* Edited by JF H, E F, RC B, DW K, R P, RR W, (Eds.), 5 edn. Ontario (Canada): B.C. Decker Inc. Hamilton; 2000: 573-84.

[4] Mitsiades CS, Mitsiades NS, Bronson RT, Chauhan D, Munshi N, Treon SP, Maxwell CA, Pilarski L, Hideshima T, Hoffman RM, Anderson KC: *Fluorescence imaging of multiple myeloma cells in a clinically relevant SCID/NOD in vivo model: biologic and clinical implications*. Cancer research 2003, 63(20):6689-96.

[5] Pinho SS, Carvalho S, Cabral J, Reis CA, Gartner F: *Canine tumors: a spontaneous animal model of human carcinogenesis*. Transl Res 2012, 159(3):165-72.

[6] Khanna C, Lindblad-Toh K, Vail D, London C, Bergman P, Barber L, Breen M, Kitchell B, McNeil E, Modiano JF, Niemi S, Comstock KE, Ostrander E, Westmoreland S, Withrow S: *The dog as a cancer model*. Nature biotechnology 2006, 24(9):1065-6.

[7] Bergman PJ: *Cancer immunotherapy*. Topics in companion animal medicine 2009, 24(3):130-6.

[8] MacEwen EG: *Spontaneous tumors in dogs and cats: models for the study of cancer biology and treatment*. Cancer metastasis reviews 1990, 9(2):125-36.

[9] Withrow SJ, MacEwen EG: *Small Animal Clinical Oncology*, 3 edn. Philadelphia (USA): W.B. Saunders Co.; 2001.

[10] Vail DM, MacEwen EG: *Spontaneously occurring tumors of companion animals as models for human cancer*. Cancer investigation 2000, 18(8):781-92.

[11] Bronson RT: *Variation in age at death of dogs of different sexes and breeds*. American journal of veterinary research 1982, 43(11):2057-9.

[12] Kelsey JL, Moore AS, Glickman LT: *Epidemiologic studies of risk factors for cancer in pet dogs*. Epidemiologic reviews 1998, 20(2):204-17.

[13] Patterson DF: *Companion animal medicine in the age of medical genetics*. Journal of veterinary internal medicine / American College of Veterinary Internal Medicine 2000, 14(1):1-9.

[14] Ostrander EA, Wayne RK: *The canine genome*. Genome research 2005, 15(12):1706-16.

[15] Marconato L, Gelain ME, Comazzi S: *The dog as a possible animal model for human non-Hodgkin lymphoma: a review*. Hematological oncology 2012.

[16] Thomas R, Smith KC, Gould R, Gower SM, Binns MM, Breen M: *Molecular cytogenetic analysis of a novel high-grade canine T-lymphoblastic lymphoma demonstrating co-expression of CD3 and CD79a cell markers*. Chromosome Res 2001, 9(8):649-57.

[17] Thomas R, Seiser EL, Motsinger-Reif A, Borst L, Valli VE, Kelley K, Suter SE, Argyle D, Burgess K, Bell J, Lindblad-Toh K, Modiano JF, Breen M: *Refining tumor-associated aneuploidy through 'genomic recoding' of recurrent DNA copy number aberrations in 150 canine non-Hodgkin lymphomas*. Leuk Lymphoma 2011, 52(7):1321-35.

[18] Thomas R, Smith KC, Ostrander EA, Galibert F, Breen M: *Chromosome aberrations in canine multicentric lymphomas detected with comparative genomic hybridisation and a panel of single locus probes*. British journal of cancer 2003, 89(8):1530-7.

[19] Ponce F, Marchal T, Magnol JP, Turinelli V, Ledieu D, Bonnefont C, Pastor M, Delignette ML, Fournel-Fleury C: *A morphological study of 608 cases of canine malignant lymphoma in France with a focus on comparative similarities between canine and human lymphoma morphology*. Veterinary pathology 2010, 47(3):414-33.

[20] Lindblad-Toh K, Wade CM, Mikkelsen TS, Karlsson EK, Jaffe DB, Kamal M, Clamp M, Chang JL, Kulbokas EJ, 3rd, Zody MC, Mauceli E, Xie X, Breen M, Wayne RK, Ostrander EA, Ponting CP, Galibert F, Smith DR, DeJong PJ, Kirkness E, Alvarez P, Biagi T, Brockman W, Butler J, Chin CW, Cook A, Cuff J, Daly MJ, DeCaprio D, Gnerre S, Grabherr M, Kellis M, Kleber M, Bardeleben C, Goodstadt L, Heger A, Hitte C, Kim L, Koepfli KP, Parker HG, Pollinger JP, Searle SM, Sutter NB, Thomas R, Webber C, Baldwin J, Abebe A, Abouelleil A, Aftuck L, Ait-Zahra M, Aldredge T, Allen N, An P, Anderson S, Antoine C, Arachchi H, Aslam A, Ayotte L, Bachantsang P, Barry A, Bayul T, Benamara M,

Berlin A, Bessette D, Blitshteyn B, Bloom T, Blye J, Boguslavskiy L, Bonnet C, Boukhgalter B, Brown A, Cahill P, Calixte N, Camarata J, Cheshatsang Y, Chu J, Citroen M, Collymore A, Cooke P, Dawoe T, Daza R, Decktor K, DeGray S, Dhargay N, Dooley K, Dooley K, Dorje P, Dorjee K, Dorris L, Duffey N, Dupes A, Egbiremolen O, Elong R, Falk J, Farina A, Faro S, Ferguson D, Ferreira P, Fisher S, FitzGerald M, Foley K, Foley C, Franke A, Friedrich D, Gage D, Garber M, Gearin G, Giannoukos G, Goode T, Goyette A, Graham J, Grandbois E, Gyaltsen K, Hafez N, Hagopian D, Hagos B, Hall J, Healy C, Hegarty R, Honan T, Horn A, Houde N, Hughes L, Hunnicutt L, Husby M, Jester B, Jones C, Kamat A, Kanga B, Kells C, Khazanovich D, Kieu AC, Kisner P, Kumar M, Lance K, Landers T, Lara M, Lee W, Leger JP, Lennon N, Leuper L, LeVine S, Liu J, Liu X, Lokyitsang Y, Lokyitsang T, Lui A, Macdonald J, Major J, Marabella R, Maru K, Matthews C, McDonough S, Mehta T, Meldrim J, Melnikov A, Meneus L, Mihalev A, Mihova T, Miller K, Mittelman R, Mlenga V, Mulrain L, Munson G, Navidi A, Naylor J, Nguyen T, Nguyen N, Nguyen C, Nguyen T, Nicol R, Norbu N, Norbu C, Novod N, Nyima T, Olandt P, O'Neill B, O'Neill K, Osman S, Oyono L, Patti C, Perrin D, Phunkhang P, Pierre F, Priest M, Rachupka A, Raghuraman S, Rameau R, Ray V, Raymond C, Rege F, Rise C, Rogers J, Rogov P, Sahalie J, Settipalli S, Sharpe T, Shea T, Sheehan M, Sherpa N, Shi J, Shih D, Sloan J, Smith C, Sparrow T, Stalker J, Stange-Thomann N, Stavropoulos S, Stone C, Stone S, Sykes S, Tchuinga P, Tenzing P, Tesfaye S, Thoulutsang D, Thoulutsang Y, Topham K, Topping I, Tsamla T, Vassiliev H, Venkataraman V, Vo A, Wangchuk T, Wangdi T, Weiand M, Wilkinson J, Wilson A, Yadav S, Yang S, Yang X, Young G, Yu Q, Zainoun J, Zembek L, Zimmer A, Lander ES: *Genome sequence, comparative analysis and haplotype structure of the domestic dog*. Nature 2005, 438(7069):803-19.

[21] Fleischer S, Sharkey M, Mealey K, Ostrander EA, Martinez M: *Pharmacogenetic and metabolic differences between dog breeds: their impact on canine medicine and the use of the dog as a preclinical animal model*. The AAPS journal 2008, 10(1):110-9.

[22] Hansen K, Khanna C: *Spontaneous and genetically engineered animal models; use in preclinical cancer drug development*. Eur J Cancer 2004, 40(6):858-80.

[23] Kumar GR, Subazini TK, Subha K, Rajadurai CP, Prabakar L: *CanGeneBase (CGB)--a database on cancer related genes*. Bioinformation 2009, 3(10):422-4.

[24] Murua Escobar H, Meyer B, Richter A, Becker K, Flohr AM, Bullerdiek J, Nolte I: *Molecular characterization of the canine HMGB1*. Cytogenetic and genome research 2003, 101(1):33-8.

[25] Murua Escobar H, Soller JT, Sterenczak KA, Sperveslage JD, Schlueter C, Burchardt B, Eberle N, Fork M, Nimzyk R, Winkler S, Nolte I, Bullerdiek J: *Cloning and characterization of the canine receptor for advanced glycation end products*. Gene 2006, 369:45-52.

[26] Walker JM, Goodwin GH, Johns EW, Wietzes P, Gaastra W: *A comparison of the amino-terminal sequences of two calf-thymus chromatin non-histone proteins*. International journal of peptide and protein research 1977, 9(3):220-3.

[27] Bustin M: *Revised nomenclature for high mobility group (HMG) chromosomal proteins*. Trends in biochemical sciences 2001, 26(3):152-3.

[28] Ferrari S, Ronfani L, Calogero S, Bianchi ME: *The mouse gene coding for high mobility group 1 protein (HMG1)*. J Biol Chem 1994, 269(46):28803-8.

[29] Kaplan DJ, Duncan CH: *Full length cDNA sequence for bovine high mobility group 1 (HMG1) protein*. Nucleic Acids Res 1988, 16(21):10375.

[30] Paonessa G, Frank R, Cortese R: *Nucleotide sequence of rat liver HMG1 cDNA*. Nucleic Acids Res 1987, 15(21):9077.

[31] Tsuda K, Kikuchi M, Mori K, Waga S, Yoshida M: *Primary structure of non-histone protein HMG1 revealed by the nucleotide sequence*. Biochemistry 1988, 27(16):6159-63.

[32] Reeck GR, Isackson PJ, Teller DC: *Domain structure in high molecular weight high mobility group nonhistone chromatin proteins*. Nature 1982, 300(5887):76-8.

[33] Thomas JO: *HMG1 and 2: architectural DNA-binding proteins*. Biochemical Society transactions 2001, 29(Pt 4):395-401.

[34] Weir HM, Kraulis PJ, Hill CS, Raine AR, Laue ED, Thomas JO: *Structure of the HMG box motif in the B-domain of HMG1*. Embo J 1993, 12(4):1311-9.

[35] Wolffe AP: *Architectural transcription factors*. Science 1994, 264(5162):1100-1.

[36] Bustin M, Reeves R: *High-mobility-group chromosomal proteins: architectural components that facilitate chromatin function*. Progress in nucleic acid research and molecular biology 1996, 54:35-100.

[37] Bustin M: *Regulation of DNA-dependent activities by the functional motifs of the high-mobility-group chromosomal proteins*. Mol Cell Biol 1999, 19(8):5237-46.

[38] Agresti A, Bianchi ME: *HMGB proteins and gene expression*. Current opinion in genetics & development 2003, 13(2):170-8.

[39] Jiao Y, Wang HC, Fan SJ: *Growth suppression and radiosensitivity increase by HMGB1 in breast cancer*. Acta pharmacologica Sinica 2007, 28(12):1957-67.

[40] Agresti A, Lupo R, Bianchi ME, Muller S: *HMGB1 interacts differentially with members of the Rel family of transcription factors*. Biochemical and biophysical research communications 2003, 302(2):421-6.

[41] Jayaraman L, Moorthy NC, Murthy KG, Manley JL, Bustin M, Prives C: *High mobility group protein-1 (HMG-1) is a unique activator of p53*. Genes & development 1998, 12(4):462-72.

[42] Stros M, Muselikova-Polanska E, Pospisilova S, Strauss F: *High-affinity binding of tumor-suppressor protein p53 and HMGB1 to hemicatenated DNA loops*. Biochemistry 2004, 43(22):7215-25.

[43] Onate SA, Prendergast P, Wagner JP, Nissen M, Reeves R, Pettijohn DE, Edwards DP: *The DNA-bending protein HMG-1 enhances progesterone receptor binding to its target DNA sequences*. Mol Cell Biol 1994, 14(5):3376-91.

[44] Verrier CS, Roodi N, Yee CJ, Bailey LR, Jensen RA, Bustin M, Parl FF: *High-mobility group (HMG) protein HMG-1 and TATA-binding protein-associated factor TAF(II)30 affect estrogen receptor-mediated transcriptional activation*. Molecular endocrinology (Baltimore, Md 1997, 11(8):1009-19.

[45] Zhang CC, Krieg S, Shapiro DJ: *HMG-1 stimulates estrogen response element binding by estrogen receptor from stably transfected HeLa cells*. Molecular endocrinology (Baltimore, Md 1999, 13(4):632-43.

[46] Lange SS, Mitchell DL, Vasquez KM: *High mobility group protein B1 enhances DNA repair and chromatin modification after DNA damage*. Proc Natl Acad Sci U S A 2008, 105(30):10320-5.

[47] Lange SS, Reddy MC, Vasquez KM: *Human HMGB1 directly facilitates interactions between nucleotide excision repair proteins on triplex-directed psoralen interstrand crosslinks*. DNA repair 2009, 8(7):865-72.

[48] Pil PM, Lippard SJ: *Specific binding of chromosomal protein HMG1 to DNA damaged by the anticancer drug cisplatin*. Science 1992, 256(5054):234-7.

[49] Hughes EN, Engelsberg BN, Billings PC: *Purification of nuclear proteins that bind to cisplatin-damaged DNA. Identity with high mobility group proteins 1 and 2*. J Biol Chem 1992, 267(19):13520-7.

[50] Billings PC, Davis RJ, Engelsberg BN, Skov KA, Hughes EN: *Characterization of high mobility group protein binding to cisplatin-damaged DNA*. Biochemical and biophysical research communications 1992, 188(3):1286-94.

[51] Huang JC, Zamble DB, Reardon JT, Lippard SJ, Sancar A: *HMG-domain proteins specifically inhibit the repair of the major DNA adduct of the anticancer drug cisplatin by human excision nuclease*. Proc Natl Acad Sci U S A 1994, 91(22):10394-8.

[52] He Q, Liang CH, Lippard SJ: *Steroid hormones induce HMG1 overexpression and sensitize breast cancer cells to cisplatin and carboplatin*. Proc Natl Acad Sci U S A 2000, 97(11):5768-72.

[53] Mitkova E, Ugrinova I, Pashev IG, Pasheva EA: *The inhibitory effect of HMGB-1 protein on the repair of cisplatin-damaged DNA is accomplished through the acidic domain*. Biochemistry 2005, 44(15):5893-8.

[54] Calogero S, Grassi F, Aguzzi A, Voigtlander T, Ferrier P, Ferrari S, Bianchi ME: *The lack of chromosomal protein Hmg1 does not disrupt cell growth but causes lethal hypoglycaemia in newborn mice*. Nature genetics 1999, 22(3):276-80.

[55] Wang H, Bloom O, Zhang M, Vishnubhakat JM, Ombrellino M, Che J, Frazier A, Yang H, Ivanova S, Borovikova L, Manogue KR, Faist E, Abraham E, Andersson J, Andersson U, Molina PE, Abumrad NN, Sama A, Tracey KJ: *HMG-1 as a late mediator of endotoxin lethality in mice*. Science 1999a, 285(5425):248-51.

[56] Li J, Kokkola R, Tabibzadeh S, Yang R, Ochani M, Qiang X, Harris HE, Czura CJ, Wang H, Ulloa L, Wang H, Warren HS, Moldawer LL, Fink MP, Andersson U, Tracey KJ, Yang H: *Structural basis for the proinflammatory cytokine activity of high mobility group box 1*. Molecular medicine (Cambridge, Mass 2003, 9(1-2):37-45.

[57] Andersson U, Tracey KJ: *HMGB1 as a mediator of necrosis-induced inflammation and a therapeutic target in arthritis*. Rheum Dis Clin North Am 2004, 30(3):627-37, xi.

[58] Park JS, Svetkauskaite D, He Q, Kim JY, Strassheim D, Ishizaka A, Abraham E: *Involvement of toll-like receptors 2 and 4 in cellular activation by high mobility group box 1 protein*. J Biol Chem 2004, 279(9):7370-7.

[59] Yu M, Wang H, Ding A, Golenbock DT, Latz E, Czura CJ, Fenton MJ, Tracey KJ, Yang H: *HMGB1 signals through toll-like receptor (TLR) 4 and TLR2*. Shock 2006, 26(2):174-9.

[60] Huttunen HJ, Fages C, Kuja-Panula J, Ridley AJ, Rauvala H: *Receptor for advanced glycation end products-binding COOH-terminal motif of amphoterin inhibits invasive migration and metastasis*. Cancer research 2002, 62(16):4805-11.

[61] Huttunen HJ, Rauvala H: *Amphoterin as an extracellular regulator of cell motility: from discovery to disease*. J Intern Med 2004, 255(3):351-66.

[62] Yang H, Ochani M, Li J, Qiang X, Tanovic M, Harris HE, Susarla SM, Ulloa L, Wang H, DiRaimo R, Czura CJ, Roth J, Warren HS, Fink MP, Fenton MJ, Andersson U, Tracey KJ: *Reversing established sepsis with antagonists of endogenous high-mobility group box 1*. Proc Natl Acad Sci U S A 2004, 101(1):296-301.

[63] Scaffidi P, Misteli T, Bianchi ME: *Release of chromatin protein HMGB1 by necrotic cells triggers inflammation*. Nature 2002, 418(6894):191-5.

[64] Messmer D, Yang H, Telusma G, Knoll F, Li J, Messmer B, Tracey KJ, Chiorazzi N: *High mobility group box protein 1: an endogenous signal for dendritic cell maturation and Th1 polarization*. J Immunol 2004, 173(1):307-13.

[65] Yang D, Chen Q, Yang H, Tracey KJ, Bustin M, Oppenheim JJ: *High mobility group box-1 protein induces the migration and activation of human dendritic cells and acts as an alarmin*. J Leukoc Biol 2007, 81(1):59-66.

[66] Palumbo R, Sampaolesi M, De Marchis F, Tonlorenzi R, Colombetti S, Mondino A, Cossu G, Bianchi ME: *Extracellular HMGB1, a signal of tissue damage, induces mesoangioblast migration and proliferation*. J Cell Biol 2004, 164(3):441-9.

[67] Bell CW, Jiang W, Reich CF, 3rd, Pisetsky DS: *The extracellular release of HMGB1 during apoptotic cell death*. Am J Physiol Cell Physiol 2006, 291(6):C1318-25.

[68] Jiang W, Bell CW, Pisetsky DS: *The relationship between apoptosis and high-mobility group protein 1 release from murine macrophages stimulated with lipopolysaccharide or polyinosinic-polycytidylic acid*. J Immunol 2007, 178(10):6495-503.

[69] Kazama H, Ricci JE, Herndon JM, Hoppe G, Green DR, Ferguson TA: *Induction of immunological tolerance by apoptotic cells requires caspase-dependent oxidation of high-mobility group box-1 protein*. Immunity 2008, 29(1):21-32.

[70] Yang H, Hreggvidsdottir HS, Palmblad K, Wang H, Ochani M, Li J, Lu B, Chavan S, Rosas-Ballina M, Al-Abed Y, Akira S, Bierhaus A, Erlandsson-Harris H, Andersson U, Tracey KJ: *A critical cysteine is required for HMGB1 binding to Toll-like receptor 4 and activation of macrophage cytokine release*. Proc Natl Acad Sci U S A 2010, 107(26):11942-7.

[71] Yang H, Lundback P, Ottosson L, Erlandsson-Harris H, Venereau E, Bianchi ME, Al-Abed Y, Andersson U, Tracey KJ, Antoine DJ: *Redox modification of cysteine residues regulates the cytokine activity of high mobility group box-1 (HMGB1)*. Molecular medicine (Cambridge, Mass 2012, 18:250-9.

[72] Andersson U, Wang H, Palmblad K, Aveberger AC, Bloom O, Erlandsson-Harris H, Janson A, Kokkola R, Zhang M, Yang H, Tracey KJ: *High mobility group 1 protein (HMG-1) stimulates proinflammatory cytokine synthesis in human monocytes*. J Exp Med 2000, 192(4):565-70.

[73] Lotze MT, Tracey KJ: *High-mobility group box 1 protein (HMGB1): nuclear weapon in the immune arsenal*. Nat Rev Immunol 2005, 5(4):331-42.

[74] Semino C, Angelini G, Poggi A, Rubartelli A: *NK/iDC interaction results in IL-18 secretion by DCs at the synaptic cleft followed by NK cell activation and release of the DC maturation factor HMGB1*. Blood 2005, 106(2):609-16.

[75] Wang H, Vishnubhakat JM, Bloom O, Zhang M, Ombrellino M, Sama A, Tracey KJ: *Proinflammatory cytokines (tumor necrosis factor and interleukin 1) stimulate release of high mobility group protein-1 by pituicytes*. Surgery 1999b, 126(2):389-92.

[76] Kawahara K, Setoyama K, Kikuchi K, Biswas KK, Kamimura R, Iwata M, Ito T, Morimoto Y, Hashiguchi T, Takao S, Maruyama I: *HMGB1 release in co-cultures of porcine endothelial and human T cells*. Xenotransplantation 2007, 14(6):636-41.

[77] Kawahara K, Hashiguchi T, Kikuchi K, Tancharoen S, Miura N, Ito T, Oyama Y, Nawa Y, Biswas KK, Meng X, Morimoto Y, Shrestha B, Sameshima H, Maruyama I: *Induction of high mobility group box 1 release from serotonin-stimulated human umbilical vein endothelial cells*. International journal of molecular medicine 2008, 22(5):639-44.

[78] Rouhiainen A, Imai S, Rauvala H, Parkkinen J: *Occurrence of amphoterin (HMG1) as an endogenous protein of human platelets that is exported to the cell surface upon platelet activation*. Thrombosis and haemostasis 2000, 84(6):1087-94.

[79] Ivanov S, Dragoi AM, Wang X, Dallacosta C, Louten J, Musco G, Sitia G, Yap GS, Wan Y, Biron CA, Bianchi ME, Wang H, Chu WM: *A novel role for HMGB1 in TLR9-mediated inflammatory responses to CpG-DNA*. Blood 2007, 110(6):1970-81.

[80] Abraham E, Arcaroli J, Carmody A, Wang H, Tracey KJ: *HMG-1 as a mediator of acute lung inflammation*. J Immunol 2000, 165(6):2950-4.

[81] Ulloa L, Ochani M, Yang H, Tanovic M, Halperin D, Yang R, Czura CJ, Fink MP, Tracey KJ: *Ethyl pyruvate prevents lethality in mice with established lethal sepsis and systemic inflammation*. Proc Natl Acad Sci U S A 2002, 99(19):12351-6.

[82] Wähämaa H, Vallerskog T, Qin S, Lunderius C, LaRosa G, Andersson U, Harris HE: *HMGB1-secreting capacity of multiple cell lineages revealed by a novel HMGB1 ELISPOT assay*. J Leukoc Biol 2007, 81(1):129-36.

[83] Kuniyasu H, Yano S, Sasaki T, Sasahira T, Sone S, Ohmori H: *Colon cancer cell-derived high mobility group 1/amphoterin induces growth inhibition and apoptosis in macrophages*. Am J Pathol 2005, 166(3):751-60.

[84] Liu S, Stolz DB, Sappington PL, Macias CA, Killeen ME, Tenhunen JJ, Delude RL, Fink MP: *HMGB1 is secreted by immunostimulated enterocytes and contributes to cytomix-induced hyperpermeability of Caco-2 monolayers*. Am J Physiol Cell Physiol 2006, 290(4):C990-9.

[85] Fujii K, Luo Y, Sasahira T, Denda A, Ohmori H, Kuniyasu H: *Co-treatment with deoxycholic acid and azoxymethane accelerates secretion of HMGB1 in IEC6 intestinal epithelial cells*. Cell proliferation 2009, 42(5):701-9.

[86] Gardella S, Andrei C, Ferrera D, Lotti LV, Torrisi MR, Bianchi ME, Rubartelli A: *The nuclear protein HMGB1 is secreted by monocytes via a non-classical, vesicle-mediated secretory pathway*. EMBO Rep 2002, 3(10):995-1001.

[87] Bonaldi T, Talamo F, Scaffidi P, Ferrera D, Porto A, Bachi A, Rubartelli A, Agresti A, Bianchi ME: *Monocytic cells hyperacetylate chromatin protein HMGB1 to redirect it towards secretion*. EMBO J 2003, 22(20):5551-60.

[88] Choi YR, Kim H, Kang HJ, Kim NG, Kim JJ, Park KS, Paik YK, Kim HO: *Overexpression of high mobility group box 1 in gastrointestinal stromal tumors with KIT mutation*. Cancer research 2003, 63(9):2188-93.

[89] Xiang YY, Wang DY, Tanaka M, Suzuki M, Kiyokawa E, Igarashi H, Naito Y, Shen Q, Sugimura H: *Expression of high-mobility group-1 mRNA in human gastrointestinal adenocarcinoma and corresponding non-cancerous mucosa*. Int J Cancer 1997, 74(1):1-6.

[90] Poser I, Golob M, Buettner R, Bosserhoff AK: *Upregulation of HMG1 leads to melanoma inhibitory activity expression in malignant melanoma cells and contributes to their malignancy phenotype*. Mol Cell Biol 2003, 23(8):2991-8.

[91] Brezniceanu ML, Volp K, Bosser S, Solbach C, Lichter P, Joos S, Zornig M: *HMGB1 inhibits cell death in yeast and mammalian cells and is abundantly expressed in human breast carcinoma*. FASEB J 2003, 17(10):1295-7.

[92] Flohr AM, Rogalla P, Meiboom M, Borrmann L, Krohn M, Thode-Halle B, Bullerdiek J: *Variation of HMGB1 expression in breast cancer*. Anticancer research 2001, 21(6A):3881-5.

[93] Kuniyasu H, Chihara Y, Kondo H, Ohmori H, Ukai R: *Amphoterin induction in prostatic stromal cells by androgen deprivation is associated with metastatic prostate cancer*. Oncol Rep 2003, 10(6):1863-8.

[94] Meyer B, Murua Escobar H, Hauke S, Richter A, Winkler S, Rogalla P, Flohr AM, Bullerdiek J, Nolte I: *Expression pattern of the HMGB1 gene in sarcomas of the dog*. Anticancer research 2004, 24(2B):707-10.

[95] Cabart P, Kalousek I, Jandova D, Hrkal Z: *Differential expression of nuclear HMG1, HMG2 proteins and H1(zero) histone in various blood cells*. Cell Biochem Funct 1995, 13(2):125-33.

[96] Meyer A, Staratschek-Jox A, Springwald A, Wenk H, Wolf J, Wickenhauser C, Bullerdiek J: *Non-Hodgkin lymphoma expressing high levels of the danger-signalling protein HMGB1*. Leuk Lymphoma 2008, 49(6):1184-9.

[97] Meyer A, Eberle N, Bullerdiek J, Nolte I, Simon D: *High-mobility group B1 proteins in canine lymphoma: prognostic value of initial and sequential serum levels in treatment outcome following combination chemotherapy*. Veterinary and comparative oncology 2010, 8(2):127-37.

[98] Schlueter C, Weber H, Meyer B, Rogalla P, Roser K, Hauke S, Bullerdiek J: *Angiogenetic signaling through hypoxia: HMGB1: an angiogenetic switch molecule*. Am J Pathol 2005, 166(4):1259-63.

[99] Zhang CL, Shu MG, Qi HW, Li LW: *Inhibition of tumor angiogenesis by HMGB1 A box peptide*. Med Hypotheses 2008, 70(2):343-5.

[100] Hori O, Brett J, Slattery T, Cao R, Zhang J, Chen JX, Nagashima M, Lundh ER, Vijay S, Nitecki D, et al.: *The receptor for advanced glycation end products (RAGE) is a cellular binding site for amphoterin. Mediation of neurite outgrowth and co-expression of rage and amphoterin in the developing nervous system*. J Biol Chem 1995, 270(43):25752-61.

[101] Park JS, Gamboni-Robertson F, He Q, Svetkauskaite D, Kim JY, Strassheim D, Sohn JW, Yamada S, Maruyama I, Banerjee A, Ishizaka A, Abraham E: *High mobility group box 1 protein interacts with multiple Toll-like receptors*. Am J Physiol Cell Physiol 2006, 290(3):C917-24.

[102] Tian J, Avalos AM, Mao SY, Chen B, Senthil K, Wu H, Parroche P, Drabic S, Golenbock D, Sirois C, Hua J, An LL, Audoly L, La Rosa G, Bierhaus A, Naworth P, Marshak-Rothstein A, Crow MK, Fitzgerald KA, Latz E, Kiener PA, Coyle AJ: *Toll-like receptor 9-dependent activation by DNA-containing immune complexes is mediated by HMGB1 and RAGE*. Nature immunology 2007, 8(5):487-96.

[103] El Mezayen R, El Gazzar M, Seeds MC, McCall CE, Dreskin SC, Nicolls MR: *Endogenous signals released from necrotic cells augment inflammatory responses to bacterial endotoxin*. Immunology letters 2007, 111(1):36-44.

[104] Chen GY, Tang J, Zheng P, Liu Y: *CD24 and Siglec-10 selectively repress tissue damage-induced immune responses*. Science 2009, 323(5922):1722-5.

[105] Bianchi ME: *HMGB1 loves company*. J Leukoc Biol 2009, 86(3):573-6.

[106] Aderem A, Ulevitch RJ: *Toll-like receptors in the induction of the innate immune response*. Nature 2000, 406(6797):782-7.

[107] Akira S, Takeda K, Kaisho T: *Toll-like receptors: critical proteins linking innate and acquired immunity*. Nature immunology 2001, 2(8):675-80.

[108] Takeda K, Kaisho T, Akira S: *Toll-like receptors*. Annual review of immunology 2003, 21:335-76.

[109] Bauer S, Kirschning CJ, Hacker H, Redecke V, Hausmann S, Akira S, Wagner H, Lipford GB: *Human TLR9 confers responsiveness to bacterial DNA via*

species-specific CpG motif recognition. Proc Natl Acad Sci U S A 2001b, 98(16):9237-42.

[110] Bauer M, Redecke V, Ellwart JW, Scherer B, Kremer JP, Wagner H, Lipford GB: *Bacterial CpG-DNA triggers activation and maturation of human CD11c-, CD123+ dendritic cells*. J Immunol 2001a, 166(8):5000-7.

[111] Kandimalla ER, Zhu FG, Bhagat L, Yu D, Agrawal S: *Toll-like receptor 9: modulation of recognition and cytokine induction by novel synthetic CpG DNAs*. Biochemical Society transactions 2003, 31(Pt 3):654-8.

[112] Agrawal S, Kandimalla ER: *Modulation of Toll-like Receptor 9 Responses through Synthetic Immunostimulatory Motifs of DNA*. Annals of the New York Academy of Sciences 2003, 1002:30-42.

[113] Cornelie S, Hoebeke J, Schacht AM, Bertin B, Vicogne J, Capron M, Riveau G: *Direct evidence that toll-like receptor 9 (TLR9) functionally binds plasmid DNA by specific cytosine-phosphate-guanine motif recognition*. J Biol Chem 2004, 279(15):15124-9.

[114] Krieg AM: *TLR9 and DNA 'feel' RAGE*. Nature immunology 2007, 8(5):475-7.

[115] Rauvala H, Rouhiainen A: *Physiological and pathophysiological outcomes of the interactions of HMGB1 with cell surface receptors*. Biochimica et biophysica acta 2010, 1799(1-2):164-70.

[116] Neeper M, Schmidt AM, Brett J, Yan SD, Wang F, Pan YC, Elliston K, Stern D, Shaw A: *Cloning and expression of a cell surface receptor for advanced glycosylation end products of proteins*. J Biol Chem 1992, 267(21):14998-5004.

[117] Schmidt AM, Vianna M, Gerlach M, Brett J, Ryan J, Kao J, Esposito C, Hegarty H, Hurley W, Clauss M, et al.: *Isolation and characterization of two binding proteins for advanced glycosylation end products from bovine lung which are present on the endothelial cell surface*. J Biol Chem 1992, 267(21):14987-97.

[118] Yan SD, Chen X, Fu J, Chen M, Zhu H, Roher A, Slattery T, Zhao L, Nagashima M, Morser J, Migheli A, Nawroth P, Stern D, Schmidt AM: *RAGE and amyloid-beta peptide neurotoxicity in Alzheimer's disease*. Nature 1996, 382(6593):685-91.

[119] Hofmann MA, Drury S, Fu C, Qu W, Taguchi A, Lu Y, Avila C, Kambham N, Bierhaus A, Nawroth P, Neurath MF, Slattery T, Beach D, McClary J, Nagashima M, Morser J, Stern D, Schmidt AM: *RAGE mediates a novel*

proinflammatory axis: a central cell surface receptor for S100/calgranulin polypeptides. Cell 1999, 97(7):889-901.

[120] Chavakis T, Bierhaus A, Al-Fakhri N, Schneider D, Witte S, Linn T, Nagashima M, Morser J, Arnold B, Preissner KT, Nawroth PP: *The pattern recognition receptor (RAGE) is a counterreceptor for leukocyte integrins: a novel pathway for inflammatory cell recruitment*. J Exp Med 2003, 198(10):1507-15.

[121] Hofmann MA, Drury S, Hudson BI, Gleason MR, Qu W, Lu Y, Lalla E, Chitnis S, Monteiro J, Stickland MH, Bucciarelli LG, Moser B, Moxley G, Itescu S, Grant PJ, Gregersen PK, Stern DM, Schmidt AM: *RAGE and arthritis: the G82S polymorphism amplifies the inflammatory response*. Genes Immun 2002, 3(3):123-35.

[122] Schmidt AM, Yan SD, Yan SF, Stern DM: *The multiligand receptor RAGE as a progression factor amplifying immune and inflammatory responses*. The Journal of clinical investigation 2001, 108(7):949-55.

[123] Chavakis T, Bierhaus A, Nawroth PP: *RAGE (receptor for advanced glycation end products): a central player in the inflammatory response*. Microbes and infection / Institut Pasteur 2004, 6(13):1219-25.

[124] Lue LF, Walker DG, Brachova L, Beach TG, Rogers J, Schmidt AM, Stern DM, Yan SD: *Involvement of microglial receptor for advanced glycation endproducts (RAGE) in Alzheimer's disease: identification of a cellular activation mechanism*. Experimental neurology 2001, 171(1):29-45.

[125] Lue LF, Yan SD, Stern DM, Walker DG: *Preventing activation of receptor for advanced glycation endproducts in Alzheimer's disease*. Current drug targets 2005, 4(3):249-66.

[126] Chen X, Walker DG, Schmidt AM, Arancio O, Lue LF, Yan SD: *RAGE: a potential target for Abeta-mediated cellular perturbation in Alzheimer's disease*. Current molecular medicine 2007, 7(8):735-42.

[127] Park L, Raman KG, Lee KJ, Lu Y, Ferran LJ, Jr., Chow WS, Stern D, Schmidt AM: *Suppression of accelerated diabetic atherosclerosis by the soluble receptor for advanced glycation endproducts*. Nature medicine 1998, 4(9):1025-31.

[128] Cipollone F, Iezzi A, Fazia M, Zucchelli M, Pini B, Cuccurullo C, De Cesare D, De Blasis G, Muraro R, Bei R, Chiarelli F, Schmidt AM, Cuccurullo F, Mezzetti A: *The receptor RAGE as a progression factor amplifying arachidonate-dependent*

inflammatory and proteolytic response in human atherosclerotic plaques: role of glycemic control. Circulation 2003, 108(9):1070-7.

[129] Yan SF, Ramasamy R, Schmidt AM: *Mechanisms of disease: advanced glycation end-products and their receptor in inflammation and diabetes complications*. Nature clinical practice 2008, 4(5):285-93.

[130] Yan SF, Ramasamy R, Schmidt AM: *The receptor for advanced glycation endproducts (RAGE) and cardiovascular disease*. Expert reviews in molecular medicine 2009, 11:e9.

[131] Goova MT, Li J, Kislinger T, Qu W, Lu Y, Bucciarelli LG, Nowygrod S, Wolf BM, Caliste X, Yan SF, Stern DM, Schmidt AM: *Blockade of receptor for advanced glycation end-products restores effective wound healing in diabetic mice*. Am J Pathol 2001, 159(2):513-25.

[132] Logsdon CD, Fuentes MK, Huang EH, Arumugam T: *RAGE and RAGE ligands in cancer*. Current molecular medicine 2007, 7(8):777-89.

[133] Stern D, Yan SD, Yan SF, Schmidt AM: *Receptor for advanced glycation endproducts: a multiligand receptor magnifying cell stress in diverse pathologic settings*. Advanced drug delivery reviews 2002, 54(12):1615-25.

[134] Brett J, Schmidt AM, Yan SD, Zou YS, Weidman E, Pinsky D, Nowygrod R, Neeper M, Przysiecki C, Shaw A, et al.: *Survey of the distribution of a newly characterized receptor for advanced glycation end products in tissues*. Am J Pathol 1993, 143(6):1699-712.

[135] Burke AP, Kolodgie FD, Zieske A, Fowler DR, Weber DK, Varghese PJ, Farb A, Virmani R: *Morphologic findings of coronary atherosclerotic plaques in diabetics: a postmortem study*. Arterioscler Thromb Vasc Biol 2004, 24(7):1266-71.

[136] Malherbe P, Richards JG, Gaillard H, Thompson A, Diener C, Schuler A, Huber G: *cDNA cloning of a novel secreted isoform of the human receptor for advanced glycation end products and characterization of cells co-expressing cell-surface scavenger receptors and Swedish mutant amyloid precursor protein*. Brain research 1999, 71(2):159-70.

[137] Schlueter C, Hauke S, Flohr AM, Rogalla P, Bullerdiek J: *Tissue-specific expression patterns of the RAGE receptor and its soluble forms--a result of regulated alternative splicing?* Biochimica et biophysica acta 2003, 1630(1):1-6.

[138] Yonekura H, Yamamoto Y, Sakurai S, Petrova RG, Abedin MJ, Li H, Yasui K, Takeuchi M, Makita Z, Takasawa S, Okamoto H, Watanabe T, Yamamoto H:

Novel splice variants of the receptor for advanced glycation end-products expressed in human vascular endothelial cells and pericytes, and their putative roles in diabetes-induced vascular injury. The Biochemical journal 2003, 370(Pt 3):1097-109.

[139] Park IH, Yeon SI, Youn JH, Choi JE, Sasaki N, Choi IH, Shin JS: *Expression of a novel secreted splice variant of the receptor for advanced glycation end products (RAGE) in human brain astrocytes and peripheral blood mononuclear cells*. Molecular immunology 2004, 40(16):1203-11.

[140] Ding Q, Keller JN: *Splice variants of the receptor for advanced glycosylation end products (RAGE) in human brain*. Neuroscience letters 2005a, 373(1):67-72.

[141] Ding Q, Keller JN: *Evaluation of rage isoforms, ligands, and signaling in the brain*. Biochimica et biophysica acta 2005b, 1746(1):18-27.

[142] Geroldi D, Falcone C, Emanuele E, D'Angelo A, Calcagnino M, Buzzi MP, Scioli GA, Fogari R: *Decreased plasma levels of soluble receptor for advanced glycation end-products in patients with essential hypertension*. Journal of hypertension 2005, 23(9):1725-9.

[143] Hudson BI, Carter AM, Harja E, Kalea AZ, Arriero M, Yang H, Grant PJ, Schmidt AM: *Identification, classification, and expression of RAGE gene splice variants*. Faseb J 2008, 22(5):1572-80.

[144] Rojas A, Gonzalez I, Morales E, Perez-Castro R, Romero J, Figueroa H: *Diabetes and cancer: Looking at the multiligand/RAGE axis*. World journal of diabetes 2011, 2(7):108-13.

[145] Sakurai S, Yamamoto Y, Tamei H, Matsuki H, Obata K, Hui L, Miura J, Osawa M, Uchigata Y, Iwamoto Y, Watanabe T, Yonekura H, Yamamoto H: *Development of an ELISA for esRAGE and its application to type 1 diabetic patients*. Diabetes research and clinical practice 2006, 73(2):158-65.

[146] Raucci A, Cugusi S, Antonelli A, Barabino SM, Monti L, Bierhaus A, Reiss K, Saftig P, Bianchi ME: *A soluble form of the receptor for advanced glycation endproducts (RAGE) is produced by proteolytic cleavage of the membrane-bound form by the sheddase a disintegrin and metalloprotease 10 (ADAM10)*. Faseb J 2008, 22(10):3716-27.

[147] Kalea AZ, Schmidt AM, Hudson BI: *Alternative splicing of RAGE: roles in biology and disease*. Front Biosci 2011, 16:2756-70.

[148] Geroldi D, Falcone C, Emanuele E: *Soluble receptor for advanced glycation end products: from disease marker to potential therapeutic target*. Current medicinal chemistry 2006, 13(17):1971-8.

[149] Rojas A, Delgado-Lopez F, Gonzalez I, Perez-Castro R, Romero J, Rojas I: *The receptor for advanced glycation end-products: A complex signaling scenario for a promiscuous receptor*. Cellular signalling 2012, 25(3):609-14.

[150] Pullerits R, Bokarewa M, Dahlberg L, Tarkowski A: *Decreased levels of soluble receptor for advanced glycation end products in patients with rheumatoid arthritis indicating deficient inflammatory control*. Arthritis research & therapy 2005, 7(4):R817-24.

[151] Emanuele E, D'Angelo A, Tomaino C, Binetti G, Ghidoni R, Politi P, Bernardi L, Maletta R, Bruni AC, Geroldi D: *Circulating levels of soluble receptor for advanced glycation end products in Alzheimer disease and vascular dementia*. Archives of neurology 2005, 62(11):1734-6.

[152] Challier M, Jacqueminet S, Benabdesselam O, Grimaldi A, Beaudeux JL: *Increased serum concentrations of soluble receptor for advanced glycation endproducts in patients with type 1 diabetes*. Clinical chemistry 2005, 51(9):1749-50.

[153] Katakami N, Matsuhisa M, Kaneto H, Matsuoka TA, Sakamoto K, Nakatani Y, Ohtoshi K, Hayaishi-Okano R, Kosugi K, Hori M, Yamasaki Y: *Decreased endogenous secretory advanced glycation end product receptor in type 1 diabetic patients: its possible association with diabetic vascular complications*. Diabetes care 2005, 28(11):2716-21.

[154] Tan KC, Shiu SW, Chow WS, Leng L, Bucala R, Betteridge DJ: *Association between serum levels of soluble receptor for advanced glycation end products and circulating advanced glycation end products in type 2 diabetes*. Diabetologia 2006, 49(11):2756-62.

[155] Basta G, Sironi AM, Lazzerini G, Del Turco S, Buzzigoli E, Casolaro A, Natali A, Ferrannini E, Gastaldelli A: *Circulating soluble receptor for advanced glycation end products is inversely associated with glycemic control and S100A12 protein*. The Journal of clinical endocrinology and metabolism 2006, 91(11):4628-34.

[156] Holman RR, Paul SK, Bethel MA, Matthews DR, Neil HA: *10-year follow-up of intensive glucose control in type 2 diabetes*. The New England journal of medicine 2008, 359(15):1577-89.

[157] Gerstein HC, Miller ME, Byington RP, Goff DC, Jr., Bigger JT, Buse JB, Cushman WC, Genuth S, Ismail-Beigi F, Grimm RH, Jr., Probstfield JL, Simons-Morton DG, Friedewald WT: *Effects of intensive glucose lowering in type 2 diabetes*. The New England journal of medicine 2008, 358(24):2545-59.

[158] Patel A, MacMahon S, Chalmers J, Neal B, Billot L, Woodward M, Marre M, Cooper M, Glasziou P, Grobbee D, Hamet P, Harrap S, Heller S, Liu L, Mancia G, Mogensen CE, Pan C, Poulter N, Rodgers A, Williams B, Bompoint S, de Galan BE, Joshi R, Travert F: *Intensive blood glucose control and vascular outcomes in patients with type 2 diabetes*. The New England journal of medicine 2008, 358(24):2560-72.

[159] Falcone C, Emanuele E, D'Angelo A, Buzzi MP, Belvito C, Cuccia M, Geroldi D: *Plasma levels of soluble receptor for advanced glycation end products and coronary artery disease in nondiabetic men*. Arterioscler Thromb Vasc Biol 2005, 25(5):1032-7.

[160] Ramasamy R, Yan SF, Herold K, Clynes R, Schmidt AM: *Receptor for advanced glycation end products: fundamental roles in the inflammatory response: winding the way to the pathogenesis of endothelial dysfunction and atherosclerosis*. Annals of the New York Academy of Sciences 2008, 1126:7-13.

[161] Lindsey JB, de Lemos JA, Cipollone F, Ayers CR, Rohatgi A, Morrow DA, Khera A, McGuire DK: *Association between circulating soluble receptor for advanced glycation end products and atherosclerosis: observations from the Dallas Heart Study*. Diabetes care 2009, 32(7):1218-20.

[162] Ghidoni R, Benussi L, Glionna M, Franzoni M, Geroldi D, Emanuele E, Binetti G: *Decreased plasma levels of soluble receptor for advanced glycation end products in mild cognitive impairment*. J Neural Transm 2008, 115(7):1047-50.

[163] Sternberg Z, Weinstock-Guttman B, Hojnacki D, Zamboni P, Zivadinov R, Chadha K, Lieberman A, Kazim L, Drake A, Rocco P, Grazioli E, Munschauer F: *Soluble receptor for advanced glycation end products in multiple sclerosis: a potential marker of disease severity*. Mult Scler 2008, 14(6):759-63.

[164] Ilzecka J: *Serum-soluble receptor for advanced glycation end product levels in patients with amyotrophic lateral sclerosis*. Acta Neurol Scand 2009, 120(2):119-22.

[165] Sparvero LJ, Asafu-Adjei D, Kang R, Tang D, Amin N, Im J, Rutledge R, Lin B, Amoscato AA, Zeh HJ, Lotze MT: *RAGE (Receptor for Advanced Glycation*

Endproducts), RAGE Ligands, and their role in Cancer and Inflammation. J Transl Med 2009, 7(1):17.

[166] Liotta LA, Clair T: *Cancer. Checkpoint for invasion*. Nature 2000, 405(6784):287-8.

[167] Yan SD, Schmidt AM, Anderson GM, Zhang J, Brett J, Zou YS, Pinsky D, Stern D: *Enhanced cellular oxidant stress by the interaction of advanced glycation end products with their receptors/binding proteins*. J Biol Chem 1994, 269(13):9889-97.

[168] Lander HM, Tauras JM, Ogiste JS, Hori O, Moss RA, Schmidt AM: *Activation of the receptor for advanced glycation end products triggers a p21(ras)-dependent mitogen-activated protein kinase pathway regulated by oxidant stress*. J Biol Chem 1997, 272(28):17810-4.

[169] Huttunen HJ, Fages C, Rauvala H: *Receptor for advanced glycation end products (RAGE)-mediated neurite outgrowth and activation of NF-kappaB require the cytoplasmic domain of the receptor but different downstream signaling pathways*. J Biol Chem 1999, 274(28):19919-24.

[170] Taguchi A, Blood DC, del Toro G, Canet A, Lee DC, Qu W, Tanji N, Lu Y, Lalla E, Fu C, Hofmann MA, Kislinger T, Ingram M, Lu A, Tanaka H, Hori O, Ogawa S, Stern DM, Schmidt AM: *Blockade of RAGE-amphoterin signalling suppresses tumour growth and metastases*. Nature 2000, 405(6784):354-60.

[171] Kostova N, Zlateva S, Ugrinova I, Pasheva E: *The expression of HMGB1 protein and its receptor RAGE in human malignant tumors*. Mol Cell Biochem 2009, 337(1-2):251-8.

[172] Lalla E, Lamster IB, Feit M, Huang L, Spessot A, Qu W, Kislinger T, Lu Y, Stern DM, Schmidt AM: *Blockade of RAGE suppresses periodontitis-associated bone loss in diabetic mice*. The Journal of clinical investigation 2000, 105(8):1117-24.

[173] Hanford LE, Enghild JJ, Valnickova Z, Petersen SV, Schaefer LM, Schaefer TM, Reinhart TA, Oury TD: *Purification and characterization of mouse soluble receptor for advanced glycation end products (sRAGE)*. J Biol Chem 2004, 279(48):50019-24.

[174] Chen Y, Yan SS, Colgan J, Zhang HP, Luban J, Schmidt AM, Stern D, Herold KC: *Blockade of late stages of autoimmune diabetes by inhibition of the receptor for advanced glycation end products*. J Immunol 2004, 173(2):1399-405.

[175] Arancio O, Zhang HP, Chen X, Lin C, Trinchese F, Puzzo D, Liu S, Hegde A, Yan SF, Stern A, Luddy JS, Lue LF, Walker DG, Roher A, Buttini M, Mucke L, Li W, Schmidt AM, Kindy M, Hyslop PA, Stern DM, Du Yan SS: *RAGE potentiates Abeta-induced perturbation of neuronal function in transgenic mice*. Embo J 2004, 23(20):4096-105.

[176] Tang D, Kang R, Zeh HJ, 3rd, Lotze MT: *High-mobility group box 1 and cancer*. Biochimica et biophysica acta 2010, 1799(1-2):131-40.

[177] Liliensiek B, Weigand MA, Bierhaus A, Nicklas W, Kasper M, Hofer S, Plachky J, Grone HJ, Kurschus FC, Schmidt AM, Yan SD, Martin E, Schleicher E, Stern DM, Hammerling GG, Nawroth PP, Arnold B: *Receptor for advanced glycation end products (RAGE) regulates sepsis but not the adaptive immune response*. The Journal of clinical investigation 2004, 113(11):1641-50.

[178] Yang H, Tracey KJ: *Targeting HMGB1 in inflammation*. Biochimica et biophysica acta 2010, 1799(1-2):149-56.

[179] Maeda S, Hikiba Y, Shibata W, Ohmae T, Yanai A, Ogura K, Yamada S, Omata M: *Essential roles of high-mobility group box 1 in the development of murine colitis and colitis-associated cancer*. Biochemical and biophysical research communications 2007, 360(2):394-400.

[180] van Beijnum JR, Buurman WA, Griffioen AW: *Convergence and amplification of toll-like receptor (TLR) and receptor for advanced glycation end products (RAGE) signaling pathways via high mobility group B1 (HMGB1)*. Angiogenesis 2008, 11(1):91-9.

[181] Hsieh HL, Schafer BW, Sasaki N, Heizmann CW: *Expression analysis of S100 proteins and RAGE in human tumors using tissue microarrays*. Biochemical and biophysical research communications 2003, 307(2):375-81.

[182] Mantell LL, Parrish WR, Ulloa L: *Hmgb-1 as a therapeutic target for infectious and inflammatory disorders*. Shock 2006, 25(1):4-11.

[183] Bianchi ME, Manfredi AA: *High-mobility group box 1 (HMGB1) protein at the crossroads between innate and adaptive immunity*. Immunological reviews 2007, 220:35-46.

[184] Suda K, Takeuchi H, Ishizaka A, Kitagawa Y: *High-mobility-group box chromosomal protein 1 as a new target for modulating stress response*. Surgery today 2010, 40(7):592-601.

[185] Klune JR, Billiar TR, Tsung A: *HMGB1 preconditioning: therapeutic application for a danger signal?* J Leukoc Biol 2008, 83(3):558-63.

[186] Izuishi K, Tsung A, Jeyabalan G, Critchlow ND, Li J, Tracey KJ, Demarco RA, Lotze MT, Fink MP, Geller DA, Billiar TR: *Cutting edge: high-mobility group box 1 preconditioning protects against liver ischemia-reperfusion injury*. J Immunol 2006, 176(12):7154-8.

[187] Dumitriu IE, Baruah P, Bianchi ME, Manfredi AA, Rovere-Querini P: *Requirement of HMGB1 and RAGE for the maturation of human plasmacytoid dendritic cells*. Eur J Immunol 2005a, 35(7):2184-90.

[188] Dumitriu IE, Bianchi ME, Bacci M, Manfredi AA, Rovere-Querini P: *The secretion of HMGB1 is required for the migration of maturing dendritic cells*. J Leukoc Biol 2007, 81(1):84-91.

[189] Manfredi AA, Capobianco A, Esposito A, De Cobelli F, Canu T, Monno A, Raucci A, Sanvito F, Doglioni C, Nawroth PP, Bierhaus A, Bianchi ME, Rovere-Querini P, Del Maschio A: *Maturing dendritic cells depend on RAGE for in vivo homing to lymph nodes*. J Immunol 2008, 180(4):2270-5.

[190] Steinman RM, Kaplan G, Witmer MD, Cohn ZA: *Identification of a novel cell type in peripheral lymphoid organs of mice. V. Purification of spleen dendritic cells, new surface markers, and maintenance in vitro*. J Exp Med 1979, 149(1):1-16.

[191] Dumitriu IE, Baruah P, Manfredi AA, Bianchi ME, Rovere-Querini P: *HMGB1: guiding immunity from within*. Trends Immunol 2005b, 26(7):381-7.

[192] Dumitriu IE, Baruah P, Valentinis B, Voll RE, Herrmann M, Nawroth PP, Arnold B, Bianchi ME, Manfredi AA, Rovere-Querini P: *Release of high mobility group box 1 by dendritic cells controls T cell activation via the receptor for advanced glycation end products*. J Immunol 2005c, 174(12):7506-15.

[193] Altmann S, Lange S, Pommerencke J, Murua Escobar H, Bullerdiek J, Nolte I, Freund M, Junghanss C: *High Mobility Group Box 1-Protein expression in canine haematopoietic cells and influence on canine peripheral blood mononuclear cell proliferative activity*. Vet Immunol Immunopathol 2008.

[194] Foley R, Tozer R, Wan Y: *Genetically modified dendritic cells in cancer therapy: implications for transfusion medicine*. Transfus Med Rev 2001, 15(4):292-304.

[195] Nencioni A, Brossart P: *Cellular immunotherapy with dendritic cells in cancer: current status*. Stem Cells 2004, 22(4):501-13.

[196] Hsu FJ, Benike C, Fagnoni F, Liles TM, Czerwinski D, Taidi B, Engleman EG, Levy R: *Vaccination of patients with B-cell lymphoma using autologous antigen-pulsed dendritic cells*. Nature medicine 1996, 2(1):52-8.

[197] Muthumani G, Laddy DJ, Sundaram SG, Fagone P, Shedlock DJ, Kannan S, Wu L, Chung CW, Lankaraman KM, Burns J, Muthumani K, Weiner DB: *Co-immunization with an optimized plasmid-encoded immune stimulatory interleukin, high-mobility group box 1 protein, results in enhanced interferon-gamma secretion by antigen-specific CD8 T cells*. Immunology 2009, 128(1 Suppl):e612-20.

[198] de Vries IJ, Krooshoop DJ, Scharenborg NM, Lesterhuis WJ, Diepstra JH, Van Muijen GN, Strijk SP, Ruers TJ, Boerman OC, Oyen WJ, Adema GJ, Punt CJ, Figdor CG: *Effective migration of antigen-pulsed dendritic cells to lymph nodes in melanoma patients is determined by their maturation state*. Cancer research 2003, 63(1):12-7.

[199] Nagaraj S, Ziske C, Schmidt-Wolf IG: *Dendritic cell, the immunotherapeutic cell for cancer*. The Indian journal of medical research 2004, 119(4):133-8.

[200] Boudreau JE, Bonehill A, Thielemans K, Wan Y: *Engineering dendritic cells to enhance cancer immunotherapy*. Mol Ther 2011, 19(5):841-53.

[201] Tekle E, Astumian RD, Chock PB: *Electroporation by using bipolar oscillating electric field: an improved method for DNA transfection of NIH 3T3 cells*. Proc Natl Acad Sci U S A 1991, 88(10):4230-4.

[202] Felgner PL, Gadek TR, Holm M, Roman R, Chan HW, Wenz M, Northrop JP, Ringold GM, Danielsen M: *Lipofection: a highly efficient, lipid-mediated DNA-transfection procedure*. Proc Natl Acad Sci U S A 1987, 84(21):7413-7.

[203] Menendez P, Bueno C, Wang L, Bhatia M: *Human embryonic stem cells: potential tool for achieving immunotolerance?* Stem cell reviews 2005, 1(2):151-8.

[204] Papapetrou EP, Zoumbos NC, Athanassiadou A: *Genetic modification of hematopoietic stem cells with nonviral systems: past progress and future prospects*. Gene therapy 2005, 12 Suppl 1:S118-30.

[205] Brenner MK: *Emerging applications of gene transfer in the hematopoietic cancers*. Journal of pediatric hematology/oncology 1997, 19(1):1-6.

[206] Haviernik P, Bunting KD: *Safety concerns related to hematopoietic stem cell gene transfer using retroviral vectors*. Current gene therapy 2004, 4(3):263-76.

[207] Tirlapur UK, König K: *Targeted transfection by femtosecond laser*. Nature 2002a, 418(6895):290-1.

[208] Stevenson D, Agate B, Tsampoula X, Fischer P, Brown CT, Sibbett W, Riches A, Gunn-Moore F, Dholakia K: *Femtosecond optical transfection of cells: viability and efficiency*. Optics express 2006, 14(16):7125-33.

[209] Kohli V, Acker JP, Elezzabi AY: *Reversible permeabilization using high-intensity femtosecond laser pulses: applications to biopreservation*. Biotechnology and bioengineering 2005, 92(7):889-99.

[210] Tirlapur UK, König K: *Femtosecond near-infrared laser pulses as a versatile non-invasive tool for intra-tissue nanoprocessing in plants without compromising viability*. Plant J 2002b, 31(3):365-74.

[211] Rosi NL, Giljohann DA, Thaxton CS, Lytton-Jean AK, Han MS, Mirkin CA: *Oligonucleotide-modified gold nanoparticles for intracellular gene regulation*. Science 2006, 312(5776):1027-30.

[212] Qiao F-Y, Liu J, Li F-R, Kong X-L, Zhang H-L, Zhou H-X: *Antibody and DNA dual-labeled gold nanoparticles: stability and reactivity.* Applied Surface Science 2008, 254(10):2941–6.

[213] Dahl JA, Maddux BL, Hutchison JE: *Toward greener nanosynthesis*. Chemical reviews 2007, 107(6):2228-69.

[214] Mafuné F, Kohno JY, Takeda Y, Kondow T: *Dissociation and aggregation of gold nanoparticles under laser irradiation*. The Journal of Physical Chemistry 2001, 105:9050-6.

[215] Mafuné F, Kohno JY, Takeda Y, Kondow T: *Full Physical Preparation of Size-Selected Gold Nanoparticles in Solution: Laser Ablation and Laser-Induced Size Control.* The Journal of Physical Chemistry 2002, 106 (31) 7575–7.

[216] Petersen S, Soller JT, Wagner S, Richter A, Bullerdiek J, Nolte I, Barcikowski S, Murua Escobar H: *Co-transfection of plasmid DNA and laser-generated gold nanoparticles does not disturb the bioactivity of GFP-HMGB1 fusion protein*. Journal of nanobiotechnology 2009b, 7:6.

[217] Wang YS, Chi KH, Liao KW, Liu CC, Cheng CL, Lin YC, Cheng CH, Chu RM: *Characterization of canine monocyte-derived dendritic cells with phenotypic and functional differentiation*. Can J Vet Res 2007, 71(3):165-74.

[218] Hoehn M, Kustermann E, Blunk J, Wiedermann D, Trapp T, Wecker S, Focking M, Arnold H, Hescheler J, Fleischmann BK, Schwindt W, Buhrle C: *Monitoring*

of implanted stem cell migration in vivo: a highly resolved in vivo magnetic resonance imaging investigation of experimental stroke in rat. Proc Natl Acad Sci U S A 2002, 99(25):16267-72.

[219] Unger EC: *How can superparamagnetic iron oxides be used to monitor disease and treatment?* Radiology 2003, 229(3):615-6.

[220] Yeh TC, Zhang W, Ildstad ST, Ho C: *In vivo dynamic MRI tracking of rat T-cells labeled with superparamagnetic iron-oxide particles*. Magn Reson Med 1995, 33(2):200-8.

[221] Schulze E, Ferrucci JT, Jr., Poss K, Lapointe L, Bogdanova A, Weissleder R: *Cellular uptake and trafficking of a prototypical magnetic iron oxide label in vitro*. Investigative radiology 1995, 30(10):604-10.

[222] Moore A, Weissleder R, Bogdanov A, Jr.: *Uptake of dextran-coated monocrystalline iron oxides in tumor cells and macrophages*. J Magn Reson Imaging 1997, 7(6):1140-5.

[223] Weissleder R, Cheng HC, Bogdanova A, Bogdanov A, Jr.: *Magnetically labeled cells can be detected by MR imaging*. J Magn Reson Imaging 1997, 7(1):258-63.

[224] Schoepf U, Marecos EM, Melder RJ, Jain RK, Weissleder R: *Intracellular magnetic labeling of lymphocytes for in vivo trafficking studies*. BioTechniques 1998, 24(4):642-6, 8-51.

[225] Dodd SJ, Williams M, Suhan JP, Williams DS, Koretsky AP, Ho C: *Detection of single mammalian cells by high-resolution magnetic resonance imaging*. Biophysical journal 1999, 76(1 Pt 1):103-9.

[226] Ahrens ET, Feili-Hariri M, Xu H, Genove G, Morel PA: *Receptor-mediated endocytosis of iron-oxide particles provides efficient labeling of dendritic cells for in vivo MR imaging*. Magn Reson Med 2003, 49(6):1006-13.

[227] Pintaske J, Helms G, Bantleon R, Kehlbach R, Wiskirchen J, Claussen CD, Schick F: *[A preparation technique for quantitative investigation of SPIO-containing solutions and SPIO-labelled cells by MRI]*. Biomedizinische Technik 2005, 50(6):174-80.

[228] de Vries IJ, Lesterhuis WJ, Barentsz JO, Verdijk P, van Krieken JH, Boerman OC, Oyen WJ, Bonenkamp JJ, Boezeman JB, Adema GJ, Bulte JW, Scheenen TW, Punt CJ, Heerschap A, Figdor CG: *Magnetic resonance tracking of dendritic cells in melanoma patients for monitoring of cellular therapy*. Nature biotechnology 2005, 23(11):1407-13.

[229] Verdijk P, Scheenen TW, Lesterhuis WJ, Gambarota G, Veltien AA, Walczak P, Scharenborg NM, Bulte JW, Punt CJ, Heerschap A, Figdor CG, de Vries IJ: *Sensitivity of magnetic resonance imaging of dendritic cells for in vivo tracking of cellular cancer vaccines*. Int J Cancer 2007, 120(5):978-84.

[230] Küstermann E, Himmelreich U, Kandal K, Geelen T, Ketkar A, Wiedermann D, Strecker C, Esser J, Arnhold S, Hoehn M: *Efficient stem cell labeling for MRI studies*. Contrast media & molecular imaging 2008, 3(1):27-37.

[231] Baumjohann D, Hess A, Budinsky L, Brune K, Schuler G, Lutz MB: *In vivo magnetic resonance imaging of dendritic cell migration into the draining lymph nodes of mice*. Eur J Immunol 2006, 36(9):2544-55.

[232] Bhawal UK, Ozaki Y, Nishimura M, Sugiyama M, Sasahira T, Nomura Y, Sato F, Fujimoto K, Sasaki N, Ikeda MA, Tsuji K, Kuniyasu H, Kato Y: *Association of expression of receptor for advanced glycation end products and invasive activity of oral squamous cell carcinoma*. Oncology 2005, 69(3):246-55.

[233] Sterenczak KA, Willenbrock S, Barann M, Klemke M, Soller JT, Eberle N, Nolte I, Bullerdiek J, Murua Escobar H: *Cloning, characterisation, and comparative quantitative expression analyses of receptor for advanced glycation end products (RAGE) transcript forms*. Gene 2009, 434(1-2):35-42.

[234] Holbrook JA, Neu-Yilik G, Hentze MW, Kulozik AE: *Nonsense-mediated decay approaches the clinic*. Nature genetics 2004, 36(8):801-8.

[235] Sterenczak KA, Kleinschmidt S, Wefstaedt P, Eberle N, Hewicker-Trautwein M, Bullerdiek J, Nolte I, Murua Escobar H: *Quantitative PCR and immunohistochemical analyses of HMGB1 and RAGE expression in canine disseminated histiocytic sarcoma (malignant histiocytosis)*. Anticancer research 2011, 31(5):1541-8.

[236] Vazzana N, Santilli F, Cuccurullo C, Davi G: *Soluble forms of RAGE in internal medicine*. Internal and emergency medicine 2009, 4(5):389-401.

[237] Santilli F, Vazzana N, Bucciarelli LG, Davi G: *Soluble forms of RAGE in human diseases: clinical and therapeutical implications*. Current medicinal chemistry 2009, 16(8):940-52.

[238] Takeuchi A, Yamamoto Y, Tsuneyama K, Cheng C, Yonekura H, Watanabe T, Shimizu K, Tomita K, Yamamoto H, Tsuchiya H: *Endogenous secretory receptor for advanced glycation endproducts as a novel prognostic marker in chondrosarcoma*. Cancer 2007, 109(12):2532-40.

[239] Tesarova P, Kalousova M, Jachymova M, Mestek O, Petruzelka L, Zima T: *Receptor for advanced glycation end products (RAGE)--soluble form (sRAGE) and gene polymorphisms in patients with breast cancer*. Cancer investigation 2007, 25(8):720-5.

[240] Jing R, Cui M, Wang J, Wang H: *Receptor for advanced glycation end products (RAGE) soluble form (sRAGE): a new biomarker for lung cancer*. Neoplasma 2010, 57(1):55-61.

[241] Moy KA, Jiao L, Freedman ND, Weinstein SJ, Sinha R, Virtamo J, Albanes D, Stolzenberg-Solomon RZ: *Soluble receptor for advanced glycation end products and risk of liver cancer*. Hepatology (Baltimore, Md 2013.

[242] Jiao L, Weinstein SJ, Albanes D, Taylor PR, Graubard BI, Virtamo J, Stolzenberg-Solomon RZ: *Evidence that serum levels of the soluble receptor for advanced glycation end products are inversely associated with pancreatic cancer risk: a prospective study*. Cancer research 2011a, 71(10):3582-9.

[243] Jiao L, Taylor PR, Weinstein SJ, Graubard BI, Virtamo J, Albanes D, Stolzenberg-Solomon RZ: *Advanced glycation end products, soluble receptor for advanced glycation end products, and risk of colorectal cancer*. Cancer Epidemiol Biomarkers Prev 2011b, 20(7):1430-8.

[244] Sterenczak KA, Joetzke AE, Willenbrock S, Eberle N, Lange S, Junghanss C, Nolte I, Bullerdiek J, Simon D, Murua Escobar H: *High-mobility group B1 (HMGB1) and receptor for advanced glycation end-products (RAGE) expression in canine lymphoma*. Anticancer research 2010, 30(12):5043-8.

[245] Ruan J, Hajjar K, Rafii S, Leonard JP: *Angiogenesis and antiangiogenic therapy in non-Hodgkin's lymphoma*. Ann Oncol 2009, 20(3):413-24.

[246] Wolfesberger B, Guija de Arespacohaga A, Willmann M, Gerner W, Miller I, Schwendenwein I, Kleiter M, Egerbacher M, Thalhammer JG, Muellauer L, Skalicky M, Walter I: *Expression of vascular endothelial growth factor and its receptors in canine lymphoma*. Journal of comparative pathology 2007, 137(1):30-40.

[247] Ono M, Torisu H, Fukushi J, Nishie A, Kuwano M: *Biological implications of macrophage infiltration in human tumor angiogenesis*. Cancer Chemother Pharmacol 1999, 43 Suppl:S69-71.

[248] Nieters A, Beckmann L, Deeg E, Becker N: *Gene polymorphisms in Toll-like receptors, interleukin-10, and interleukin-10 receptor alpha and lymphoma risk*. Genes Immun 2006, 7(8):615-24.

[249] Smith TJ, Yamamoto K, Kurata M, Yukimori A, Suzuki S, Umeda S, Sugawara E, Kojima Y, Sawabe M, Nakagawa Y, Suzuki K, Crawley JT, Kitagawa M: *Differential expression of Toll-like receptors in follicular lymphoma, diffuse large B-cell lymphoma and peripheral T-cell lymphoma*. Experimental and molecular pathology 2010, 89(3):284-90.

[250] Wang L, Zhao Y, Qian J, Sun L, Lu Y, Li H, Li Y, Yang J, Cai Z, Yi Q: *Toll-like receptor-4 signaling in mantle cell lymphoma : Effects on tumor growth and immune evasion*. Cancer 2012.

[251] Rendon-Mitchell B, Ochani M, Li J, Han J, Wang H, Yang H, Susarla S, Czura C, Mitchell RA, Chen G, Sama AE, Tracey KJ: *IFN-gamma induces high mobility group box 1 protein release partly through a TNF-dependent mechanism*. J Immunol 2003, 170(7):3890-7.

[252] Ulloa L, Batliwalla FM, Andersson U, Gregersen PK, Tracey KJ: *High mobility group box chromosomal protein 1 as a nuclear protein, cytokine, and potential therapeutic target in arthritis*. Arthritis Rheum 2003, 48(4):876-81.

[253] Andersson U, Erlandsson-Harris H, Yang H, Tracey KJ: *HMGB1 as a DNA-binding cytokine*. J Leukoc Biol 2002, 72(6):1084-91.

[254] Park JS, Arcaroli J, Yum HK, Yang H, Wang H, Yang KY, Choe KH, Strassheim D, Pitts TM, Tracey KJ, Abraham E: *Activation of gene expression in human neutrophils by high mobility group box 1 protein*. Am J Physiol Cell Physiol 2003, 284(4):C870-9.

[255] Soller JT, Murua-Escobar H, Willenbrock S, Janssen M, Eberle N, Bullerdiek J, Nolte I: *Comparison of the human and canine cytokines IL-1(alpha/beta) and TNF-alpha to orthologous other mammalians*. J Hered 2007, 98(5):485-90.

[256] Ulloa L, Messmer D: *High-mobility group box 1 (HMGB1) protein: friend and foe*. Cytokine Growth Factor Rev 2006, 17(3):189-201.

[257] Baumgart J, Bintig W, Ngezahayo A, Willenbrock S, Murua Escobar H, Ertmer W, Lubatschowski H, Heisterkamp A: *Quantified femtosecond laser based opto-perforation of living GFSHR-17 and MTH53 a cells*. Optics express 2008, 16(5):3021-31.

[258] Pitsillides CM, Joe EK, Wei X, Anderson RR, Lin CP: *Selective cell targeting with light-absorbing microparticles and nanoparticles*. Biophysical journal 2003, 84(6):4023-32.

[259] Yao C, Qu X, Zhang Z: *Laser-based transfection with conjugated gold nanoparticles*. Chinese Optics Letters 2009, 7 (10):898-900.

[260] Schomaker M, Baumgart J, Ngezahayo A, Bullerdiek J, Nolte I, Murua Escobar H, Lubatschowski H, Heisterkamp A: *Plasmonic perforation of living cells using ultrashort laser pulses and gold nanoparticles*. Proceedings of the SPIE 7192, Plasmonics in Biology and Medicine VI, 71920U 2009.

[261] Schomaker M, Fehlauer H, Bintig W, Ngezahayo A, Nolte I, Murua Escobar H, Lubatschowski H, Heisterkamp A: *Fs- laser cell perforation using gold nanoparticles of different shapes*. Proceedings of the SPIE, Volume 7589, pp 75890C-75890C-5 (2010) 2010.

[262] Schomaker M, Baumgart J, Motekaitis D, Heinemann D, Krawinkel J, Pangalos M, Bintig W, Boulais E, Lachaine R, St.-Louis Lalonde B, Ngezahayo A, Meunier M, Heisterkamp A: *Mechanisms of gold nanoparticle mediated ultrashort laser cell membrane perforation.* Proceedings of the SPIE 2011.

[263] Heinemann D, Schomaker M, Motekaitis D, Krawinkel J, Killian D, Murua Escobar H, Junghanss C, Heisterkamp A: *Gold nanoparticle mediated cell manipulation using fs and ps laser pulses for cell perforation and transfection*. Proceedings of the SPIE 2011:7918-25.

[264] Kalies S, Birr T, Heinemann D, Schomaker M, Ripken T, Heisterkamp A, Meyer H: *Enhancement of extracellular molecule uptake in plasmonic laser perforation*. J Biophotonics 2013.

[265] Petersen S, Jakobi J, Barcikowski S: *In situ bioconjugation - Novel laser based approach to pure nanoparticle-conjugates*. Applied Surface Science 2009a, 255(10):5435-8.

[266] *Durán MC, *Willenbrock S, Barchanski A, Muller JM, Maiolini A, Soller JT, Barcikowski S, Nolte I, Feige K, Murua Escobar H, authorship ec: *Comparison of nanoparticle-mediated transfection methods for DNA expression plasmids: efficiency and cytotoxicity*. Journal of nanobiotechnology 2011, 9:47.

[267] Darquet AM, Cameron B, Wils P, Scherman D, Crouzet J: *A new DNA vehicle for nonviral gene delivery: supercoiled minicircle*. Gene therapy 1997, 4(12):1341-9.

[268] Kreiss P, Cameron B, Rangara R, Mailhe P, Aguerre-Charriol O, Airiau M, Scherman D, Crouzet J, Pitard B: *Plasmid DNA size does not affect the physicochemical properties of lipoplexes but modulates gene transfer efficiency*. Nucleic Acids Res 1999, 27(19):3792-8.

[269] Yin W, Xiang P, Li Q: *Investigations of the effect of DNA size in transient transfection assay using dual luciferase system*. Anal Biochem 2005, 346(2):289-94.

[270] Willenbrock S, Braun O, Baumgart J, Lange S, Junghanss C, Heisterkamp A, Nolte I, Bullerdiek J, Murua Escobar H: *TNF-alpha induced secretion of HMGB1 from non-immune canine mammary epithelial cells (MTH53A)*. Cytokine 2012b, 57(2):210-20.

[271] Parkkinen J, Rauvala H: *Interactions of plasminogen and tissue plasminogen activator (t-PA) with amphoterin. Enhancement of t-PA-catalyzed plasminogen activation by amphoterin*. J Biol Chem 1991, 266(25):16730-5.

[272] Ossowski L, Biegel D, Reich E: *Mammary plasminogen activator: correlation with involution, hormonal modulation and comparison between normal and neoplastic tissue*. Cell 1979, 16(4):929-40.

[273] Wernette CM, Smith BF, Barksdale ZL, Hecker R, Baker HJ: *CpG oligodeoxynucleotides stimulate canine and feline immune cell proliferation*. Vet Immunol Immunopathol 2002, 84(3-4):223-36.

[274] Hartmann G, Weeratna RD, Ballas ZK, Payette P, Blackwell S, Suparto I, Rasmussen WL, Waldschmidt M, Sajuthi D, Purcell RH, Davis HL, Krieg AM: *Delineation of a CpG phosphorothioate oligodeoxynucleotide for activating primate immune responses in vitro and in vivo*. J Immunol 2000, 164(3):1617-24.

[275] Krieg AM, Yi AK, Matson S, Waldschmidt TJ, Bishop GA, Teasdale R, Koretzky GA, Klinman DM: *CpG motifs in bacterial DNA trigger direct B-cell activation*. Nature 1995, 374(6522):546-9.

[276] Walker PS, Scharton-Kersten T, Krieg AM, Love-Homan L, Rowton ED, Udey MC, Vogel JC: *Immunostimulatory oligodeoxynucleotides promote protective immunity and provide systemic therapy for leishmaniasis via IL-12- and IFN-gamma-dependent mechanisms*. Proc Natl Acad Sci U S A 1999, 96(12):6970-5.

[277] Hartmann G, Weiner GJ, Krieg AM: *CpG DNA: a potent signal for growth, activation, and maturation of human dendritic cells*. Proc Natl Acad Sci U S A 1999, 96(16):9305-10.

[278] Ballas ZK, Rasmussen WL, Krieg AM: *Induction of NK activity in murine and human cells by CpG motifs in oligodeoxynucleotides and bacterial DNA*. J Immunol 1996, 157(5):1840-5.

[279] Krieg AM: *Direct immunologic activities of CpG DNA and implications for gene therapy*. J Gene Med 1999a, 1(1):56-63.

[280] Decker T, Schneller F, Kronschnabl M, Dechow T, Lipford GB, Wagner H, Peschel C: *Immunostimulatory CpG-oligonucleotides induce functional high affinity IL-2 receptors on B-CLL cells: costimulation with IL-2 results in a highly immunogenic phenotype*. Experimental hematology 2000, 28(5):558-68.

[281] Haferlach C, Dicker F, Schnittger S, Kern W, Haferlach T: *Comprehensive genetic characterization of CLL: a study on 506 cases analysed with chromosome banding analysis, interphase FISH, IgV(H) status and immunophenotyping*. Leukemia 2007, 21(12):2442-51.

[282] Struski S, Gervais C, Helias C, Herbrecht R, Audhuy B, Mauvieux L: *Stimulation of B-cell lymphoproliferations with CpG-oligonucleotide DSP30 plus IL-2 is more effective than with TPA to detect clonal abnormalities*. Leukemia 2009, 23(3):617-9.

[283] Reimann-Berg N, Murua Escobar H, Kiefer Y, Mischke R, Willenbrock S, Eberle N, Nolte I, Bullerdiek J: *Cytogenetic analysis of CpG-oligonucleotide DSP30 plus Interleukin-2-Stimulated canine B-Cell lymphoma cells reveals the loss of one X Chromosome as the sole abnormality*. Cytogenetic and genome research 2011, 135(1):79-82.

[284] Abruzzese E, Rao PN, Slatkoff M, Cruz J, Powell BL, Jackle B, Pettenati MJ: *Monosomy X as a recurring sole cytogenetic abnormality associated with myelodysplastic diseases*. Cancer Genet Cytogenet 1997, 93(2):140-6.

[285] Bueno JL, Watson A, Dainton MG, Hughes DM, Killick S, Treleaven JG, Swansbury GJ: *Monosomy X as the sole cytogenetic abnormality in acute lymphoblastic leukemia: a report of two new patients*. Leuk Lymphoma 1999, 32(3-4):381-4.

[286] Kurata K, Iwata A, Masuda K, Sakaguchi M, Ohno K, Tsujimoto H: *Identification of CpG oligodeoxynucleotide sequences that induce IFN-gamma production in canine peripheral blood mononuclear cells*. Vet Immunol Immunopathol 2004, 102(4):441-50.

[287] Ren J, Sun L, Yang L, Wang H, Wan M, Zhang P, Yu H, Guo Y, Yu Y, Wang L: *A novel canine favored CpG oligodeoxynucleotide capable of enhancing the efficacy of an inactivated aluminum-adjuvanted rabies vaccine of dog use*. Vaccine 2010, 28(12):2458-64.

[288] Fitting J, Killian D, Junghanss C, Willenbrock S, Murua Escobar H, Lange S, Nolte I, Barth S, Tur MK: *Generation of recombinant antibody fragments that target canine dendritic cells by phage display technology*. Veterinary and comparative oncology 2011, 9(3):183-95.

[289] Akins EJ, Dubey P: *Noninvasive imaging of cell-mediated therapy for treatment of cancer*. J Nucl Med 2008, 49 Suppl 2:180S-95S.

[290] Mosca PJ, Clay TM, Morse MA, Lyerly HK: *Immune monitoring*. Cancer Treat Res 2005, 123:369-88.

[291] Chan WC, Nie S: *Quantum dot bioconjugates for ultrasensitive nonisotopic detection*. Science 1998, 281(5385):2016-8.

[292] Bruchez M, Jr., Moronne M, Gin P, Weiss S, Alivisatos AP: *Semiconductor nanocrystals as fluorescent biological labels*. Science 1998, 281(5385):2013-6.

[293] Chan WC, Maxwell DJ, Gao X, Bailey RE, Han M, Nie S: *Luminescent quantum dots for multiplexed biological detection and imaging*. Curr Opin Biotechnol 2002, 13(1):40-6.

[294] Derfus AM, Chan WCW, Bhatia SN: *Probing the Cytotoxicity of Seminconductor Quantum Dots*. Nano Letters 2004, 4(1):11-8.

[295] Cai W, Hsu AR, Li ZB, Chen X: *Are quantum dots ready for in vivo imaging in human subjects?* Nanoscale Res Lett 2007, 2(6):265-81.

[296] Intes X: *Time-domain optical mammography SoftScan: initial results*. Acad Radiol 2005, 12(8):934-47.

[297] Taroni P, Danesini G, Torricelli A, Pifferi A, Spinelli L, Cubeddu R: *Clinical trial of time-resolved scanning optical mammography at 4 wavelengths between 683 and 975 nm*. Journal of biomedical optics 2004, 9(3):464-73.

[298] Willenbrock S, Knippenberg S, Meier M, Hass R, Wefstaedt P, Nolte I, Murua Escobar H, Petri S: *In vivo MRI of intraspinally injected SPIO-labelled human CD34+ cells in a transgenic mouse model of ALS*. In vivo (Athens, Greece) 2012a, 26(1):31-8.

[299] Dunning MD, Lakatos A, Loizou L, Kettunen M, ffrench-Constant C, Brindle KM, Franklin RJ: *Superparamagnetic iron oxide-labeled Schwann cells and olfactory*

ensheathing cells can be traced in vivo by magnetic resonance imaging and retain functional properties after transplantation into the CNS. J Neurosci 2004, 24(44):9799-810.

[300] Jendelova P, Herynek V, Urdzikova L, Glogarova K, Kroupova J, Andersson B, Bryja V, Burian M, Hajek M, Sykova E: *Magnetic resonance tracking of transplanted bone marrow and embryonic stem cells labeled by iron oxide nanoparticles in rat brain and spinal cord*. Journal of neuroscience research 2004, 76(2):232-43.

[301] Zhang Y, Cheng G, Yang K, Fan R, Xu Z, Chen L, Li Q, Yang A, Jin B: *A novel function of granulocyte colony-stimulating factor in mobilization of human hematopoietic progenitor cells*. Immunol Cell Biol 2009a, 87(5):428-32.

[302] Zhang Y, Wang L, Fu Y, Song H, Zhao H, Deng M, Zhang J, Fan D: *Preliminary investigation of effect of granulocyte colony stimulating factor on amyotrophic lateral sclerosis*. Amyotroph Lateral Scler 2009b, 10(5-6):430-1.

[303] Liesveld JL, Bechelli J, Rosell K, Lu C, Bridger G, Phillips G, 2nd, Abboud CN: *Effects of AMD3100 on transmigration and survival of acute myelogenous leukemia cells*. Leukemia research 2007, 31(11):1553-63.

[304] Larochelle A, Krouse A, Metzger M, Orlic D, Donahue RE, Fricker S, Bridger G, Dunbar CE, Hematti P: *AMD3100 mobilizes hematopoietic stem cells with long-term repopulating capacity in nonhuman primates*. Blood 2006, 107(9):3772-8.

[305] Meng E, Guo Z, Wang H, Jin J, Wang J, Wu C, Wang L: *High mobility group box 1 protein inhibits the proliferation of human mesenchymal stem cells and promotes their migration and differentiation along osteoblastic pathway*. Stem Cells Dev 2008, 17(4):805-13.

[306] Mou Y, Hou Y, Chen B, Hua Z, Zhang Y, Xie H, Xia G, Wang Z, Huang X, Han W, Ni Y, Hu Q: *In vivo migration of dendritic cells labeled with synthetic superparamagnetic iron oxide*. International journal of nanomedicine 2011, 6:2633-40.

[307] de Chickera SN, Snir J, Willert C, Rohani R, Foley R, Foster PJ, Dekaban GA: *Labelling dendritic cells with SPIO has implications for their subsequent in vivo migration as assessed with cellular MRI*. Contrast media & molecular imaging 2011a, 6(4):314-27.

[308] Tavare R, Sagoo P, Varama G, Tanriver Y, Warely A, Diebold SS, Southworth R, Schaeffter T, Lechler RI, Razavi R, Lombardi G, Mullen GE: *Monitoring of in*

vivo function of superparamagnetic iron oxide labelled murine dendritic cells during anti-tumour vaccination. PLoS One 2011, 6(5):e19662.

[309] de Chickera S, Willert C, Mallet C, Foley R, Foster P, Dekaban GA: *Cellular MRI as a suitable, sensitive non-invasive modality for correlating in vivo migratory efficiencies of different dendritic cell populations with subsequent immunological outcomes*. Int Immunol 2011b, 24(1):29-41.

10. Danksagung / Acknowledgement

Herrn Prof. Dr. Jörn Bullerdiek danke ich für die Überlassung des Themas und für die Begutachtung und Diskussion dieser Arbeit. Vielen Dank dafür, dass in den Endzügen alles so schnell ging. Ich danke ihm des Weiteren für die Möglichkeit, Teile der Laborarbeiten im Zentrum für Humangenetik in Bremen durchzuführen und für die damit verbundene wissenschaftliche Betreuung.

Herrn Prof. Dr. Andreas Dotzauer danke ich vielmals für die spontane Bereitschaft zur Übernahme des Zweitgutachtens.

Herrn PD Dr. Murua Escobar danke ich für die exzellente Betreuung, die Unterstützung und das Vertrauen in mich, wodurch das Gelingen dieser Arbeit erst möglich wurde. Danke für die vielen Erfahrungen, die ich während meiner Promotionszeit in den verschiedensten Bereichen sammeln durfte; selbst Laborumzüge schocken mich jetzt nicht mehr. Auch für die Teilnahme am Prüfungsausschuss bedanke ich mich.

Bei Frau Prof. Dr. Kathrin Maedler möchte ich mich ebenfalls für die Teilnahme am Prüfungsausschuss bedanken.

Herrn Prof. Dr. Ingo Nolte danke ich für die vertrauensvolle Zusammenarbeit und die vielen Möglichkeiten, die er mir eröffnet hat. Ich bedanke mich für das stete Interesse an meiner Arbeit und dessen Vorankommen. Weiterhin möchte ich mich dafür bedanken, dass ich einen Großteil meiner Arbeit in den Laboren der Klinik für Kleintiere durchführen durfte.

Ich möchte mich bei den mittlerweile zahlreichen aktuellen und ehemaligen Mitgliedern unserer Arbeitsgruppe bedanken, die mich während meiner Promotionszeit auf die eine oder andere Weise unterstützt haben. Dankeschön für das gute Teamwork und das freundliche Arbeits- und Büroklima an: Siegfried Wagner, Dr. Carolina Maria Durán Graeff, Dr. Deniz Dziallas, Dr. Jan Soller, Dr. Katharina Sterenczak, Mohammed Amine Moulay, Wen Liu, Susanne Hammer, Julia Matena, Sari Eble, Annika Schnoor, Nicole Dörffer, Alesya Kuryanouych, Jan Schwarze und Olga Braun.

Bei den Mitarbeitern des ZHG Bremen bedanke ich mich für die gute Zusammenarbeit und das nette Arbeitsklima. Ein besonderer Dank geht dabei an

Dr. Nicola Reimann-Berg („Irgendwann entdeckt man doch sein Herz für Metaphasen…"), Dr. Andreas Richter und Marietta Müller, die trotz der Entfernung zwischen Bremen und Hannover den Kontakt nicht abreißen lassen haben.

Mein Dank geht auch an alle Mitglieder des Teilprojektes A2 des Transregio 37 für die vielen interdisziplinären Erfahrungen, die ich während der Bearbeitungsphase des Projektes sammeln durfte. Dabei geht ein besonderes Dankeschön an Markus Schomaker für die „neuen" Einblicke in die Methode der Lasertransfektion und die sehr unterhaltsamen kollaborativen Doktorandengespräche.

Dankeschön an das gesamte Team der Klinik für Kleintiere für das freundliche Arbeitsklima und die gute Zusammenarbeit. Dabei möchte ich besonders Regina Carlson für die geduldige Hilfe bei den Flowzytometrie-Messungen danken.

Steffi D., Vani und Nicky danke ich für die stets aufmunternden und lieben Worte in all den Jahren. Sweetums, du bist die Beste. Danke, dass du in allen Lebenslagen immer für mich da bist.

An meine Unimädels Miri, Bine, Jasmin, Steffi G. und Ines geht ein Dankeschön für die moralische Unterstützung und die tollen gemeinsamen Roadtrips, die mir immer geholfen haben, den Kopf wieder frei zu bekommen. Mit Jannsen-Reisen kommt man überall gut an.

Danke auch an Dani und Caro für die gemütlichen und kommunikativen Abende in Hannover - geteiltes Leid ist halbes Leid.

Ein ganz besonderer Dank geht an meine Eltern, meinen Bruder und meine Omi, die mich auf meinem bisherigen Lebensweg immer unterstützt und ermutigt haben und an mich und an das Gelingen dieser Arbeit geglaubt haben.

Abschließend möchte ich mich von ganzem Herzen bei meinem Freund Dennis bedanken, der mich durch alle Höhen und Tiefen begleitet hat und besonders in schwierigen und stressigen Zeiten immer für mich da war. Danke.